DENSIFICATION AND CYCLIC TRIAXIAL TESTING OF LEIGHTON-BUZZARD 120/200 SAND

by

MARK DAVID BUCKNAM

B.S.C.E., Tufts University
(1980)

SUBMITTED TO THE DEPARTMENT OF
CIVIL ENGINEERING IN PARTIAL
FULFILLMENT OF THE
REQUIREMENTS FOR THE
DEGREE OF

MASTER OF SCIENCE

at the

MASSACHUSETTS INSTITUTE OF TECHNOLOGY

September 1981

Signature of Author _____
Department of Civil Engineering
September 17, 1981

Certified by _____
Thesis Supervisor

Accepted by _____
Chairman, Department Committee

DENSIFICATION AND CYCLIC TRIAXIAL TESTING OF LEIGHTON-BUZZARD 120/200 Sand

by

MARK DAVID BUCKNAM

Submitted to the Department of Civil Engineering on September 17, 1981 in partial fulfillment of the requirements for the Degree of Master of Science in Civil Engineering.

ABSTRACT

The cyclic loading of saturated sands in triaxial tests has been intensely studied in the past 15 years. The results of such tests have been used primarily to determine the liquefaction behavior of various sand deposits during earthquake shaking. However, there are many geometry-related problems associated with comparing the stress condition in a triaxial test with that believed to exist in the field. More recently, the cyclic triaxial test has been used to study the behavior of soils beneath offshore structures. Here, the applied stresses can be made to closely resemble those of various elements beneath the actual structure.

One of the limitations of laboratory testing of reconstituted sand samples for the above mentioned reasons, is that the soil fabric (structure) is usually quite different from that of the in-situ soil. It has been shown, for instance, that the liquefaction strength can vary by as much as 200%, depending on how the sample is formed.

The purpose of this research was: 1) to document drained and undrained cyclic triaxial test results for use in estimating densification in centrifuge tests, and 2) to investigate the differences in the cyclic behavior between samples prepared by the conventional moist tamped method and the wet rodding method - a method used to prepare samples in centrifuge tests.

The drained analysis consisted primarily of determining a relationship for volumetric strain in terms of peak-to-peak shear strain and cycle number. This relationship is shown to work quite well for predicting the densification behavior of the test sand in drained cyclic tests. The effect of sample preparation method on the densification behaviour of Leighton-Buzzard 120/200 Sand is discussed in depth. Results show that the moist tamped samples have a greater tendency toward densification than the wet rodded samples when compacted to the same void ratio.

The liquefaction behavior of the sand in undrained cyclic tests is also addressed in this thesis. Results are presented in the form of liquefaction strength curves to show the effects of sample preparation method. It was found that the cyclic shear stress ratio required to cause initial liquefaction in N cycles in the wet rodded samples was approximately 5-15 percent less than that for the moist tamped samples. Normalized plots of pore pressure development show that the method of preparation has no distinguishable effect on pore pressure accumulation. It is concluded that the differences in the undrained cyclic behaviour are mainly a result of the differences in soil structure.

Thesis Supervisor: Professor Robert V. Whitman

ACKNOWLEDGMENT

I would like to thank my thesis supervisor, Professor Robert V. Whitman, and good friend, Philip Lambe, for their continued guidance and support during my year at M.I.T.

I am also grateful to my family, and my wife, Cheri, who provided the endless encouragement I needed throughout the year.

TABLE OF CONTENTS

LIST OF TABLES

LIST OF FIGURES

LIST OF SYMBOLS

A	-	Constant in Equation 4.2, $A = 10^{a_N}$ for cycle N.
a_N	-	Volumetric strain at $\gamma_{pp} = 0.01\%$ at cycle N.
B	-	Pore Pressure coefficient for isotropic stress, $B = \Delta u / \Delta\sigma_c$.
b	-	Slope of volumetric strain - shear strain data.
CAD	-	Anisotropically consolidated drained test.
$\overline{CIU}$	-	Isotropically consolidated undrained test.
cm	-	Centimeter.
D	-	Diameter of triaxial sample.
DC	-	Drained Cyclic test.
D_r	-	Relative density.
D_{10}	-	Grain diameter at which 10% is finer.
D_{50}	-	Mean grain diameter.
D_{60}	-	Grain diameter at which 60% is finer.
D_{90}	-	Grain diameter at which 90% is finer.
E	-	Young's modulus.
E_v	-	Modulus calculated from drained tests (Equation 4.9), $E_v = \Delta\sigma_v / \Delta\varepsilon_v$
ESP	-	Effective Stress Path.
e	-	Void ratio.
e_c	-	Void ratio after consolidation.
e_o	-	Initial void ratio.
G	-	Shear modulus, $G = \frac{E}{2(\mu+1)}$
G	-	Specific gravity.
H	-	Height of triaxial sample.
in	-	Inch.

K_c - Consolidation stress ratio.

K_o - Coefficient of lateral stress at rest.

kg - Kilogram.

m - Meter.

mm - Millimeter.

min - Minute.

N - Number of cycles.

N_L - Number of cycles to initial liquefaction in undrained cyclic test.

$N_{(\varepsilon_{v_{pp}} = 1\%)}$ - Number of cycles to 1% peak-to-peak vertical strain.

$N_{(\varepsilon_{v_{pp}} = 5\%)}$ - Number of cycles to 5% peak-to-peak vertical strain.

n - Porosity.

N_c - Porosity after consolidation.

p - "p-value", mean normal stress, $p = \frac{\sigma_v + \sigma_h}{2}$

$\bar{p}$ - Mean effective normal stress, $\bar{p} = \frac{\bar{\sigma}_v + \bar{\sigma}_h}{2}$

$\bar{p}_o$ - Initial mean effective normal stress.

psi - Pounds per square inch.

q - "q-value", mean shear stress, $q = \frac{\sigma_1 - \sigma_3}{2}$

q_m - Mean shear stress about which cyclic test is run.

$q_m/\bar{p}_o$ - Mean shear stress ratio in cyclic test.

Δq_{cy} - Half the total change in shear stress in a cyclic test, $\Delta q_{cy} = \frac{\sigma_1 - \sigma_3}{2}$

$\Delta q_{cy}/\bar{p}_o$ - Shear stress ratio in cyclic test.

sec - Second.

T	-	Cyclic load period, seconds.
TSP	-	Total Stress Path.
U	-	Coefficient of Uniformity.
u	-	Pore Pressure.
u_b	-	Back pressure in triaxial test.
u_c	-	Undrained cyclic test.
u_i	-	Degree of undercompaction.
u_s	-	Steady-state pore pressure.
$\dot{u}$	-	Pore pressure change.
V_c	-	Volume after consolidation.
$\dot{V}$	-	Volume change.
W_c	-	Total cyclic hanger weight in kg.
W_h	-	Static hanger weight in kg.
W_s	-	Deadweight on static hanger in kg.
α^*	-	Angle of rotation on flywheel.
$\bar{\alpha}$	-	Inclination of the K_f-line.
γ	-	Shear strain.
ε	-	Strain (see subscripts).
ε_{acc}	-	Accumulated (residual) strain.
ε_{vol}	-	Volumetric strain (= $\dot{V}/V$).
μ	-	Poisson's ratio.
θ	-	Inclination of the effective stress path of a load cycle.
σ	-	Total stress (see subscripts).
$\bar{\sigma}$	-	Effective stress (denoted by bar).
$\bar{\sigma}_c$	-	Effective consolidation stress.
$\Delta\sigma$	-	Change in stress.

$\Delta\sigma_c$ - Change in cell pressure.

$\Delta\sigma_v$ - Vertical cyclic stress.

τ - Shear stress (see subscripts).

$\bar{\phi}$ - Angle of internal friction.

$\bar{\phi}_{cyc}$ - Angle of friction from cyclic tests.

$\bar{\phi}_{st}$ - Angle of friction from static loading after cyclic test.

FREQUENTLY USED SUBSCRIPTS

v,h - Denotes stresses or strains in vertical and horizontal direction.

pp - Denotes peak-to-peak strains.

o - Denotes initial stress state.

c - Denotes consolidation stress.

ε - Denotes strain.

u - Denotes pore pressure.

res - Denotes residual strain.

x,y - Denotes stress or strains on x and y planes or x and y direction.

CHAPTER ONE - INTRODUCTION

Adequate solutions to many problems in geotechnical engineering require the knowledge of the dynamic properties of soils. Attempts to determine dynamic properties of soils stem from questions, such as: "How will the foundation at a particular building respond to a strong motion earthquake", or "What will be the behavior of a particular offshore structure that is subjected to cyclic wave loadings". Other examples in geotechnical engineering which involve dynamic behavior of cohesionless soils are: (1) dynamic response of machine foundations, (2) pavement design, and (3) vibratory densification.

Prediction of foundation response to seismic loading involves two main catagories of soil behavior. First is the determination of stiffness and damping properties of the soil as a function of cycling, to permit prediction of wave propagation and dynamic response of a soil mass. The second area is the prediction of large deformations and strength reduction resulting from pore water pressure buildup in undrained loading conditions. Field loading frequencies are relatively high, and inertial effects are important.

Wave loadings on off-shore structures cause cyclic stresses to be imparted on the foundation soils. Of concern in this situation are the possibilities of (1) large deformations and strength reduction due to pore pressure buildup, and (2) deformations caused by volume change from cycling. Stiffness

properties are required for deformation prediction, and strength properties are required for stability prediction. In addition to cyclic stresses imparted by the foundation, there are static pore pressure fluctuations caused by the waves.

Machine foundation response involves very low amplitude stresses and strains. Volume change and pore pressure buildup are generally negligible. Pavement design involves stiffness changes and cumulative deformation of granular layers beneath pavements subjected to repeated traffic loading. Inertial and strain-rate-effects are usually neglected. Vibratory densification involves volume change due to repetitive loading and vibration at relatively high frequencies. Drained conditions usually prevail and inertial effects are usually present.

The major soil properties and characteristics which are used in soil dynamics and earthquake engineering are (Woods, 1978):

1. Dynamic moduli,
2. Poisson's ratio,
3. Damping and attenuation,
4. Liquefaction parameters - cyclic shearing stress ratio, cyclic deformation, and pore pressure response,
5. Shearing strength in terms of strain-rate-effects.

Some of these properties are best measured in the field (in-situ) and some in the laboratory. Many analytical techniques currently used to evaluate some of the soil dynamic problems mentioned above require the use of low strain amplitude soil

moduli as determined in-situ. On the other hand, it is often important to understand something about the behavior of soil under loading conditions not initially prevalent in-situ, thus requiring laboratory investigations. Consequently, both in-situ and laboratory studies are necessary for adequate solution to many dynamic soil problems.

Laboratory investigations of dynamic soil properties are often conducted by means of the following type of tests: cyclic triaxial tests (Castro, 1969; Ishihara and Yasuda, 1972; Lee and Albaisa, 1974: Lee and Fitton, 1969; Lee and Focht, 1975; Finn, Pickering and Bransby, 1971; Peacock and Seed, 1968), cyclic torsional shear tests (Drnevich, 1972; Ishihara and Kawaguchi, 1970; Ishihara and Li, 1972; and Yoshimi and Oh-Oka, 1970, 1973), shaking table tests (De Alba, et al, 1975; Emery, Finn and Lee, 1972; Finn, Emery and Gupta, 1970; Mori, 1976; Pyke, Chan and Seed, 1974; Tanimoto, 1967; Whitman, 1970; and Yoshimi, 1967), and resonant column tests (Drnevich, 1967, 1972; Hardin, 1965, 1970; Hardin and Music, 1965).

Current research being conducted by M.I.T. and Cambridge University deals with the centrifugal modelling of reconstituted soil at the Cambridge University centrifuge facility. Although the principles behind centrifuge testing have been around for many years, it has been only recently that tremendous advances in the technology for running such tests have been made (Schofield, 1981). Bucky (1931) recognized that in order "to produce, at corresponding points in a small scale

model, the same unit stresses that exist in the full scale structure, the weight of the material of the model must be increased in the same ratio that the scale of the model is decreased with respect to the full scale structure. The effect of an increase in weight may be obtained by the use of a centrifugal force, the model being placed in a suitable revolving apparatus". Such tests have been run by P. Lambe (1981) and P. Lambe and Whitman (1980) on Leighton-Buzzard 120/200 Sand for the purpose of studying the behavior of a column of sand under a dynamic loading condition. Saturated sand samples described by P. Lambe (1981) were prepared by a technique termed "wet rodding" (see Chapter Three). It was the purpose of this test program to conduct drained and undrained cyclic triaxial tests on Leighton-Buzzard 120/200 Sand prepared by this method of sample formation. Results of the tests would:

1. provide data for use in predicting response of soil in centrifuge tests, and
2. tell something about the effect of sample preparation method on the drained and undrained behavior of the test sand.

Several tests on samples prepared by the moist tamped method - a generally accepted method of preparation used in cyclic triaxial testing of cohesionless soils - were performed for comparison with the test results of wet rodded samples.

Chapter Two describes the drained and undrained cyclic triaxial testing of sand. This chapter discusses the differences in stress condition between a sample subjected to a

cyclic triaxial-type loading, and those stress conditions peculiar to elements of soil in earthquake and offshore structure loading environments. Chapter Two also gives a detailed description of Leighton-Buzzard 120/200 Sand.

Chapter Three discusses the method of wet rodding in detail. In particular, it addresses the issue of applying the method, as used for large-diameter centrifuge samples, to triaxial tests.

Chapter Four discusses the results of seven drained cyclic tests. Presented is a relationship to be used for the prediction of volumetric strain in cyclic triaxial tests. The relationship expresses volumetric strain in terms of peak-to-peak shear strain and cycle number. The influence of sample formation technique and cyclic shear stress ratio on the drained behavior is discussed.

Chapter Five gives the results of eight undrained cyclic tests and compares them with published results. As can be expected, the method of preparation is found to have a significant effect on the liquefaction strength of Leighton-Buzzard 120/200 Sand. This difference in strength is attributed to the differences in the soil structure of the two types of samples (wet rodded and moist tamped). An explanation for the difference in behavior is hypothesized, based on Mulilis, et al (1975).

Chapter Six summarizes the findings of this investigation, concluding that,

1. the method of sample preparation significantly affects the drained cyclic behavior of Leighton-Buzzard 120/200 Sand, as well as the undrained behavior,
2. the prediction of volumetric strains using the analysis by Hadge (1979) works for Leighton-Buzzard 120/200 Sand, and
3. more tests and a detailed fabric study are necessary in order to fully understand why the wet rodded samples displayed less of a tendency toward volumetric straining in drained tests, yet when tested undrained, they exhibited a lower liquefaction strength.

CHAPTER TWO - CYCLIC TRIAXIAL TESTING OF SATURATED SAND

The behavior of saturated sand under cyclic loading has been considered by many investigators in the past fifteen years. Most of the earlier studies emphasized the liquefaction potential of sand deposits due to vertically propagating shear waves from strong motion earthquakes. More recent investigations have included the densification behavior of dry and saturated sands subjected to cyclic loading. Results of the many test programs, directed at the topic of cyclic loading of soils, indicate that the liquefaction behavior of saturated sand is influenced primarily by the following factors:

1. soil type and gradation,
2. initial effective confining stress,
3. intensity of shaking or the cyclic shear stress,
4. duration of shaking or number of applied stress cycles,
5. void ratio or density,
6. previous strain history,
7. lateral earth pressure coefficient or degree of overconsolidation,
8. soil structure or fabric.

The drained cyclic behavior of sand, whether tested dry or saturated, is believed to be influenced mostly by these factors:

1. degree of shear strain,
2. density of material,
3. confining pressure.

Perhaps the most important factor determining the behavior of sand subjected to some loading is the drainage condition. When a soil element is subjected to cyclic loading, plastic and elastic deformations occur. If the time required for full drainage is short, compared to the time during which the load is applied, full drainage will occur and densification of the soil will prevail. If, however, the time required for drainage is long, the element will behave in an undrained fashion, in which there is no volume change, and there will be a change in pore water pressure. It has been shown (Hadge, 1979; Silver and Seed, 1971) that a cycle of loading creates a certain potential for volume change, which is reflected in the magnitude of the pore water pressure change.

The completely drained and completely undrained conditions are ideal and are most easily simulated in the laboratory. Field conditions, however, are seldom either of these two cases. It is necessary, therefore, to exhibit caution when applying the results of laboratory investigations to field situations, where actual soil behavior may be significantly different than predicted, as a result of inappropriate assumptions of drainage conditions. Little is known about the cyclic behavior of soil under partially drained conditions.

This chapter will discuss the use of the standard triaxial test, modified to induce a cyclic shear stress on the

sample, to observe the cyclic behavior of sand under drained and undrained conditions. The ability of the cyclic triaxial test to reproduce the stress conditions of two field situations is addressed. The first case is that of an earthquake loading (level ground conditions) and the second is that of an offshore structure imparting cyclic stresses on the foundation soils.

Also discussed in this chapter are the two types of tests performed in this investigation. Fundamental information, such as the applied stress conditions and typical test results, is presented for each type of test. Finally, the test sand used in this investigation is described.

2.1 In-Situ Stress Conditions for Soil Elements in Cyclic Loading Environments

Figure II-1a depicts a soil element located some distance beneath the ground surface. The "at-rest" stresses acting on that element are given in Figure II-1b. In this condition the major and minor principal stresses are acting vertically and horizontally, respectively. The magnitude of the effective horizontal stress is some fraction of the effective vertical stress, which is reflected in the value of K_o, the coefficient of lateral stress at rest. The value of K_o is extremely difficult to measure reliably in the field. A normally consolidated sand deposit sedimented over a large lateral area will generally undergo less compression in the horizontal direction than in the vertical direction, and will typically have a

value of K_o between 0.4 and 0.5 (Lambe and Whitman, 1969). For normally consolidated sands K_o is commonly assumed equal to $1-\sin\bar{\phi}$ (Jaky 1944, $\bar{\phi}$ = effective angle of friction). Larger values of K_o result from overconsolidation, where some amount of horizontal stress is "locked-in" to the soil structure as overburden is removed. In an extreme case K_o could be as high as 2 or 3. It is expected that K_o for marine sediments may range between 0.4 and more than 2.0 (Hedberg, 1977).

Figure II-1a shows Mohr circles of stress and stress points associated with values of K_o = 0.5, 1.0 and 2.0 for the element. The stress point with coordinates $p = (\sigma_v + \sigma_h)/2$ and $q = (\sigma_v - \sigma_h)/2$ is the point of maximum shear stress on the Mohr circle of total stress. In terms of effective stresses, the stress point with coordinates $\bar{p} = p - u_s$ and q is the point of maximum shear stress on the Mohr circle of effective stress, as shown on Figure II-1c. The stress point can completely describe a Mohr circle and can, therefore, be used to replace it.

A line connecting stress points for an element subjected to a particular loading sequence is called a stress path. Shown in Figure II-2 are the stress points and stress path for a simple loading sequence. Here the vertical stress on an element is increased until failure. Failure occurs when the stress path reaches the K_f-line, which is inclined at angle . The K_f-line is related to the Mohr-Coulomb failure envelope (which is inclined at angle $\bar{\alpha}$ from the origin for cohesionless soil) by $\tan\bar{\alpha} = \sin\bar{\phi}$. The stress path is particularly useful

when describing complicated loading conditions. Lambe and Whitman (1969), and Lambe and Marr (1981) describe the stress path method in great detail. This paper will make use of the stress path plotted on a p-q diagram (Figure II-2) to describe all stress conditions.

Figure II-3a idealizes the stresses induced on the same element due to the upward propagation of shear waves in the soil deposit during an earthquake. The applied stresses, though somewhat random in pattern, are considered cyclic in nature, and cause complete shear stress reversal on the faces of the element (conditions 2 and 3). Figure II-3b shows these stresses idealized on a p-q diagram for the simple case where the applied shear stresses of conditions 2 and 3 are equal in magnitude. As a result of the shear stress reversal, there is a rotation of principal stresses, through some angle, Θ, to the right and left of its initial position. Because the vertical stress does not change during shaking, and the horizontal stress is presumed also to be constant, the resulting stress path is generally taken to be vertical ($\bar{p}_o$ constant). The value of q depends on the magnitude and direction of the shear stresses induced by the earthquake. Although this model is only a simple idealization of real behavior, it tells us two important things about the stresses in level ground resulting from an earthquake:

1. The stress path follows some vertical path ($\bar{p}_o$ constant), exhibiting complete shear stress reversal; the magnitude of shear stress, q, is completely random, and depends on the ground motion.

2. During the excitation, the principal stresses rotate continuously (also in a random fashion) about the at-rest position; the degree of rotation, Θ, cannot exceed 90 degrees.

Figure II-4a depicts two soil elements A and B located beneath an offshore gravity structure. The effective static foundation stresses acting on the elements are given in Figure II-4b. These effective stresses are broken into two components: the initial effective geostatic stresses (denoted by subscript "o"), and those effective stresses induced by the placement of the structure. Depending on the location of the elements beneath the structure, shear stresses may or may not exist on horizontal planes following placement of the structure. Element A, located directly beneath the centerline of the structure, has no shear stresses acting on horizontal planes, while element B does. In other terms, the major and minor principal stresses of element B do not act in vertical and horizontal directions, respectively, as they do in element A. The importance of initial shear stresses existing prior to any applied shear stresses is discussed in detail in the following sections. The initial stress condition of element B is similar to that of an element within a slope or embankment. Figure II-4c shows the stress points and stress paths associated with the loading of the elements from the initial geostatic stress condition to that condition depicted in Figure II-4b, where the foundation load is applied to the elements. Typical values of K_o equal to 0.5, 1.0 and 2.0 are used.

Figure II-5a shows elements A and B under the cyclic loading conditions which result from the structure's response to storm waves. The stress conditions for these elements are shown in Figure II-5b, and the resulting stress paths in Figure II-5c. The storm conditions impart a cyclic component of both effective normal stress and shear stress on the element. Vertical and horizontal cyclic normal stresses will be small on element A and large on element B. The dashed portion of the stress path of Figure II-4c represents the cyclic loading of the elements. Although the cyclic loading will actually vary in terms of magnitude and duration, it is represented here as a uniform cycle of loading of constant magnitude.

2.2 Application of Cyclic Triaxial Testing to Investigate Cyclic Loading Problems

Application of the standard triaxial test to determine properties associated with the cyclic loading of soils was fist developed by Seed and Lee (1966). It was recognized that, although the cyclic triaxial test could not provide the quality of information that simple shear tests could about response of soils to earthquake loadings, it provided a practical and convenient alternative (Seed, 1979). The cyclic triaxial test has since been used in numerous investigators, (see references, Chapter One).

The direct application of the cyclic triaxial test to earthquake loading problems, such as that idealized in Figure

II-3, is limited because the field conditions differ from those developed in cyclic triaxial tests (Peacock and Seed, 1968). The important differences are listed below:

1. In the triaxial test, the major principal stress can act only in a vertical or horizontal direction; no reorientation, other than full orientation through 90° is possible. As mentioned in the previous section, in the ground there is a continuous cyclic rotation of the principal stress direction through some angle, θ, to the right and left of its initial position.
2. In the field the soil element is initially consolidated under K_o-conditions. In cyclic triaxial tests, the sample must be initially consolidated isotropically in order to produce a symmetrically reversing shear stress (representative of level ground conditions).
3. In the field, deformations are presumed to occur under plane-strain conditions, whereas deformations occur in all three principal stress directions in the triaxial test.
4. In the field the cyclic stress conditions are reasonably symmetric; in a typical cyclic triaxial test, the intermediate principal stress is equal to the minor principal stress during axial compression, but equal to the major principal stress during lateral compression.

Application of the cyclic triaxial test to earthquake problems requires the use of a correction factor to allow for these limitations (Finn, et al, 1971; Seed and Peacock, 1971; and Castro, 1975).

The cyclic triaxial test is particularly useful, however, in reproducing stress conditions beneath structures such as that shown in Figures II-4 and II-5. In such a case, the stress paths which represent expected in-site loading conditions can be closely reproduced in the laboratory with a cyclic triaxial apparatus. The only major limitation is, of course, that the cyclic stress path can only be inclined 45 degrees, i.e. the apparatus can not induce cyclic shear stresses on horizontal and vertical planes. Sections 2.3 and 2.4 illustrate typical stress paths for anisotropically and isotropically consolidated, stress controlled, cyclic triaxial tests, respectively.

2.3 Anisotropically-Consolidated, Drained, Cyclic Triaxial Tests

Two types of stress-controlled tests were performed in this investigation of Leighton-Buzzard 120/200 Sand:

1. Anisotropically-Consolidated, Drained, Cyclic Triaxial Compression Tests (CAD Cyclic),
2. Isotropically-Consolidated, Undrained, Cyclic Triaxial Tests, with pore pressure measurements ($\overline{\text{CIU}}$ Cyclic).

This section describes the CAD cyclic triaxial test. Section 2.3.1 describes the stresses applied to the triaxial specimen in terms of total and effective stress paths. Appendix B discusses the laboratory testing procedure in greater detail.

There exists little information pertaining to drained cyclic triaxial tests. Hadge (1979) has completed a comprehensive study of drained cyclic triaxial behavior of sand, proposing a relationship between pore pressure buildup in undrained tests, and volumetric strain in drained tests. The majority of literature which does address the question of densification of sand, is based on results from cyclic simple shear tests (Cuellar, et al 1977; Youd, 1972; Silver and Seed, 1971). An interesting result of Youd's (1972) test program is that there appeared to be no significant difference between the behavior of dry Monterey Sand and the same sand tested in a saturated, but completely drained, condition.

2.3.1 Applied Stresses

Figure II-6 illustrates on a p-q plot the sequence of stresses that were applied to a triaxial specimen to determine the densification behavior of Leighton-Buzzard 120/200 Sand. Shown is the effective stress path (ESP), total stress path (TSP), and total stress path minus static pore pressure (TSP-u_s). The sequence of applied stresses corresponds closely to those stresses which act on element B in Figure II-5.

The stresses are applied as follows:

1. The sample is first subjected to a small confining stress, induced by the water pressure within the

triaxial cell, and an axial (vertical) stress which is induced by the vertical piston engaged at the top of the sample. At this time, the backpressure, u_b, is zero (drainage line to sample is open to atmospheric pressure), and the vertical stress on the sample, σ_v, is assumed to be equal to the confining pressure, $\sigma_c = \sigma_h$. Hence, the effective stresses in the sample are as follows:

$$\bar{\sigma}_{vo} = \sigma_v - u \qquad \text{Equation 2.1}$$

$$\bar{\sigma}_{ho} = \sigma_h - u \qquad \text{Equation 2.2}$$

Since $u = 0$ and $\sigma_v = \sigma_c = \sigma_h$, $\sigma_{vo} = \sigma_{ho}$ and sample exists in an isotropic state of stress.

2. The total horizontal and vertical stresses are increased to σ_v and σ_h while maintaining constant effective stresses within the sample equal to $\bar{\sigma}_{ho}$ and $\bar{\sigma}_{vo}$. This is done by raising the backpressure, u_b, in the sample by an amount equal to u_s. The effective stresses in the sample become:

$$\bar{\sigma}_{vo} = \sigma_v - u_s \qquad \text{Equation 2.3}$$

$$\bar{\sigma}_{ho} = \sigma_h - u_s \qquad \text{Equation 2.4}$$

This step is referred to as "backpressuring".

3. The triaxial sample is anisotropically-consolidated to stress levels σ_{vc} ($\bar{\sigma}_{vc}$) and σ_{hc} ($\bar{\sigma}_{hc}$) at constant backpressure, u_b. The initial mean effective normal stress, $\bar{p}_o$, is given by:

$$\bar{p}_o = \frac{\bar{\sigma}_{vc} + \bar{\sigma}_{hc}}{2} = \frac{(1 + K_c)\ \bar{\sigma}_{vc}}{2} \qquad \text{Equation 2.5}$$

and the mean total normal stress, p_o, is given by

$$p = \bar{p}_o + u_b \qquad \text{Equation 2.6}$$

The mean shear stress is:

$$q_m = \frac{\sigma_{vc} - \sigma_{hc}}{2} = \frac{\bar{\sigma}_{vc} - \bar{\sigma}_{hc}}{2} = \frac{(1-K_c)\ \bar{\sigma}_{vc}}{2} \qquad \text{Equation 2.7}$$

Thus, by setting the value of K_c equal to K_o, the state of stress is analogous to that shown in Figure II-1, for a particular value of K_o.

4. The cyclic component of shear stress, Δq_{cy}, is applied to the sample. This is accomplished by cycling the vertical stress on the sample by $\pm\ \Delta\sigma_v$, which causes a change of shear stress, $\pm\ \Delta q_{cy}$, of $\pm\ \Delta\sigma_v/2$.

Because the sample is drained, there is no change in pore water pressure, $\Delta u=o$, and the effective stress path is the same as the total stress path minus static pore pressure.

2.3.2 <u>Typical Test Results</u>

Figure II-7 shows the effective stress path for an anisotropically-consolidated, drained, cyclic triaxial test on Oosterschelde Fine Sand (see grain size characteristics, Section 2.5) as reported by Hadge (1979). Given in Figure II-8 are the results of the test, showing how the effective

stresses, $\bar{p}$ and q, and vertical and volumetric strains change with the number of cycles of applied shear stress.

Figure II-8 shows that there is a maximum and a minimum value of vertical strain within each cycle. This is referred to as the cyclic vertical strain. With the completion of each cycle, there is a resulting accumulated vertical strain level called the residual vertical strain. After a large number of cycles, there is very little effect of subsequent cycling on the residual strains. The sample, at this point, has developed a higher resistance to further straining under the same stress condition.

The volumetric strain, $\varepsilon_{vol} = \Delta V/V$, exhibits behavior similar to that of the vertical strain. There is a cyclic volumetric strain within each cycle, and a residual volumetric strain which accumulates at a gradually decreasing rate.

2.3.3 Shear Strains in the Cyclic Triaxial Test

It has been recognized that a change in shear stress is the primary cause of volume change in a sand specimen tested either in a simple shear test or a triaxial test. Although a change of octahedral stress may induce volume change, the change is quite small, especially for dense sands (Ko and Scott, 1967; El-Sohby and Andrawes, 1972). Silver and Seed (1971) and Youd (1972) concluded from simple shear tests on sand, that the cyclic shear strain may well be a fundamental parameter determining the volume change behavior of cohesionless soil under dynamic loading conditions.

Although shear strains cannot be directly measured in the triaxial test, they can be calculated from direct measurements of volumetric strain and vertical strain. From Mohr's circle of strain, illustrated in Figure II-9, it is shown that:

$$\gamma = \varepsilon_1 - \varepsilon_3 \qquad \text{Equation 2.8}$$

where γ is the maximum shear strain within the sample, ε_1 is the major principal strain, and ε_3 is the minor principal strain. The major principal strain in a triaxial test corresponds to the vertical strain measured during the test. The minor principal strain corresponds to the maximum lateral strain of the sample, which is not measured. The major and minor principal strains are, by definition, related to the volumetric strain, ε_{vol}, by

$$\varepsilon_{vol} = \varepsilon_1 + \varepsilon_2 + \varepsilon_3 \qquad \text{Equation 2.9}$$

It is assumed from this equation, that the strains are uniform with the sample, which is generally not the case with a triaxial test. Axial symmetry in a triaxial test allows the equating of the intermediate principal strain, ε_2, to the minor principal strain, ε_3. Equation 2.9 now becomes:

$$\varepsilon_{vol} = \varepsilon_1 + 2\varepsilon_3 \qquad \text{Equation 2.10}$$

Equation 2.10 is rearranged to arrive at a term for the minor principal strain, ε_3, as follows:

$$\varepsilon_3 = \frac{\varepsilon_{vol} - \varepsilon_1}{2} \qquad \text{Equation 2.11}$$

Substituting this equation into equation 2.8, an expression for shear strain is derived as follows:

$$\gamma = \varepsilon_1 - \frac{\varepsilon_{vol} - \varepsilon_1}{2} = \frac{3}{2}\varepsilon_1 - \frac{1}{2}\varepsilon_{vol} \qquad \text{Equation 2.12}$$

Thus, if it is assumed that Equation 2.9 applies to a triaxial specimen, Equation 2.12 allows the calculation of the cyclic shear strain.

As discussed in Section 2.3.2, the volumetric and vertical strains in a cyclic triaxial test exhibit minimum and maximum values within any particular cycle. These values correspond to the maximum and minimum applied stresses on the sample. For stress controlled tests, such as those described for this investigation, the applied cyclic stresses are quite constant. This constancy is shown in Figure II.8 where q_{max} and q_{min}, and $\bar{p}_{max}$ and $\bar{p}_{min}$ are plotted versus cycle number. As a result of the cycling nature the volumetric and vertical strains, the shear strain within the sample also reaches a maximum and a minimum value during any particular cycle. The difference between the maximum shear strain, γ_{max}, and the minimum shear strain, γ_{min}, within a cycle is referred to as the peak-to-peak shear strain, γ_{pp}:

$$\gamma_{pp} = \gamma_{max} - \gamma_{min} \qquad \text{Equation 2.13}$$

Hadge (1979) found that although the maximum and minimum shear strains increased with each cycle, the peak-to-peak shear strains remained relatively constant for all cycles.

2.3.4 Determination of Modulus from Triaxial Tests

In addition to the liquefaction characteristics of soils, Young's modulus, E, and damping ratio, D, can be determined from strain-controlled cyclic triaxial tests (Figure II-10). In these tests a servo-system applies uniform cycles of controlled deformation. Young's modulus is determined from the ratio of applied axial stress to axial strain ($E = \Delta\sigma_v / \Delta\varepsilon_v$). Shear modulus, G, can then be computed from

$$G = E/2\ (\mu + 1) \qquad \text{Equation 2.14}$$

where μ is Poisson's ratio. Silver and Park (1975) performed strain-controlled cyclic triaxial tests on dry sand to investigate the dynamic stress-strain properties of crystal silica No. 20 sand.

2.4 Isotropically-Consolidated, Undrained, Cyclic Triaxial Tests

This section describes the $\overline{CIU}$ cyclic triaxial test as typically run to determine the liquefaction characteristics of sands. The stress condition imposed on the sample is discussed briefly in Section 2.4.1. Because most critical conditions

are likely to be those associated with zero shear stress on horizontal and vertical planes prior to cyclic stress application (Seed and Lee, 1969) - a condition analogous in earthquake problems to soil response under essentially level ground - most undrained cyclic tests are performed on isotropically-consolidated (K_c=1) samples. Although the behavior of sand in undrained cyclic tests on anisotropically-consolidated samples is well documented (Hedberg, 1977; Castro, 1975), peak pore pressure ratios of 100% (see definitions Chapter Five) followed by total strength loss (complete liquefaction) is unlikely, and investigators were somewhat less interested in it. Recently, however, these anisotropic stress conditions have gained more attention, as a result of work with offshore structures.

The undrained cyclic tests performed in this investigation were isotropically-consolidated and tested through the initial liquefaction stage - a condition in which the pore water pressure equals the initial effective confining pressure at zero shear stress. Following initial liquefaction, important problems develop within the sample (Chapter Five). Therefore, the use of the number of cycles required to reach initial liquefaction, N_L, allows comparison of this test data to results of similar tests on other sands, without the interference of these problems. Section 2.4.2 presents typical test results for cyclic isotropic tests.

2.4.1 Applied Stresses

Figure II-11 illustrates on a p-q plot the sequence of stresses applied to a triaxial specimen to observe the un-

drained behavior of Leighton-Buzzard 120/200 Sand. This sequence of applied stresses resembles those acting on element A in Figure II-4 and II-5, for the case where $K_o = 1$. The stresses are applied in the manner as for the anisotropically-consolidated sample described in Section 2.3.1, with the exception of Step 3. Here, the sample is isotropically-consolidated (K_c=1) to stress levels σ_{vc} and σ_{hc} ($\bar{\sigma}_{vc}$ and $\bar{\sigma}_{hc}$), at constant backpressure u_b, such that $\sigma_{vc} = \sigma_{hc}$. The initial mean effective normal stress, $\bar{p}_o$, is given by

$$\bar{p}_o = \frac{\bar{\sigma}_{vc} + \bar{\sigma}_{hc}}{2} = \bar{\sigma}_{vc} = \bar{\sigma}_{hc}$$

The mean shear stress,

$$q_m = \frac{\bar{\sigma}_{vc} - \bar{\sigma}_{hc}}{2} = 0$$

The cyclic component of shear stress, Δq_{cy}, is applied to the specimen as described in Step 4.

2.4.2 <u>Typical Test Results</u>

Figure II-12 shows the effective stress paths, total stress path, and total stress path minus static pore pressure for a typical isotropically-consolidated, undrained, cyclic triaxial test performed on Oosterschelde Fine Sand as reported by T. William Lambe and Associates (1977). Figure II-13 gives the development of vertical strain and pore pressure with each cycle of applied shear stress. Within each cycle the pore pressure attains a maximum and minimum value, corresponding to the maximum and minimum stresses applied to the sample. The difference between the maximum and minimum values is referred

to as the cyclic pore pressure. At the completion of each cycle (mean load on the specimen), there exists an accumulated pore pressure. This pore pressure is referred to as the residual pore pressure, and gradually increases with each cycle. As a result of the accumulated pore pressures, the effective stresses decrease with each cycle, causing a leftward movement of the effective stress path relative to the total stress path minus static pore pressure. This leftward movement is shown in Figure II-12, as the effective stresses are plotted for several different cycles during the test. The movement of the effective stress path, however, is restricted by the K_f-line, as shown for cycle 21.

Vertical strain within the sample also cycles between a maximum and minimum value for any particular cycle (Figure II-13). Thus the cyclic vertical strain is similarly defined for undrained tests as for drained tests, even though no volume change occurs. The residual vertical strains accumulate slowly until the pore water pressures reach a value close to the confining stress. At this time, the strains become suddenly large. Residual peak-to-peak vertical strains of 10% or more are common for samples which experience peak cyclic pore pressure ratios of 100% (initial liquefaction). The test results shown in Figure II-12 and II-13 indicate that the sample of Oosterschelde Fine Sand reached initial liquefaction in 19 cycles.

The results of liquefaction tests are often presented in the form shown in Figure II-14 (Mulilis, et al, 1975). In

this figure the cyclic stress ratio, $\Delta q_{cy}/\bar{p}_o$, is plotted versus the logarithm of the number of cycles required to obtain initial liquefaction, and peak-to-peak (double amplitude) vertical strains of 2.5, 5 and 10 percent. In this particular case the sample was prepared by moist tamping in layers. From the figure it is evident that the number of cycles to cause initial liquefaction, or significant vertical strains, at cyclic stress ratios less than $\pm$ 0.25, becomes quite large. It is of interest to note that, compared to cyclic simple shear tests, cyclic triaxial tests indicate a higher resistance to liquefaction (Seed, 1979). The stress ratio for simple shear tests is defined as $\pm \Delta\tau_{xy}/\bar{\sigma}_{yo}$, where $\Delta\tau_{xy}$ is the alternating shear stress in the X, Y plane, and $\bar{\sigma}_{yo}$ is the initial effective vertical confining pressure. Finn, et al (1971) concluded that if the differences in the stress conditions of both tests is taken into account, equal resistances to liquefaction are obtained within the slight scatter of experimental data.

Pore pressures generated during soil liquefaction are a fundamental concern. Seed, et al (1976) present an analytical procedure for evaluating general characteristics of pore water pressure buildup and subsequent dissipation in sand deposits both during and following a period of earthquake shaking. By observing the rate of pore pressure buildup in cyclic loading tests, it has been found that the rate of buildup generally lies within a fairly narrow band when plotted on a graph of pore pressure ratio, $\Delta u/\bar{p}_o$ (= $\Delta u/\bar{\sigma}_{3c}$ for cyclic simple shear

tests), and cycle number normalized to the number of cycles to initial liquefaction, N/N_L. Figure II-15 shows pore pressure buildup data presented in this form for Monterey Sand and Sacramento River Sand as reported by Lee and Albaisa (1974). The data was generated from cyclic triaxial tests. Knowing N and N_L for a particular soil, one can enter figures such as those presented in Figure II-15, and estimate the maximum pore pressure which will be generated by the design earthquake. This topic is covered further in Chapter Five.

2.5 Leighton-Buzzard 120/200 Sand

All tests described herein were performed on Leighton-Buzzard 120/200 Sand, a uniform fine sand with grains of diameter 0.07mm to 0.13mm. Figure II-16 shows the grain size distribution for Leighton-Buzzard 120/200 Sand, along with the grain size curves for Monterey No. 0, Sacramento River, and Oosterschelde Fine Sands. The mean grain size, D_{50}, is approximately 0.12mm for Leighton-Buzzard Sand. The coefficient of uniformity ($U=D_{60}/D_{10}$) is 1.33, indicating a uniform sand. The test sand has approximately 1.4% fines content (percent by weight passing the No. 200 sieve). The specific gravity was determined to be 2.65 by the method described by Lambe (1951). Morris (1979) determined the maximum void ratio, e_{max} to be 1.025 and the minimum void ratio, e_{min}, to be 0.65.

Scanning electron microscope (SEM) pictures (photomicrographs) were taken of the sand, as shown in Figures II-17 through II-20. Each figure shows a) unsheared sand grains, b) sheared sand grains, and c) unsheared "recycled" sand. Shear-

ing consisted of applying 10,000 cycles to a triaxial specimen in a drained test at a cyclic stress ratio $\Delta q_{cy}/\bar{p}_o = 0.333$. The recycled sand was washed and oven-dried several times for the purpose of conserving sand during the development of the rodding method (Bucknam, 1981). The SEM and XRD analysis was performed on the recycled sand to determine if the washing technique used would remove all the glycerin from the sand.

Figures II-17 through II-20 show the sand magnified 50, 200, 500 and 1000 times, respectively. From these figures it can be seen that the sand has a subrounded shape. A striking feature of this sand is the large amount of secondary quartz present. Clues to the presence of secondary quartz are the very rough surface on some grains, and the very odd grain shapes (upper edge of Figure II-18a). Figure II-20 shows very marked evidence of the extreme amount of secondary quartz in Leighton-Buzzard 120/200 Sand. Optical properties in polarized light also confirm an abundance of secondary quartz. X-ray diffraction indicates secondary quartz because although quartz was the only detected crystalline phase, the peak amplitudes were about three-fourths what would be expected from quartz. Chemistry determined during SEM examination showed only silicon.

It could not be determined conclusively whether or not mineral grains were completely fractured as a result of shearing. The real cracks, such as those shown in Figures II-19a and II-19b, appeared to occur in the secondary quartz.

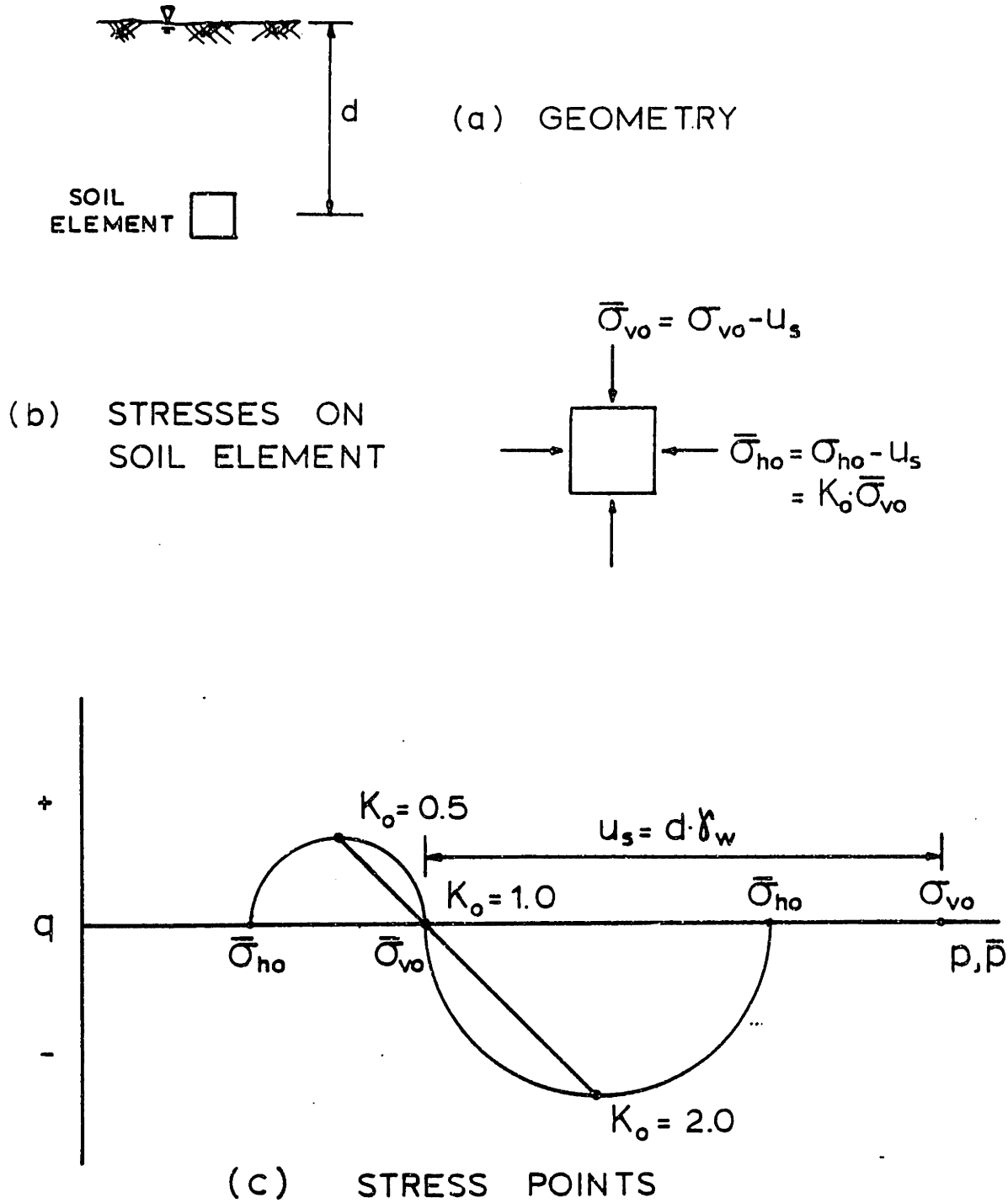

IN SITU STRESS CONDITION

FIGURE II-1

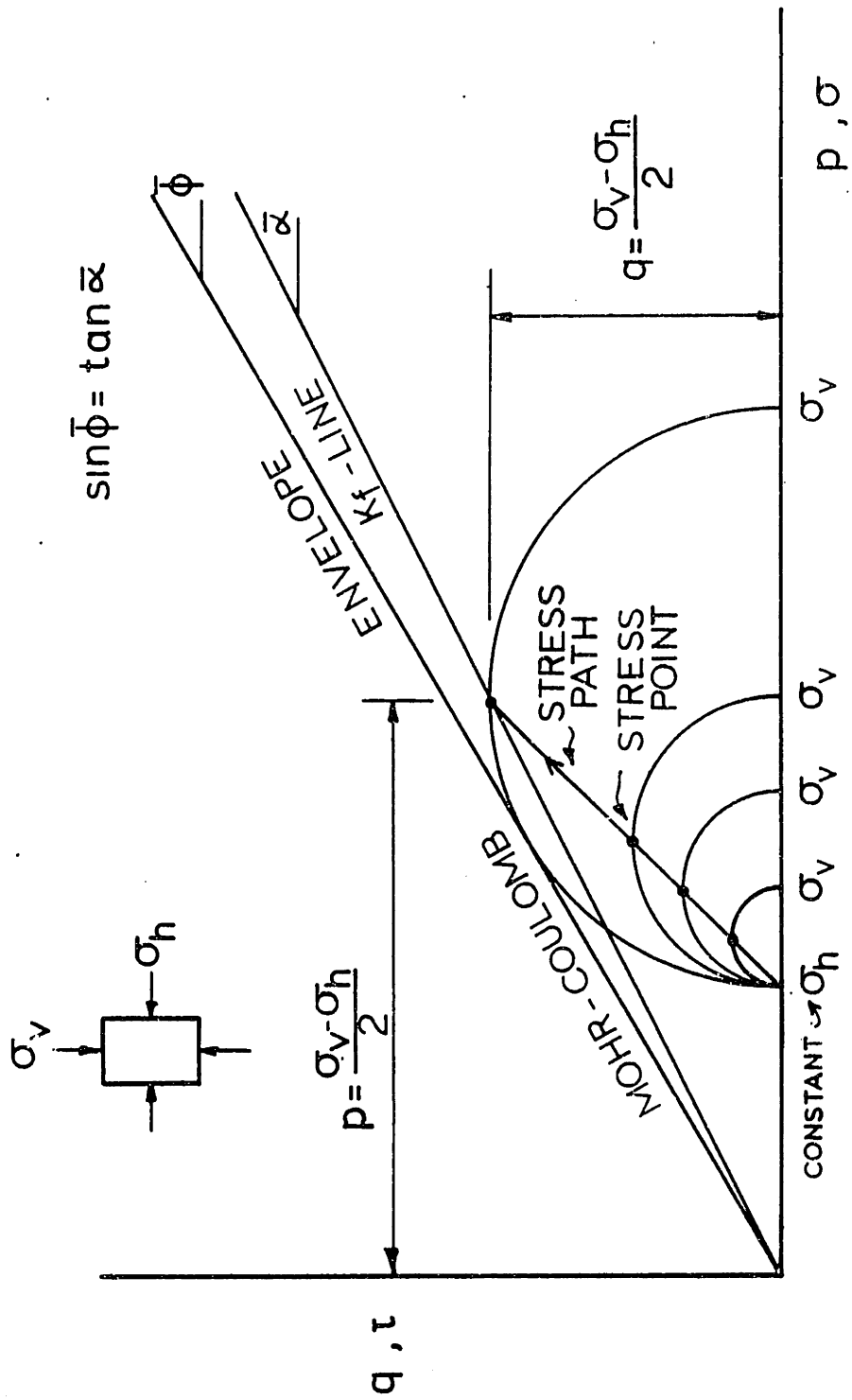

STRESS POINTS AND STRESS PATH

FIGURE II-2

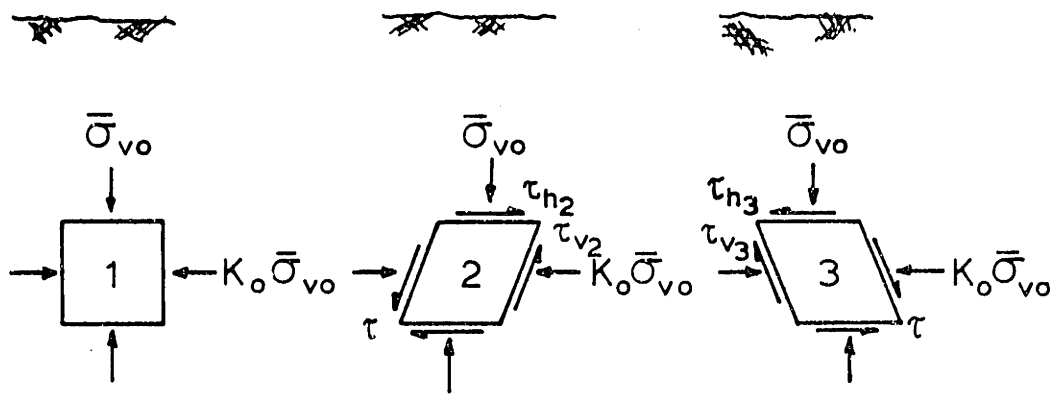

(a)

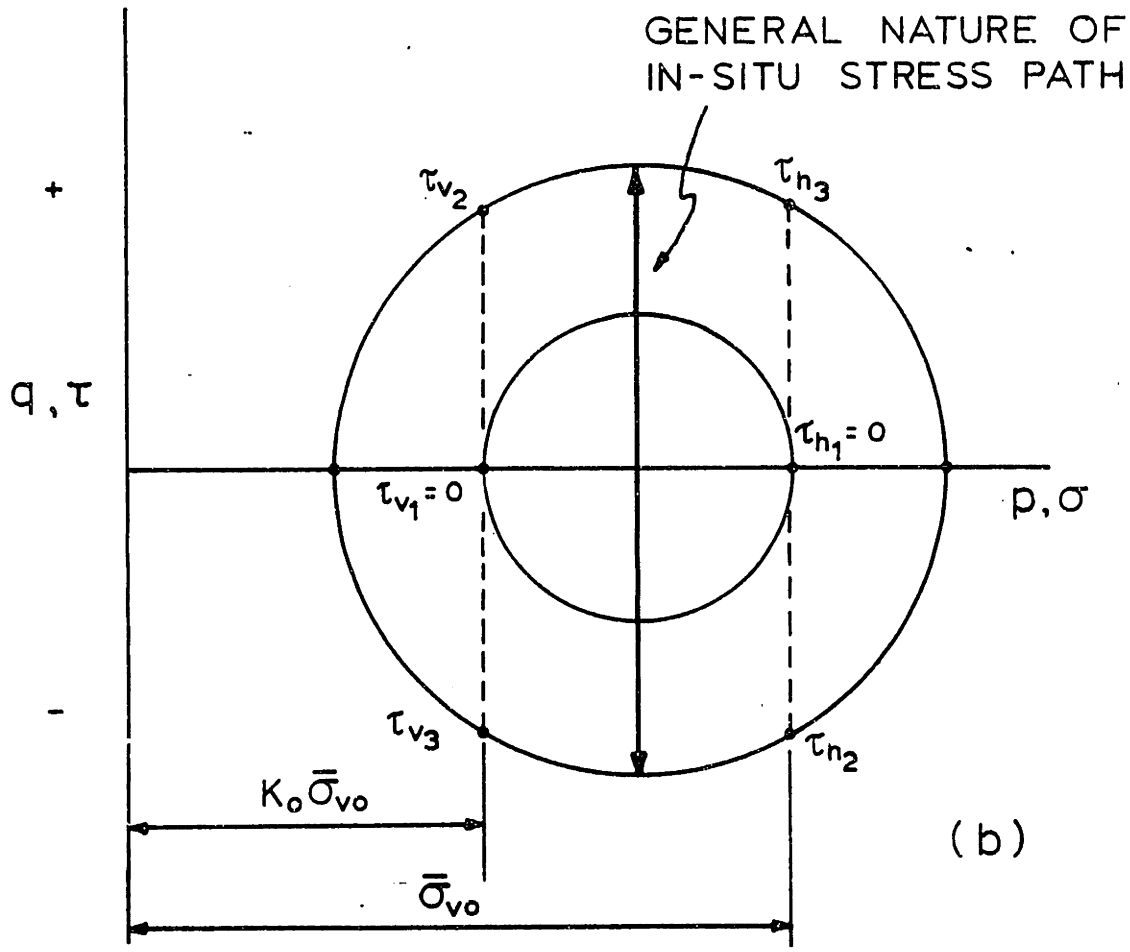

(b)

CYCLIC STRESS CONDITION FOR SOIL ELEMENT UNDER EARTHQUAKE LOADING

FIGURE II-3

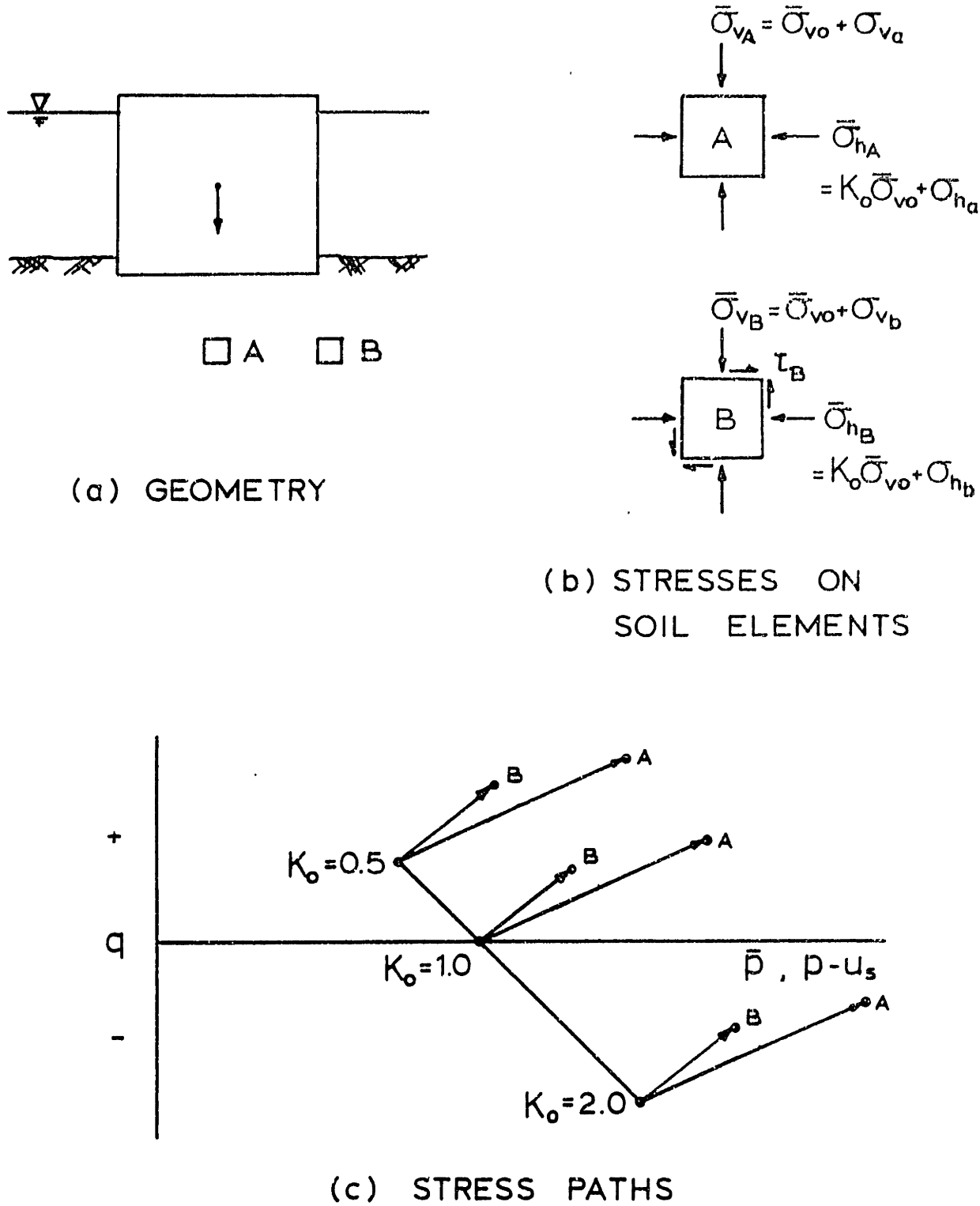

STATIC STRESS CONDITION FOR SOIL ELEMENTS BENEATH OCEAN STRUCTURE

FIGURE II-4

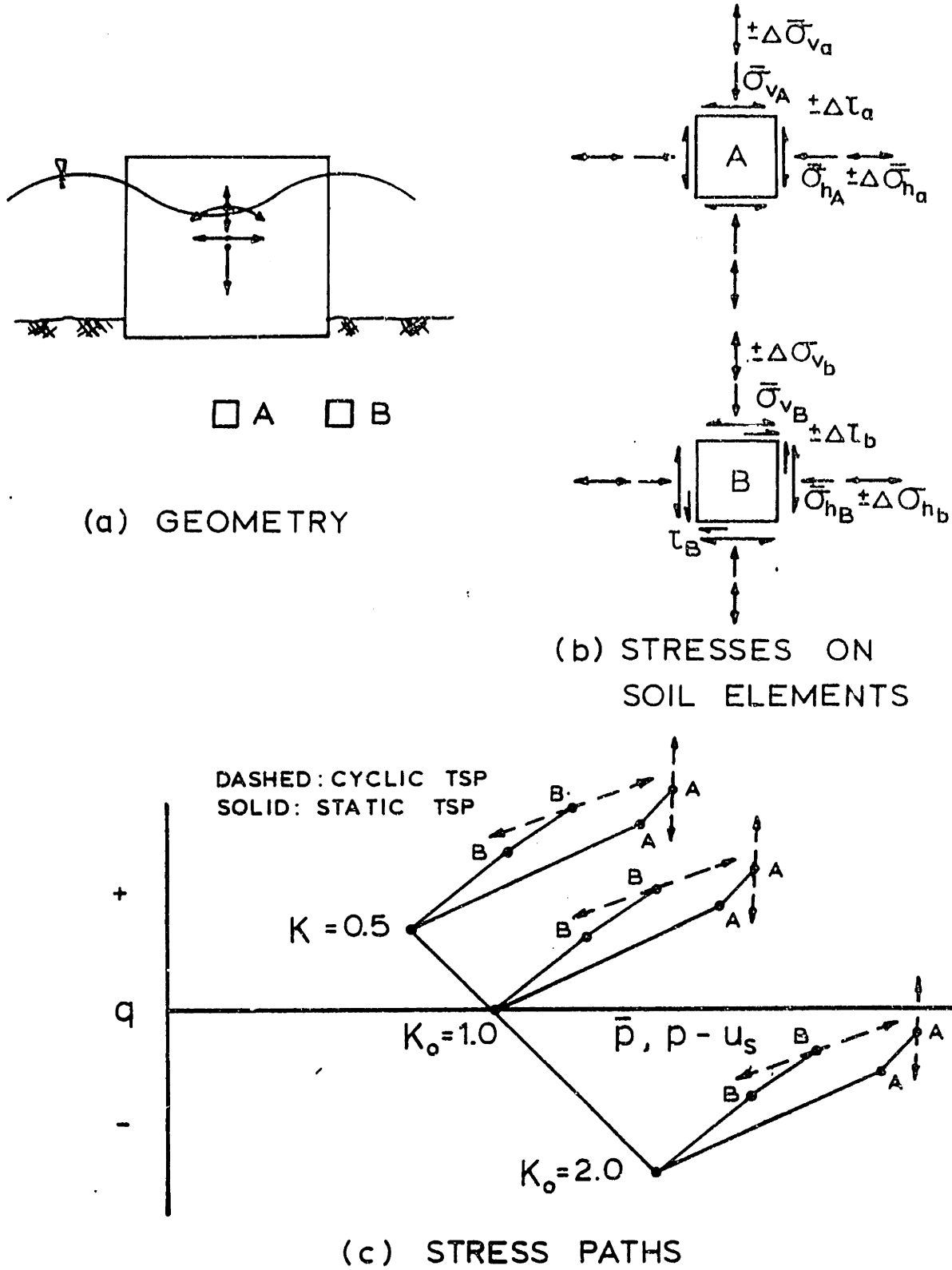

CYCLIC STRESS CONDITION FOR SOIL ELEMENTS BENEATH OCEAN STRUCTURE

FIGURE II-5

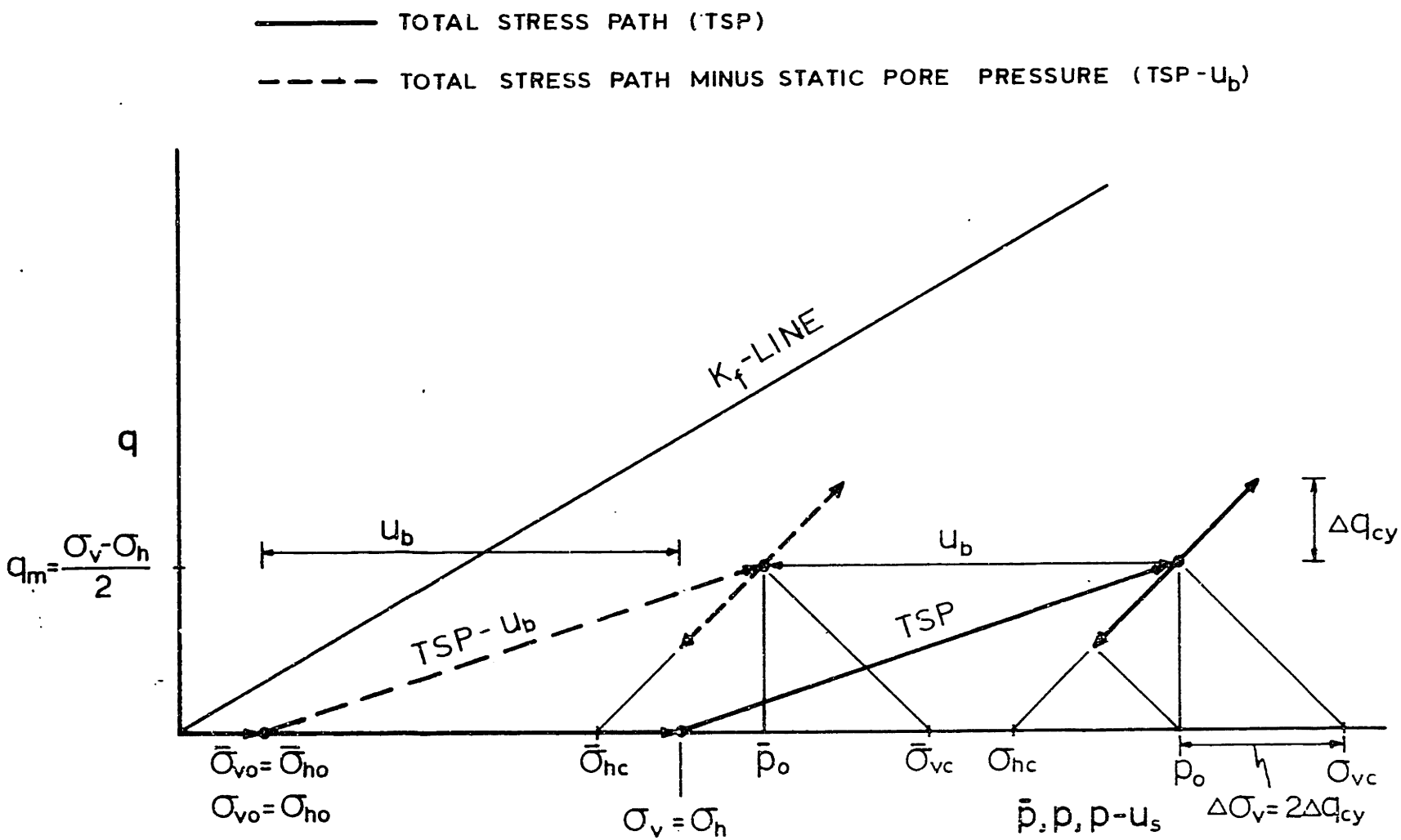

APPLIED STRESSES IN CAD CYCLIC TRIAXIAL TEST

FIGURE II-6

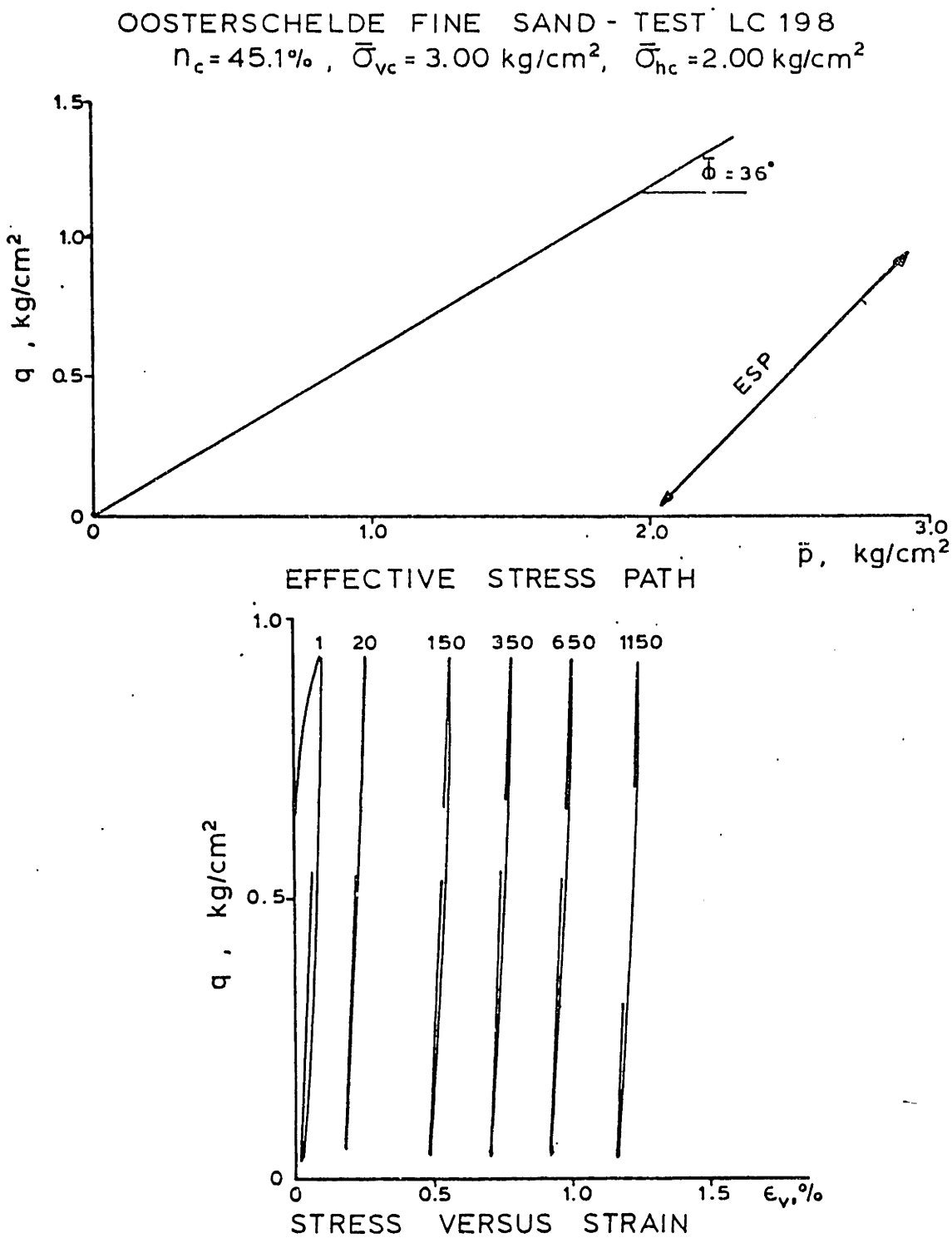

EFFECTIVE STRESS PATH AND STRESS-STRAIN PLOTS FOR CAD CYCLIC TEST ON OOSTERSCHELDE FINE SAND (AFTER HADGE, 1979)

FIGURE II-7

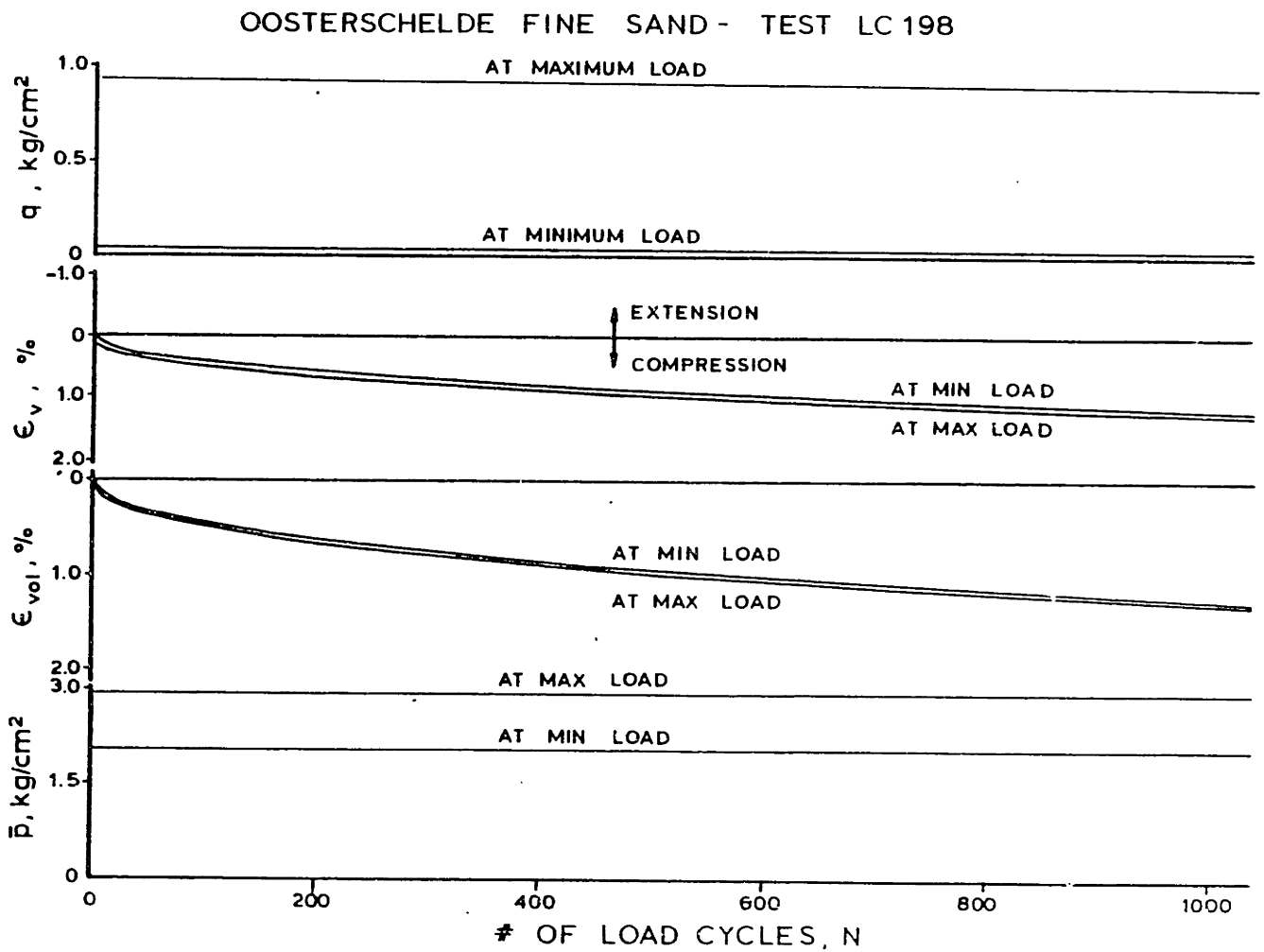

SUMMARY OF STRESS AND STRAIN DEVELOPMENT FOR CAD CYCLIC TEST ON OOSTERSCHELDE FINE SAND

(AFTER HADGE, 1979)

FIGURE II-8

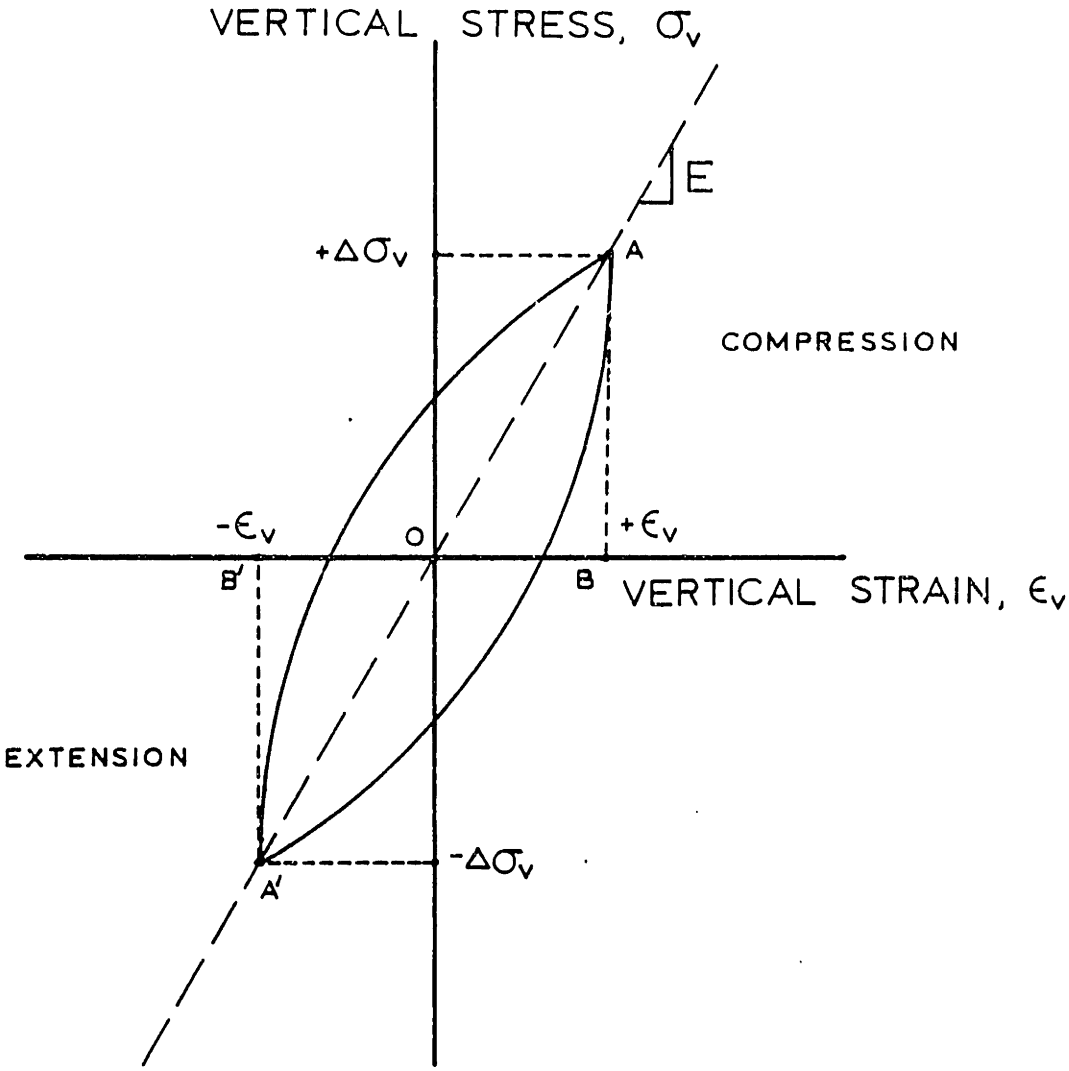

$$D = \frac{1}{2\pi} \frac{\text{AREA OF HYSTERESIS LOOP}}{\text{AREA OF TRIANGLE AOB \& A'OB'}}$$

EQUIVALENT HYSTERETIC STRESS-STRAIN PROPERTIES FROM CYCLIC TRIAXIAL TEST

FIGURE II-9

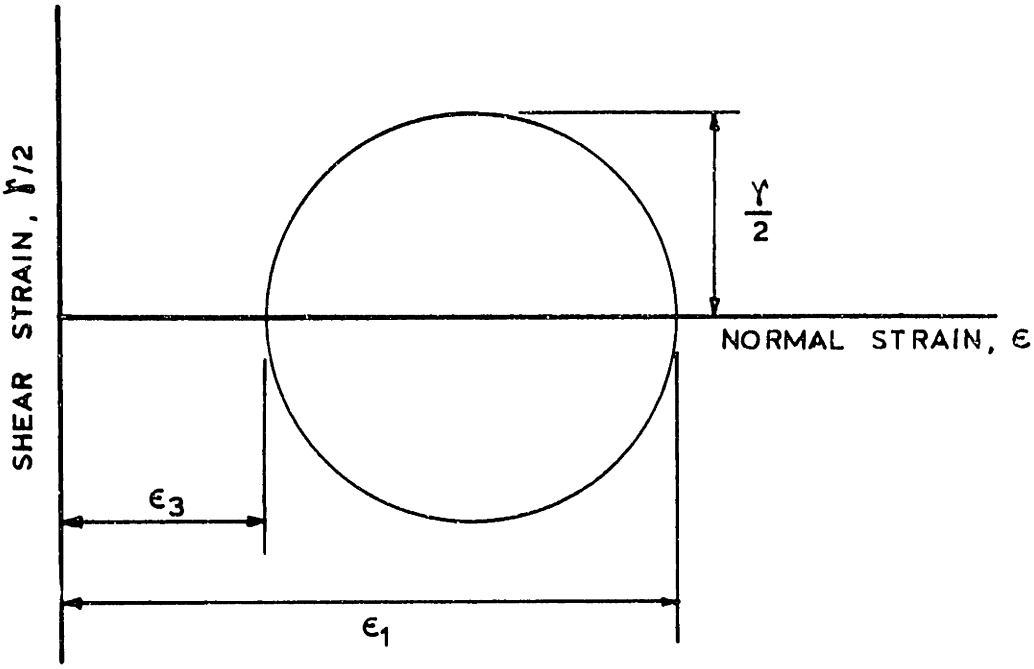

γ = MAXIMUM SHEAR STRAIN

ϵ_1 = MAJOR PRINCIPAL STRAIN, δ_1/H

ϵ_3 = MINOR PRINCIPAL STRAIN, δ_3/R

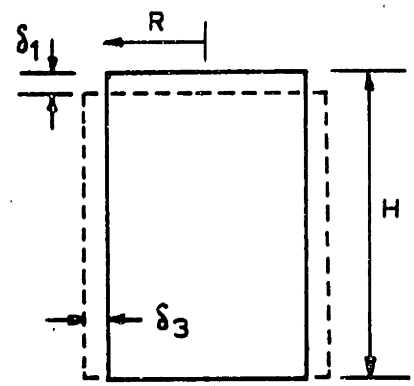

$$\left(\frac{\gamma}{2}\right)_{MAX} = \frac{\epsilon_1 - \epsilon_3}{2} \quad \text{OR} \quad \gamma = \epsilon_1 - \epsilon_3$$

MOHR'S CIRCLE OF STRAIN

FIGURE II-10

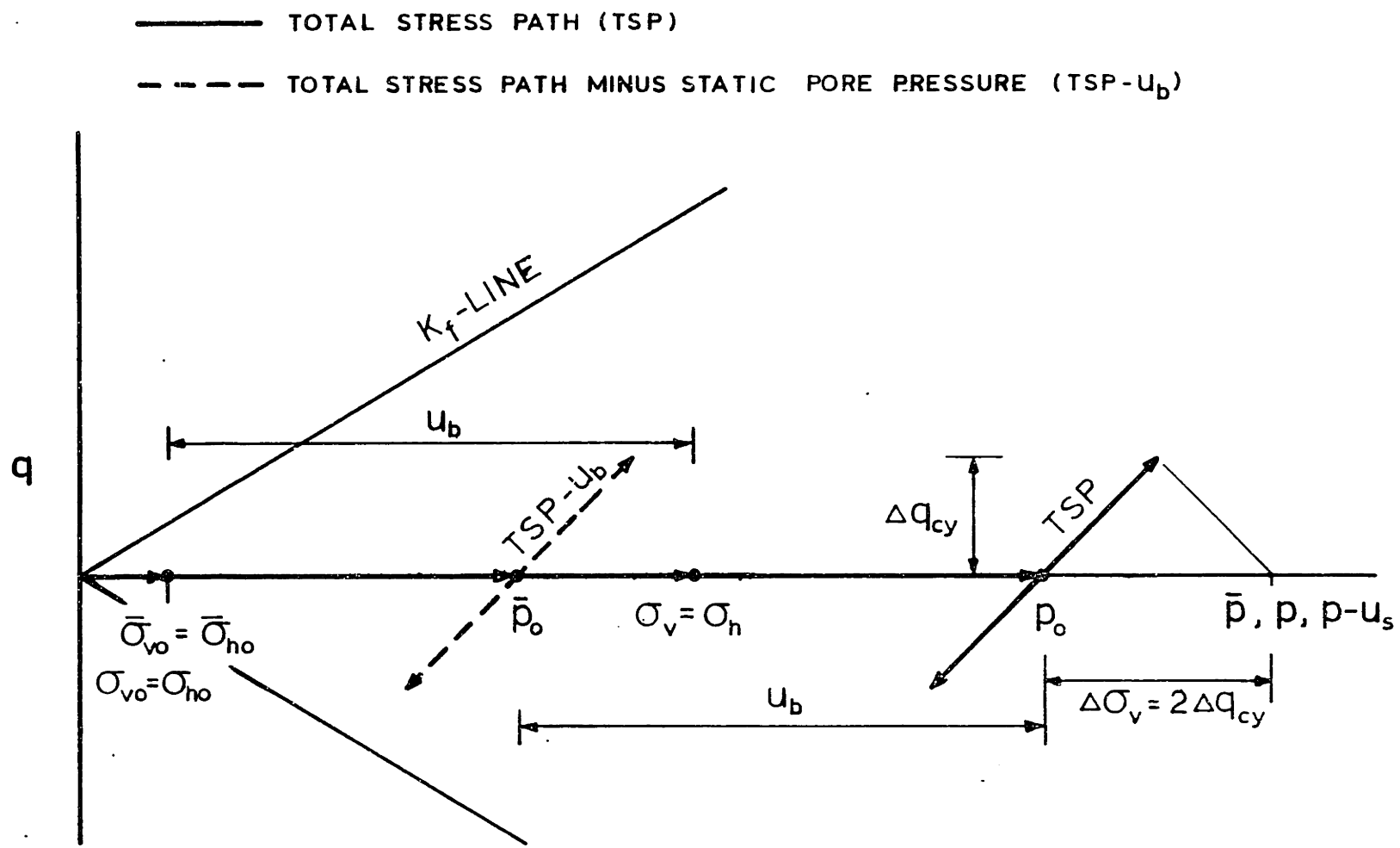

APPLIED STRESSES IN $\overline{CIU}$ CYCLIC TRIAXIAL TEST

FIGURE II-11

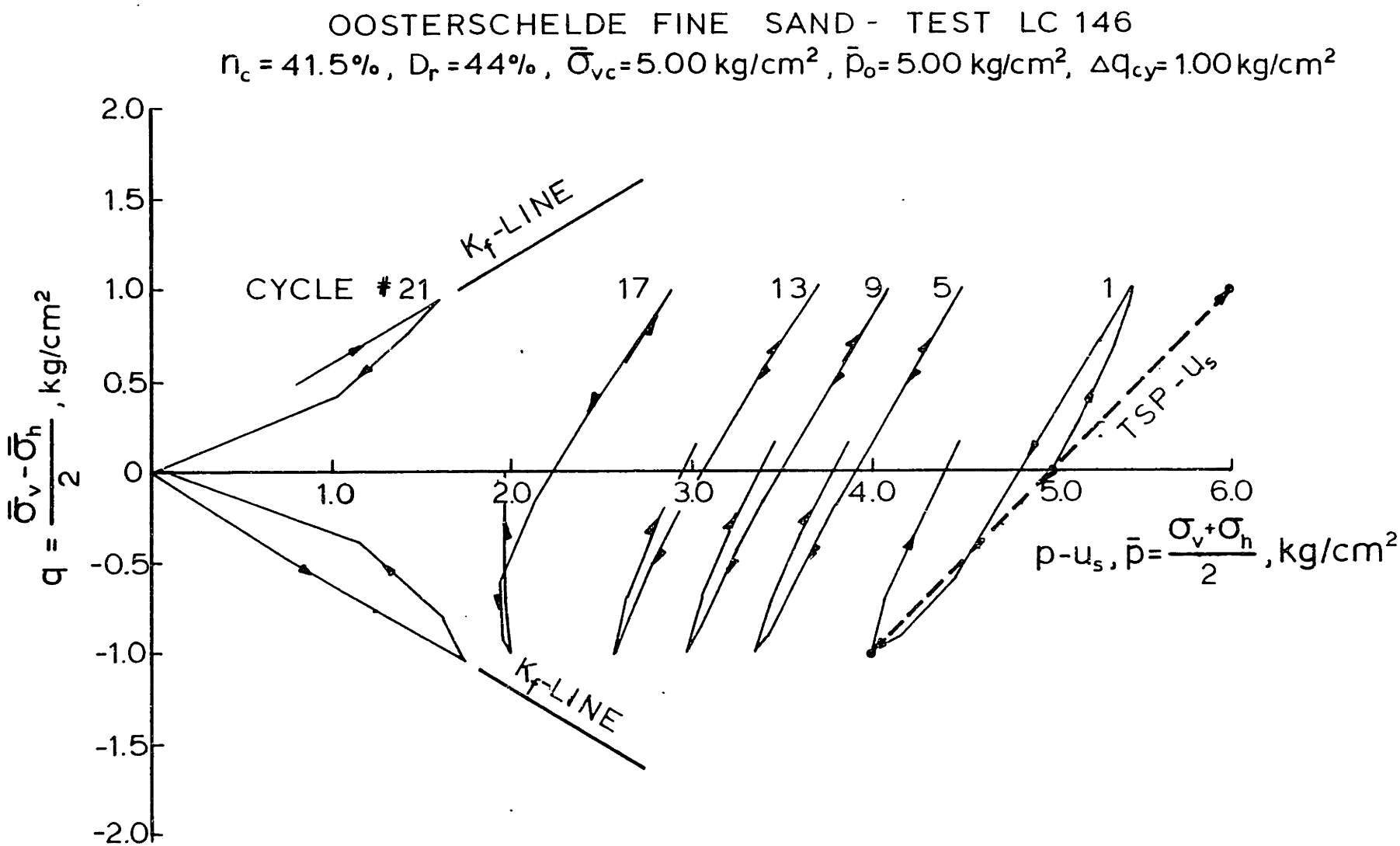

EFFECTIVE STRESS PATH FOR $\overline{CIU}$ CYCLIC TEST ON OOSTERSCHELDE FINE SAND (AFTER LAMBE AND ASSOCIATES, 1977)

FIGURE II-12

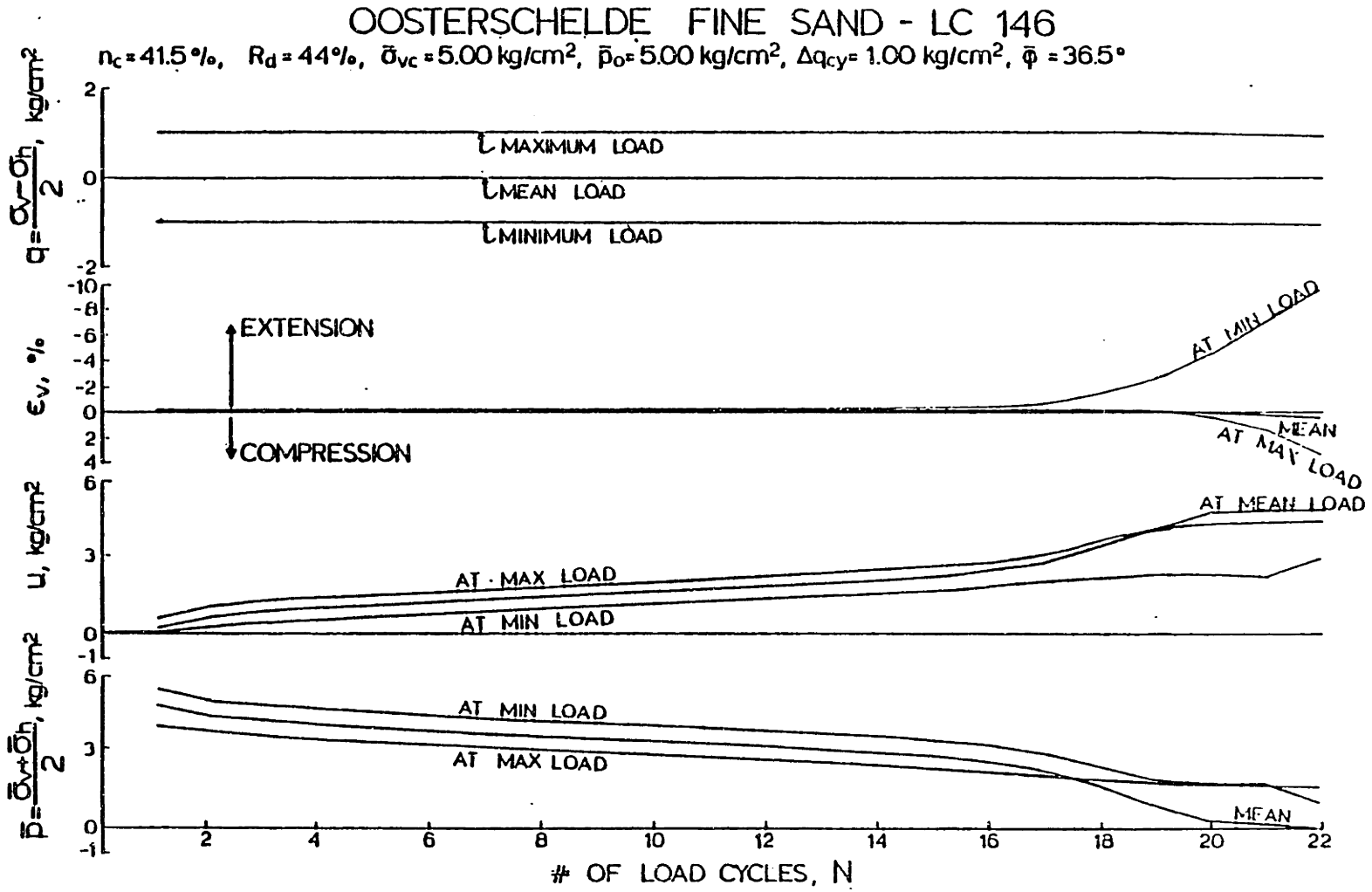

SUMMARY OF STRESS, STRAIN AND PORE PRESSURE DEVELOPMENT FOR $\overline{CIU}$ CYCLIC TEST ON OOSTERSCHELDE FINE SAND (AFTER LAMBE AND ASSOCIATES, 1977)

FIGURE II-13

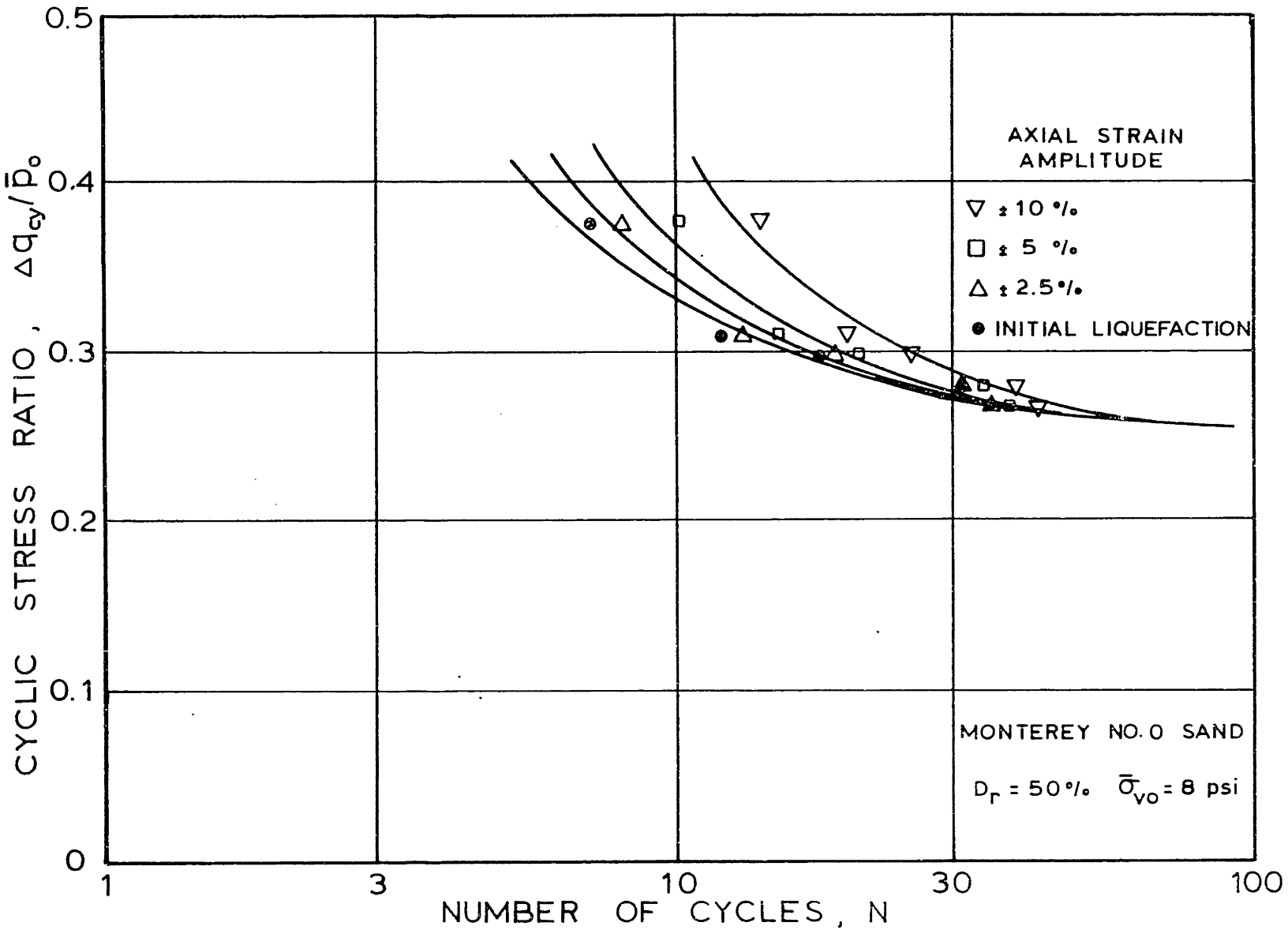

CYCLIC STRESS RATIO VERSUS NUMBER OF CYCLES FOR SAMPLES TAMPED MOIST IN LAYERS (AFTER MULILIS, et al, 1975)

FIGURE II-14

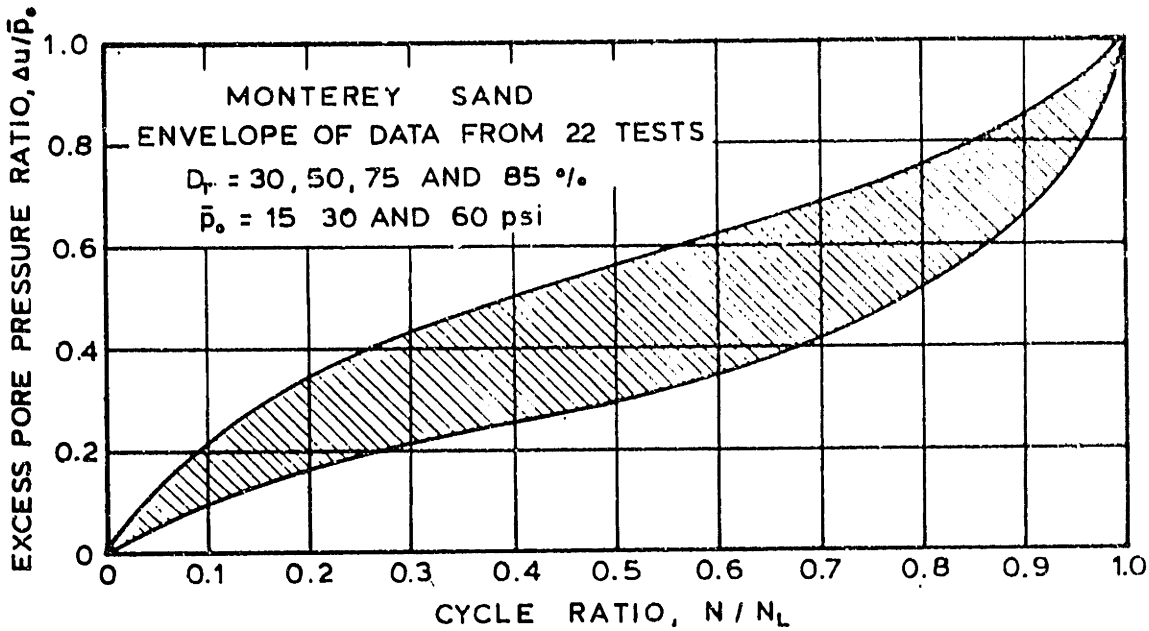

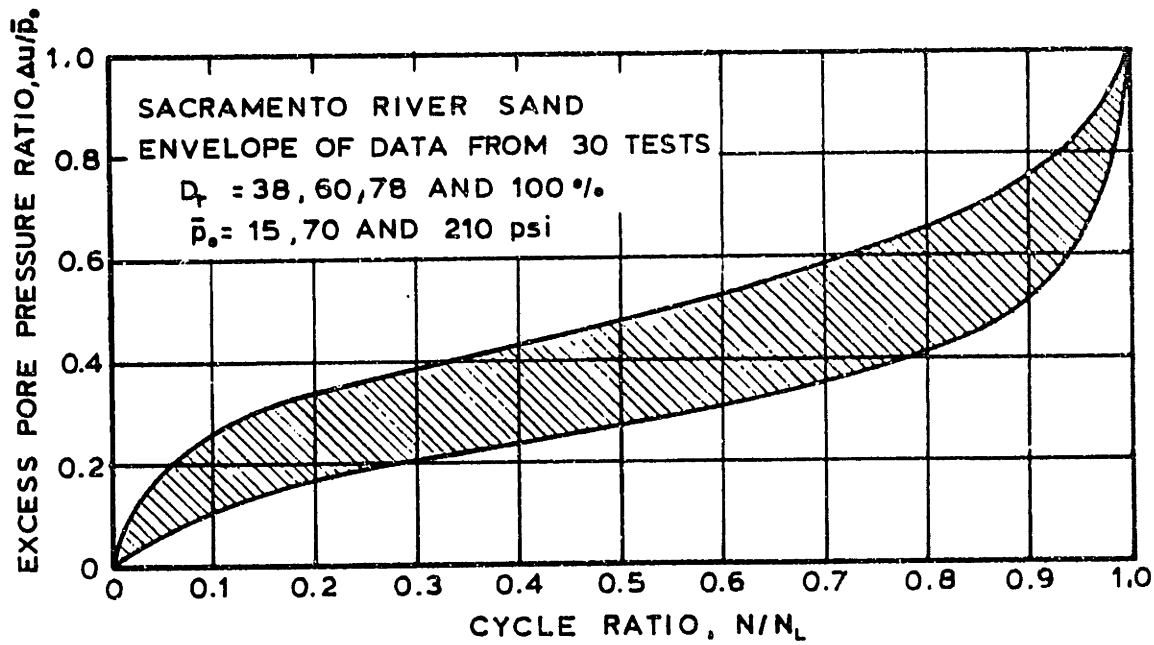

NORMALIZED PORE PRESSURE DATA FROM CYCLIC TRIAXIAL TESTS (FROM LEE AND ALBAISA, 1974)

FIGURE II-15

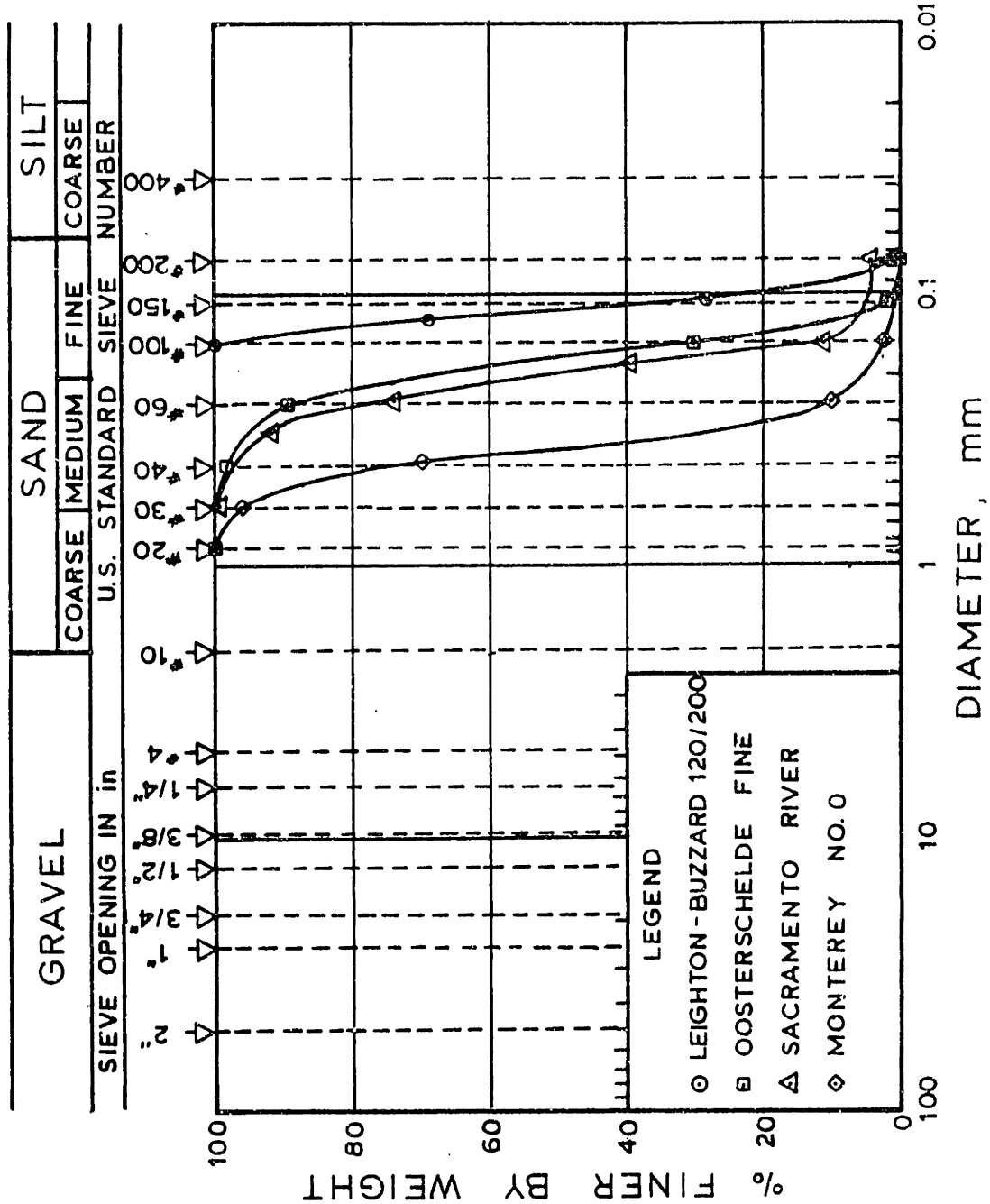

GRAIN SIZE DISTRIBUTION FOR DIFFERENT SANDS

FIGURE II-16

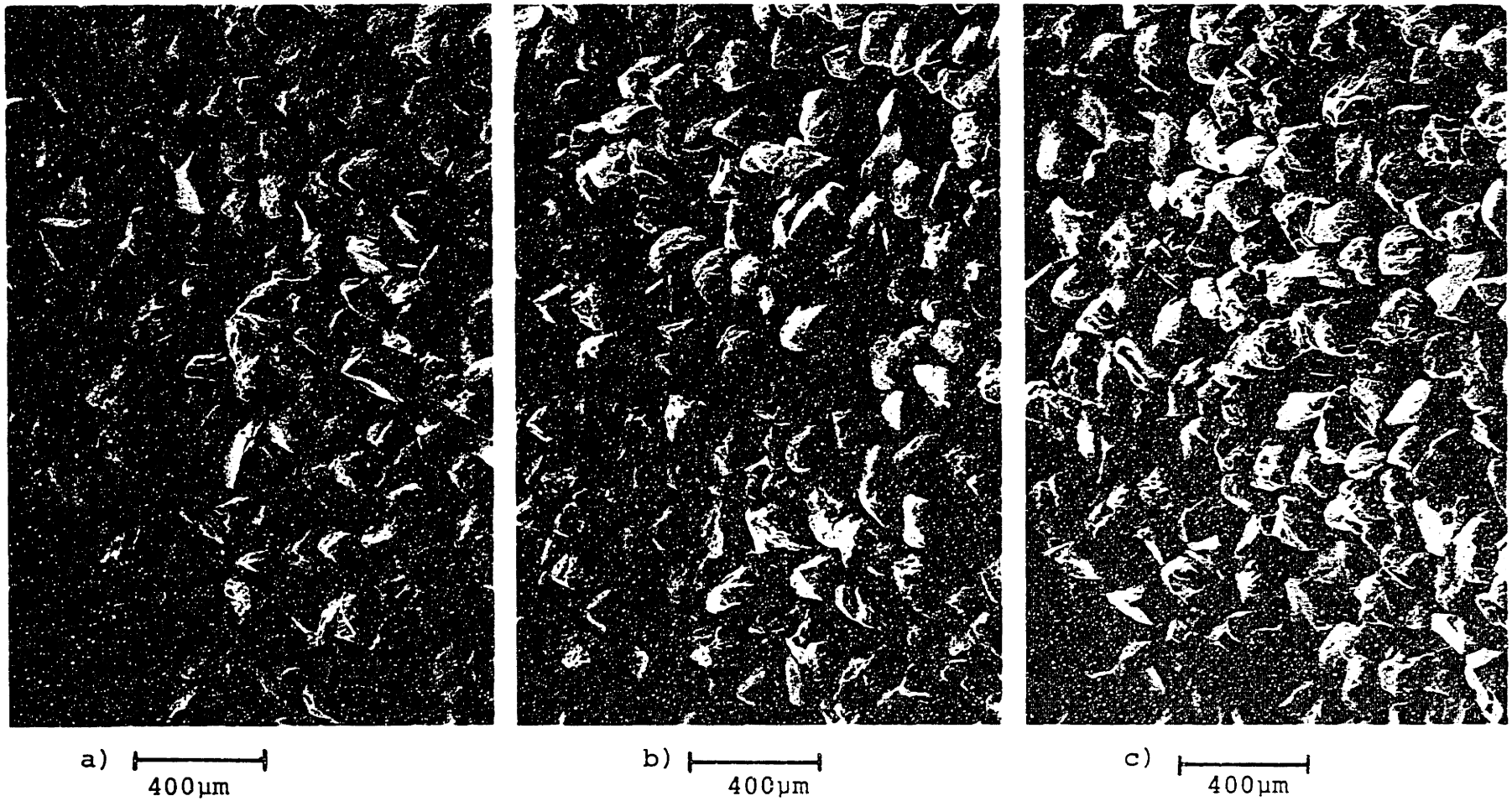

Scanning Electron Photomicrographs of Leighton Sand at 50X:
a) not sheared; b) sheared; c) recycled.

FIGURE II-17

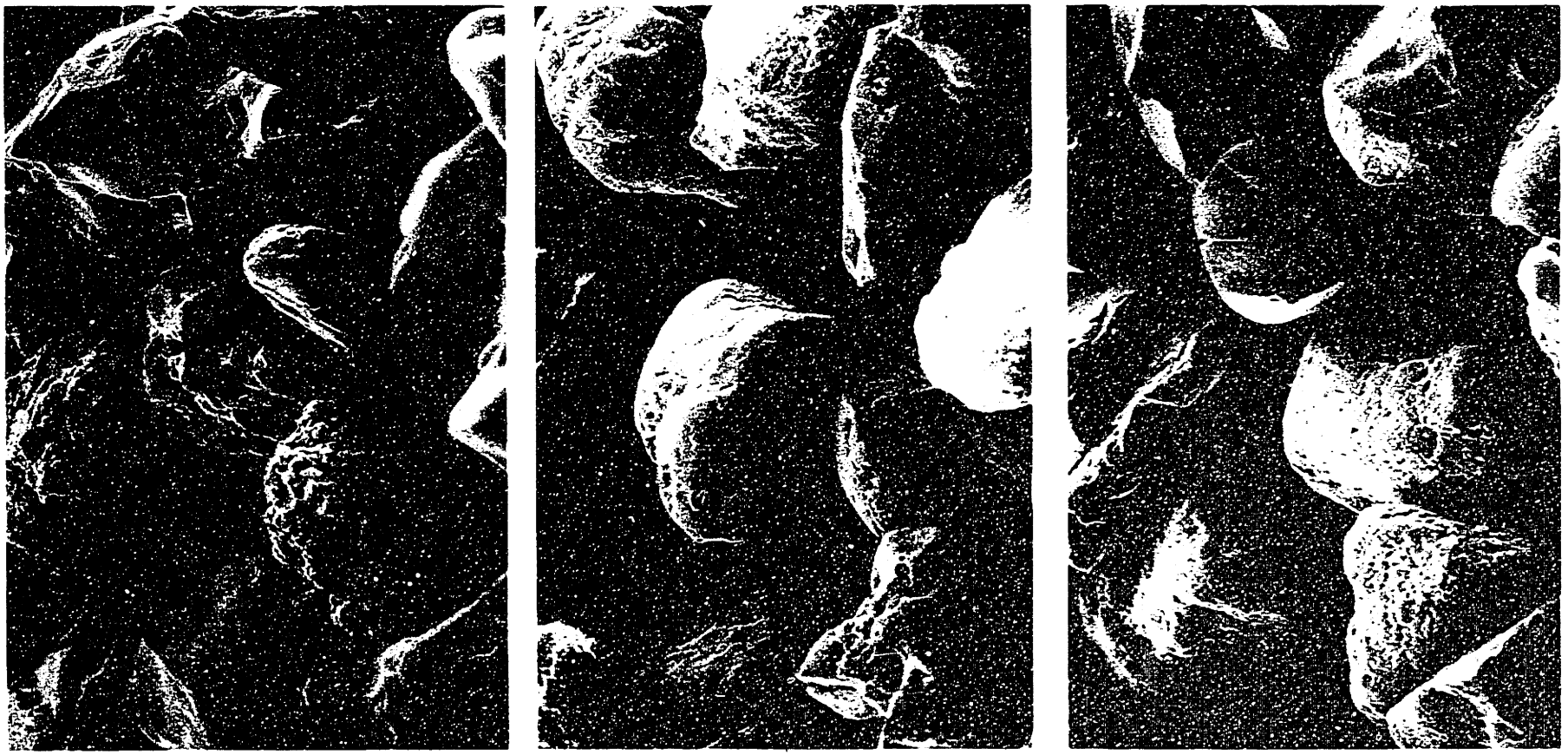

a) 100μm b) 100μm c) 100μm

Scanning Electron Photomicrographs of Leighton Sand at 200X:
a) not sheared; b) sheared; c) recycled.

FIGURE II-18

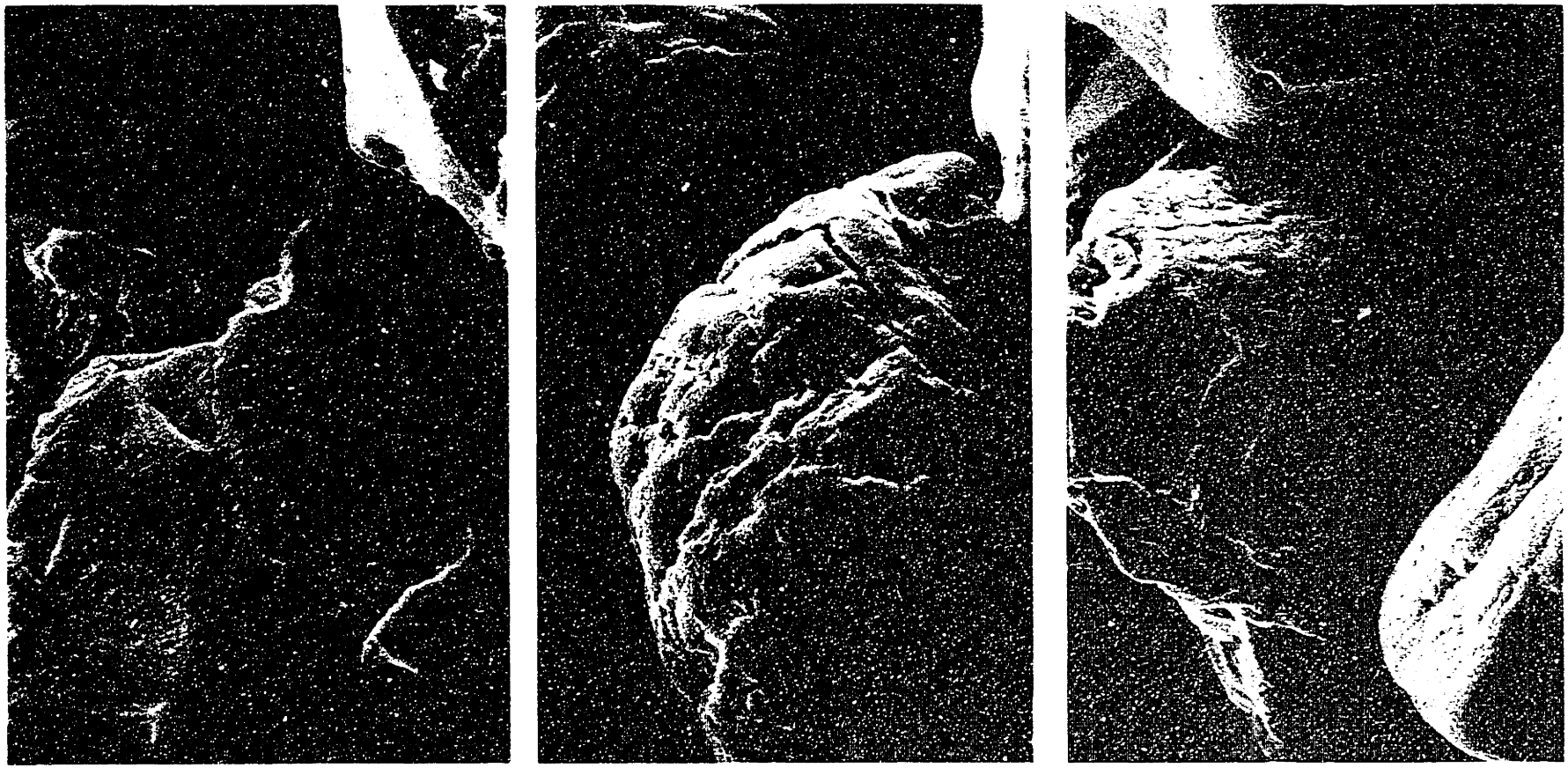

a) 40μm b) 40μm c) 40μm

Scanning Electron Photomicrographs of Leighton Sand at 500X
a) not sheared; b) sheared; c) recycled.

FIGURE II-19

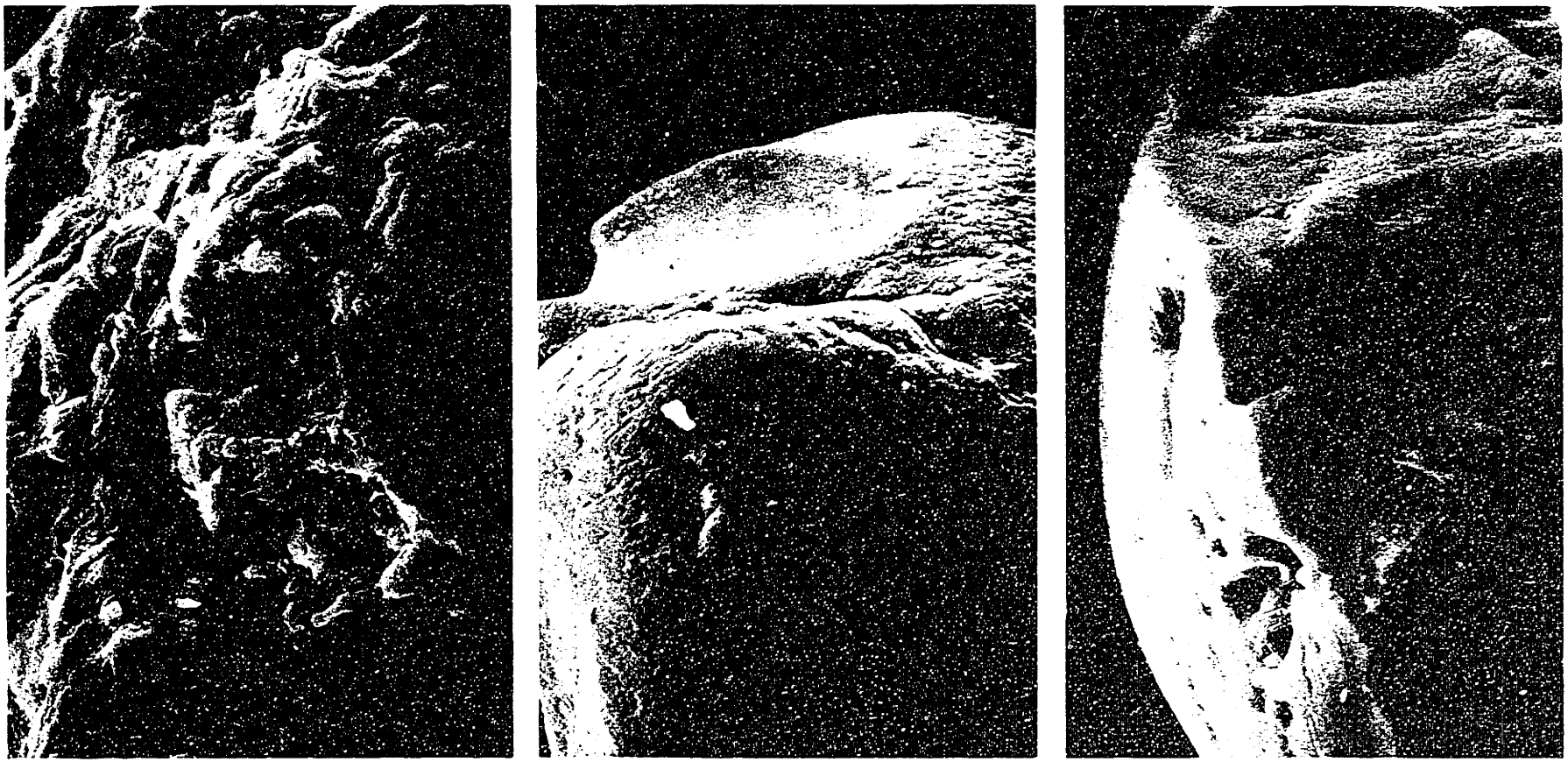

a) 20μm b) 20μm c) 20μm

Scanning Electron Photomicrographs of Leighton Sand at 1000X:
a) & b) not sheared; c) sheared.

FIGURE II-20

CHAPTER THREE - SAMPLE PREPARATION TECHNIQUE

Recent laboratory investigations, such as those by Ladd (1974, 1977) and Mulilis, et al, (1975), have shown that, although the liquefaction potential for saturated sands increases with decreasing relative density, or increasing void ratio (all other factors remaining equal), the method of soil preparation and resulting soil structure becomes a major factor influencing the liquefaction of the sand. This is a consideration which was generally overlooked by early investigators.

This chapter first summarizes the effect of sample preparation technique on the cyclic behavior of saturated sand as reported in the literature. The remainder of the chapter is devoted to the description of a sample preparation technique termed "wet rodding". This technique was developed for the purpose of preparing large-diameter, saturated sand samples for centifuge testing (Bucknam, 1981). The method was adapted for use in triaxial testing in order to determine the cyclic behavior of the test sand prepared this way, and to compare this behavior to that of the same sand prepared by other methods of preparation. Actual drained and undrained cyclic triaxial behavior of Leighton-Buzzard 120/200 Sand prepared by the wet rodding technique is discussed in Chapters Four and Five, respectively.

3.1 Effect of Sample Preparation Technique on Cyclic Behavior of Sand

Ladd (1974) used two methods of sample preparation to form specimens for stress-controlled cyclic triaxial tests. The first method was "dry vibration", whereby the specimen was compacted in four layers using a Vibro-Grave tool attached to a 1-1/2-inch (38mm) diameter compaction foot. Each layer was compacted to the dry-unit weight required to obtain the prescribed relative density. The bottom layers were initially slightly undercompacted, since compaction of each succeeding layer densified the sand below it. The second method was "wet-tamping" (later referred to as moist tamping), whereby the specimen was compacted in eight layers at a water content of approximately 9%. Each layer was compacted by hand with a 1-inch (25mm) diameter compaction foot. Three different sands were used in the analysis. Mean grain size, D_{50}, ranged from 0.16mm to 0.52mm. Test results showed that for a given number of cycles required to obtain a peak-to-peak vertical strain of 10%, the cyclic strength of specimens prepared using the wet-tamping method was approximately double that of the specimens prepared by the dry-vibration method.

Figure III-1 shows the results of similar tests as reported by Mulilis, et al (1975). Stress controlled cyclic triaxial tests were performed on samples of Monterey No. 0 Sand (see grain size characteristics Section 3.2) prepared eight different ways to the same average relative density. In Figure III-1 the cyclic stress ratio, $\pm \Delta q_{cy}/\bar{p}_o$, is plotted versus

the number of cycles to cause a peak pore pressure ratio of 100% (initial liquefaction) and ±2.5 axial strain. Results of the test program show that, for a given number of cycles, the stress ratio required to achieve initial liquefaction can vary by as much as 200%. Tests on other sands, however, showed that the magnitude of the effect of sample preparation technique used may be a function of the type of sand. Fabric studies and electrical conductivity measurements of the samples prepared using the different methods indicated that the arrangement and orientation of the contacts between sand grains was probably a primary reason for the observed differences in the cyclic strength of sand (refer to Chapter Five).

The affect of sample preparation technique on the drained and undrained cyclic behavior of Leighton-Buzzard 120/200 Sand is presented in Chapters Four and Five, respectively.

Ladd (1978) recommends the use of the moist tamped method of sample preparation (with undercompaction of the lower layers) for the application of cyclic triaxial testing to real problems. In cyclic triaxial tests, the moist tamping method generally produces a sample with a higher liquefaction strength than those compacted by most other methods (Figure III-1). Undisturbed samples, which are believed to best represent in situ conditions, yield liquefaction strengths higher than most laboratory-compacted samples of the same material. Thus it is recommended that moist-tamping (with undercompaction) be used because it produces samples with strengths closest to what is believed to be the actual in situ

strength. The use of the moist-tamping method (with undercompaction) to prepare 1.4-inch diameter triaxial samples for this investigation is described in detail in Appendix B.

3.2 Wet Rodding Sample Preparation Method

The wet rodding sample preparation method was developed for the purpose of preparing large diameter saturated sand samples for centrifuge testing (Bucknam, 1981). There were several important requirements that the preparation method had to meet in order to be successfully employed as part of the centrifuge testing program. Below is a list of the most important requirements.

1. The sample had to be prepared in a saturated state, then densified to a specific, predetermined void ratio.
2. The sample had to be prepared in layers so that electronic instrument sensors could be placed at various intermediate heights within the sample.
3. It was necessary that the method of preparation be one that would insure a uniform density distribution within the sample.
4. The method of preparation had to insure that the densification of upper layers would not disturb the instrumentation already placed within lower layers, i.e. by causing them to settle or reorientate.
5. The method had to be one which was fairly simple, did not require complicated equipment, and would

form samples of a desired void ratio repeatably from test to test.

The wet rodding method of sample preparation adequately satisfied the above requirements and has since been successfully used to prepare 5.25-inch diameter samples for centrifuge testing (P. Lambe, 1981). The wet rodding method is outlined below. The sequence of steps corresponds to a schematic shown in Figure III-2.

1. The sample container (mold) is filled to the top with water (preferably de-aired, distilled). An extension collar is attached to the top of the container to allow the water level to rise without spillage as sand is added.
2. Enough sand is "rained" into the water-filled container to form the first layer. The sand is rained uniformly over the whole cross-sectional area of the container. This insures that the sand settles out in a level manner. The intensity of raining is maintained at approximately 1.2 grams/min/cm^2. The sand settles out at near maximum void ratio.
3. Densification of the sand layer is achieved by pushing a cylindrical rod of diameter d_{rod} to the bottom of the layer N_r times in a random fashion. The number of pushes of the rod, N_r, to achieve the desired void ratio is experimentally determined for a particular size container and rod.

4. The remaining layers are formed and densified in the same manner, using the same amount of sand and the same value of N_r. The only difference is that the rod is pushed approximately 1/16 to 1/8 of an inch into the top of the lower layer (provided it will not interfere with electrical equipment) in order to densify a thin loose zone which is believed to occur at the top of each layer (Bucknam, 1981).

Qualitative X-radiographic analysis (Bucknam, 1981; Taverna, 1977) indicates that samples prepared by the wet-rodding method are generally uniform with respect to the vertical direction. Radiographs were taken of individual layers in the vertical direction in order to determine the uniformity of the sand in the lateral direction. The radiographs showed spots which indicated there were loose zones in the places where the rod was pushed into the sand. It is speculated that these loose zones extend to the bottom of the layer in a columnar fashion. However, a three-dimensional fabric study using radiographs would be necessary to determine whether or not this is true. Subsequent rodding action in the vicinity of one of these loose zones appeared to densify it, based on the radiographs taken. The degree of subsequent densification depends on the proximity of the rodding to the loose zone, as indicated by the different shades of the spots on the radiographs (Bucknam, 1981). A smaller diameter rod was used in order to minimize the size of these loose zones.

No information is available regarding the lateral uniformity of samples prepared using other methods, such as those reported by Mulilis, et al (1975). It is possible that the moist-rodding method, as reported by Mulilis, et al (1975), may have lateral uniformity problems similar to those of the wet-rodding method described herein.

It was determined from radiographs of 6-inch samples of Leighton-Buzzard 120/200 Sand that the formation and densification of overlying layers has no distinguishable effect on the underlying layers. This was determined by taking radiographs at different stages as the sample was formed. It has not been established, however, how much of a change in density can be detected by the radiographic analysis performed for this investigation at the M.I.T. radiographic facility. Thus, the term "qualitative" X-radiographic analysis is used.

Determination of the degree of saturation of sand samples formed in this manner was not made. Bieganousky (1976) reported that the degree of saturation for large bin samples of Reid Bedford Model Sand, prepared by raining the test sand through water, was approximately 97%.

3.3 Application of the Wet Rodding Method to Triaxial Specimens

The wet rodding method of sample preparation was used to form triaxial specimens for the purpose of observing the cyclic behavior of Leighton-Buzzard 120/200 Sand. The procedure is essentially the same as that outlined briefly in the previous section, however, extra measures are taken to insure

a high degree of saturation of the sample after densification (see Appendix B). The steps of the preparation procedure which directly relate to the formation and densification of the sand within the triaxial mold are given here for the reader's benefit.

1. The amount of air-dried sand to be used is calculated using the desired void ratio and the volume of the split mold. This sand is divided equally into two parts (for a two-layer sample). The sand is weighed and kept in separate containers.
2. The primary and secondary rubber membranes (previously described) are affixed to the bottom pedestal of the triaxial cell base and sealed with O-rings. A bronze disk is set inside the primary membrane on top of the pedestal, and the split mold is set in place. The primary membrane is stretched upward through the mold and pulled over the sides at the top. The secondary membrane remains rolled up at the base, in a void space between the bottom of the mold and the pedestal. A vacuum is applied to the mold to hold the primary membrane tight against the inside of the mold. An extension collar is secured to the top of the mold by means of a large rubber band which is fastened to the base. The collar is kept water tight so to allow water to rise above the top of the mold when the sand is rained into the mold.

3. By means of a screw pump connected to the bottom drainage line, the mold is completely filled with de-aired, distilled water.

4. The first portion of sand is rained gently into the water-filled mold to form the first layer. The sand settles uniformly at the bottom of the mold at near maximum void ratio. The water which is displaced rises within the extension collar.

5. Rodding is performed with a steel wire rod approximately 0.042 inches in diameter, and sufficiently long enough to extend well above the extension collar. The first layer is densified by pushing the rod to the bottom of the mold a total of 50 times in a random fashion, being sure to cover the whole cross-sectional area. The downstroke of the rod should be brisk. However, because of friction between the rod and the particles within the sample, the upstroke should be gentle. This prevents soil grains from being pulled upward and out of layer. Rodding should be done in sets of five or ten pushes, with a 30 to 60 second pause in between to allow for some settling action to occur. This enhances the repeatability of the technique.

6. The second layer is rained into the mold in a similar fashion. Again, 50 pushes of the rod are used to densify this upper layer. The downstroke is extended 1/16 to 1/8 of an inch into the top of the lower (first) layer.

7. Upon completion of the densification of the sand within the mold, the water inside the extension collar, (above the sample) is carefully removed. This is done by siphoning the water out of the collar with a small diameter tube (or with a pipette) until the water level is only about 1/4-inch above the top of the sand sample. The remainder of this water is removed and the sample is drained by very slowly backscrewing the screw pump until an air bubble is seen in the hose connecting the screw pump to the triaxial base.

8. The extension collar is removed from the top of the mold. The sand level is usually slightly above the top of the mold at this point. The top bronze disk is placed on the sample and pushed downward (and slightly rotated) in order to level the sample and provide good seating between the sand and the top cap.

9. The housing containing the top cap/piston is fastened to the base. The top cap/piston is lowered onto the sample and the bronze disk, and held firmly in position while the piston is clamped.

10. The vacuum is released and the primary membrane is stretched over the top cap and sealed with O-rings.

11. A slight vacuum of 0.2 to 0.4 kg/cm^2 is applied to the sample with the screw pump. The split mold is removed.

The moist tamped method of sample formation (with undercompaction) is described in detail in Appendix B. This method was used by Hedberg (1977) for cyclic triaxial tests on Oosterschelde Fine Sand. The samples were compacted in five layers at a water content of 10%, using a degree of undercompaction of 5%. The same parameters were used in this test program.

Five III-3 shows radiographs of triaxial samples prepared by the wet rodding method (Figure III-3a) and the moist tamped method (Figure III-3b). It is clear from this figure that the moist tamped sample shows significantly greater layering effects than does the wet rodded sample. All five layers of the moist tamped sample appear identical, i.e., the bottom layer (which was 5% undercompacted) showing no distinguishable differences from the top layer (which received no undercompaction). Within each layer, however, there is a very significant change in density. The top of each layer appears much denser than the lower portion of each layer. This result has been observed by others (Mulilis, et al, 1975; Taverna, 1977) for most tamped (undercompacted) samples. The observation of such drastic non-uniformities within the individual layers contributes to the belief that such samples, although generally yielding liquefaction strengths closest to those of undisturbed samples, are the least uniform of any type of sample so far used in triaxial testing. The wet rodded sample (Figure III-3a), on the other hand, appears quite uniform with depth. Little, if any, layering is observed within this sample.

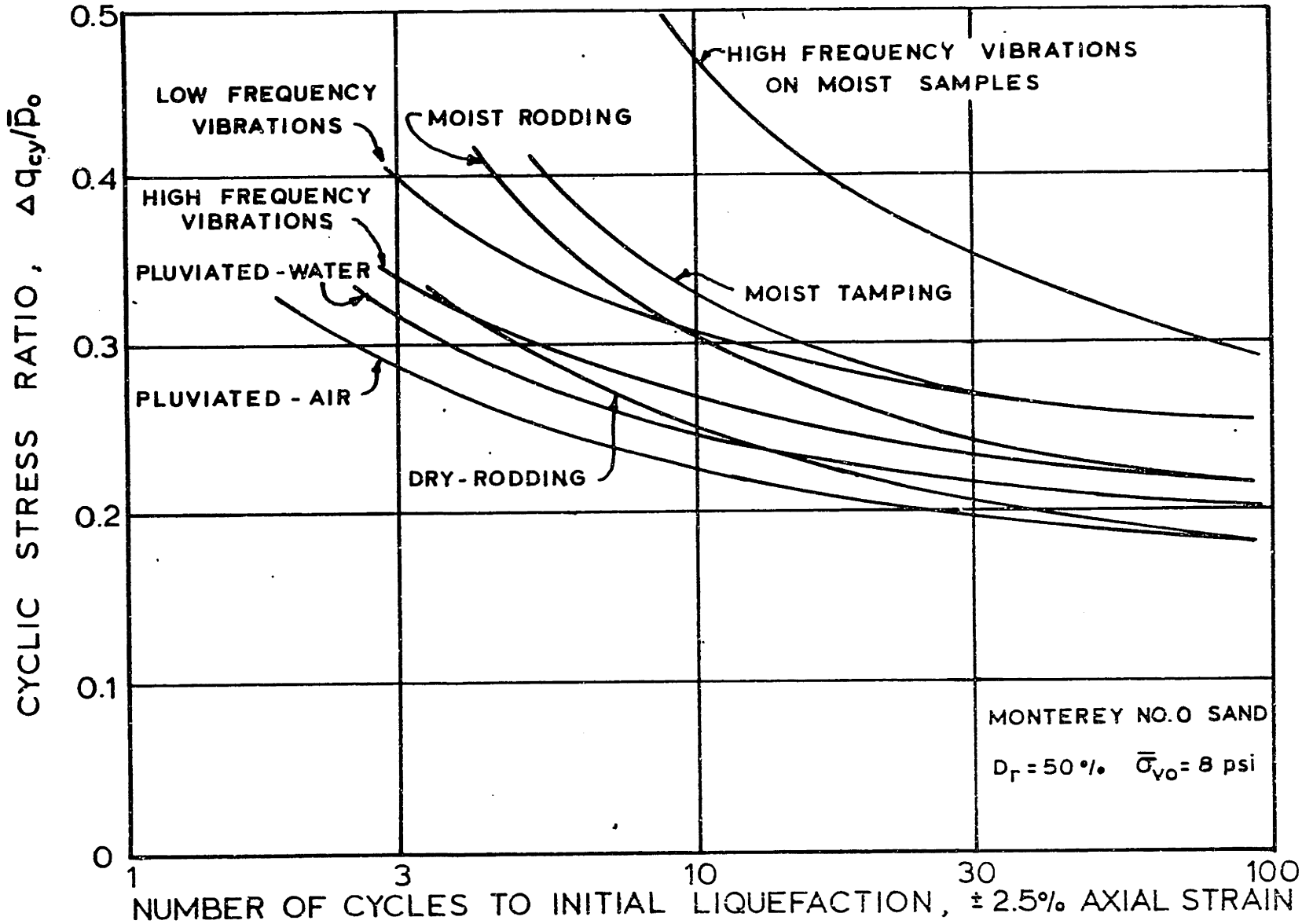

CYCLIC STRESS RATIO VERSUS NUMBER OF CYCLES FOR DIFFERENT COMPACTION PROCEDURES (AFTER MULILIS, et al, 1975)

FIGURE III-1

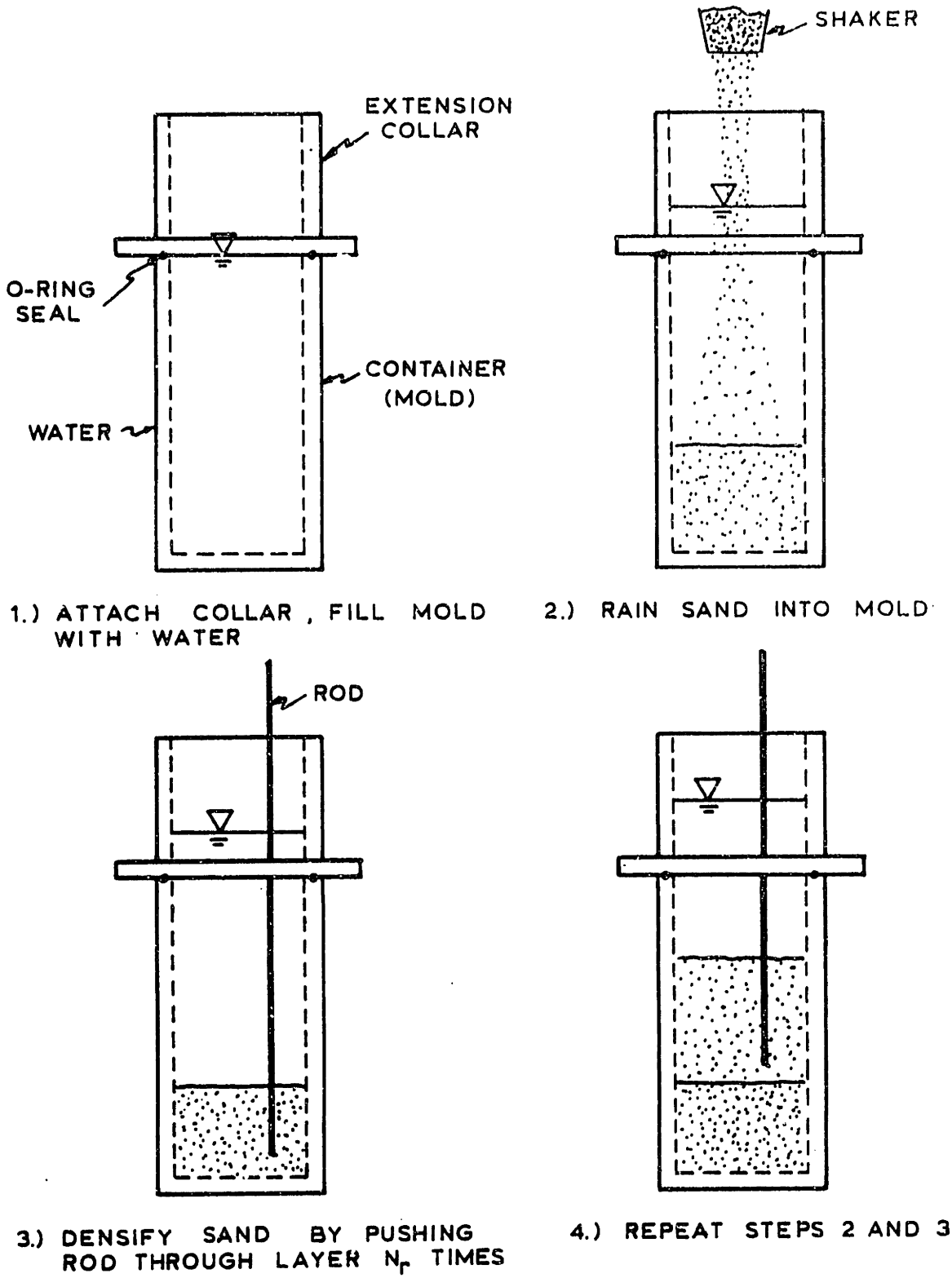

SCHEMATIC OF WET RODDING METHOD

FIGURE III-2

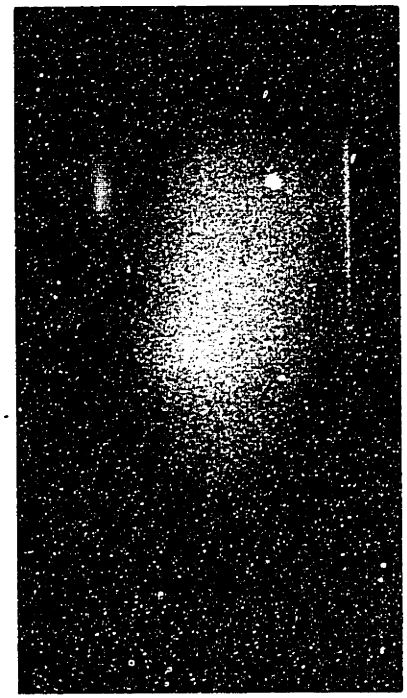

a) wet rodded

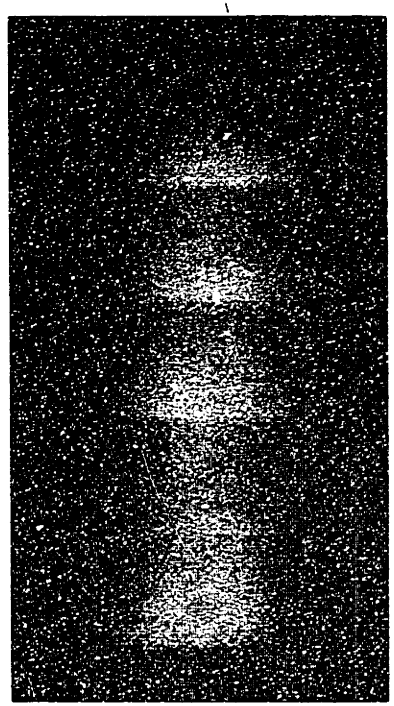

b) moist tamped
(under compacted)

Radiographs of Triaxial Samples

FIGURE III-3

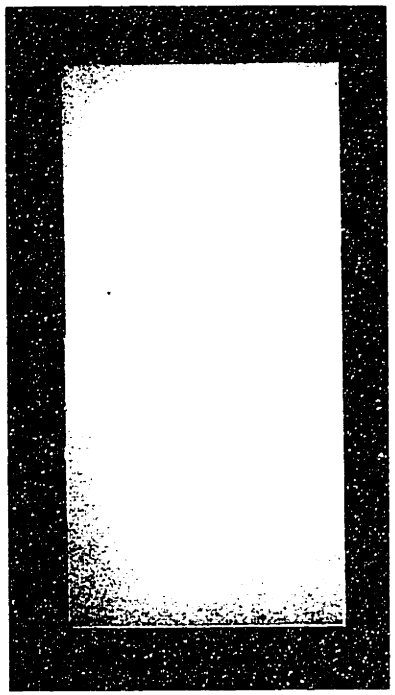

a) wet rodded

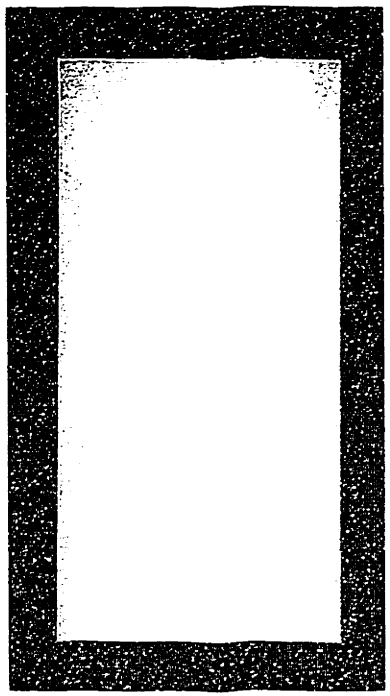

b) moist tamped
(under compacted)

Radiographs of Triaxial Samples

FIGURE III-3

CHAPTER FOUR - DENSIFICATION BEHAVIOR OF LEIGHTON-BUZZARD 120/200 SAND

This chapter examines the densification (accumulation of volumetric strain) of Leighton-Buzzard 120/200 Sand in drained cyclic triaxial compression tests. A simple relationship for volumetric strain in terms of cycle number, N, and peak-to-peak shear strain, γ_{pp}, is presented, based upon an analysis by Hadge (1979). Although Hadge shows that initial density and stress condition influences the degree of shear strain in a triaxial test, these factors were not considered in this investigation because of the limited number of tests performed. Instead, it is the purpose of this chapter to:

1. provide data to permit the estimation of densification of this sand as a result of cyclic loading,
2. shed some light on the influence of method of sample preparation on the densification of Leighton-Buzzard 120/200 sand under these loading conditions.

4.1 Test Results

Figure IV-1 gives the total and effective stress paths for the seven anisotropically consolidated drained cyclic compression tests run on Leighton-Buzzard 120/200 Sand. These stress paths correspond to the cyclic component of the applied stresses as depicted in Figure II-7. All tests were taken through 1000 load cycles.

Results of Test DC8 are shown in Figures IV-2, IV-3 and IV-4. The sample was prepared by the wet rodding method for this test. The applied cyclic shear stress ratio, $\pm \Delta q_{cy}/\bar{p}_o$ = 0.75. The effective stress path is shown in Figure IV-2, as generated by the computer reduction program (see Appendix B). This effective stress path is essentially identical to the corresponding stress path depicted in Figure IV-1. Figure IV-3 gives the stress, q, versus vertical strain, ε_v, for cycles N = 1, 5, 10, 50, 100, 250, 500 and 1000. The accumulation of vertical and volumetric strain, as well as stress q and $\bar{p}$, are plotted versus cycle number N in Figure IV-4. As discussed in Section 2.3.2, the vertical and volumetric strains cycle between maximum and minimum values, and exhibit residual strains which increase with each cycle at a decreasing rate. Figure IV-4 gives the stresses and strains as determined at the maximum, minimum, and mean load positions. This is done by adjusting the cyclic machine so data is recorded at times as close as possible to these three load positions (see Appendix B). As a result, the data recorded at mean load (see Figure IV-4) is not necessarily the same as the average of the data recorded at maximum and minimum loads. In other words, the "at mean load" line is not always exactly centered between the "at maximum load" and the "at minimum load" lines.

In general the results of this test closely resemble the results of similar tests on Oosterschelde Fine Sand as reported in Section 2.3.2 (Figure II-8 and II-9). Table 4-1 summarizes the test results of all the drained cyclic compression

tests performed in this investigation. Tests DC10 and DC11 were run on samples of Leighton-Buzzard 120/200 sand prepared by the moist tamping (undercompaction) method. All other tests were performed on samples prepared by the wet rodding method. Table 4-2 summarizes the volumetric strain development as measured during the tests. Table 4-3 summarizes the vertical strain development. Appendix A1 gives plots of stress and strain for most drained tests performed in this investigation.

Peak-to-peak shear strains were calculated for cycles 1, 2, 5, 10, 50, 100, 250, 500 and 1000 using the equations given in Section 2.3.3. Shear strains were corrected for system compliance (see Appendix A1). These strains are tabulated in Table 4-4, and plotted versus cycle number N (on a logarithmic scale) in Figure IV-5 for each test. From Figure IV-5 it is seen that the value of peak-to-peak shear strain is relatively constant throughout all 1000 cycles for tests with low cyclic stress ratios (Tests DC6, DC7, and DC10). Tests DC8, DC9, and DC11, however, exhibit significantly larger peak-to-peak shear strains in the first cycles, compared to the rest of the test. This behavior is more drastic for Tests DC9 and DC11, which were run at cyclic stress ratios of $\pm\ \Delta q_{cy}/\bar{p}_o = 0.444$.

One explanation for the large shear strains at the beginning of Tests DC8, DC9, and DC11 is that the effective stress path comes quite close to the K_f-line at maximum shear stress, q_{max}, during each cycle (Figure IV-1). This causes large vertical strains within the sample at maximum load. However, in addition to larger vertical strains, extension strains

(measured relative to the length after q_m = 0.75 kg/cm^2 is applied) also develop as a result of either a zero shear stress condition (Test DC8 at minimum load, Figure IV-2) or a slight reversal of shear stress (Tests DC9, DC11 at minimum load, Figure IV-1). The cyclic vertical strain (difference between strains measured at maximum and minimum loads) is therefore large at the beginning of the test. At the same time, the volumetric strain is still small, but rapidly increasing. The peak-to-peak shear strain is therefore quite large during the first cycle, and decreases gradually until the sample densifies enough to resist the high shear stresses. The peak-to-peak shear strains more or less level off after cycle 50 in Tests DC9 and DC11, and after cycle 10 in Test DC8.

From the above observations, it is evident that an average peak-to-peak shear strain for all N cannot be used to describe the shear strains experienced throughout tests where large cyclic shear stress ratios are applied. This issue is further expanded upon in Section 4.3 which discusses the influence of cyclic stress ratio on peak-to-peak shear strains as determined for the tests reported herein.

Tests DC6 and DC12 were essentially identical, with the exception that Test DC6 had an initial void ratio, e_c = 0.773 (D_r = 67.2%) and Test DC12 had an initial void ratio, e_c = 0.751 (D_r = 73.1%). Sample DC6 underwent somewhat larger volumetric strains than did sample DC12 - approximately 30% larger by cycle 1000. This difference is attributed to the

difference in density of the samples. As shown on Figure IV-5 and in Table 4-3, the peak-to-peak shear strains of Test DC6 are about 10% higher than those of Test DC12. Although the difference in density is not very large, the results indicate the looser sample experiences larger shear strains than the denser. Otherwise, the comparison of these two tests suggests that the possibility of duplicating drained cyclic tests under the same test conditions (density, stress path, confining pressure) and obtaining repeatable results, is quite good.

4.2 Densification Relationship for Leighton-Buzzard 120/200 Sand

Recalling the findings of Silver and Seed (1971) and Youd (1972), the degree of shear strain is the primary factor causing densification in granular materials. Silver and Seed (1971) showed that a linear log-log relationship exists between the applied shear strain, γ_{xy}, and vertical strain, ε_v, for a given cycle number and density in simple shear tests. It is thus desireable to consider the peak-to-peak shear strain in a cyclic triaxial test, γ_{pp}, analogous to the shear strain in a cyclic simple shear test. Doing so justifies the generation of a linear log-log relationship between the volumetric strain, ε_{vol}, and peak-to-peak shear strain, γ_{pp}, which would describe the densification of a sand as observed in a cyclic triaxial compression test.

Such a log-linear expression was determined by Hadge (1979) for Oosterschelde Fine Sand. From log-log plots of ε_{vol}

versus γ_{pp} for any particular cycle N, Hadge found that the development of volumetric strain during cyclic triaxial compression tests evolved in a regular fashion. An expression of the following form would describe the data:

$$\log(\varepsilon_{vol}) = a_n + b \log(\gamma_{pp}) \qquad \text{Equation 4.1}$$

where

$a_N = \varepsilon_{vol}$ at $\gamma_{pp} = 0.01\%$

b = slope of line.

For Oosterschelde Fine Sand, b was found to be relatively constant (approximately 1.26) regardless of cycle number, based on plots for cycles 5, 10, 50, 150, 550, and 1050.

Equation 4.1 can be expressed as:

$$\varepsilon_{vol} = A\,(\gamma_{pp})^b \qquad \text{Equation 4.2}$$

where $A = 10^{a_N}$. The parameter A is therefore a function of N. Fitting a line through a log-log plot of A versus N data, Hadge found that A could be estimated for any N by

$$A = 0.685N^{.413} \qquad \text{Equation 4.3}$$

Combining Equations 4.2 and 4.3, setting b = 1.26, yields

$$\varepsilon_{vol} = 0.685N^{.413}\,(\gamma_{pp})^{1.26} \qquad \text{Equation 4.4}$$

ε_{vol} in %

γ_{pp} in %

for Oosterschelde Fine Sand.

With Equation 4.4, the ability to predict volumetric strain in a cyclic triaxial test (under the same general conditions) depends only on the knowledge of the peak-to-peak shear strain for any cycle N.

A similar analysis was conducted for Leighton-Buzzard 120/200 Sand using the results of drained cyclic compression tests on wet rodded samples. Figures IV-6 through IV-16 show plots of ε_{vol} (%) versus ε_{pp} (%) on a log-log scale for all tests at various cycles. Linear regression was used to determine the line which best fit the data and the corresponding slope, b, for the wet rodded samples (open data points). The slope b ranged from 1.22 to 1.70. Figure IV-17 is a log-log plot of A versus N for the same cycles used in Figures IV-6 through IV-16. For cycles 1-10, the data can be expressed by the following equation:

$$A = 0.423\ N^{0.983} \qquad \text{Equation 4.5}$$

For cycles 10-1000, the data in Figure IV-17 can be expressed by:

$$A = 2.19\ N^{0.271} \qquad \text{Equation 4.6}$$

The slope, b, gradually increased in the first 10 cycles from 1.22 to 1.58. This gradual increase in b is a direct result of high (but ever decreasing) peak-to-peak shear strains in the first cycles. The average value of b = 1.41. For cycles 10-1000, the value of b was more constant, ranging from 1.44 to 1.70. The average value of b = 1.59 for cycles 10-1000. Combining equations 4.5 and 4.6 each with Equation 4.2 and the

respective average value of b, the following two expressions for volumetric strain are developed:

$$\varepsilon_{vol} = 0.423\ N^{0.983}\ (\gamma_{pp})^{1.41} \text{ for } N = 1\text{-}10 \qquad \text{Equation 4.7}$$

$$\varepsilon_{vol} = 2.19\ N^{0.271}\ (\gamma_{pp})^{1.59} \text{ for } N = 10\text{-}1000 \qquad \text{Equation 4.8}$$

At cycle 10, Equations 4.7 and 4.8 are not compatible. For example, using γ_{pp} = 0.1%, Equation 4.7 yields ε_{vol} = 0.158% and Equation 4.8 yields ε_{vol} = 0.105% - approximately 50% less.

It is expected that the high shear stress ratios forced the development of a separate expression for volumetric strain during the first 10 cycles, as given by Equation 4.7. Because the non-linearity in the peak-to-peak shear strains with cycle number may be similar to the behavior of the same sand in centrifuge tests, the development of both empircal relationships was necessary. Hadge (1979) found that a single linear relationship for $A = 10^{aN}$ in terms of N would approximate his data rather well. The maximum shear strains developed in Hadge's tests, however, were about an order of magnitude less than those developed in this investigation.

For comparison, Figure IV-18 plots cummulative volumetric strain, ε_{vol}, versus cycle number, N, for a peak-to-peak shear strain γ_{pp} = 0.1% using Hadge's relationship for Oosterschelde Fine Sand (Equation 4.4), and Equation 4.8 for Leighton-Buzzard 120/200 Sand. Note that Equation 4.8 yields up to 80% higher volumetric strains than Equation 4.4.

Figure IV-19 shows the difference in percent, between the measured and predicted volumetric strains for various cycles for six drained triaxial tests. Equation 4.8 was used for cycle N = 10. Figure IV-19 shows that predictions were generally accurate to within ±50% for all tests, including those in which the moist tamped method of preparation was used (DC10, DC11). In one case (Test DC6, N=7) the prediction deviated from measured results by about 70%. Using Equation 4.7, the accuracy of the prediction seems to be somewhat dependent on cycle number, as a result of the changing b parameter. At low cycles (N=1-4), Equation 4.7 generally underpredicts the volumetric strain. This is because the value of b for these cycles (see Figure IV-6 through IV-9) is less than the average value of 1.41. As the value of b becomes greater than 1.41 (N=5-10, Figures IV-10 through IV-12), the equation has a tendency to overpredict the volumetric strain. This is reflected in the gross overestimation of volumetric strain in Test DC6, cycle N=7. The accuracy of the prediction appears to be independent of cycle number using Equation 4.8 for cycles 10 through 1000. From Figures IV-12 through IV-16, it is evident that the slope b is not dependent on cycle number, primarily because the shear strains are relatively constant over these cycles. Figure IV-19 indicates that Equation 4.8 has a greater tendency to underpredict the volumetric strains for cycles 10 through 1000. This is merely because also plotted on the figure are the data for Tests DC10 and DC11, which utilized moist tamping. Equation 4.8 definitely had a tendency to underpredict the volumetric strains observed in these two

tests. The fact that the prediction seems to be independent of cycle number for cycles 10 through 1000 is consistant with Hadge's findings.

Section 4.3 discusses the various factors influencing the degree of shear strain in drained triaxial compression tests. In particular, it discusses the effect of cyclic shear stress ratio on γ_{pp}, because this was the only factor varied in this investigation. Section 4.4 addresses the issue of how the sample preparation method affects the densification behavior.

4.3 Factors Influencing Degree of Shear Strain

Results of cyclic simple shear tests on sands indicate that the degree of shear strain experienced in a soil depends primarily on the density of the material and the effective stresses acting on it (Silver and Seed, 1971). Thus it would follow that the effective stress path and sample density would be the primary influences on peak-to-peak shear strains in cyclic triaxial tests. Hadge (1979) studied the influence of porosity, n_c; cyclic stress ratio, $\pm\Delta q_{cy}/\bar{p}_o$; mean effective stress, $\bar{p}_o$; and mean shear stress, q_m, on shear strains developed in cyclic triaxial tests on Oosterschelde Fine Sand. The following observations were made:

1. There is a gradual linear increase in γ_{pp} as porosity increases (0.007% in γ_{pp} per 1% in n_c) for values of n_c of 41.0% (D_r = 56.9%) to 46.1% (D_r = 0%).

2. The peak-to-peak shear strain increases directly with cyclic shear stress ratio for values of cyclic stress ratio ranging from 0.05 to 0.35; a slight non-linearity is required to satisfy the condition that $\gamma_{pp} = 0$ when $\Delta q_{cy}/\bar{p}_o = 0$.
3. As the mean effective stress, q_m, increases, there is a direct increase in γ_{pp} for values of $\bar{p}_o$ ranging from 1.0 kg/cm^2 to 5.0 kg/cm^2.
4. The effect of mean shear stress appears to be negligible for values of mean shear stress ratio, $q_m/\bar{p}_o$, between 0.15 and 0.30.

Tests performed in this investigation were run at essentially constant density (porosity), constant mean effective stress, and constant mean shear stress. Variable shear strains were arrived at by changing the cyclic shear stress ratio, $\Delta q_{cy}/\bar{p}_o$. This enabled the determination of the effect of cyclic shear stress ratio on peak-to-peak shear strains, as measured in these cyclic triaxial tests on Leighton-Buzzard 120/200 Sand.

As discussed in Section 4.1, it was found that the peak-to-peak shear strain was much higher in the first few cycles than in the remainder of the test for larger values of $\Delta q_{cy}/\bar{p}_o$. Figure IV-20 is a plot of peak-to-peak shear strain versus cyclic shear stress ratio for cycle N = 1. Note that the data exhibits a high degree of non-linearity. Figure IV-21 shows a similar plot for cycle N = 1000. By this cycle, γ_{pp} has essentially leveled off and become constant for all tests

(recall Figure IV-5). Figure IV-21 indicates that γ_{pp} increases linearly with cyclic stress ratio for this conditio n. Based on these results, it is evident that the peak-to-peak shear strain only increases linearly with cyclic shear stress ratio, for all N, in cases where $\Delta q_{cy}/\bar{p}_o$ is small enough to insure constant shear straining. This is consistent with Hadge's (1979) findings that γ_{pp} was directly proportional to $\Delta q_{cy}/\bar{p}_o$ for all N, for values of $\Delta q_{cy}/\bar{p}_o$ between 0.05 and 0.35 for Oosterschelde Fine Sand. The cyclic shear stress ratio ranged from 0.136 to 0.444 in this investigation.

Plotted on Figures IV-20 and IV-21, for comparison, is the relationship Hadge found for peak-to-peak shear strain, in terms of cyclic stress ratio, for Oosterschelde Fine Sand. Although there are many differences in the two cases (i.e. type of sand, density, and stress conditions), there is a similarity between the results of both test programs within the same range ($0.05 < \Delta q_{cy}/\bar{p}_o < 0.25$).

It was determined by comparing the results of Tests DC10 and DC11 to other comparable tests, that the soil structure of the specimen is also a major factor influencing the amount of densification in drained cyclic compression tests. The effect of sample preparation method is discussed separately in the following section.

4.4 Influence of Sample Preparation Method on Densification

Intuition would tell us that if the method of sample preparation had a major effect on the liquefaction characteris-

tics of sand in cyclic triaxial tests, then it would also have some significant effect on the drained behavior as well. Figure IV-22 plots the volumetric strain versus number of cycles for tests DC7 and DC10 ($\Delta q_{cy}/\bar{p}_o$ = 0.333), which were essentially identical tests, except that the samples were formed by the wet rodding and moist tamped methods, respectively. It is quite clear that there is a large difference in the degree of volume change between the two tests. The moist tamped sample, DC10, underwent approximately 50% higher volumetric strains than did the wet rodded sample, DC7. Figure IV-23 gives a similar plot for tests DC9 and DC11 ($\Delta q_{cy}/\bar{p}_o$ = 0.444) which shows that the moist tamped specimen underwent approximately 70% higher volumetric strains than the wet rodded sample. These larger volumetric strains for the moist tamped samples correspond to higher measured peak-to-peak shear strains, as plotted on Figure IV-5. The moist tamped samples (solid points on Figure IV-5) sustain approximately 10-15% higher shear strains.

Because all other factors were kept constant for these two pairs of tests, the difference in volumetric strain development can be attributed to the preparation method by which the individual samples were formed. Exactly why the moist tamped samples had a tendency towards larger volume change has not been established. Some insight to the reasons can be acquired, however, by studying the stress strain data for two similar tests.

Although these cyclic triaxial tests were not strain-controlled (which would permit the proper evaluation of Young's modulus, E), a modulus with respect to vertical stresses and strains can still be calculated. Whether this modulus is theoretically meaningful is not clear because of the continuously changing strain conditions. However, it may help to compare the stiffness of one test sample to another, at least for the first load cycle, and possibly for cycles thereafter. The modulus is calculated as follows:

$$E_v = \Delta\sigma_v / \Delta\varepsilon_v = (2\ \Delta q_{cy}) / \Delta\varepsilon_v \qquad \text{Equation 4.8}$$

where $\Delta\sigma_v$ and $\Delta\varepsilon_v$ are double amplitude (peak-to-peak) changes in stress and strain, respectively. For cycle N = 1, Equation 4.9 yields a modulus E_v = 1176 kg/cm^2 for Test DC7 (wet rodded) and E_v = 1075 kg/cm^2 for Test DC10 (moist tamped). Although this difference in modulus does not seem significant (approximately 9%), it does indicate that the wet rodded sample is somewhat stiffer in the vertical direction (Test DC7, $D_{r(N=1)}$ = 67.5%; Test DC10, $D_{r(N=1)}$ = 67.2%). At cycle N = 950, the modulus of the rodded sample E_v = 1639 kg/cm^2, and that of the moist tamped sample is equal to 1370 kg/cm^2. The total increase in stiffness is a result of increased density of the samples. The modulus of the wet rodded sample is about 16% higher than that of the moist tamped sample, and because it has undergone significantly less volumetric straining, its relative density is now lower (Test DC7, $D_{r(N=950)}$ = 68.2%; Test DC10, $D_{r(N=950)}$ = 68.7%).

Thus it appears from this brief look at the stress strain behavior, that the differences in volume changes experienced by the two types of samples may be related to the stiffness of the sample in the vertical direction. The method of sample formation is expected to be the direct cause of differences in sample stiffness. Whether a 50% or 70% difference in volumetric strain between moist tamped and wet rodded samples can be attributed totally to slight differences in vertical sample stiffness can not be determined from results of this investigation. Drained static triaxial test results for samples prepared by these two methods might be very helpful in determining if, in fact, the wet rodded samples are initially stiffer in the vertical direction (i.e., higher modulus, E_v), at the same initial density.

4.5 Summary

Six drained cyclic triaxial compression tests were performed in this investigation to determine the densification behavior of Leighton-Buzzard 120/200 Sand. Four tests (DC6-DC9) were performed on samples using the wet rodding method of sample preparation. Two tests (DC10, DC11) utilized the moist tamped method of preparation. The cyclic stress ratio, $\Delta q_{cy}/\bar{p}_o$, was changed to achieve different shear strain in the sample. All other factors ($\bar{p}_o$, q_m, and e) were essentially constant.

It was found (Figure IV-5) that at low values of $\Delta q_{cy}/\bar{p}_o$ (Tests DC6, DC7, DC12), the peak-to-peak shear strains were

generally constant for all N. At higher cyclic stress ratios, however, there were significantly larger peak-to-peak shear strains in the first 10 cycles. The value of peak-to-peak shear strain did tend to level off, however, after this point for these tests.

An analysis based on Hadge (1979), to determine an expression for volumetric strain in terms of cycle number and the value of peak-to-peak shear strain, was performed using data from four tests on wet rodded samples. The occurrance of high shear strains in the first 10 load cycles had a significant affect on the analysis. The result was the development of two separate expressions; one for cycles 1 through 10 (Equation 4.7), and another for cycles 10 through 1000 (Equation 4.8). Hadge (1979) found that one expression was adequate to estimate the densification behavior for cycles 5 through 1000 (Equation 4.4). The analysis by Hadge showed that the line describing volumetric strain versus peak-to-peak shear strain data for any N generally had a constant slope b, and an intercept (expressed in terms of the parameter A) which was directly related to the cycle number N. This was found to apply to Leighton-Buzzard Sand tests, also, for cycles 10 through 1000. For cycles 1 through 10, however, the value of b was slightly dependent upon cycle number N because of the non-linearity in the peak-to-peak shear strain versus cycle number data. As a result, Equation IV-7 generally underpredicted the volumetric strain in the first four or five cycles, but had a tendency to overpredict the volumetric strain from cycle 5 to 10. The

volumetric strain predictions using Equation 4.8 for cycles 10 through 1000 appeared to be independent of cycle number. Figure IV-19 shows that the accuracy of the predictions of volumetric strain using Equations 4.7 and 4.8 is generally within $\pm 50\%$. These expressions also adequately predicted the volumetric strains experienced in samples formed by the moist tamped method. The predictions for these two tests were usually lower for most cycles, however.

It was determined that the peak-to-peak shear strains increased with increasing cyclic stress ratio (Figures IV-20 and IV-21). The relationship was not linear for cycle 1 but was quite linear for cycle 1000. Again this is believed to be a result of the highly non-linear behavior of the peak-to-peak shear strains in the first 10 cycles. Hadge (1979) found that the peak-to-peak shear strain increased linearly with cyclic shear stress ratio for all N between $\Delta q_{cy}/\bar{p}_o$ of 0.05 and 0.35. The results of this investigation are consistent with this finding for the same range of cyclic stress ratios, and for larger ranges, provided the peak-to-peak shear strain has become constant with each load cycle (i.e. cycle 1000).

Tests performed to determine the effect of the sample preparation technique on the densification behavior of the test sand showed that the moist tamped samples had a greater tendency towards volume change (up to about 70% greater) than did the wet rodded samples. The difference in the amount of volumetric strain developed is attributed to the differences in the fabric of the samples, as governed by the method of

preparation incorporated (Figures IV-22 and IV-23). One explanation for the higher resistance of the wet rodded samples toward densification is that these samples may be stiffer in the vertical direction. This is reflected in higher calculated modulus values for the wet rodded samples at various cycles. The method of sample preparation is expected to be the direct cause of differences in sample stiffness.

TEST DC	e_c	D_r (%)	σ_{vc} (kg/cm^2)	σ_{hc} (kg/cm^2)	$\bar{p}_o$ (kg/cm^2)	Δq_{cy} (kg/cm^2)	$\frac{\Delta q_{cy}}{\bar{p}_o}$	$\frac{q_m}{\bar{p}_o}$	N_{final}	$(\varepsilon_v)_{acc}$ (%)	$(\varepsilon_{vol})_{acc}$ (%)
6	0.773	67.2	3.0	1.4	2.2	0.30	0.136	0.364	1000	.041	.073
7	0.772	67.5	3.0	1.5	2.25	0.50	0.222	0.333	950	.064	.241
8	0.749	73.6	3.0	1.5	2.25	0.75	0.333	0.333	1000	.123	.471
9	0.760	70.7	3.0	1.5	2.25	1.00	0.444	0.333	1000	.192	.902
10	0.773	67.2	3.0	1.5	2.25	0.50	0.222	0.333	1000	.083	.382
11	0.771	67.7	3.0	1.5	2.25	1.00	0.444	0.333	1000	.208	1.477
12	0.751	73.1	3.0	1.5	2.25	0.30	0.133	0.333	1000	.039	.051

SUMMARY OF DRAINED CYCLIC COMPRESSION TESTS

TABLE 4-1

DC \ N	1	2	5	10	50	100	250	500	1000
	Volumetric Strain, ε_{vol}, in %								
6	.009	.012	.017	.021	.040	.040	.050	.066	.073
7	.040	.048	.068	.081	.140*	.152*	-	.232	.241*
8	.082	.108	.149	.186	.288	.334	.386	.416	.471
9	.208	.270	.352	.416	.583	.659	.756	.829	.902
10+	.040	.054	.077	.098	.174	.215	.273	.325	.382
11+	.266	.353	.468	.564	.846	.991	1.187	1.334	1.477
12	.005	.007	.010	.013	.027	.033	.039	.045	.051

* Strain for cycle ±50 cycles different from N specified.

\+ Samples prepared by moist compaction method.

TABLE 4-2 SUMMARY OF VOLUMETRIC STRAIN DEVELOPMENT IN DRAINED CYCLIC TESTS

DC \ N	1	2	5	10	50	100	250	500	1000
	Vertical Strain, ε_v, in %								
6	-.012	-.011	-.009	-.006	.002	.006	.014	.023	.031
7	-.023	-.020	-.014	-.006	.019	.031*	-	.076	.096*
8	-.050	-.034	-.010	.011	.075	.105	.142	.167	.197
9	.061	.174	.303	.385	.568	.637	.720	.770	.812
10+	-.020	-.016	-.007	.001	.038	.057	.091	.122	.159
11+	-.017	.110	.265	.378	.670	.822	1.017	1.152	1.273
12	.002	.003	.004	.006	.010	.001	.005	.008	.012

* Strain for cycle ±50 cycles different from N specified.

\+ Samples prepared by moist compaction method.

TABLE 4-3

SUMMARY OF VERTICAL STRAIN DEVELOPMENT IN DRAINED CYCLIC TESTS

Peak-To-Peak Shear Strain, γ_{pp}, in %

DC \ N	1	2	5	10	50	100	250	500	1000
6	.053	.044	.042	.041	.040	.043	.042	.043	.041
7	.115	.079	.079	.074	.058*	.068*	-	.064	.064*
8	.258	.178	.148	.137	.128	.123	.121	.120	.123
9	.650	.446	.312	.265	.218	.208	.198	.197	.192
10+	.128	.094	.087	.085	.079	.080	.080	.081	.083
11+	.732	.497	.350	.293	.242	.228	.218	.212	.208
12	.042	.040	.041*	.039	.039	.039	.039	.040	.039

* Strain for cycle ±50 cycles different from N specified.

\+ Samples prepared by moist compaction method.

TABLE 4-4

SUMMARY OF PEAK-TO-PEAK SHEAR STRAINS IN DRAINED CYCLIC TESTS

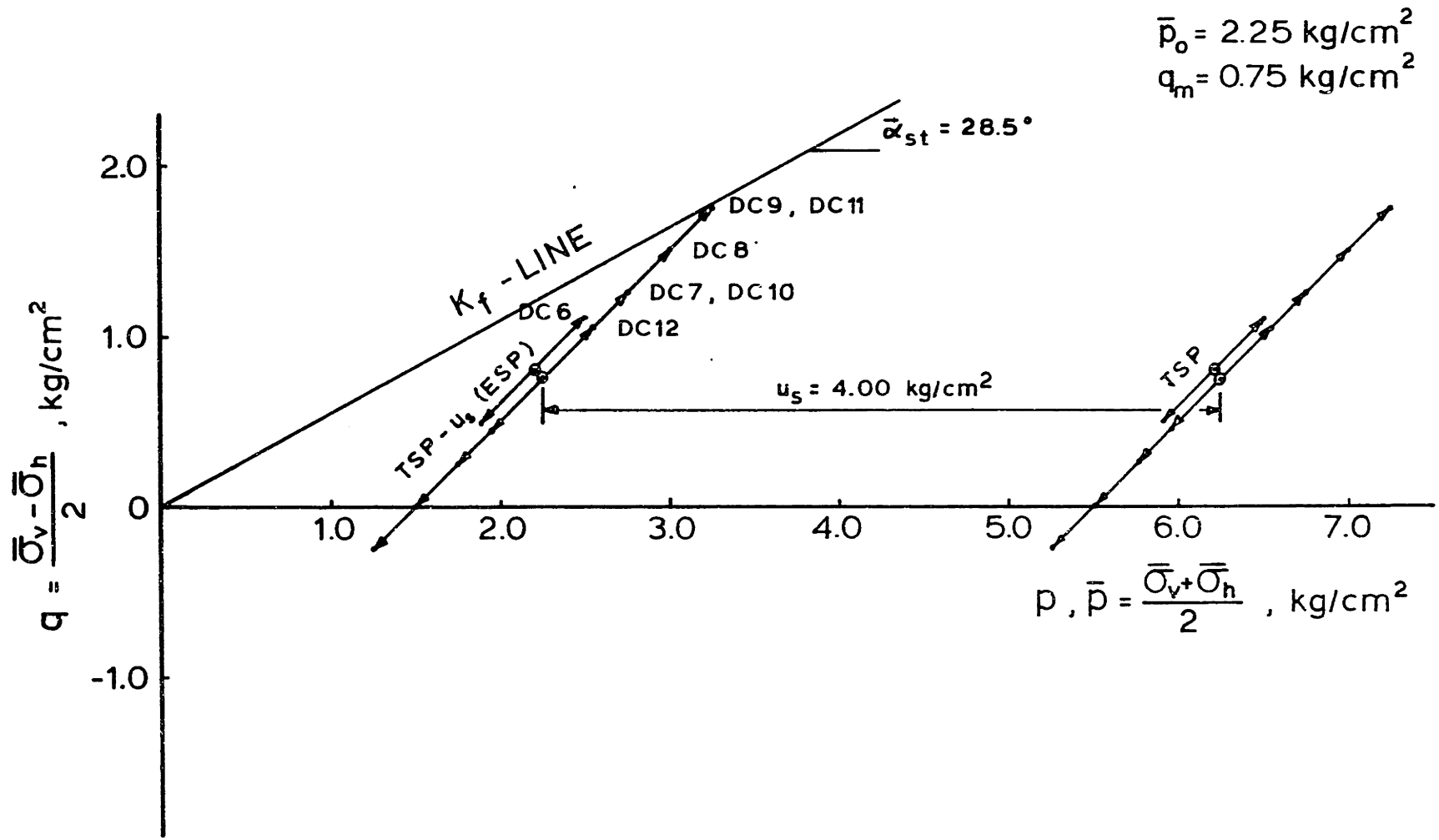

TOTAL AND EFFECTIVE STRESS PATHS
FOR CYCLIC COMPRESSION TESTS

FIGURE IV-1

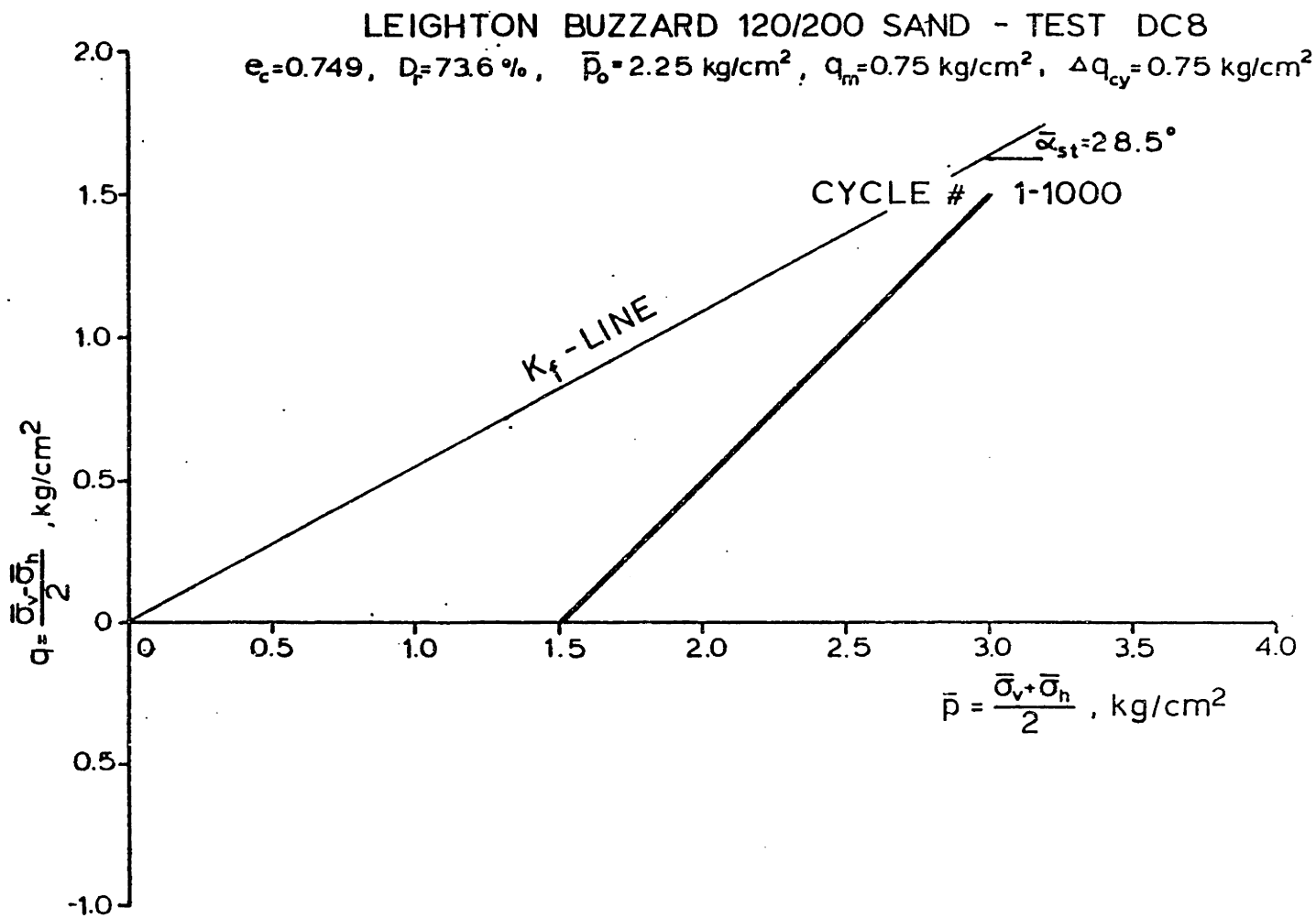

EFFECTIVE STESS PATH - TEST DC 8

FIGURE IV-2

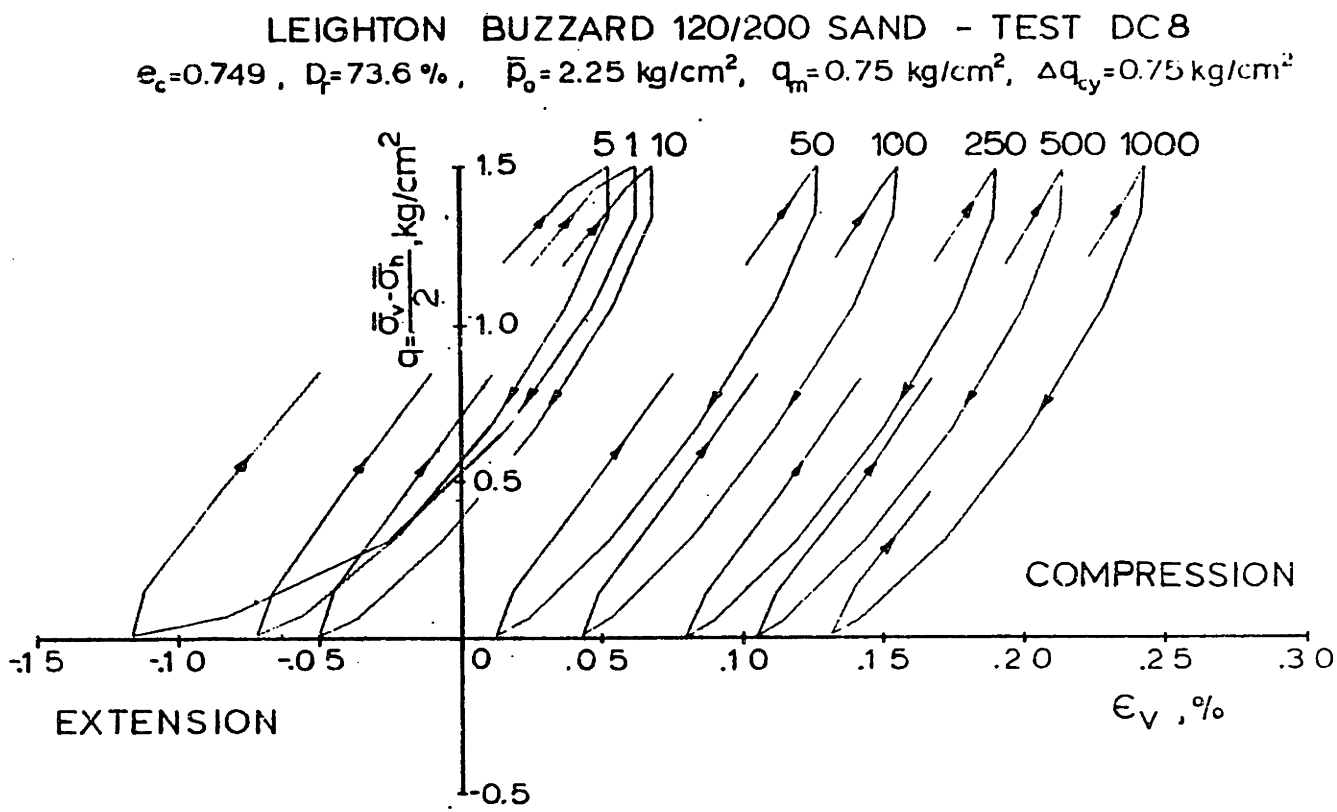

STRESS VERSUS STRAIN PLOTS FOR SELECTED CYCLES- TEST DC8

FIGURE IV-3

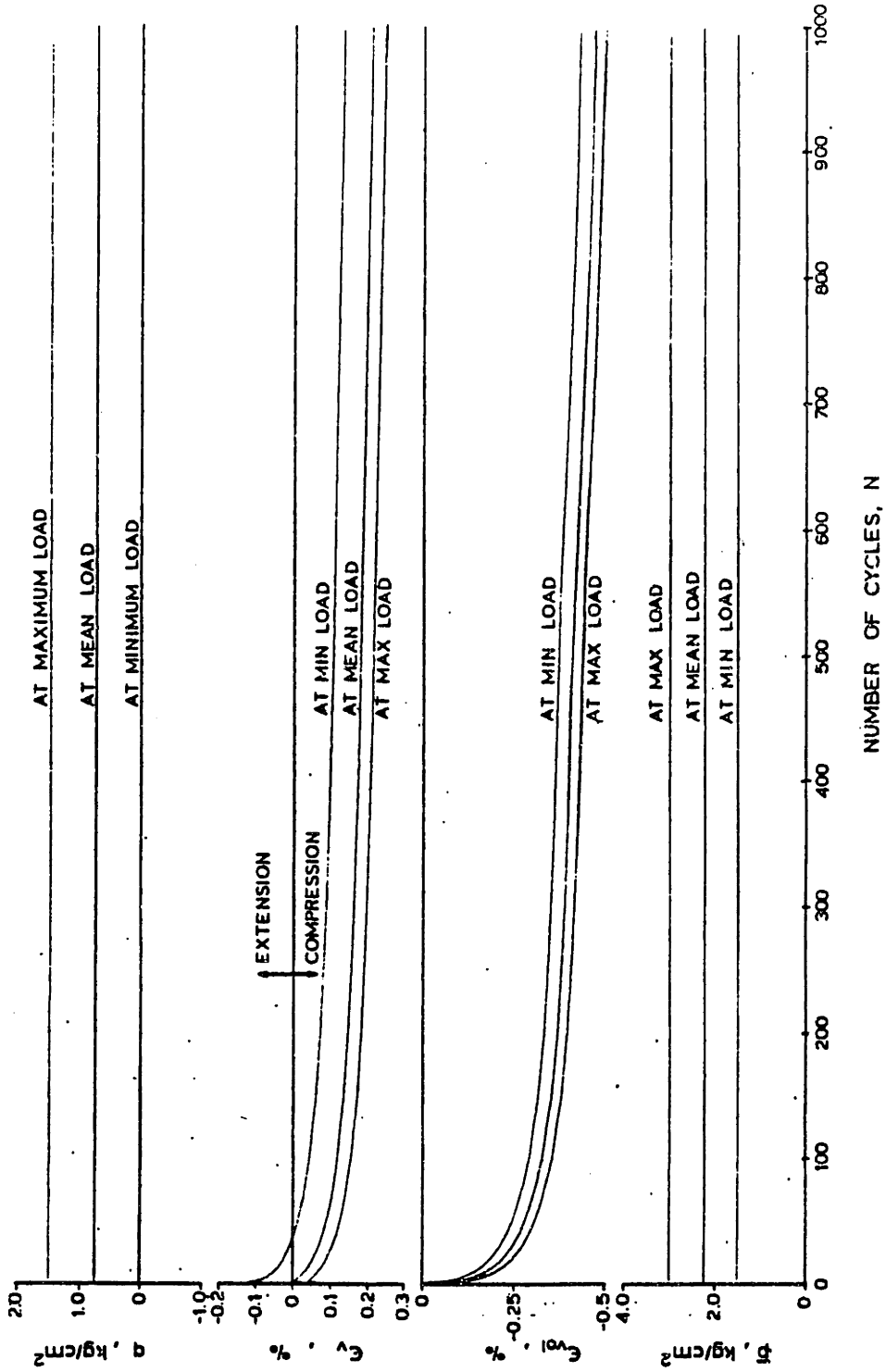

SUMMARY OF STRESS AND STRAIN DEVELOPMENT
TEST DC8

FIGURE IV-4

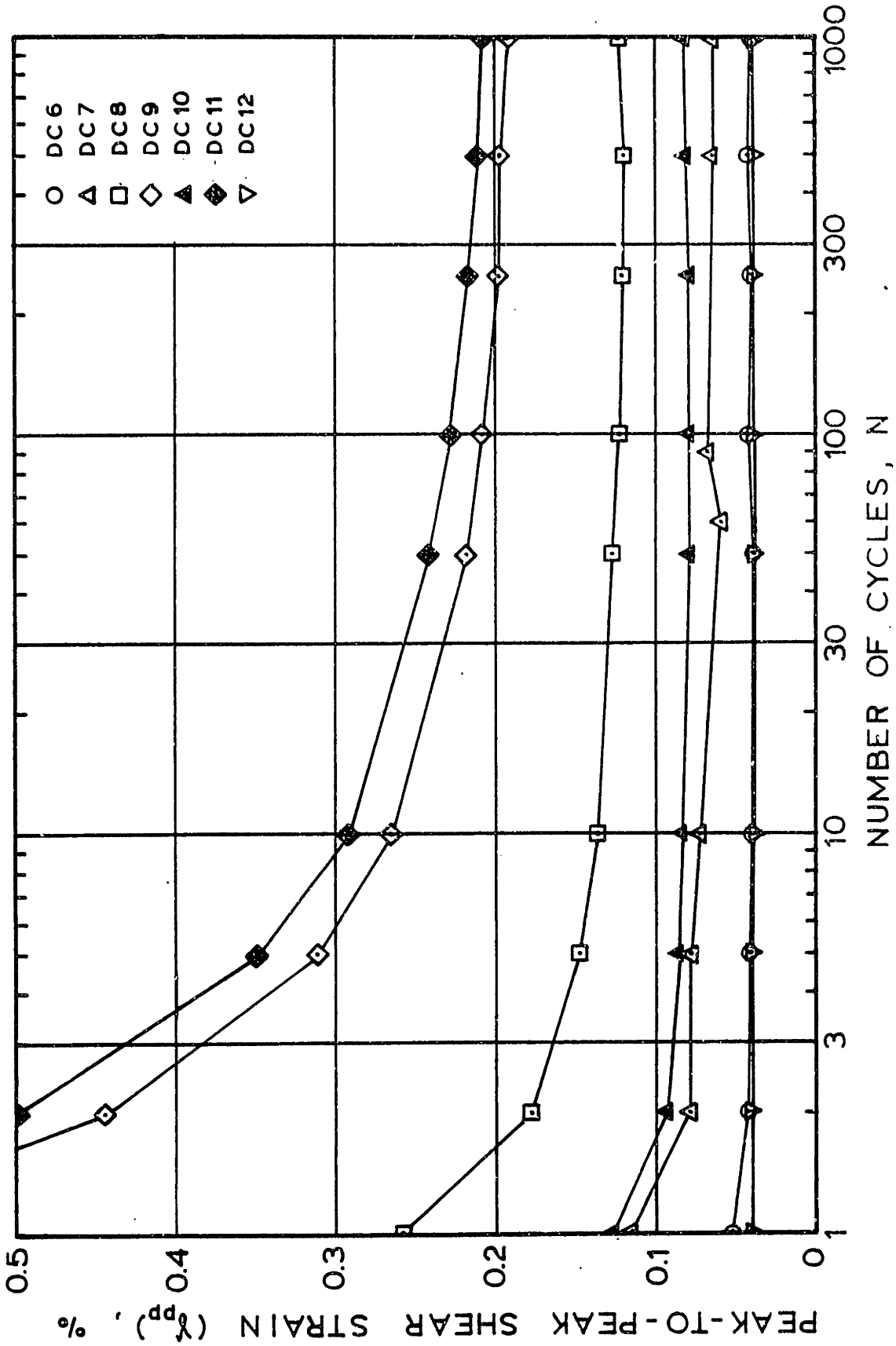

PEAK-TO-PEAK SHEAR STRAIN VERSUS CYCLE NUMBER

FIGURE IV-5

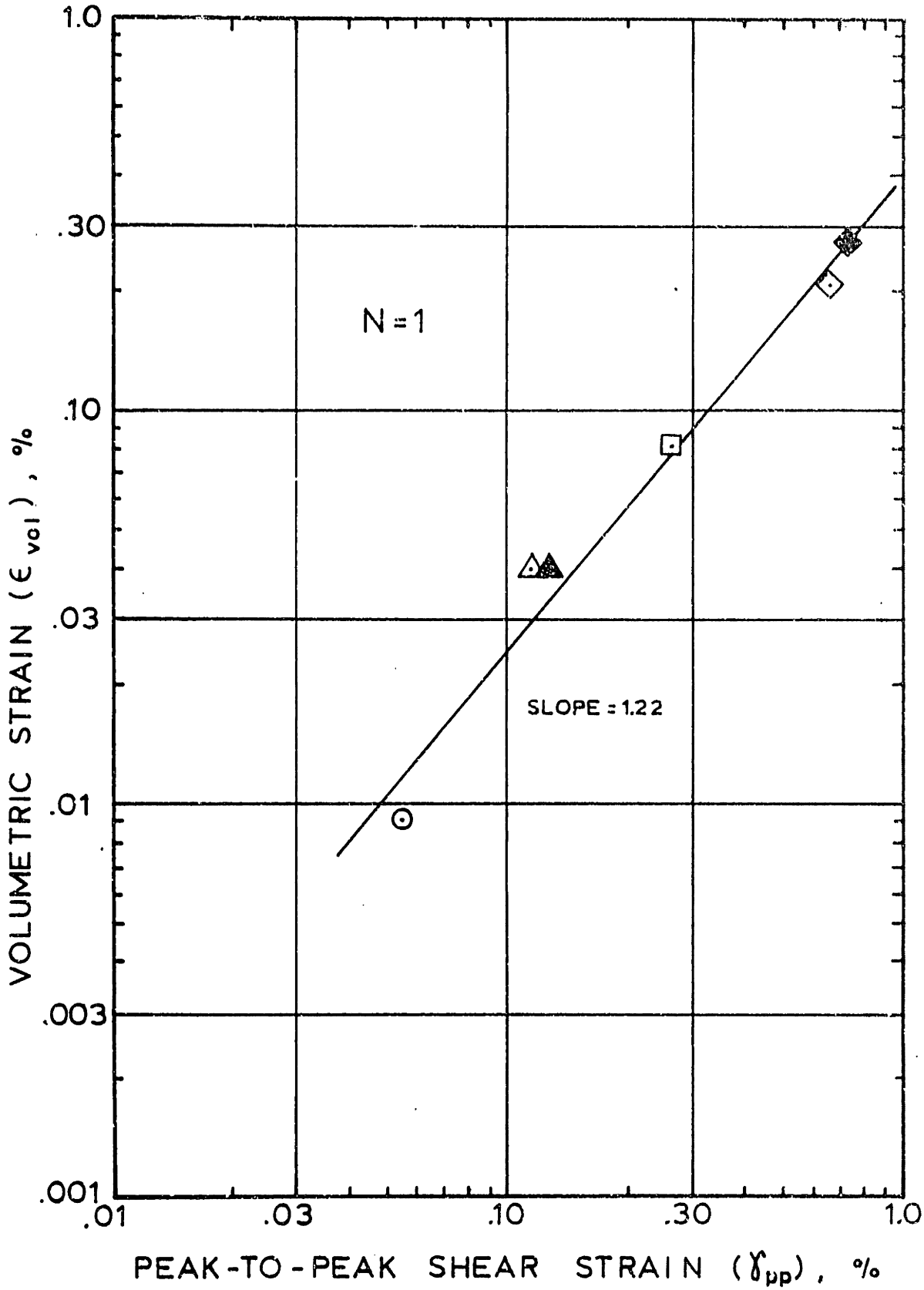

ϵ_{vol} VERSUS γ_{pp} FOR N=1

FIGURE IV-6

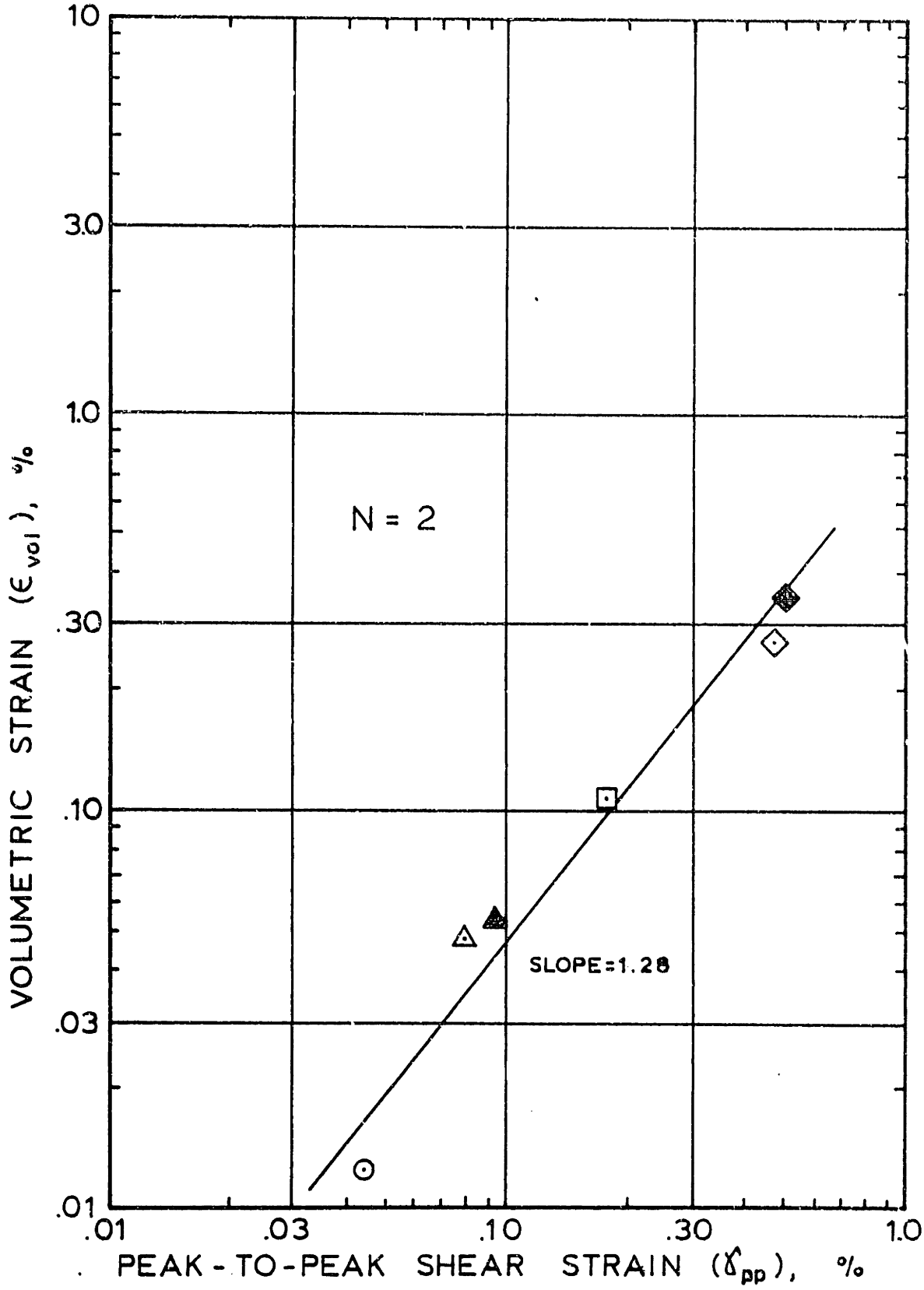

ϵ_{vol} VERSUS γ_{pp} FOR N=2

FIGURE IV-7

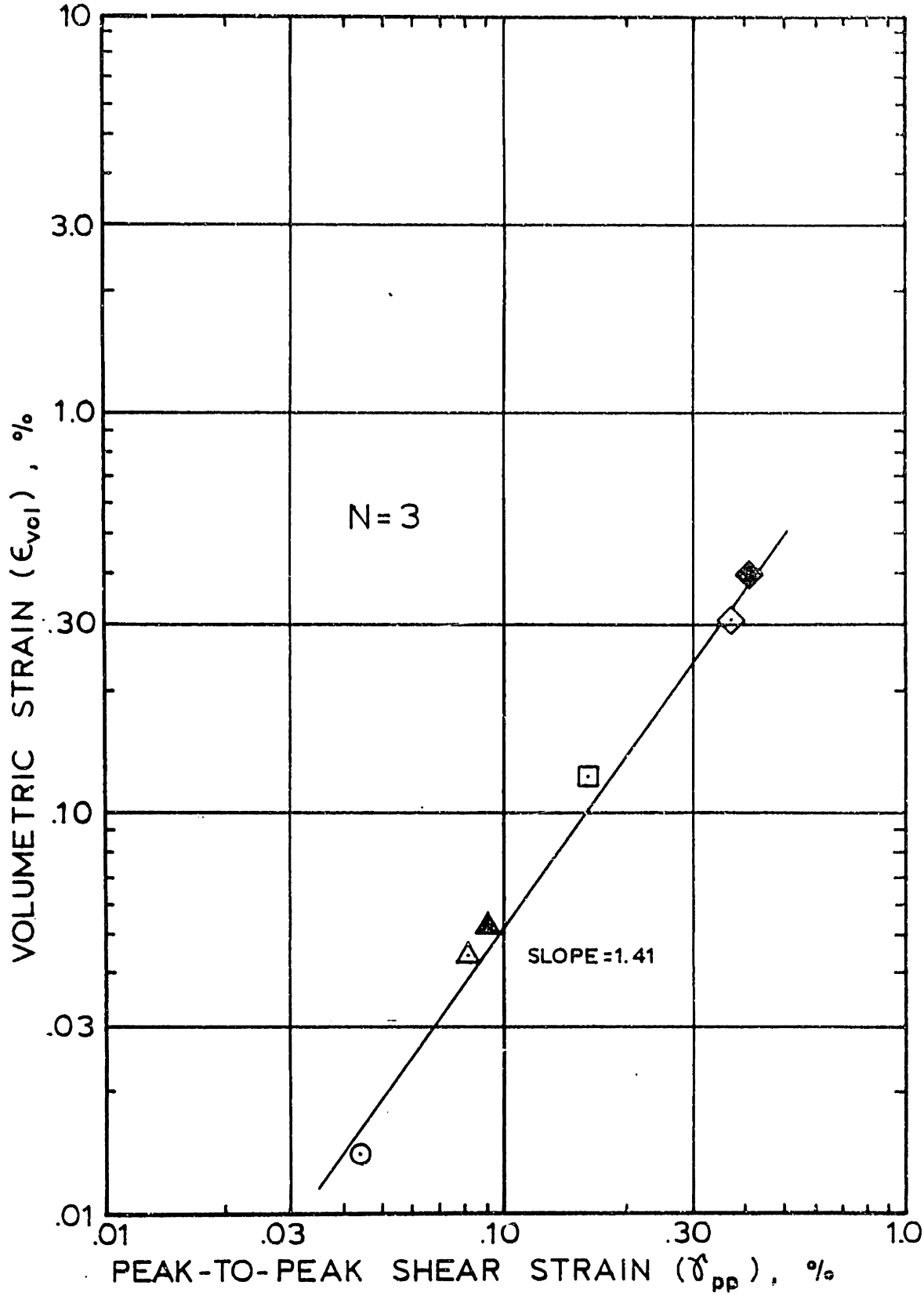

ϵ_{vol} VERSUS γ_{pp} FOR N=3

FIGURE IV-8

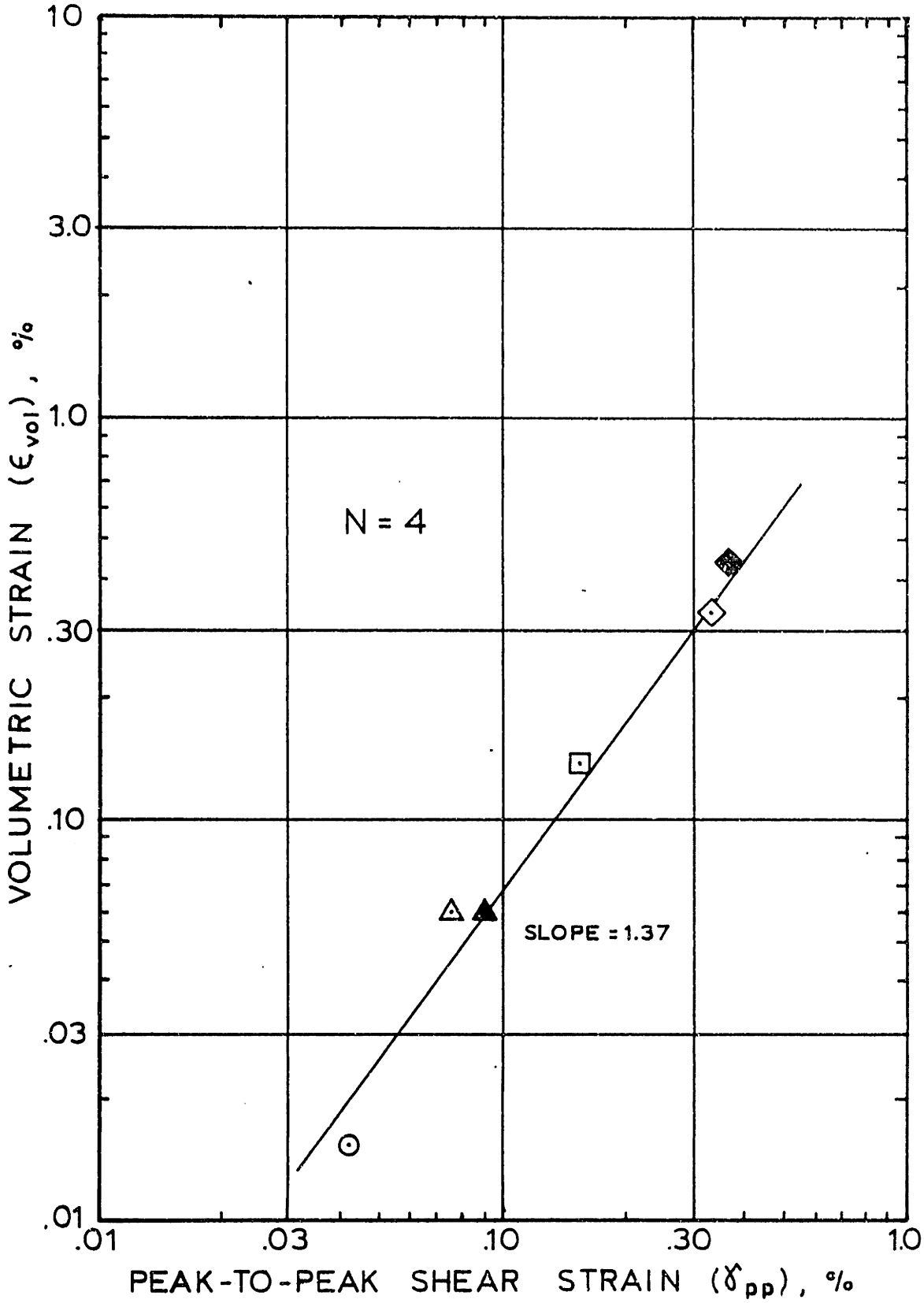

ϵ_{vol} VERSUS γ_{pp} FOR N=4

FIGURE IV-9

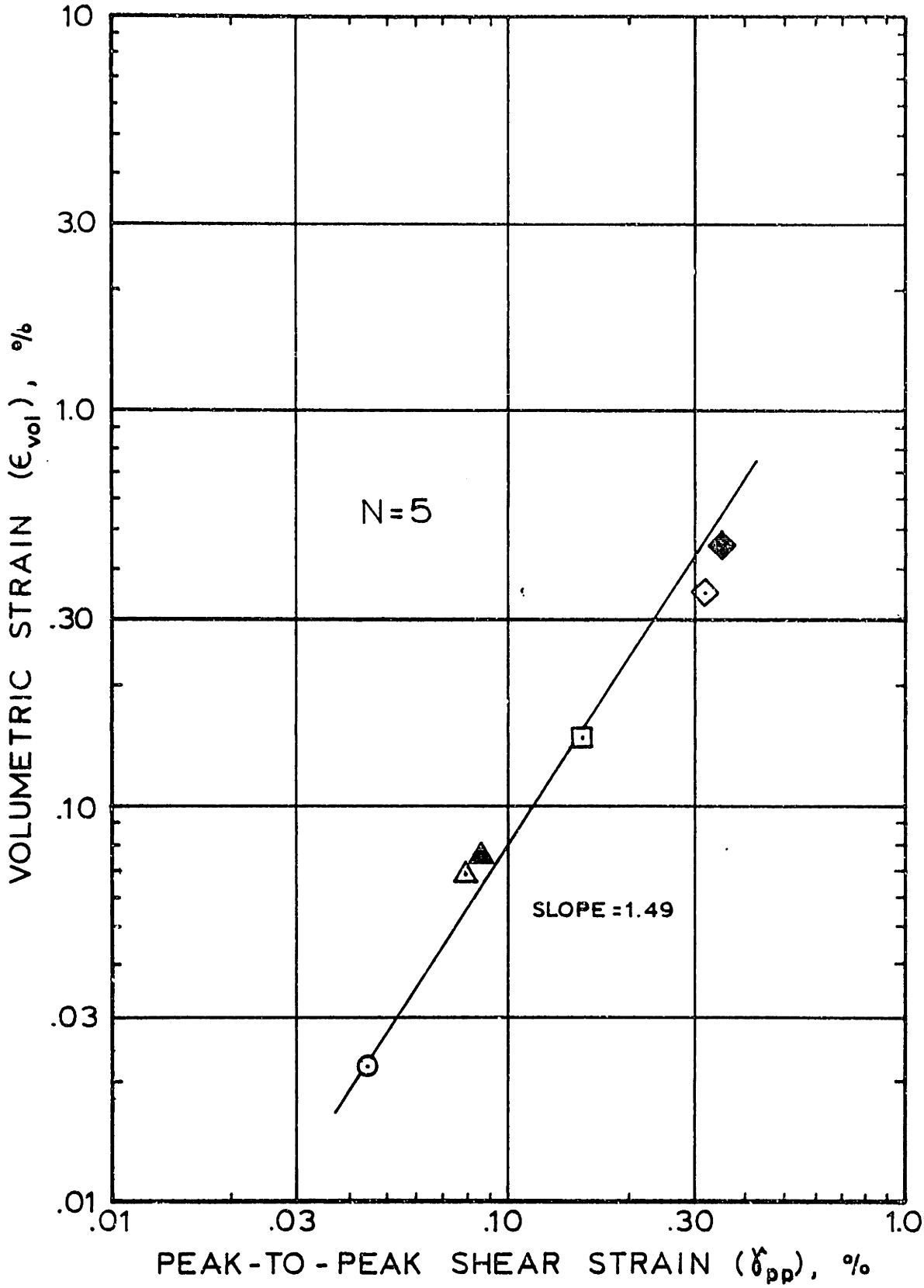

ϵ_{vol} VERSUS γ_{pp} FOR N=5

FIGURE IV-10

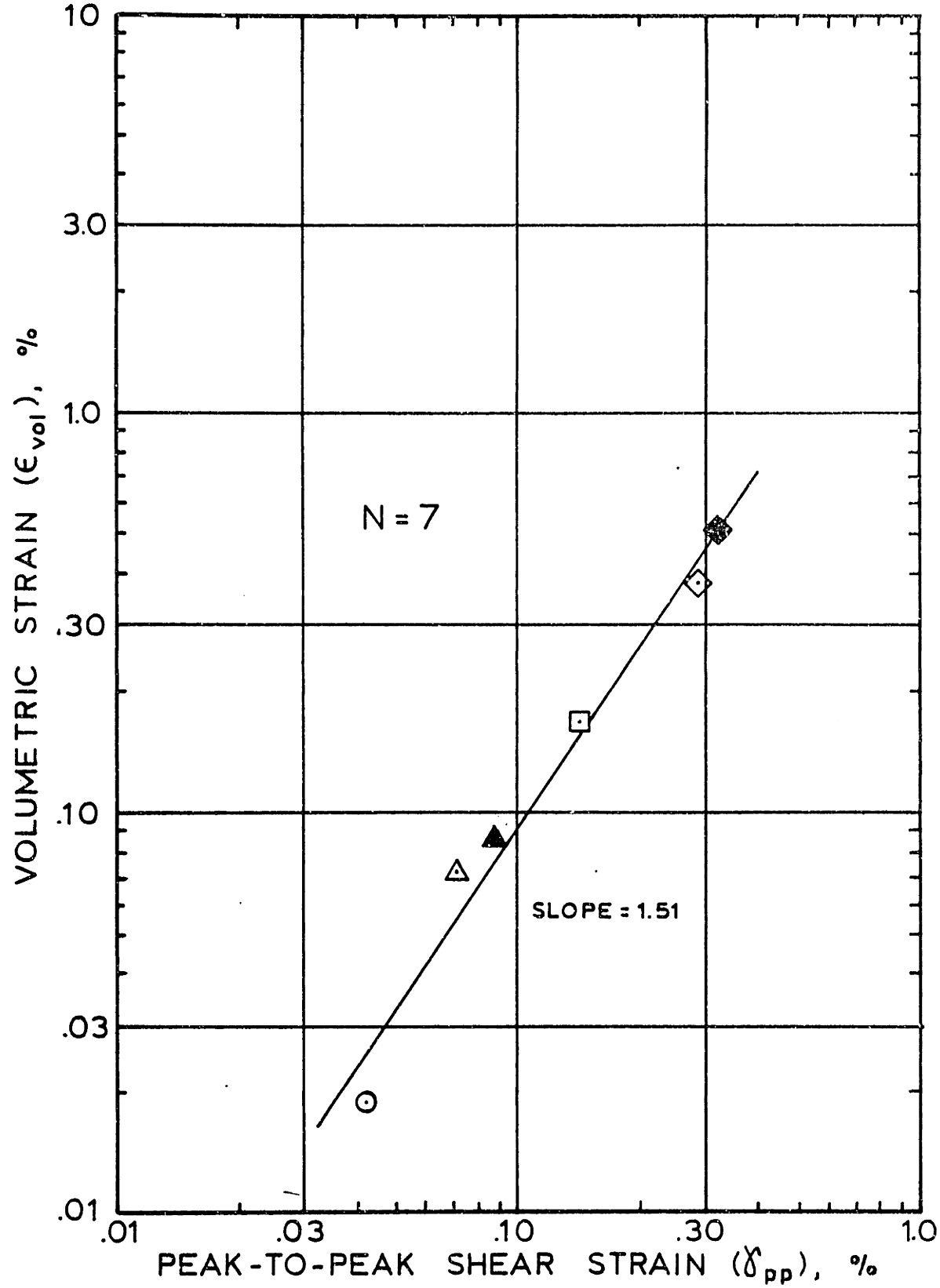

ϵ_{vol} VERSUS γ_{pp} FOR N=7

FIGURE IV-11

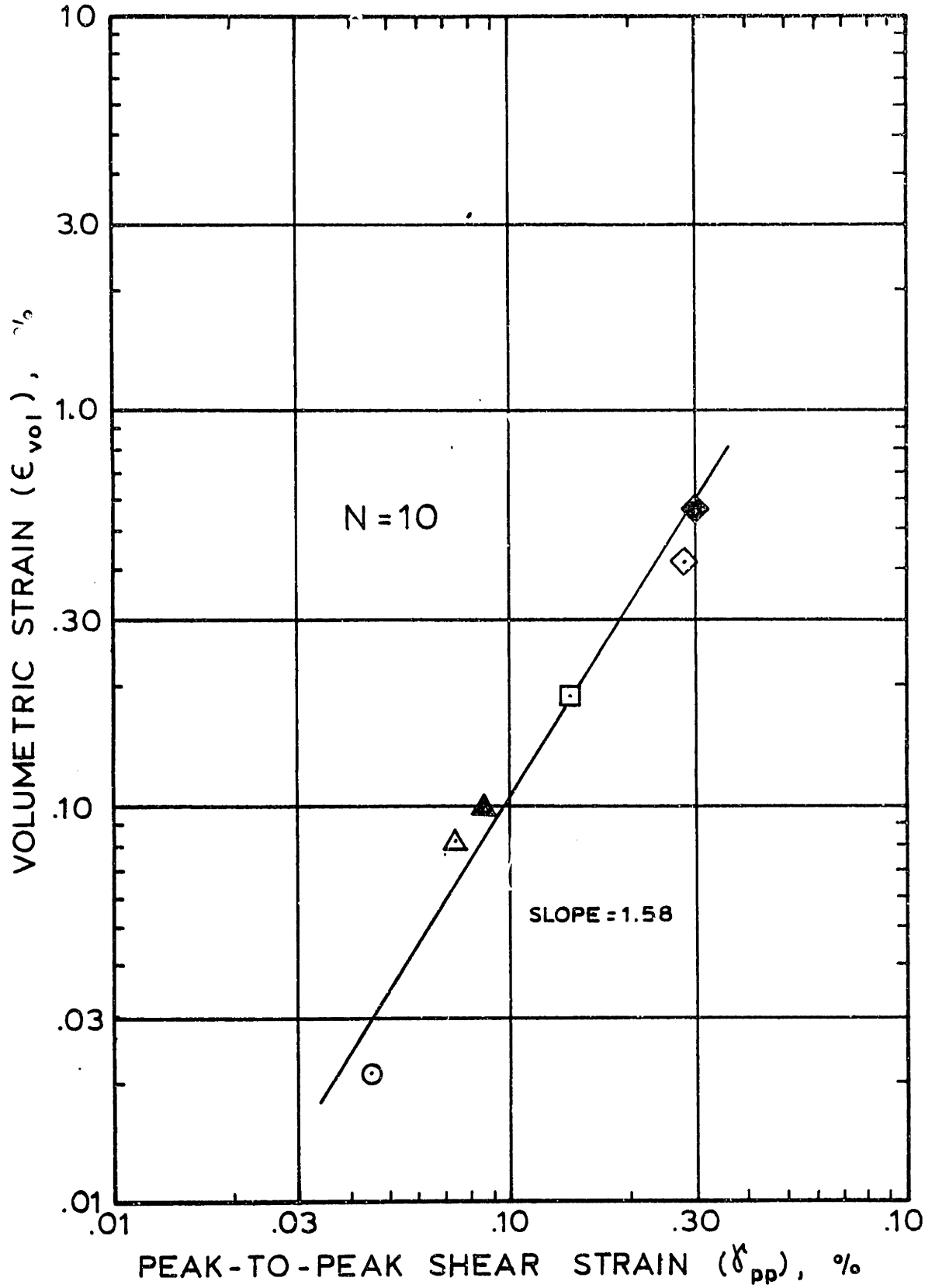

ϵ_{vol} VERSUS γ_{pp} FOR N=10

FIGURE IV-12

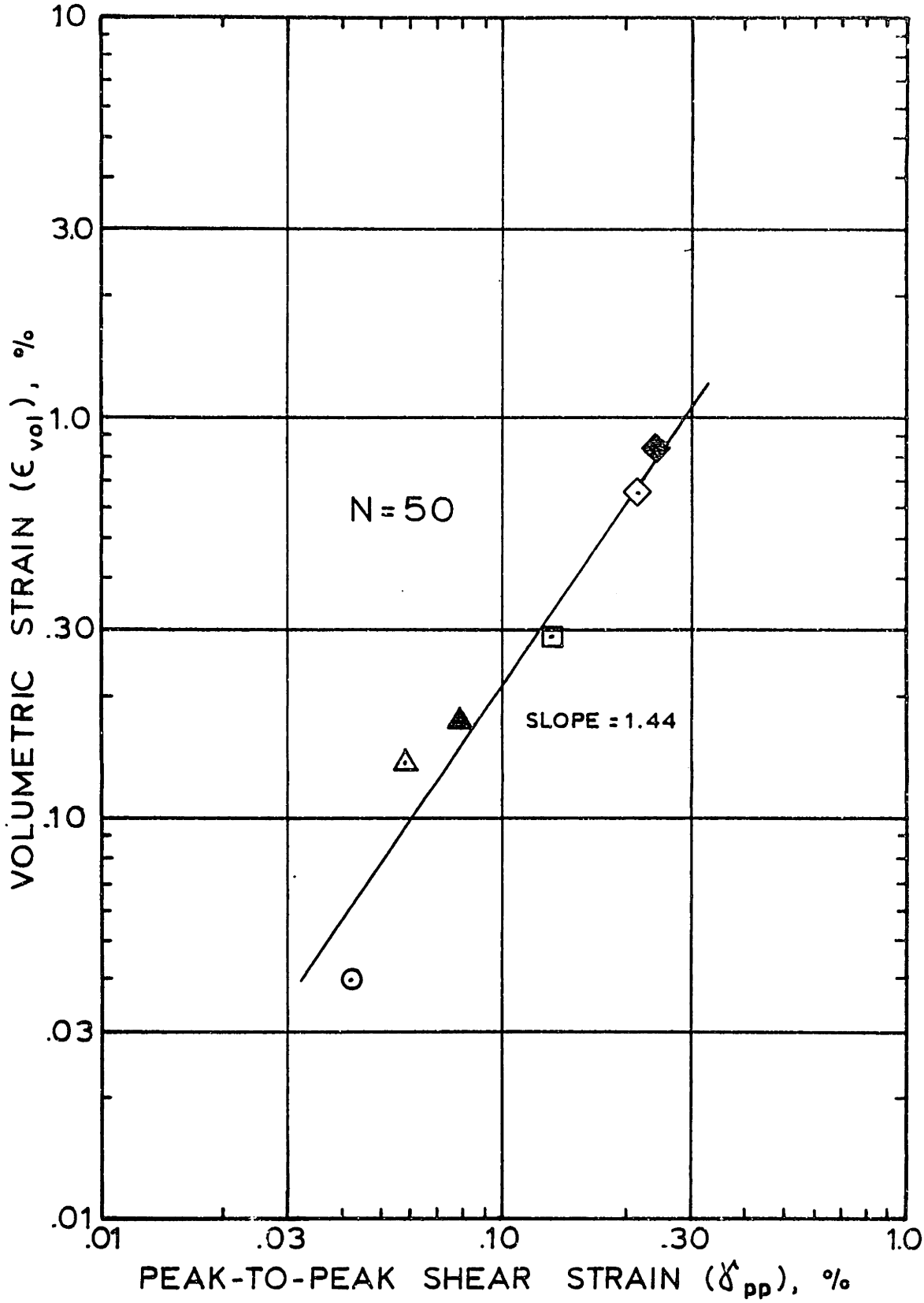

ϵ_{vol} VERSUS γ_{pp} FOR N=50

FIGURE IV-13

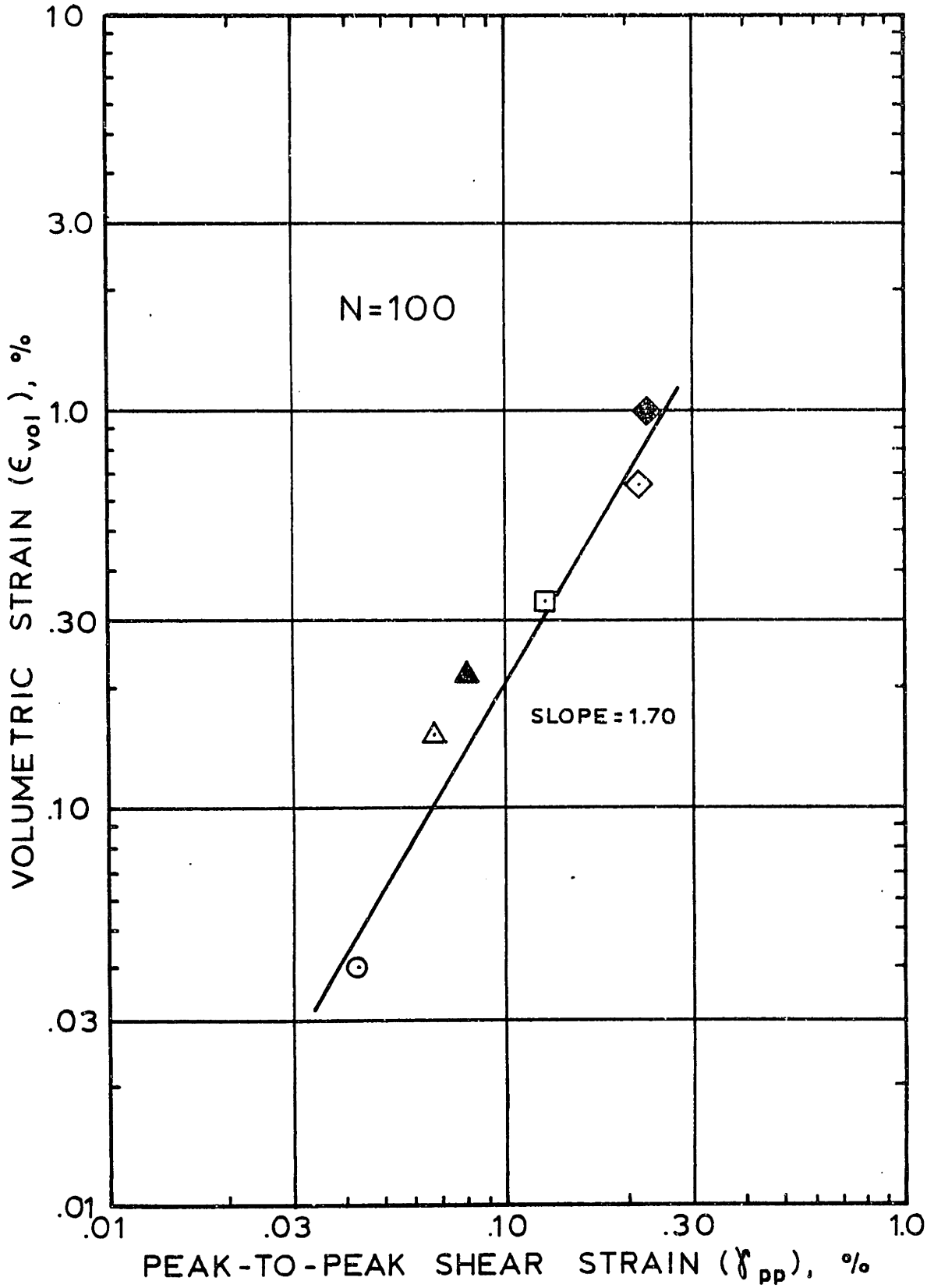

ϵ_{vol} VERSUS γ_{pp} FOR N=100

FIGURE IV-14

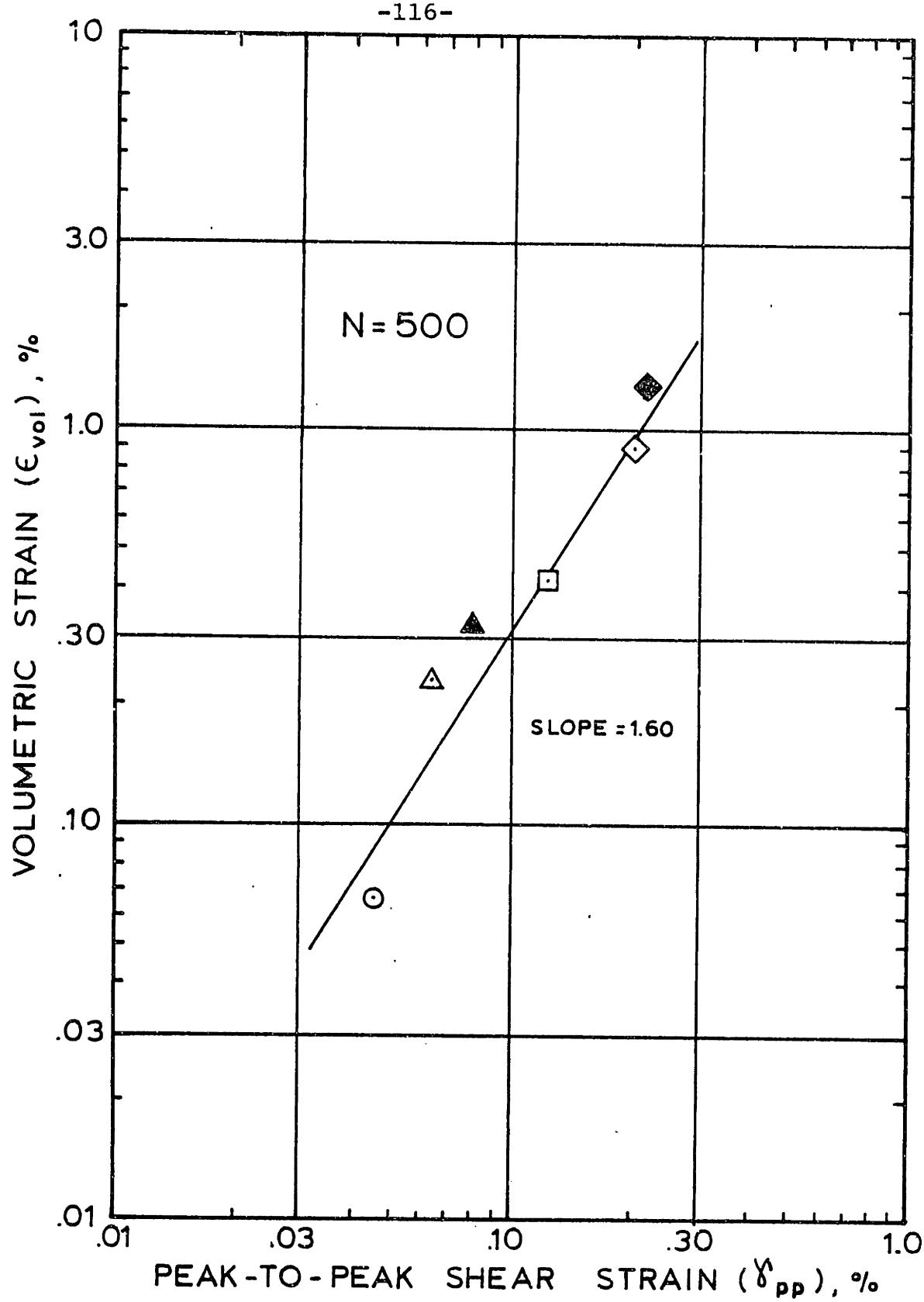

ϵ_{vol} VERSUS γ_{pp} FOR N=500

FIGURE IV-15

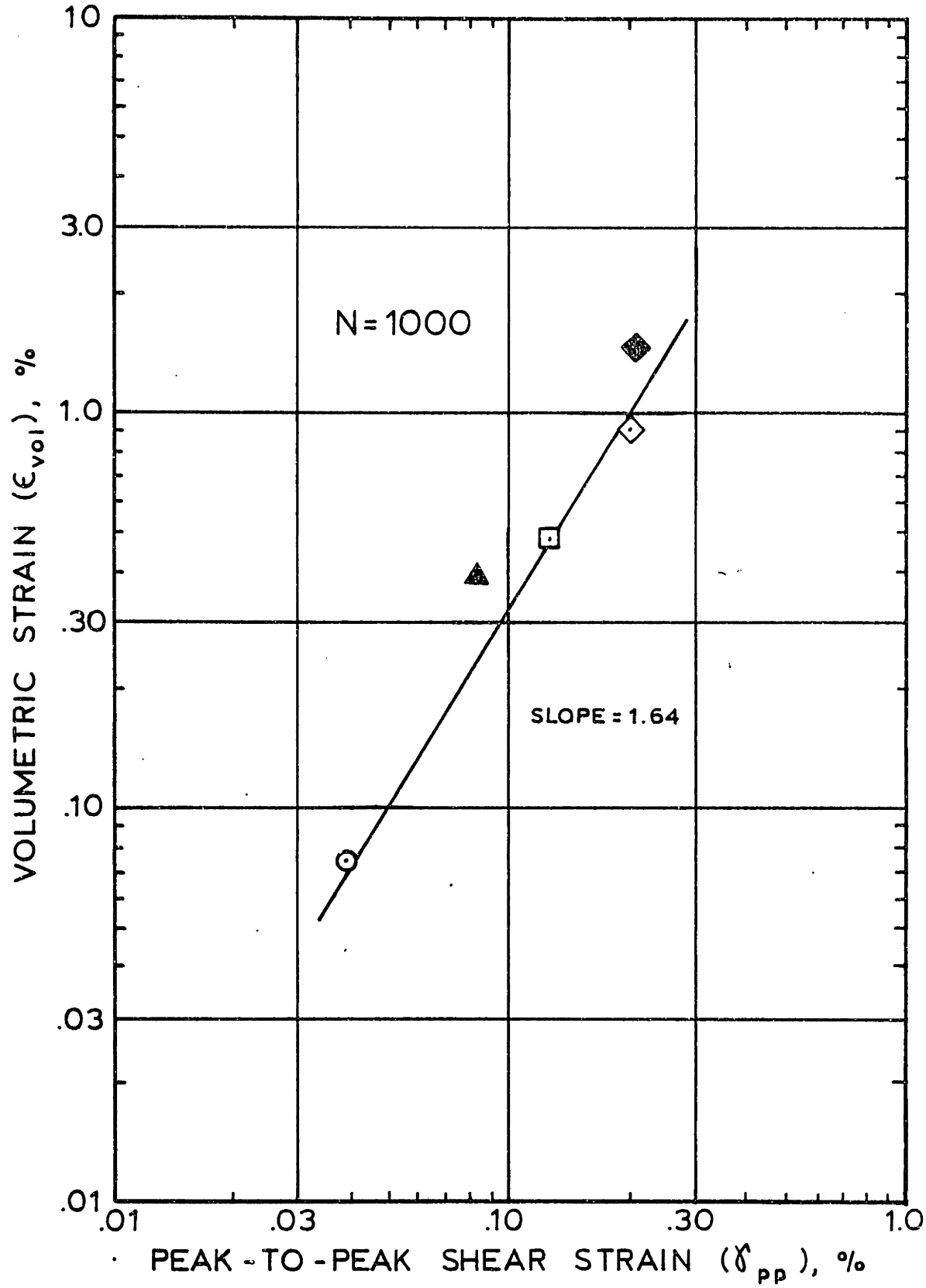

ϵ_{vol} VERSUS γ_{pp} FOR N=1000

FIGURE IV-16

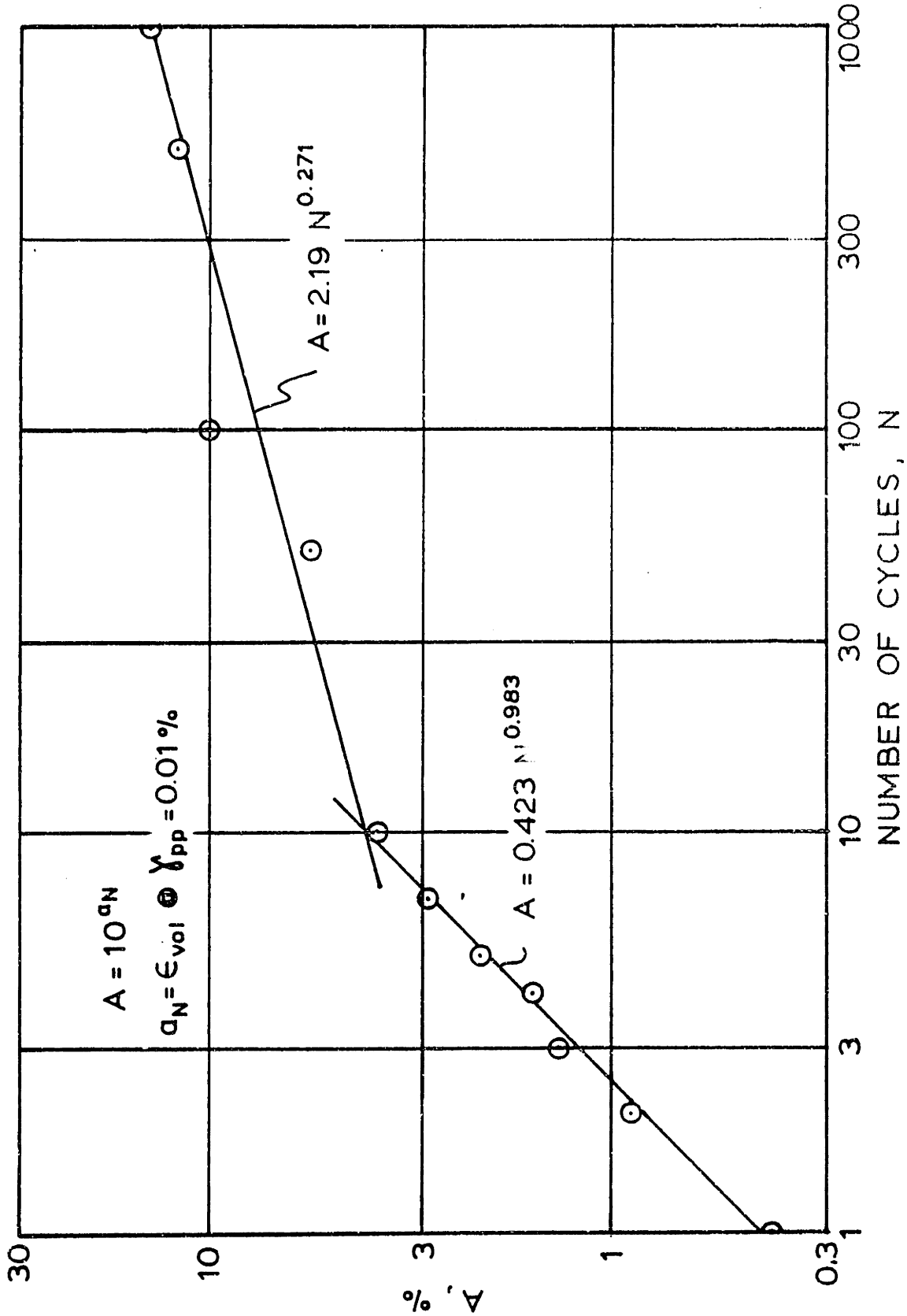

"A" VERSUS CYCLE NUMBER

FIGURE IV-17

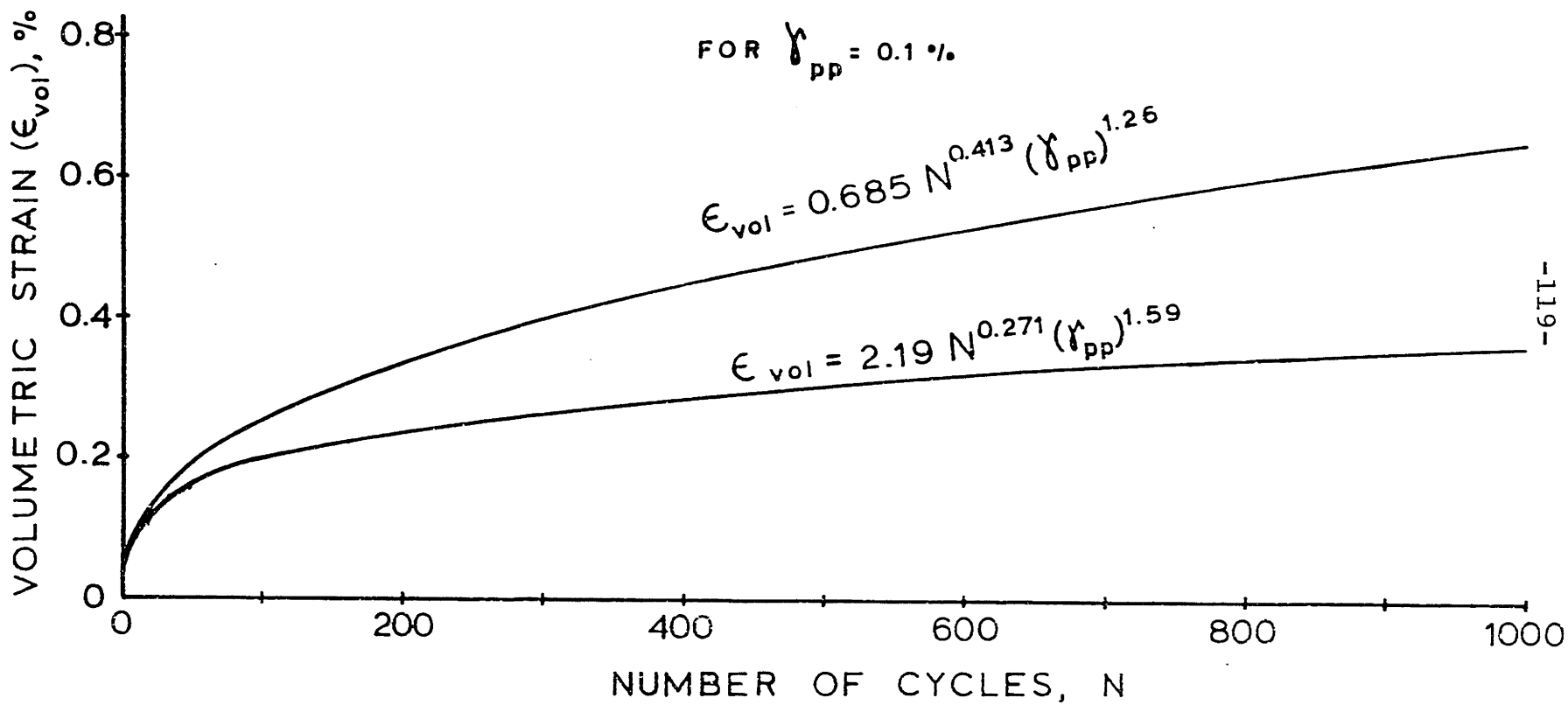

COMPARISON OF EQUATIONS 4.4 AND 4.8 FOR γ_{pp} = 0.1 %

FIGURE IV-18

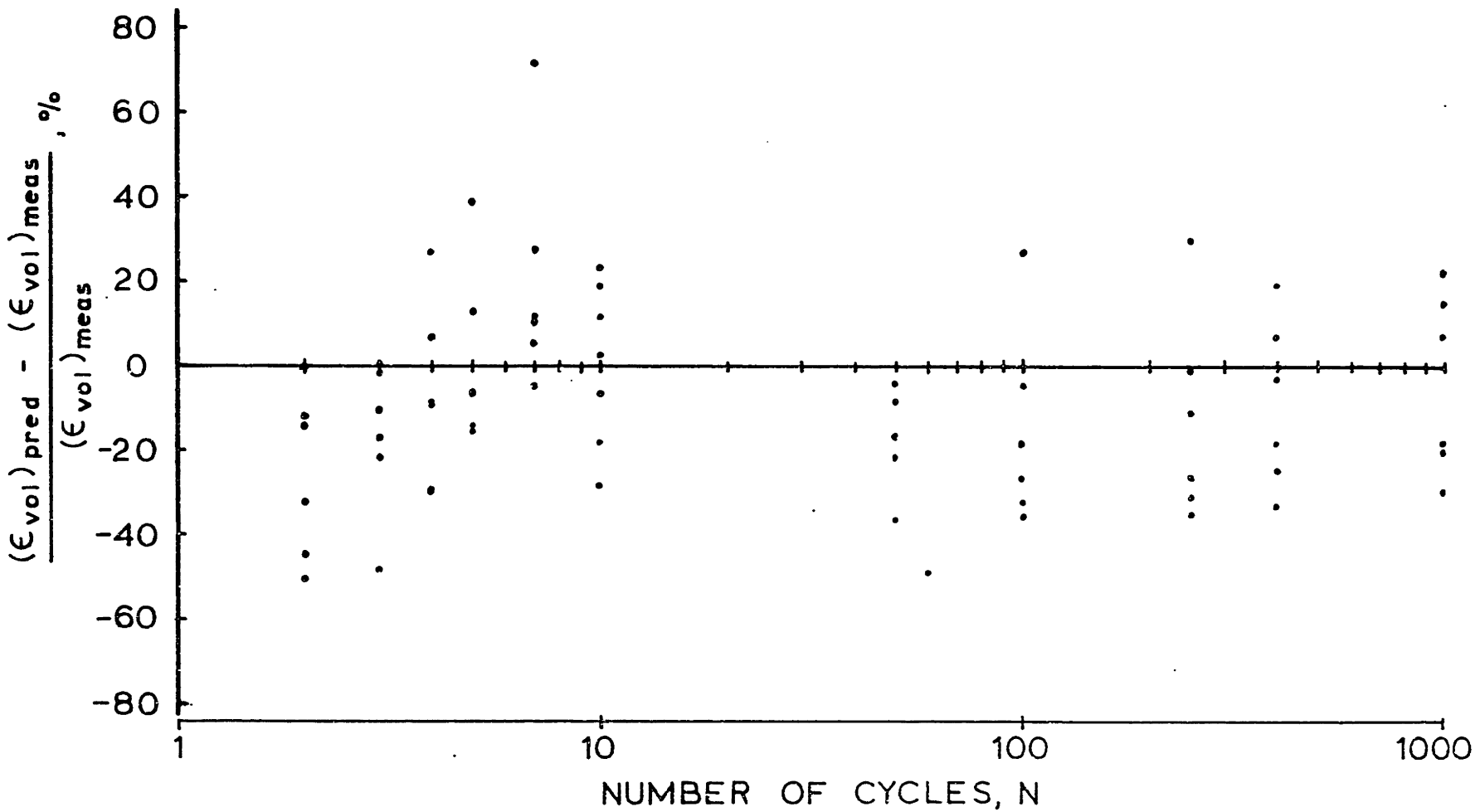

ACCURACY OF VOLUMETRIC STRAIN PREDICTIONS

FIGURE IV-19

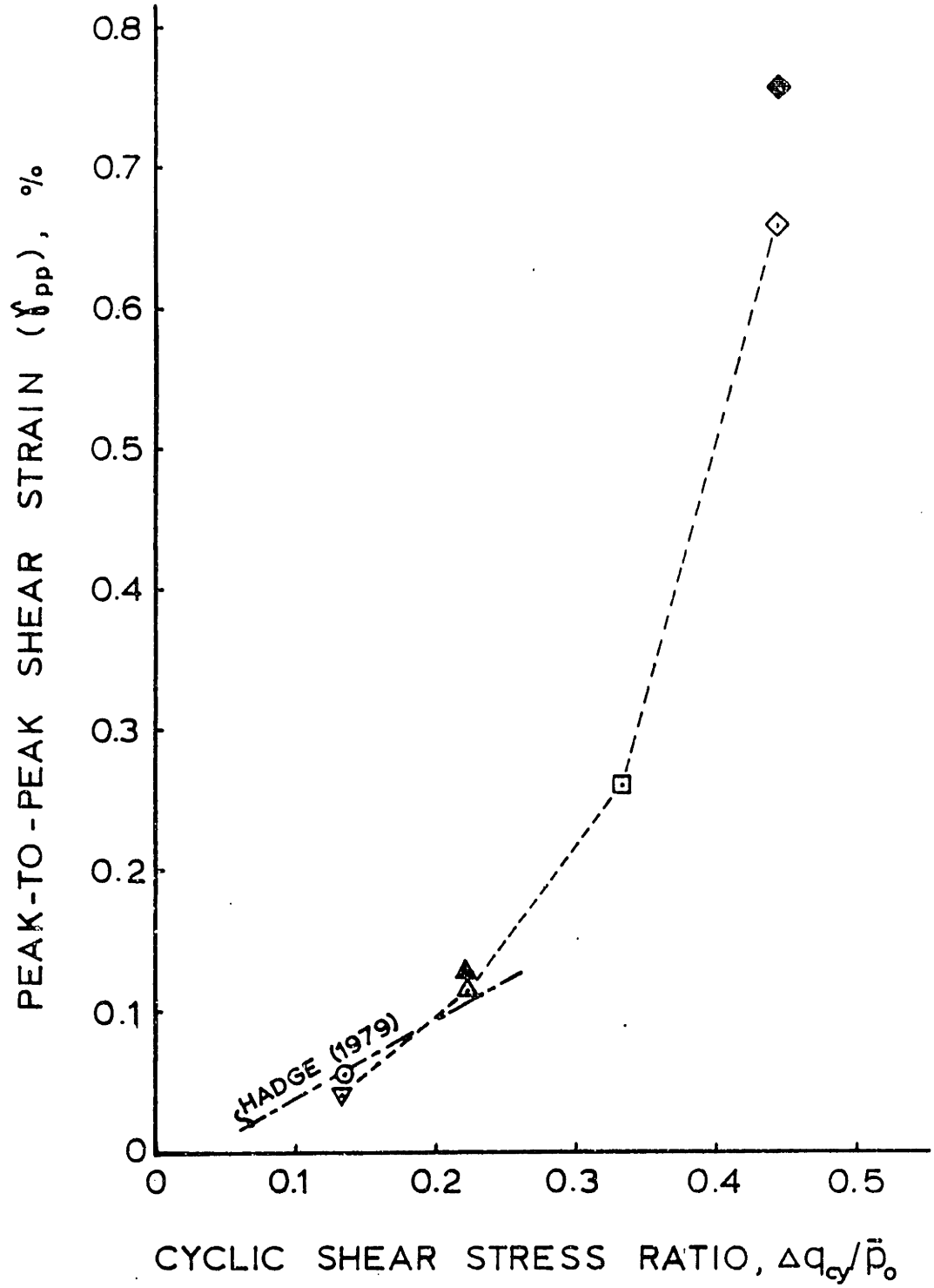

PEAK-TO-PEAK SHEAR STRAIN VERSUS CYCLIC SHEAR STRESS RATIO FOR N=1

FIGURE IV-20

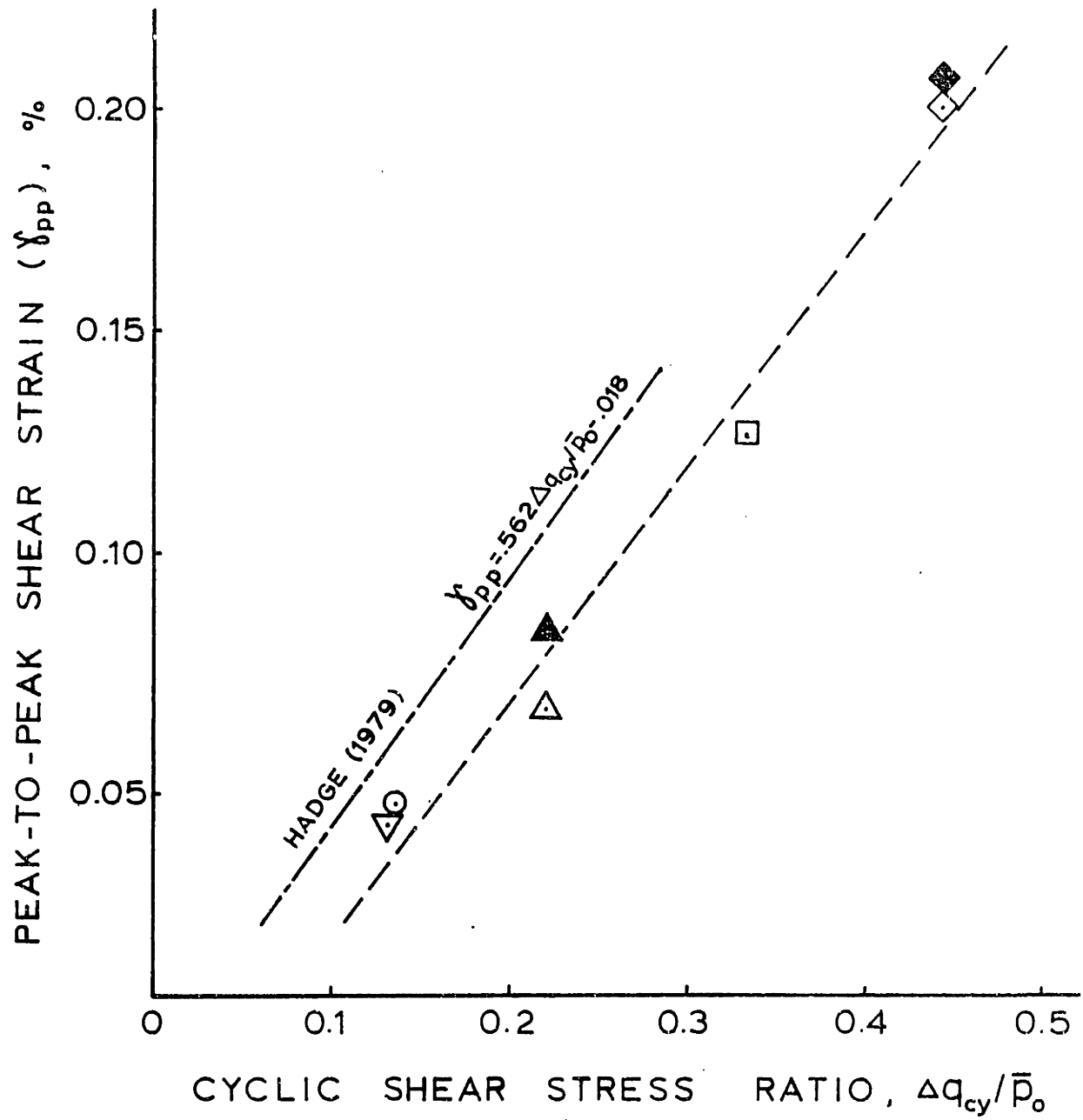

PEAK-TO-PEAK SHEAR STRAIN VERSUS CYCLIC SHEAR STRESS RATIO FOR N=1000

FIGURE IV-21

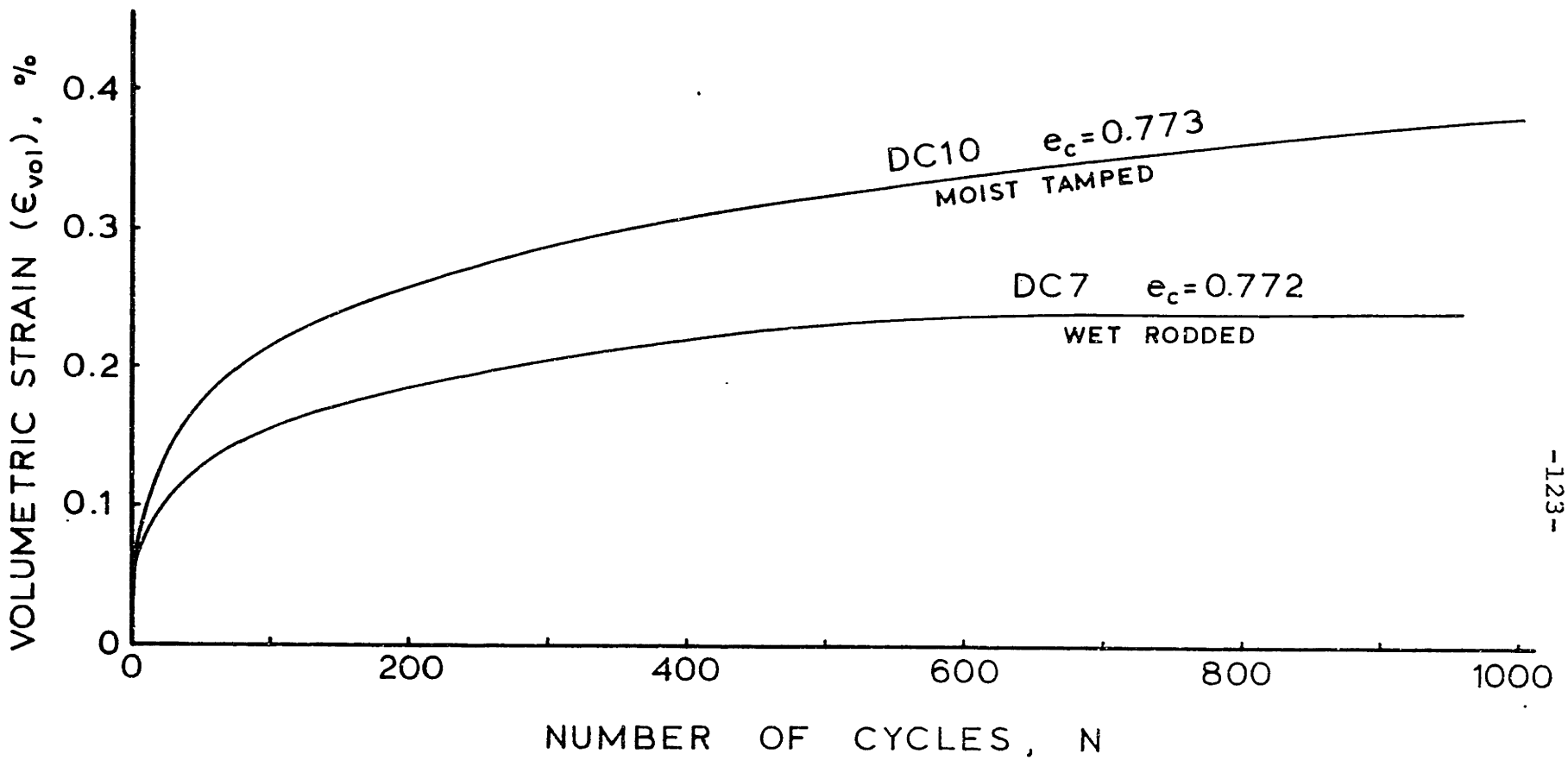

VOLUMETRIC STRAIN DEVELOPMENT FOR TESTS DC7, DC10

FIGURE IV-22

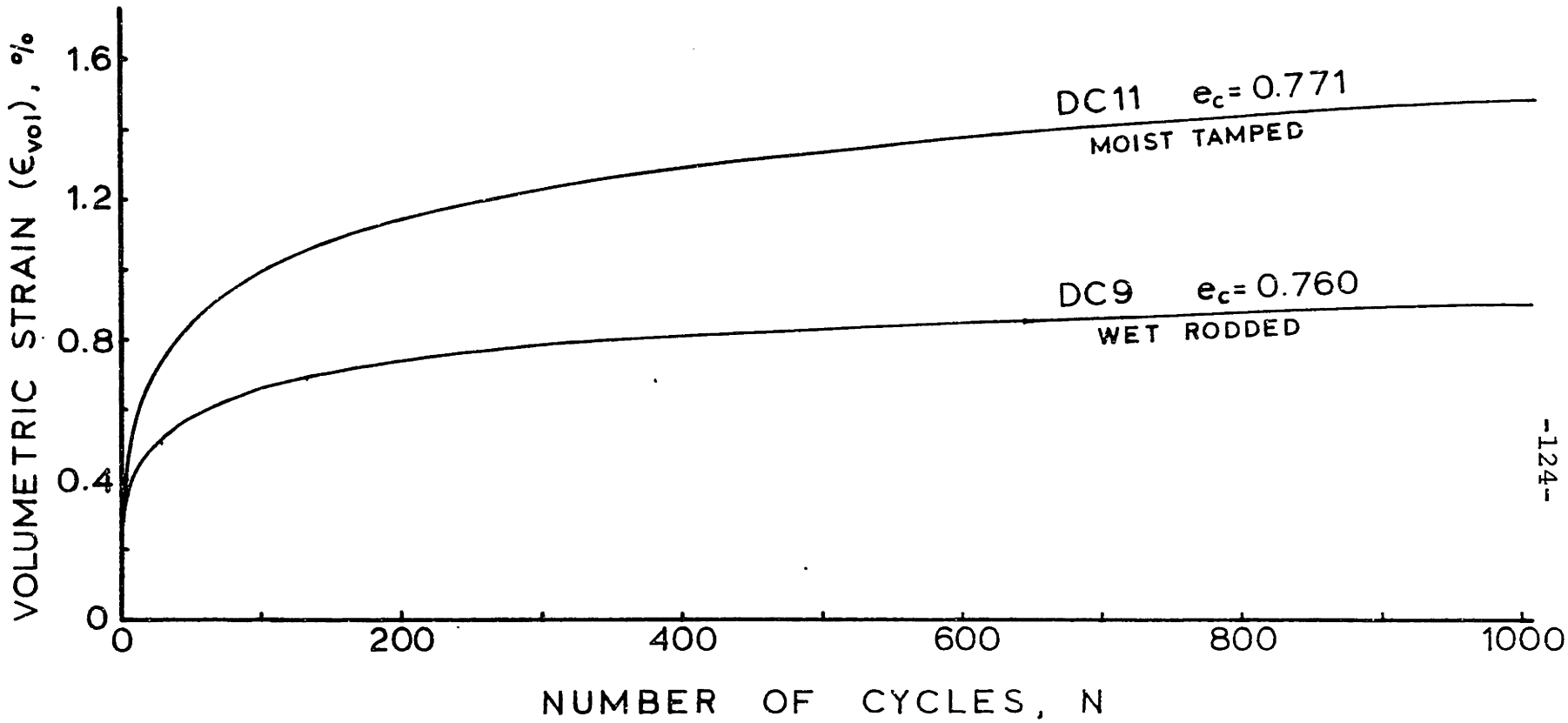

VOLUMETRIC STRAIN DEVELOPMENT FOR TESTS DC9, DC11

FIGURE IV-23

CHAPTER FIVE - LIQUEFACTION BEHAVIOR OF LEIGHTON-BUZZARD 120/200 SAND

The most common use of the cyclic triaxial apparatus is to perform undrained tests to examine the liquefaction characteristics of sands. As a result of the many investigations which have been undertaken for this purpose (see references Section 2.3), it became particularly important to describe, without confusion, the various phenomena involved when pore pressures are generated in soils by earthquakes or other cyclic motions. Seed (1979) defines the following three terms describing the liquefaction behavior of sand:

1. "Liquefaction": denotes a condition where the soil will undergo continued deformation at constant low residual stress or with low residual resistance, due to the buildup and maintenance of high pore water pressures, which reduce the effective confining pressure to a very low value; pore pressure buildup may be due either to static or cyclic stress applications and the possibility of its occurrence will depend on the void ratio or relative density of the sand and the confining pressure; it may also be caused by a critical hydraulic gradient during an upward flow of water in a sand deposit.
2. "Peak Cyclic Pore Pressure Ratio of 100%": denotes a condition where, during the course of cyclic stress applications, the residual pore water pressure on completion of any full stress cycle becomes equal to the applied confin-

ing pressure; the development of a peak cyclic pore pressure ratio of 100% has no implications concerning the magnitude of the deformations that the soil might subsequently undergo.

3. "Peak Cyclic Pore Pressure Ratio of 100% with Limited Strain Potential", or "Cyclic Mobility": denotes a condition in which cyclic stress applications develop a peak pore pressure ratio of 100% and subsequent cyclic stress applications cause limited strains to develop either because of the remaining resistance of the soil to deformation or because the soil dilates, the pore pressure drop, and the soil stabilizes under the applied loads.

It is according to the above definitions that these three terms will be used in this chapter. The term "initial liquefaction" will sometimes be used interchangeably with "peak pore pressure ratio of 100%".

This chapter examines the results of eight isotropically consolidated, undrained, cyclic triaxial tests on Leighton-Buzzard 120/200 Sand. The tests were designed to investigate the influence of sample preparation method on the liquefaction characteristics of the sand. This entailed generating a liquefaction strength curve (see Figure II-13), characteristic of each method of sample preparation, and observing pore pressure generation characteristics (see Figure II-14). Inferences concerning the influence of soil structure on liquefaction behavior are then made.

5.1 Test Results

Figure V-1 shows the cyclic total stress paths minus static porewater pressure (TSP-u_s) for the 8 undrained tests described in this investigation. All tests were run at an effective confining pressure, $\bar{p}_o$, of 3.0 kg/cm^2, and a back pressure, $u_b = u_s$, of 5.0 kg/cm^2. The cyclic shear stress, Δq_{cy}, ranged from 0.3 kg/cm^2 to 1.0 kg/cm^2.

Tests UC1 through UC5 were run on specimens prepared by the wet rodding method. The void ratio after consolidation, e_c, ranged from 0.737 to 0.763. This corresponded to a range of relative density, D_r, of 69.9% to 76.8%.

Tests UC6 through UC8 were run on specimens formed by the moist tamped (undercompacted) method of preparation. The void ratio, e_c, ranged from 0.764 to 0.767, which corresponds to relative densities between 68.8% and 69.6%. The rodded samples were formed in two layers, while the moist tamped samples were formed in 5 layers at a water content of 10%, and 5% undercompaction (see Appendix A).

Figure V-2 shows the total stress path minus static pore water pressure and effective stress paths for selected cycles for Test UC4 ($\Delta q_{cy}/\bar{p}_o$ = 0.175). Note the leftward progression of the effective stress path with each cycle of loading as the pore water pressure gradually increases. The first cycle of loading produces a larger increment of residual pore pressure than any of the subsequent cycles. This particular test attained a peak pore pressure ratio of 100% (initial liquefaction) at cycle 63, at which time the pore pressure reached 3.0

kg/cm^2 and the effective confining stress within the sample was close to zero. This condition can only exist, however, when the shear stress, q, equals zero. For positive and negative values of q, the effective confining stress is positive.

Figure V-3 shows the stress versus strain curves for the same cycles of loading as plotted in Figure V-2 for Test UC4. Both the peak-to-peak and accumulated strains remain very small, yet slightly accumulating until the effective stress path approaches the K_f-line. As seen in Figure V-3, the slight accumulation of vertical extension strains continues until about cycle 60. After cycle 60 large recoverable strains develop when the value of $\bar{p}$ and q are at or near zero, i.e. there is no confining stress. These large peak-to-peak strains center around a small, but gradually increasing, residual extension strain. As the value of q increases, dilatency within the sample leads to an increase in the mean effective stress, $\bar{p}_o$, limiting the amount of cyclic straining. Note from Figure V-2 that the effective stress path follows the K_f-line during loading and unloading at this stage (cycles 65, 67). This phenomenon is caused by a dilative behavior of the sand, and is what Seed (1979) denotes "peak cyclic pore pressure ratio of 100% with limited strain potential" or cyclic mobility.

"Complete" liquefaction occurs only in very loose samples where the specimen exhibits a total loss of strength, showing no dilation during failure. During complete liquefaction, the sample experiences continued, unrecoverable straining on the

order of 20% or so, if not to the limits of the testing apparatus. This, however, was not the case in the tests reported in this investigation, all of which showed clear signs of dilational behavior.

Within two or three cycles following initial liquefaction, during cyclic mobility, the samples showed signs of necking. This usually occurred at the top of the sample, but sometimes at the bottom. Casagrande (1979) concluded that there is a radical redistribution of water content within sand samples subjected to cyclic triaxial loadings, leading to a softening at the top of the specimen. Gradually the sample deforms by alternate necking and buldging. This, according to Casagrande, is a phenomenon which would not exist in the field. The redistribution of water content is particularly severe, according to his test results, when peak pore pressure ratios reach well above 50% of the confining pressure. Therefore, he suggests the use of the parameter N_{50}, rather than N_L (number of cycles to initial liquefaction), in analysis. The reason for this, is because the measured data is considered unreliable following a massive redistribution of water content in the test specimen. Data up to the cycle of necking are valid, but data beyond should be discarded (Lee, 1976).

Based on these findings, only data recorded through initial liquefaction will be used, because all tests showed signs of necking and buldging shortly thereafter. The parameter N_L will be used, however, for the purpose of comparison with published results.

Figure V-4 shows plots of the cyclic stresses $\bar{p}_o$ and q, vertical strain, ε_v, and pore pressure, Δu, versus cycle number for Test UC4. As mentioned earlier, there is a very slight increase in residual vertical (extension) strain until only a few cycles prior to initial liquefaction. Pore pressures increase gradually until just before initial liquefaction, when they increase rather suddenly.

The test results described above are quite similar to those of Oosterschelde Fine Sand (Figures II-12 and II-13). A complete summary of all tests is provided by Table 5-1. Plots for all tests are given in Appendix A2.

5.2 Factors Influencing the Liquefaction Characteristics of Saturated Sand

The number of cycles to reach intitial liquefaction in a saturated sand sample has been found to be primarily a function of the void ratio of the specimen; the effective consolidation pressure; and the magnitude of the cyclic deviator stress, or in other terms, the magnitude of the cyclic shear stress ratio, $\Delta q_{cy}/\bar{p}_o$. In a broader sense, however, the soil structure of the sample has a major effect on the liquefaction strength (see Chapter Three).

For the eight tests conducted in this investigation, the void ratio and effective confining pressure were kept relatively constant. It was, therefore, possible to determine the effect of cyclic stress ratio and sample preparation method (soil fabric) on the liquefaction behavior of Leighton-Buzzard

120/200 Sand samples formed by the wet rodding and the moist tamped methods of preparation. The average void ratio for these tests is about 0.757 $\pm$.02 (D_r approximately 71.5%). The effective consolidation stress was 3.00 kg/cm^2 for all tests. Figure V-5 clearly shows that increasing the cyclic shear stress ratio in a cyclic isotropic test causes initial liquefaction in fewer cycles of loading. These results are consistent with the findings of Mulilis, et al (1975) and others (Figure II-14).

It has been recognized (Castro, et al, 1977; Peacock and Seed, 1968; Seed and Lee, 1967) that the number of cycles required to cause initial liquefaction increases with increasing confining pressure. Increased effective confining pressure also means larger deformations if liquefaction is induced.

Seed and Idriss (1967) point out that the stresses developed in a sand deposit during an earthquake are unaffected by small changes in relative density. However, the cyclic stresses required to cause liquefaction are particularly sensitive to small changes in relative density. It has been shown by many investigators that the cyclic stress required to cause liquefaction in a given number of cycles increases with the initial relative density. In other terms, a denser sand will have a higher liquefaction strength than a looser sand, provided all other factors remain equal. It was not the intention of this investigation to quantitatively determine the effect of effective confining pressure and relative density on the liquefaction behavior of Leighton-Buzzard 120/200 Sand. However,

the trends determined by other investigations are assumed to apply to the behavior of Leighton-Buzzard Sand as well.

Somewhat debated is the effect of grain size on the undrained liquefaction strength of cohesionless soils. Seed and Idriss (1971) presents the results of triaxial compression test data showing the effect of mean grain size, D_{50}, on the cyclic stress ratio required to cause liquefaction in 10 and 30 cycles. It is apparent from the information that as the mean grain size decreases, the required cyclic stress ratio to cause liquefaction in some number of cycles decreases. Recent investigations (Martin, Finn and Seed, 1978; Lade and Hernandez, 1977), however, have suggested that the effects of membrane penetration may be responsible for this difference in liquefaction strength. The effect of the penetration of the membrane into the specimen is to reduce the measured pore pressure, which can lead to, according to Lade and Hernandez (1977), an overestimation of resistance to undrained liquefaction. Martin, Finn and Seed (1978) have shown that the effects of membrane penetration are negligible for mean grain sizes less than 0.1 to 0.2 mm. Because the mean grain size of Leighton-Buzzard 120/200 Sand is about 0.11 mm, the effects of membrane penetration were not considered in this investigation.

It is clear from the test results depicted in Figure V-5 that the method by which the triaxial sample was formed has a significant effect on the liquefaction behavior of the test sand. This topic was discussed briefly in Chapter Three where the results of triaxial tests were presented as reported by

Mulilis, et al (1975) showing the influence of eight different methods of sample preparation on the liquefaction strength of Monterey No. 0 Sand. The following section addresses this topic in greater depth, discussing the results acquired in this investigation, and comparing them to the findings of previous researchers such as Mulilis and Ladd.

5.3 Influence of Sample Preparation Method on Liquefaction Behavior

Results of the undrained cyclic tests conducted in this investigation show that the moist tamped specimens have a greater "liquefaction strength" than the wet rodded samples. The number of cycles required to achieve initial liquefaction in the moist tamped samples was between 65% and 175% greater than for the wet rodded samples. In other words, the cyclic shear stress ratio required to cause initial liquefaction in any given number of cycles is about 5 to 15 percent higher for the moist tamped samples. The moist tamped samples are then said to have a higher "liquefaction strength" than the wet rodded samples. Figure V-5 clearly illustrates this point.

Although it is now generally accepted that the soil structure has a major affect on the liquefaction behavior of sand in laboratory tests, it has not been established exactly what variances in the fabric are responsible for the observed differences in cyclic behavior. Mulilis, et al (1975) conducted fabric studies on samples formed by three different processes to determine whether the orientation and arrangement of the

sand grains had an effect on the liquefaction strength of Monterey No. 0 Sand. A statistical determination was made of the orientation of individual grains, and the position of any one grain relative to other grains. The three methods of preparation used were plurial, tamped, and vibratory compaction.

Statistical determination of the orientation of the apparent long axis of the sand grains for the three methods of compaction were found to be similar, therefore contributing nothing to the explanation of differences in behavior. The distribution of the normals which are perpendicular to tangential planes at the point of contact between any two grains was determined for each of the three samples. Results showed that the sample formed by dry pluvial compaction had the lowest distribution of normals to tangential contact planes in the vertical direction (i.e. parallel to the major principal stress); the sample formed by moist tamped compaction had the highest distribution of normals to tangential contact planes in the vertical direction; and the sample formed by dry vibratory compaction had a distribution intermediate with that of the other two methods.

Recalling Figure III-1, the sample formed by pluvial compaction had the lowest liquefaction strength of the three, the sample formed by moist tamped compaction had the highest, and the samples formed by dry vibratory compaction had a liquefaction strength between the other two. It was thus evident to Mulilis, et al that the sample which has the highest distribu-

tion of normals to tangential contact planes in the direction parallel to the major principal stress exhibits the highest dynamic strength. Mulilis' results appear to be consistent with those of Oda (1972), who showed that triaxial samples which had the highest distribution of normals to tangential contact planes in the direction of the major principal stress exhibited the highest static strength.

It was concluded by Mulilis, et al that the various methods of sample preparation produce samples in which the contacts between sand grains are oriented differently, and that the differences in orientation may be the primary reason for the observed differences in the liquefaction behavior of the sample. The samples of Monterey No. 0 Sand were compacted to a relative density of about 50%.

Results of the work by Mulilis, et al may help to explain why the moist tamped samples tested in this investigation were found to have a higher liquefaction strength than the wet rodded samples. The rodding action is likely to cause a reorientation of particles, significantly different from that resulting from deposition into the mold, in which the arrangement of particle contacts is in some preferred direction. This reorientation of particle contacts may account for the lower cyclic strength observed in the wet rodded samples. It is quite possible that if fabric studies, such as those reported by Mulilis, were performed on the two types of samples used herein, the moist tamped samples might be found to have a higher distribution of normals to tangential contact planes in

the direction of loading. Thus it is considered important that similar fabric studies be conducted on wet rodded and moist tamped samples of Leighton-Buzzard 120/200 Sand before more definite conclusions can be drawn.

Figure III-1 shows the liquefaction strength curves for samples formed by the moist rodding and dry rodding methods, as described by Mulilis, et al (1975). Essentially the only difference between these two rodding methods and that of the moist tamping method is the size of the compacting foot. The moist tamping method utilizes a 1-inch diameter compaction foot, and the rodding methods use a 3/8-inch diameter steel rod. The dry and moist tamped methods exhibit a lower liquefaction strength than the moist tamped sample. The moist rodded method produces a curve closest to the moist rodded curve, however. This result is important because of the possible similarities in the fabric of Mulilis' dry and moist rodded samples (compacted with a 0.375-inch diameter rod) and the wet rodded samples used in this test program (compacted with a 0.042-inch diameter rod). The fact that there are similarities in the results shown in Figure III-1 and Figure V-5 is encouraging.

Ladd (1977) concludes that in addition to the differences in grain and interparticle contact orientation, variation in void ratio within the individual specimen and segregation of particles are also variences in the fabric of sand which may contribute significantly to the differences in observed liquefaction behavior in the laboratory. Mulilis, et al (1975)

conducted some research on the effect of loose zones within the sample on the liquefaction of Monterey No. 0 sand. He concluded that the strength of the specimen becomes a function of the thickness of the loose layer. Qualitative radiographic analysis (see Chapter Three) indicates that the wet rodded samples are generally more uniform than the moist tamped samples, and that neither has a distinct "loose" zone which would affect the liquefaction strength in the way Mulilis, et al determined. In addition, because the test sand is quite uniform (see Section 3.1) the effect of particle segregation can be discounted.

Mulilis (1977) concluded that, although the differences in the liquefaction strengths of a sand may be attributed to the fabric of the sample (all other factors being equal), the magnitude of this difference is likely to be dependent on the type of sand being tested. Thus it is not alarming that the two curves of Figure V-5 are quite close to each other, whereas those of Figure III-1 (especially moist tamped and dry rodded) appear to be very different - remembering, of course, that wet rodding cannot be directly compared to dry (and moist) rodding, anyway.

5.4 Pore Pressure Development in Cyclic Isotropic Tests

Section 2.4.2 briefly described the typical development of pore water pressure (see Figure II-13) through the liquefaction stage for an undrained cyclic isotropic test. The development of pore pressures in such a test can be described as follows:

1. There is a large increment of residual pore pressure developed in the first load cycle, followed by a gradual, steady increase thereafter until the effective stress path reaches the K_f-line.
2. When the K_f-line is reached, the pore pressure increases suddenly to a value equal to the initial effective confining pressure. This only occurs when the shear stress is equal to zero and is defined as initial liquefaction.
3. When the shear stress q is a value other than zero, the pore pressure decreases and the effective stresses increase. This dilative behavior only occurs after the K_f-line is reached (i.e. after initial liquefaction) and is termed cyclic mobility. Complete liquefaction is never achieved.

Results of a static triaxial compression test on Leighton-Buzzard 120/200 Sand prepared by the wet rodding method and consolidated to a void ratio of e_c = 0.753 (see Appendix C) shows that undrained monatonic loading of the sand at this density also causes similar dilative behavior at the failure line. This dilative behavior is believed to represent an important characteristic of the sand at this density in undrained tests. The static friction angle, $\bar{\Phi}_{st}$, was determined to be 34° ($\bar{\alpha}_{st}$ = 28.5°) for this test. Note that this value of $\bar{\alpha}_{st}$ is significantly less than $\bar{\alpha}_{cyc}$ = 34°, a value inferred from the effective stress path at initial liquefaction for test UC4 (Figure V-2).

As mentioned in Section 2.4.2, it is often useful to summarize pore pressure buildup data on a plot of excess pore pressure ratio, $\Delta u/\bar{p}_o$, versus cycle ratio, N/N_L. Figure II-15 shows two such non-dimensional plots summarizing over 50 tests on Sacramento River and Monterey Sand (Lee & Albaisa, 1974). Figure V-6 gives such a plot for two of the cyclic tests performed on the wet rodded samples. Data from Tests UC1 and UC5 are not plotted because in both cases the sample reached initial liquefaction in less than 5 cycles and a distinct pattern of pore pressure development was not observed. From Figure V-6 it can be seen that the development of pore pressures for Tests UC2 and UC4 is quite similar to that shown in Figure II-15 for Sacramento River and Monterey Sands.

Figure V-7 shows a similar plot for Tests UC6 and UC7 in which the samples were formed by the moist tamped method. There appears to be little or no difference in the development of pore pressures between the wet rodded samples and the moist tamped samples. This observation is more clear in Figure V-8, which combines the results of all four tests mentioned above. Note that Tests UC4 (N_L=63) and UC6 (N_L=174) have a more well-defined pattern of pore pressure development, and essentially plot atop each other on this normalized plot. The pattern of buildup is quite consistent for all tests through a cycle ratio of 50%. Because a great deal of pore pressure is generated in the last few cycles of loading, tests with a small number of cycles to initial liquefaction appear to be generating the largest pore pressures earlier than the longer lasting tests.

Therefore, on a normalized plot such as Figure V-8, the data from the shorter liquefaction tests causes what appears to be significant scatter in the results after a cycle ratio of about 50%.

Section 2.4.2 briefly mentioned the use of such normalized pore pressure development plots. Once such information has been established (whether by cyclic triaxial tests or other laboratory tests), one can estimate the rate of generation of pore water pressure in a soil deposit with reasonable accuracy (Seed, et al, 1976).

Test UC3 was terminated after 895 cycles of loading because only a very small amount of residual pore pressure had developed. Using Figure V-8, the number of cycles which would have been required to reach initial liquefaction could be estimated as follows:

1. at cycle N = 895, $\Delta u = 0.406$ kg/cm^2
2. the excess pore pressure ratio $\Delta u/\bar{p}_o = 0.406/3.00 = 0.135$
3. entering Figure V-8, N/N_L is roughly 0.02
4. N_L is therefore 895/0.02 or 44,750 cycles.

It was feared at the time that such a long-lasting test (approximately 150 hours) would be subject to significant temperature effects, and was therefore terminated.

Also plotted on Figure V-8 are the combined results of Lee and Albaisa's tests for Monterey and Sacramento River sands. Because the results of this test program are so similar, they support the claim of Lee and Albaisa (1974) that the position

of the curves is rather insensitive to the type of soil, as well as the relative density, confining pressure, and number of cycles required to cause liquefaction. In fact, it is now evident that the soil structure of the sample does not influence the position of the curves.

Seed, et al (1976) determined that the development of pore water pressure in laboratory cyclic tests is of the form

$$\frac{\Delta u}{\bar{\sigma}_o} = F\ (N/N_L) \quad \text{or} \quad r_u = F\ (r_N) \qquad \text{Equation 5.1}$$

in which $\bar{\sigma}_o$ = the effective confining pressure (equal to $\bar{p}_o$ in this paper), N = the cycle number, and N_L = the number of cycles to cause a peak cyclic pore pressure ratio of 100% under undrained conditions. An analytical expression has been assigned to the function F, such that Equation 5.1 becomes:

$$\frac{\Delta u}{\bar{\sigma}_o} = \frac{2}{\pi} \text{ Arc sin } (N/N_L)^{1/2\alpha} \qquad \text{Equation 5.2}$$

The parameter α in the expression permits the generation of various curves which will encompass the whole data band obtained from cyclic tests under different conditions. It has been found that a value of $\alpha = 0.7$ best fits the mean of the data band relating the excess pore pressure ratio, $\Delta u/\bar{p}_o$, to the cycle ratio, N/N_L, for most published results. Figure V-9 shows the pore pressure generation data for the tests reported herein, along with the curves corresponding to α-values of 1.3, 0.7 and 0.4 as given by Equation 5.2. It appears from Figure V-9 that, although an α value of 0.7 may fit the mean of the data the best, no one value of α adequately describes the data band from beginning to end.

5.5 Summary

Results of eight undrained isotropic cyclic triaxial tests on Leighton-Buzzard Sand (Figures V-2, V-3, V-4) were shown to be quite similar to results for Oosterschelde Find Sand as reported by Hedberg (1977) (Figures II-12, II-13). Five tests were performed on samples prepared by the wet rodding method, and three were performed on samples prepared by the moist tamped (undercompacted) method. All tests, except one, reached initial liquefaction in some number of cycles, N_L, which was followed by a dilative behavior of the sample at the failure line (Figure V-2) which limited strain development. This is referred to as cyclic mobility. All of the samples which liquefied showed signs of alternate necking and buldging at the top or bottom (or both) of the sample within one or two cycles following initial liquefaction. This behavior, according to Casagrande (1979), is unique to cyclic triaxial tests and is not representative to in-site soil behavior. Necking is caused by a radical redistribution of water content within the sample, resulting in a very loose zone at the top of the sample. Test data recorded after necking is not reliable.

Samples prepared by the wet rodding method were shown to have a lower liquefaction strength than those formed by the moist tamped method. A lower liquefaction strength means that a lower cyclic shear stress ratio, $\Delta q_{cy}/\bar{p}_o$, is required to bring the sample to initial liquefaction in some number of cycles. Test results illustrating this lower strength for wet rodded samples is shown in Figure V-5.

Mulilis, et al (1975) concludes that the difference in liquefaction strengths observed in samples of the same initial density prepared in different ways may be attributed to the difference in orientation of particle contacts within the samples. Specifically, he found that the samples which had a higher distribution of normals perpendicular to tangential planes in the direction of the major principal stress (vertical) had a higher liquefaction strength. Based on Mulilis' results, it is hypothesized that the differences in orientation of particle contacts within the wet rodded and moist tamped samples of the investigation account for the lower liquefaction strength of the wet rodded specimens. Without having performed detailed fabric studies, it was not possible to determine the characteristics of the fabrics resulting from the two methods of sample preparation used. It is encouraging, however, to see that Mulilis' dry and moist rodded methods (although probably quite different than the wet rodding method described herein) produced samples with lower liquefaction strengths than his moist tamped samples. Other variences in soil fabric, such as the occurrance of loose zones and particle segregation, were not believed to significantly influence the results in this investigation.

Pore pressure generation data, expressed in terms of a dimensionless plot of excess pore pressure ratio, $\Delta u/\bar{p}_o$, versus cycle ratio, N/N_L, was found to be quite similar to that of Lee and Albaisa (1974) for two other types of sand test under different conditions. The results presented for Leighton-Buz-

zard 120/200 Sand supports Lee and Albaisa's claim that the shape and position of the data band expressed in such a fashion is insensitive to the type of sand, density, confining pressure, and number of cycles necessary to cause initial liquefaction. In fact, this statement can be taken one step further in that the results appear to be insensitive to the method by which the sample is formed, based on results of tests reported herein.

The characterization of the normalized pore pressure data band (Figure V-9) by Equation 5.2 (Seed, et al, 1976) does not appear to be satisfactory for test results on Leighton-Buzzard 120/200 Sand. The use of an α value of 0.7 probably provides the best fit of the data band, but is in no way adequately descriptive of the data. Equation 5.2 and a value of $\alpha = 0.7$ does, however, provide the best fit of the mean of the shaded data band presented in Figure V-8, within which these test data results fall.

TEST UC	e_c	D_r (%)	$\bar{p}_o$ (kg/cm^2)	Δq_{cy} (kg/cm^2)	$\frac{\Delta q_{cy}}{\bar{p}_o}$	N_L	$N_{(\varepsilon_{vpp} = 5\%)}$
1	.737	76.8	3.0	1.00	0.333	1	2
2	.753	72.5	3.0	0.60	0.200	10	12
3	.752	72.8	3.0	0.30	0.100	Never Achieved	
4	.763	69.9	3.0	0.525	0.175	63	64
5	.750	73.3	3.0	0.75	0.25	3	4
6	.767	68.8	3.0	0.525	0.175	173	174
7	.764	69.6	3.0	0.60	0.200	16	17
8	.766	69.1	3.0	0.75	0.250	5	5

SUMMARY OF UNDRAINED CYCLIC ISOTROPIC TESTS

TABLE 5-1

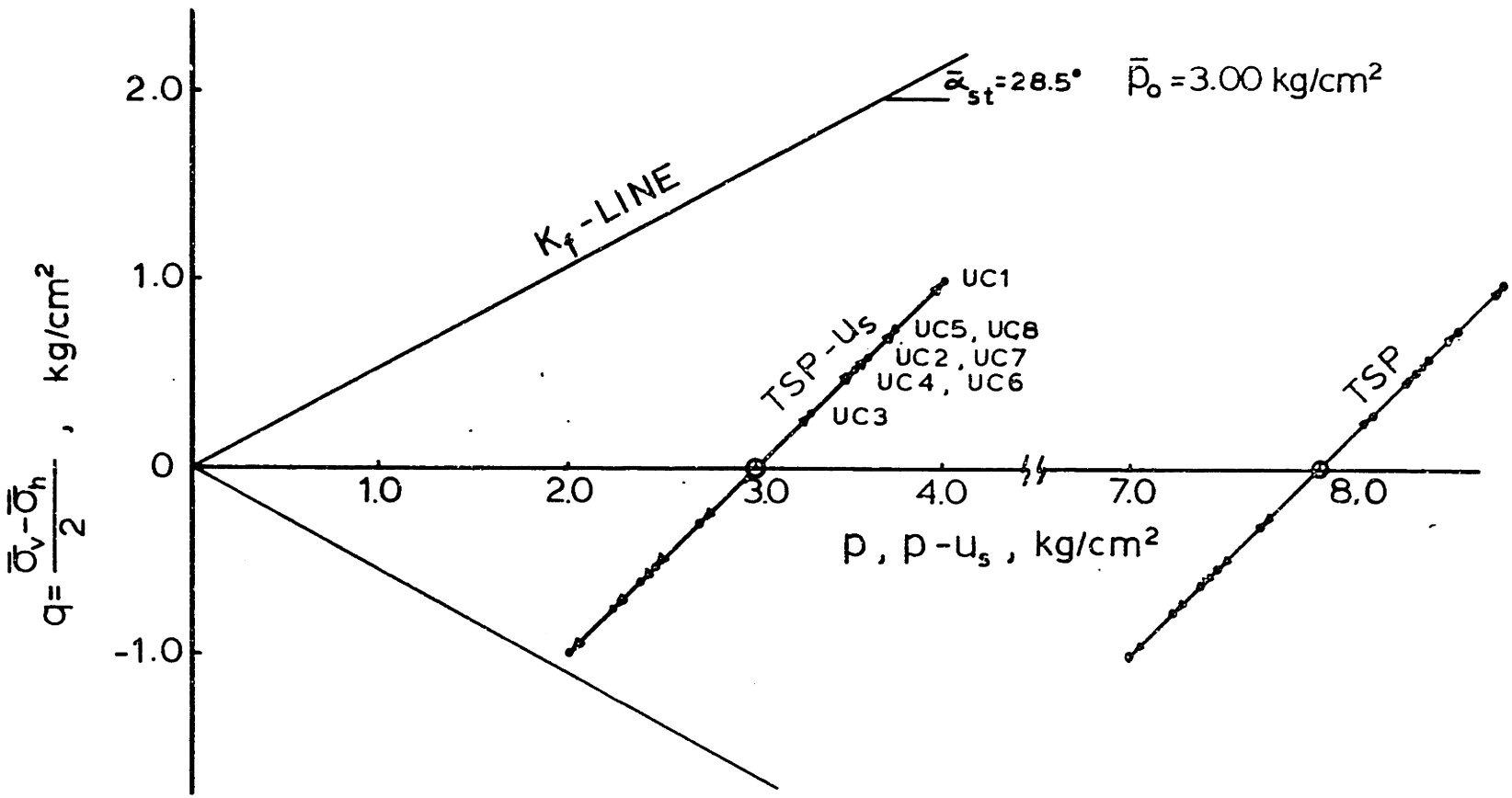

TOTAL STRESS PATHS (TSP-u_s) FOR CYCLIC ISOTROPIC TESTS

FIGURE V-1

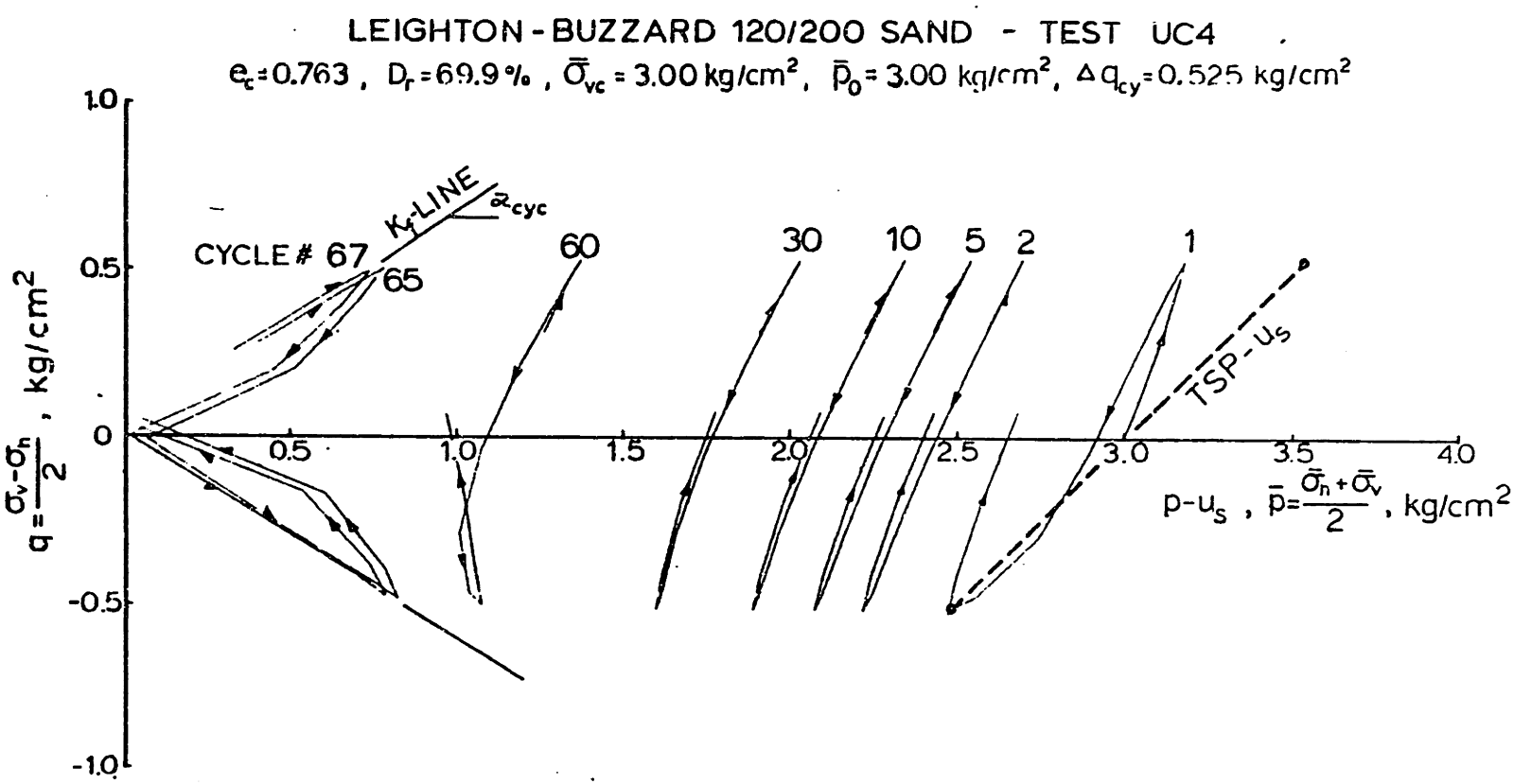

EFFECTIVE STRESS PATHS FOR SELECTED CYCLES - TEST UC4

FIGURE V-2

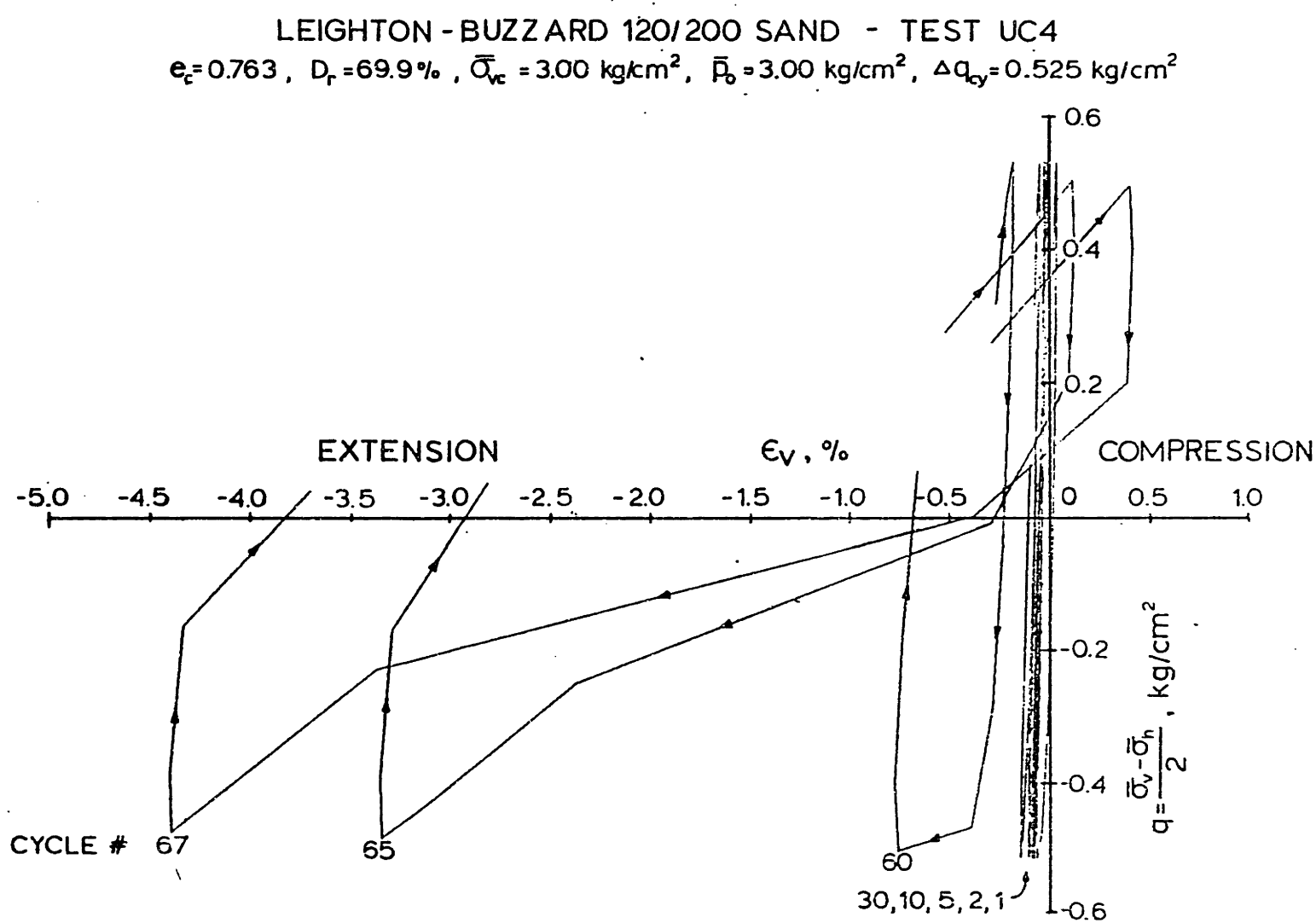

STRESS VERSUS STRAIN PLOTS FOR SELECTED CYCLES-
TEST UC4

FIGURE V-3

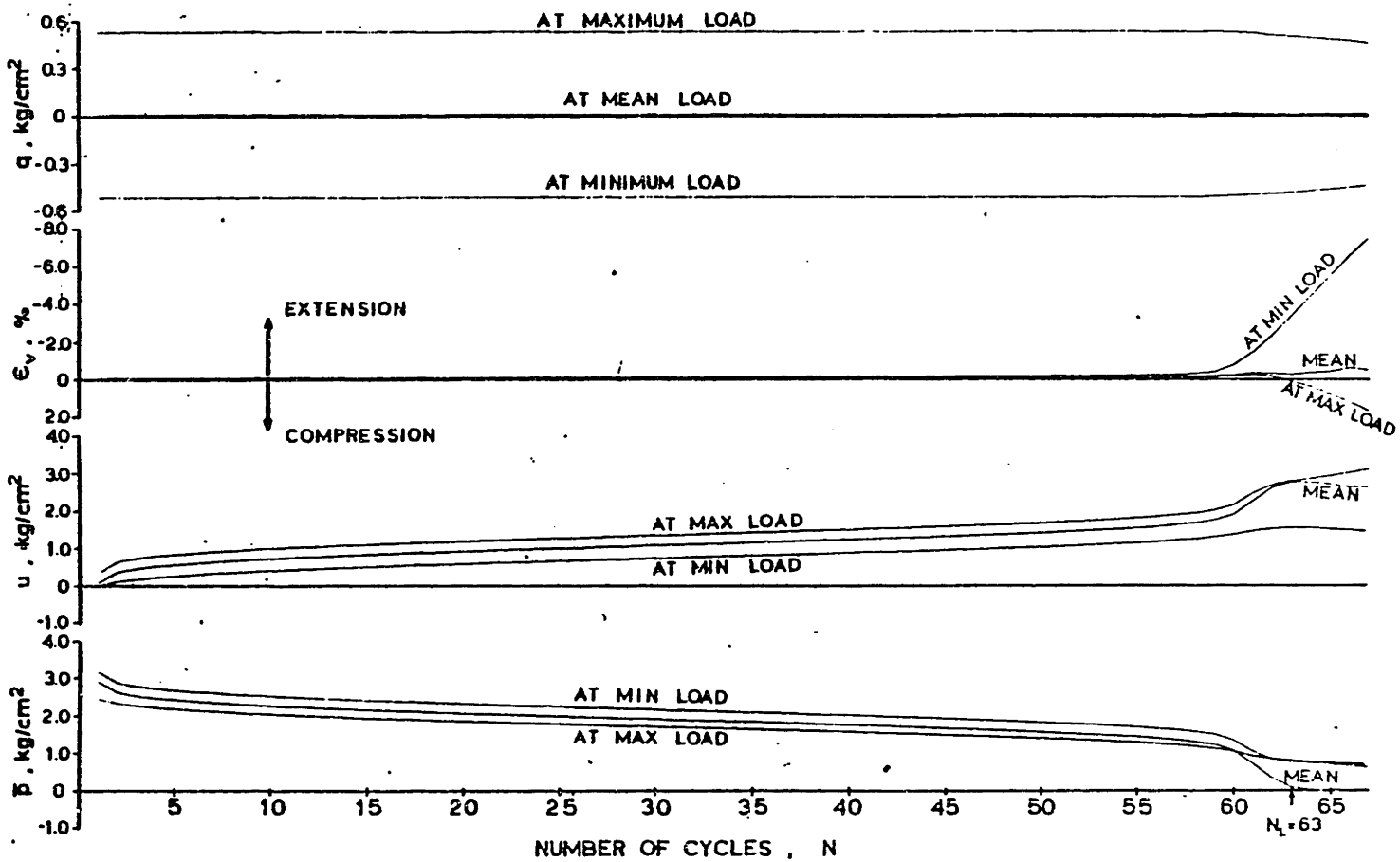

SUMMARY OF STRESS, STRAIN AND PORE PRESSURE DEVELOPMENT TEST UC4

FIGURE V-4

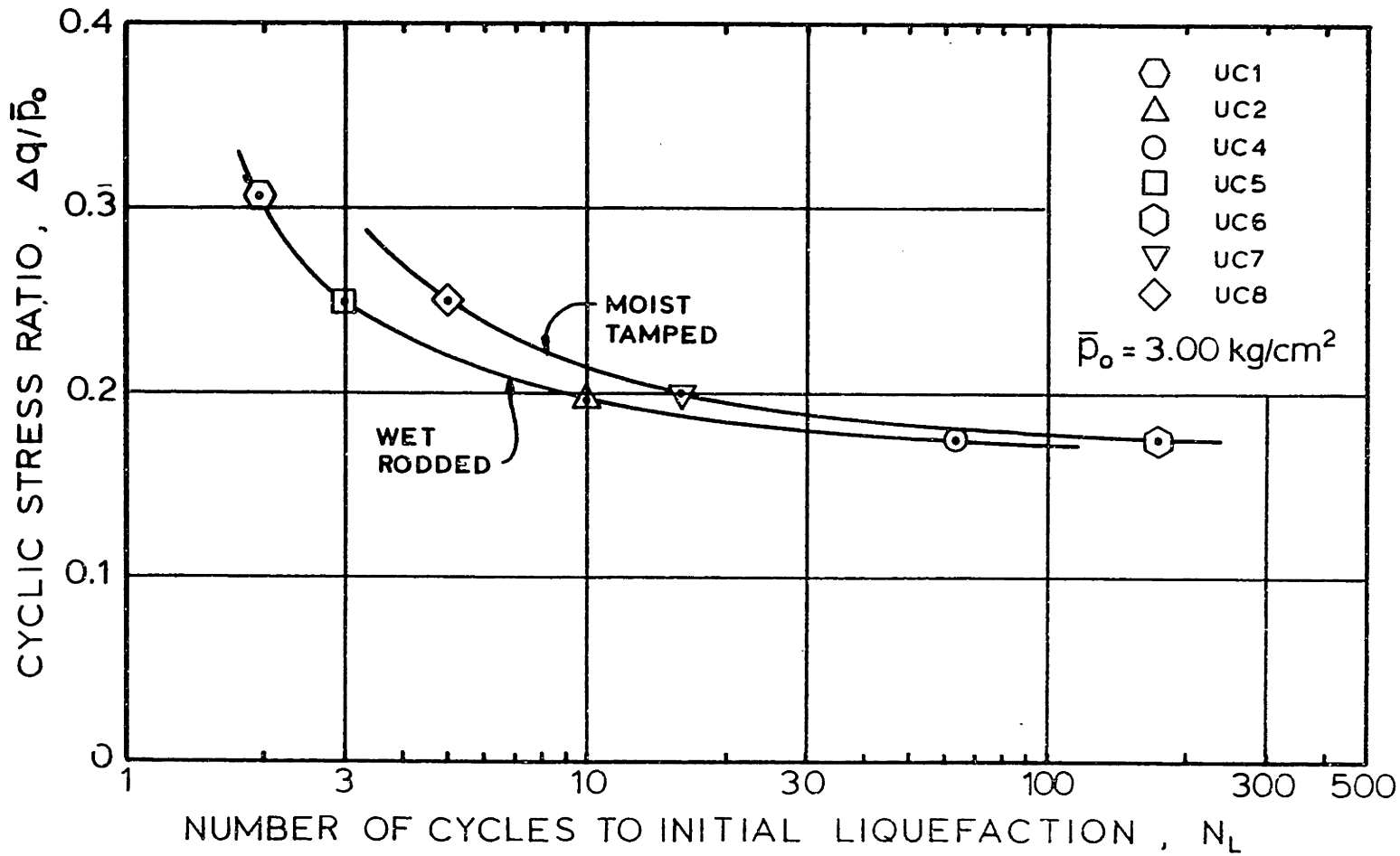

CYCLIC STRESS RATIO VERSUS NUMBER OF CYCLES FOR DIFFERENT DENSIFICATION METHODS

FIGURE V-5

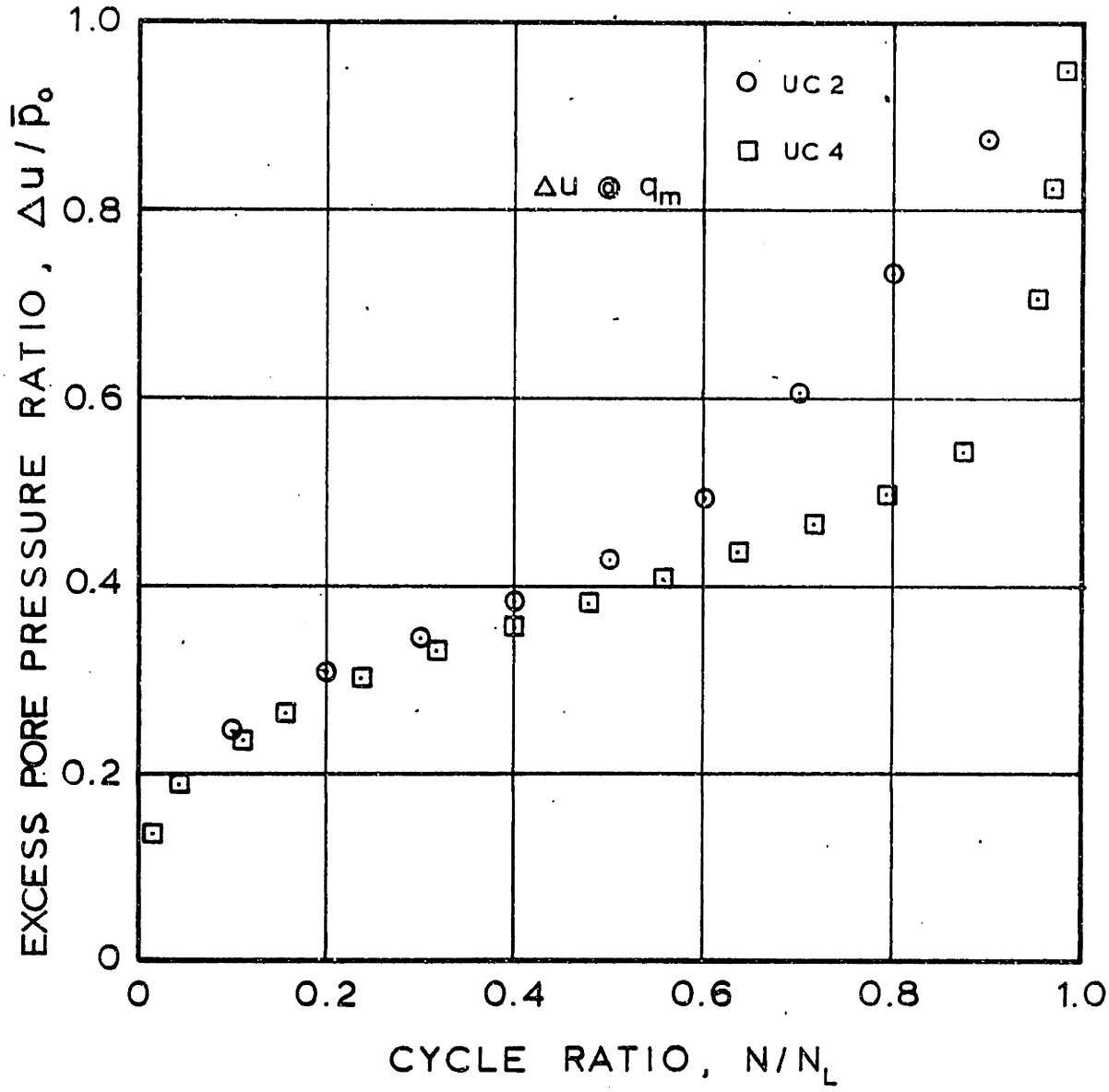

NORMALIZED PORE PRESSURE DATA
WET RODDED TRIAXIAL SAMPLES

FIGURE V-6

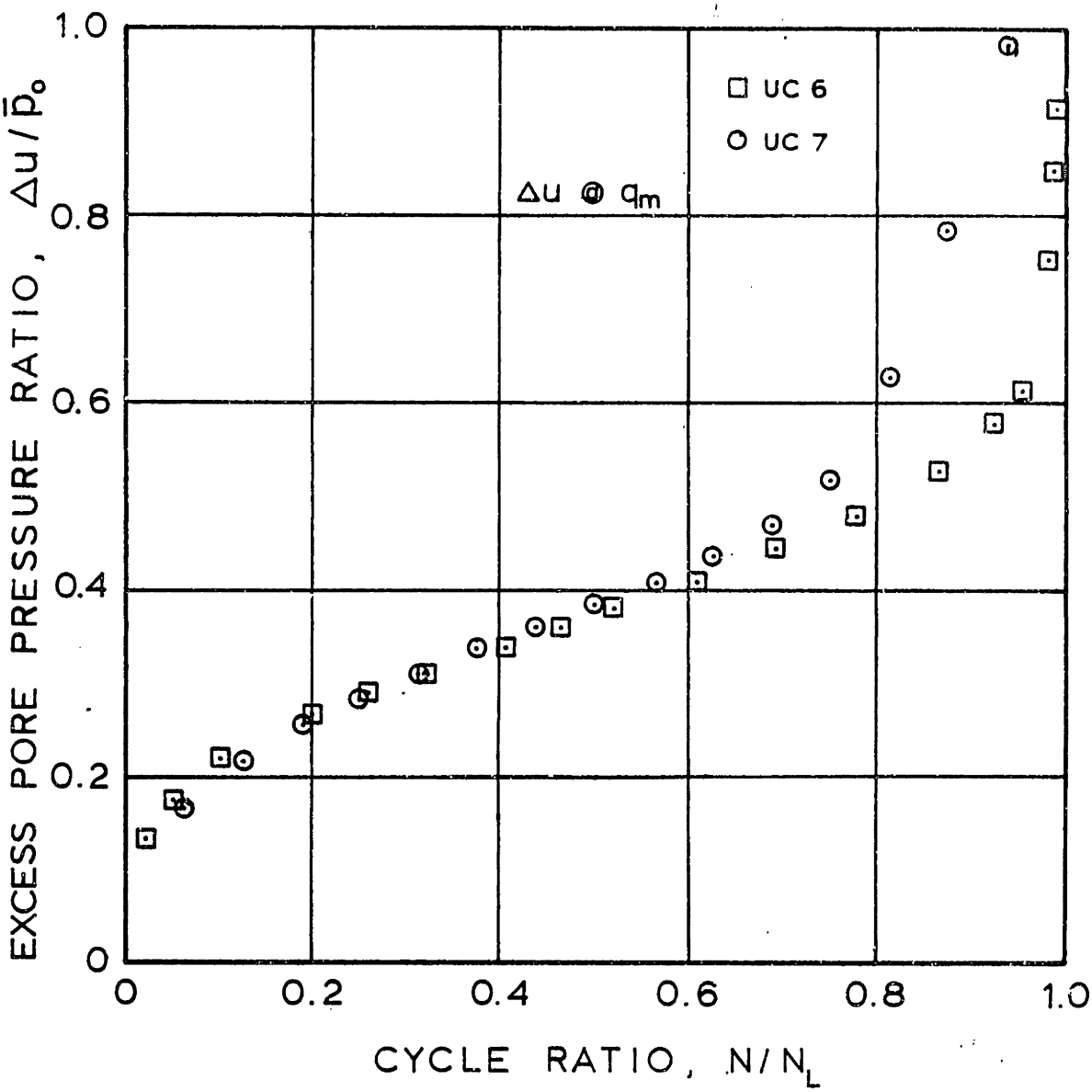

NORMALIZED PORE PRESSURE DATA
MOIST TAMPED TRIAXIAL SAMPLES

FIGURE V-7

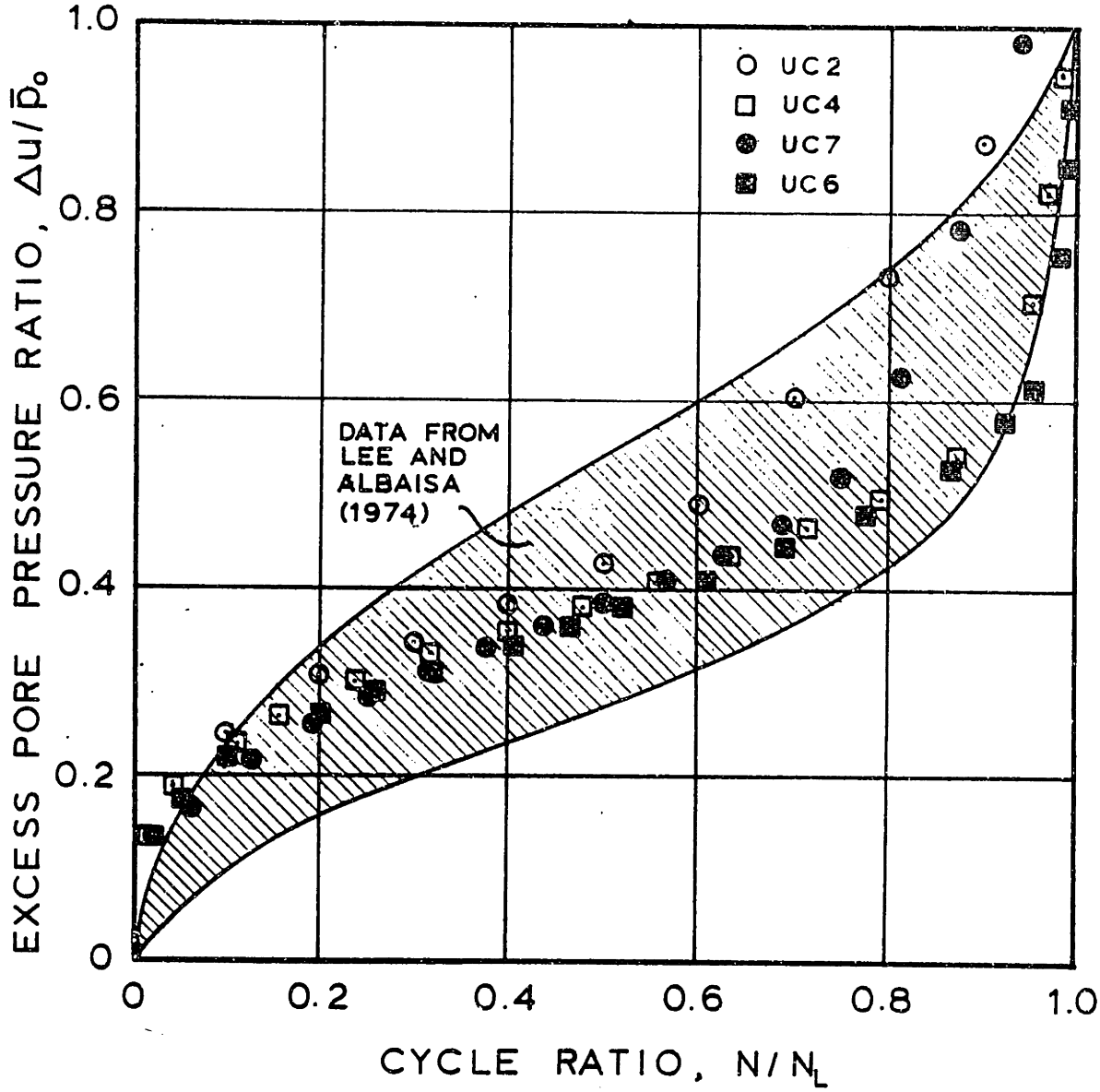

NORMALIZED PORE PRESSURE DATA
SUMMARY OF ALL TESTS

FIGURE V-8

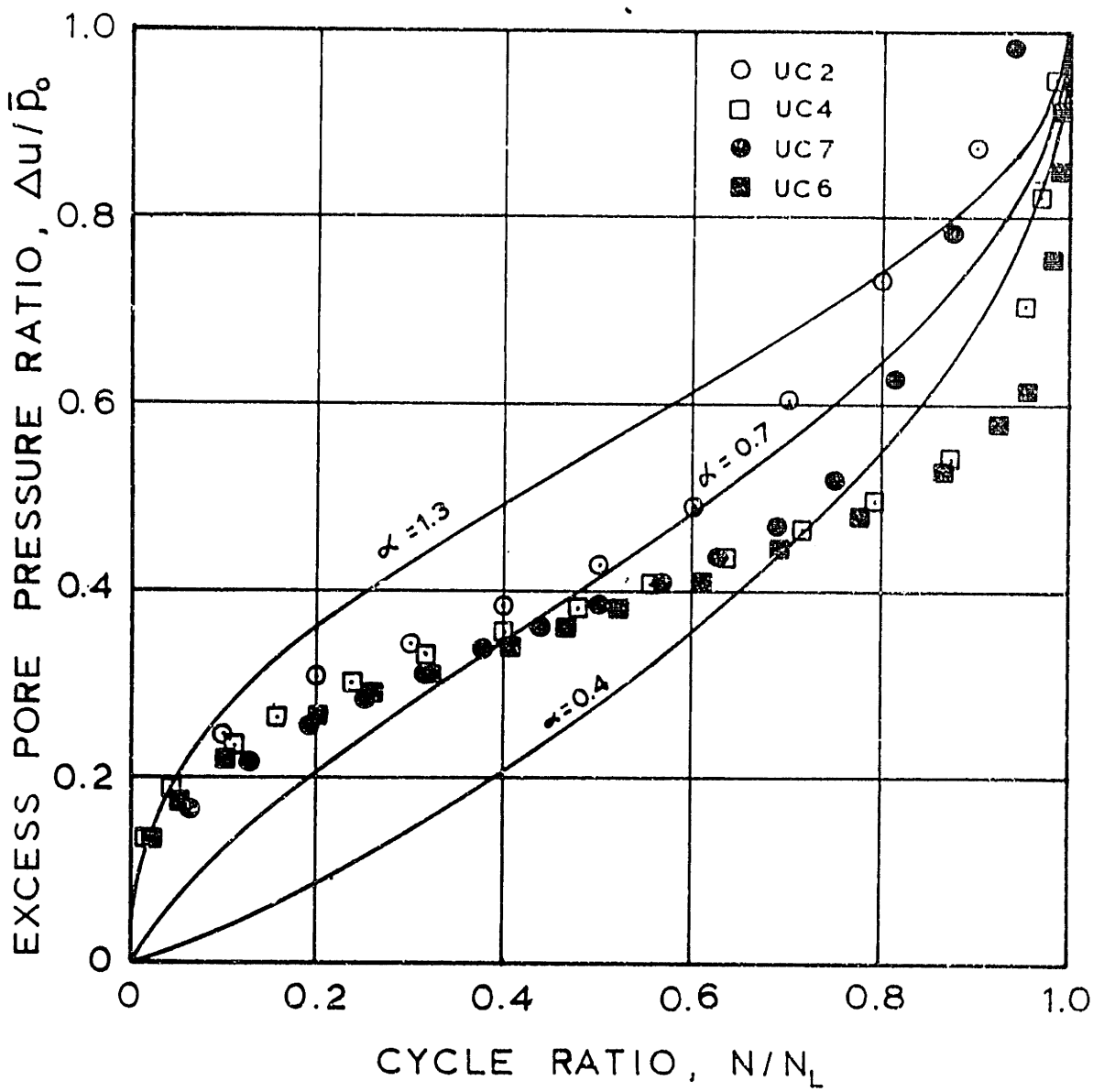

NORMALIZED PORE PRESSURE DATA
SUMMARY OF ALL TESTS

FIGURE V-9

CHAPTER SIX - SUMMARY AND CONCLUSIONS

The purpose of this investigation was to perform stress-controlled cyclic triaxial tests on Leighton-Buzzard 120/200 Sand in order to:

1. obtain data which can be used in the prediction of the response of soil in centrifuge tests,
2. compare this data with published results, paying particular attention to the influence of sample preparation method.

The wet rodding method of preparation, which was developed for use in centrifuge testing to form large-diameter samples (Lambe, 1981), was adapted for use in cyclic triaxial testing. Chapter Three outlines the procedure for preparing samples by this method. Appendix B describes the process in more detail. The moist tamped method of sample preparation (with undercompaction) was also used in this investigation for the purpose of comparison with the wet rodded test results. Qualitative X-radiographic analysis indicated that the wet rodded samples (2 layers) have little or no distinguishable layering effects, whereas the moist tamped samples (5 layers) have very marked layering effects. Radiographs of samples prepared by the moist tamped method, such as that shown in Figure III-3b, indicate that the top of each layer is somewhat more dense than the bottom of the layer. The variation in density within the samples could not be determined quantitatively with the equipment used.

Seven drained cyclic tests were performed on Leighton-Buzzard 120/200 Sand. The results of the tests, which were run at the same initial stresses and density, indicated that the wet rodding samples had a lower tendency for volume change than for identical moist tamped samples. The difference in the volumetric strain development is attributed primary to the differences in the soil structure of the samples, as governed by the methods of preparation. The stress-strain behavior of comparable tests run on both types of samples leads to the belief that the wet rodded sample is somewhat stiffer in the vertical direction than the moist tamped sample.

It was found that drained tests, run on both types of samples, with high applied cyclic shear stress ratios ($\Delta q_{cy}/\bar{p}_o > 0.25$) yielded significantly larger peak-to-peak shear strains in the first 10 cycles of the test. After that, the peak-to-peak shear strains more or less leveled off. This behavior was contrary to the findings of Hadge (1979), and is believed to be caused by the high cyclic stresses, which apparently induce large vertical extension strains (and to a lesser extent, large compression strains). The result is large peak-to-peak vertical straining, causing excessive peak-to-peak shear straining until such time when the sample has densified enough to resist the high cyclic stresses. This behavior was equally evident in both types of samples. It is, therefore, believed not to be caused by the structure of the sample.

An analysis, based on Hadge (1979), was conducted to determine a relationship for predicting of volumetric strain in

cyclic triaxial tests. The relationship expresses volumetric strain in terms of peak-to-peak shear strain and cycle number. Because of the non-linearity of the peak-to-peak shear strain data, it was necessary to develop two expressions: one for use with cycles 1 through 10, and another for use with cycles 10 through 1000. Regardless, the two expressions predicted volumetric strains quite well - generally within $\pm 50\%$. The expressions were developed from test data on wet rodded samples. When used to predict the volumetric strains in tests on moist tamped samples, the equations generally underpredict the volumetric strains, but the predictions were still within $\pm 50\%$.

Eight undrained cyclic tests were performed on Leighton-Buzzard 120/200 Sand for the purpose of studying the liquefaction behavior of the test sand prepared by the two preparation methods. Seven of the eight tests were carried through initial liquefaction, at which time the sand displayed a dilative behavior which increased effective stresses when the shear stress, q, was positive or negative, thus limiting strain development. This dilative behavior at the failure line (K_f-line) was also observed in the undrained static test described in Appendic C. Most samples necked within one or two cycles following initial liquefaction.

Results of these undrained tests showed that the wet rodded samples had a lower liquefaction strength than the moist tamped samples. The cyclic stress ratio required to cause initial liquefaction in some number of cycles was generally 5-15% lower for the wet rodded samples. The difference in liquefaction strength between the two types of samples is

attributed to differences in the fabric of the sand samples. Mulilis, et al (1975) claims that the orientation of particles and particle contacts is the primary reason for the difference between the strengths of laboratory-reconstituted samples, although the magnitude of the difference may be related to the type of material tested.

Pore pressure development for the tests described herein, expressed in a non-dimensional fashion, is similar to that of other test programs using Sacramento River and Monterey Sands. The pore pressure buildup data for Leighton-Buzzard 120/200 Sand falls within a band of data collected from a number of stress-controlled cyclic triaxial tests on Sacramento River and Monterey Sand tested under very different conditions. The pore pressure data presented in Chapter Five support the claim that this characteristic-type development of pore pressure is independent of the material being tested. Now it appears as though the method of sample formation also has no effect on pore pressure generation.

It is not clear at this time why the wet rodded samples seemed stronger (stiffer, more resistant to volume change) than the moist tamped samples in drained tests, yet had a lower liquefaction strength when tested undrained. It would seem that the sample which had the highest tendency for volume change would have a greater tendency to develop pore pressures under undrained loading conditions. This, however, was not the case. From test results presented in Chapter Four, it is suspected that the wet rodded samples are stiffer than the moist tamped samples in the vertical direction. It is possi-

ble, therefore, that the drained behavior in cyclic triaxial tests is governed primarily by the vertical modulus (i.e., Young's Modulus), whereas the undrained behavior may be primarily a function of some octahedral-type modulus. The wet rodded sample might have a fabric which would yield a lower modulus of this type, as a result of the rodding action used in the densification procedure. Results from detailed fabric studies and additional static and cyclic tests would be necessary to support such a claim, however.

LIST OF REFERENCES AND BIBLIOGRAPHY

ABBREVIATIONS

ASCE	American Society of Civil Engineers
ASTM	American Society for Testing and Materials
BOSS'76	Behavior of Offshore Structures, 1st Symposium, 1976
JGED	Journal of the Geotechnical Engineering Division
JSMFD	Journal of the Soil Mechanics and Foundation Division
MIT	Massachusetts Institute of Technology
SMFE	Soil Mechanics and Foundation Engineering

REFERENCES

Ambraseys, N. and Sarma, S. (1969), "Liquefaction of Soils induced by Earthquakes", Bulletin of the Seismological Society of America, 59, No. 2, pp. 651-664.

ATSM, "Test for Relative Density of Cohesionless Soils, ASTM, D2049-69.

Bieganousky, W.A. and Marcuson, W.F. III (1976), Laboratory Standard Penetration Tests on Reid Bedford Model and Ottawa Sands, Research Report S-76-2, U.S. Army Engineer Waterways Experiment Station.

Bishop, A.S. and Henkel, D.J. (1962), The Measurements of Soil Properties in the Triaxial Test, A. Arnold, London.

Bucknam, M.D. (1981), A Sample Preparation Method for Centrifuge Testing, MIT Internal Report.

Bucky, P.B. (1931), "Use of Models for the Study of Mining Problems", American Institute Mining and Metallurgical Engineers Tech. Pub. No. 425, pp. 3-28.

Casagrande, A. (1971), "On Liquefaction Phenomena: A Lecture to the ENCOLD and the British Geotechnical Society", Geo-Technique, 21, No. 3, pp. 197-202.

Casagrande, A. (1979), "Liquefaction and Cyclic Deformation of Sands, A Critical Review", Harvard Soil Mechanics Series No. 88.

Casagrande, A. and Rendon, F. (1978), Gyratory Shear Apparatus Design, Testing Procedures, and Test Results on Undrained Sand, Technical Report S-78-15, U.S. Army Engineer Waterways Experiment Station.

Castro, G. (1969), "Liquefaction of Sands", PhD Dissertation, Harvard University.

Castro, G. (1975), "Liquefaction and Cyclic Mobility of Saturated Sands", JGED, ASCE, 101, No. GT6, pp. 551-570.

Castro, G. and Christian, J.T. (1976), "Shear Strength of Soils and Cyclic Loading", JGED, ASCE, 102 GT9, pp. 887-894.

Castro, G. and Poulos, S.J. (1977), "Factors Affecting Liquefaction and Cyclic Mobility", JGED, ASCE, Vol. 103, No. GT6, pp. 501-506.

Cuellar, V. Bazant, Z.P., Krizek, R.J., and Silver, M.L. (1977), "Densification and Hysteresis of Sand under Cyclic Shear", JGED, ASCE, Vol. 103, No. GT5, pp. 399-416.

Cyclic Triaxial Tests on Oosterschelde Sands (1979), M.I.T. Department of Civil Engineering Report R79-24.

DeAlba, Pedro, Seed, H. Bolton, and Chan, Clarence K. (1976), "Sand Liquefaction in Large-Scale Simple Shear Tests", JGED, ASCE, Vol. 102, No. GT9, pp. 909-927.

DeAlba, P.A., Chan, C.K. and Seed, H.B. (1975), "Determination of Soil Liquefaction Characteristics by Large-Scale Laboratory Tests", Report No. EERC 75-14.

Drnevich, V.P. (1967), Effect of Strain History on the Dynamic Properties of Sand, Ph.D. Dissertation, Univ. of Michigan.

Drnevich, V.P. (1972), "Undrained Cyclic Shear of Saturated Sand", JSMFD, ASCE, 98, No. SM8, pp. 807-825.

El-Sohby, M.A. and Andrawes, K.Z. (1972) "Deformation Characteristics of Granular Materials under Hydrostatic Compression", Canadian Geotechnical Journal, 9, pp. 338-350.

Emery, J.J., Finn, W.D.L. and Lee, K.L. (1972), "Uniformity of Saturated Sand Samples", Soil Mechanics Series, University of British Columbia.

Finn, W.D.L. (1981), "Liquefaction Potential: Developments since 1976", Proc. Int. Conf. on Recent Advances in Geotechnical Earthquake Engineering and Soil Dynamics, Vol. 2, pp. 655-681.

Finn, W.D.L. and Bransby, P.O. and Pickering, D.J. (1970), "Effect of Strain History on Liquefaction of Sand", JSMFD, ASCE, 96, No. SM6, pp. 1917-1934.

Finn, W.D.L. and Byrne, P.M. (1975) "Settlements in Sands During Earthquakes", Proceedings, 2nd Canadian Conference on Earthquake Engineering, Hamilton, Ontario, pp. 1-8.

Finn, W.D.L., Emergy, J.J. and Gupta, Y.P. (1971), "Liquefaction of Large Samples of Saturated Sand on a Shaking Table", Proc. 1st Canadian Conf. on Earthquake Engrg., Vancouver, Canada, pp. 97-110.

Finn, W.D.L., Lee, K.W. and Martin, G.R. (1976), "An Effective Stress Model for Liquefaction", ASCE NCLPGE, pp. 169-198.

Finn, W.D.L., Pickering, D.J. and Bransby, P.L. (1971), "Sand Liquefaction in Triaxial and Simple Shear Tests", JSMFD, ASCE, 97, No. SM4, pp. 639-659.

Hadge, W.E., and Marr, W.A. (1979), A Relationship Between the Drained and Undrained Cyclic Behavior of Sand, S.M. Thesis, M.I.T. Department of Civil Engineering.

Haldar, A., and Tang, W.H. (1979), "Probabilistic Evaluation of Liquefaction Potential", JGED, ASCE, Vol. 105, No. GT2, pp. 145-163.

Hardin, B.O. (1965), "The Nature of Damping in Sands", JSMFD, ASCE, Vol. 91, No. SM1, Part 1, pp. 63-97.

Hardin, B.O. (1970), "Suggested Methods of Test for Shear Modulus and Damping of Soils by the Resonant Column", ASTM Special Technical Publication 479, pp. 516-529.

Hardin, B.O. and Drnevich, V.P. (1972a), "Shear Modulus and Damping in Soils: Measurement and Parameter Effects", JSMFD, ASCE, 98, No. SM6, pp. 603-624.

Hardin, B.O. and Drnevich, V.P. (1972b), "Shear Modulus and Damping in Soils: Design Equations and Curves", JSMFD, ASCE, 98, No. SM7, pp. 667-692.

Hardin, B.O., and Music, J. (1965), "Apparatus for Vibration of Soil Specimens During the Triaxial Test", Instruments and Apparatus for Soil and Rock Mechanics, ASTM STP 392, Am. Soc. Testing Mats., pp. 55-74.

Hedberg, Jan (1977) "Cyclic Stress Strain Behavior of Sand in Offshore Environment", Ph.D. Thesis, Massachusetts Institute of Technology, Department of Civil Engineering.

Ishihara, K. and Kawaguchi, N. (1970), "Triaxial Torsion Shear Tests on Saturated Sands Under Simulated Earthquake Loading Conditions", Proc. 3rd Japan Earthquake Engineering Symposium, Tokyo.

Ishihara, K. and Li, S.I. (1972), "Liquefaction of Saturated Sand in Triaxial Torsion Shear Test", Soils and Foundations, 12, No. 3, pp. 19-39.

Ishihara, K. and Yasuda, S. (1972), "Sand Liquefaction Due to Irregular Excitation", Soils and Foundations, 12i, No. 4, pp. 65-78.

Jaky, F. (1944), "The Coefficient of Earth Pressure at Rest", Journal of the Society of Hungarian Architects and Engineers, pp. 355-358.

James, R.G. (1973), Radiographic Techniques, Cambridge University Report CUED/C - Soils Ln(b).

Ko, H.Y. and Scott, R.F. (1967) "Deformation of Sand in Hydrostatic Compression", Journal of the Soil Mechanics and Foundations Division, ASCE, 93, No. SM3, pp. 137-156.

Ladd, R.S. (1974), "Specimen Preparation and Liquefaction of Sands", JGED, ASCE, 100, No. GT10, pp. 1180-1184.

Ladd, R.S. (1977), "Specimen Preparation and Cyclic Stability of Sands", JGED, ASCE, Vol. 103, No. GT6, pp. 535-547.

Ladd, R.S. (1978), "Preparing Test Specimens Using Undercompaction" Geotechnical Testing Journal, GTJODJ, Vol. 1, No. 1, pp. 16-23.

Lade, P.V. and Hernandez, S.B. (1977), "Membrane Penetration Effects in Undrained Tests", JGED, ASCE, 103, pp. 109-125.

Lambe, P.C. (1981), Dynamic Centrifugal Modelling of a Horizontal Sand Stratum, Sc.D. Thesis, M.I.T. Department of Civil Engineering.

Lambe, P.C., and Whitman, R.V. (1980), Modelling Dynamic Ground Motions by Centrifuge - First Test Series", M.I.T. Department of Civil Engineering Report R80-40.

Lambe, T.W. (1951), "Soil Testing for Engineers", John Wiley & Sons, Inc., New York.

Lambe, T.W. (1967), "Stress Path Method", JSMFD, ASCE, 93, SM6, pp. 309-339.

Lambe, T. William and Associates (1977), Static Triaxial Tests on Oosterschelde Sand, Document L-38, T. William Lambe and Associates, Carlisle, Massachusetts.

Lambe, T. William and Associates (1977), Prediction of Strain and Pore Pressure from Cyclic Triaxial Tests, Document 1-40, T.W. Lambe and Associates, Carlisle, Massachusetts.

Lambe, T.W., and Marr, W.A. (1979), "Stress Path Method: Second Edition", JGED, ASCE, Vol. 105, No. GT6, pp. 727-738.

Lambe, T.W. and Whitman, R.V. (1969), Soil Mechanics, John Wiley and Sons, Inc., New York.

Lee, K.L. (1976), "Fundamental Considerations for Cyclic Triaxial Tests on Saturated Sand", Proc. BOSS'76, 1, pp. 355-373, Trondheim, Norway.

Lee, K.L. and Albaisa, A. (1974), "Earthquake Induced Settlements in Saturated Sands", JGED, ASCE, 100, GT4, Proc. Paper 10496, pp. 387-406.

Lee, K.L. and Fitton, J.A. (1969), "Factors Affecting the Cyclic Loading Strength of Soil", Vibration Effects of Earthquakes on Soils and Foundations, ASTM Special Technical Publication, 450, Philadelphia, PA, pp. 71-95.

Lee, K.L. and Focht, J.A., Jr. (1975), "Liquefaction Potential at Ekofisk Tank in North Sea", JSMFD, ASCE, 101, GT1, pp. 1-18.

Lee, K.L. and Seed, H.B. (1967a), "Cyclic Stress Conditions Causing Liquefaction of Sand", JSMFD, ASCE, 93, No. SM1, pp. 47-70.

Lee, K.L. and Seed, H.B. (1967b), "Dynamic Strength of Anisotropically Consolidated Sand", JSMFD, ASCE, 93, No. SM5, pp. 169-190.

Lee, K.L. and Seed, H.B. (1967c), "Drained Strength Characteristics of Sands", JSMFD, ASCE, 93, SM6, pp. 117-141.

Lee, K.L. and Seed, H.B. (1970), "Undrained Strength of Anisotropically Consolidated Sand", JSMFD, ASCE, 96, SM2, pp. 411-428.

Lee, K.L., and Vernese, F.J. (1978), "End Restraint Effects on Cyclic Triaxial Strength of Sand", JGED, ASCE, Vol. 104, No. GT6, pp. 705-719.

Marcuson, W.F., III, Chmn. (1978), "Definition of Terms Related to Liquefaction", JGED, ASCE, Vol. 104, No. GT9, pp. 1197-1200.

Martin. G.R., Finn, W.D.L. and Seed, H.B. (1975), "Fundamentals of Liquefaction Under Cyclic Loading", JGED, ASCE, 101, No. GT5 Proc. Paper 11285, pp. 423-438.

Martin, G.R., Finn, W.D.L., and Seed, H.B. (1978), "Effects of System Compliance on Liquefaction Tests", JGED, ASCE, Vol. 104, No. GT4, pp. 463-478.

Martin, P.P., and Seed, H.B. (1979), "Simplified Procedure for Effective Stress nalysis of Ground Response", JGED, ASCE, Vol. 105, No GT6, pp. 739-758.

Mori, K., Seed, H.B., and Chan, C.K. (1978), "Influence of Sample Disturbance on Sand Response to Cyclic Loading", JGED, ASCE, Vol. 104, No. GT3, pp. 323-339.

Mori, K. (1976), "Factors Affecting the Liquefaction Behavior of Saturated Sands", PhD Dissertation, University of California, Berkeley.

Morris, D.V. (1979), The Centrifugal Modelling of Dynamic Soil-Structure Interaction and Earthquake Behavior, Ph.D. Thesis, Cambridge University.

Mulilis, J.P., Chan, C.J., and Seed, H.B. (1075), "The Effects of Method of Sample Preparation on the Cyclic Stress-Strain Behavior of Sands", Report No. EERC75-18.

Mulilis, J.P. et al (1977), "Effects of Sample Preparation on Sand Liquefaction", JGED, ASCE, 103, GT2, pp. 91-108.

Oda, M. (1972a), "Initial Fabrics and Their Relations to Mechanical Properties of Granular Material", Soils and Foundations, March, 12, No. 1, pp. 17-36.

Oda, M. (1972b), "The Mechanism of Fabric Changes During Compressional Deformation of Sand", Soils and Foundations, June, 12, No. 2, pp. 1-18.

Oda, M. (1972c), "Deformation Mechanism of Sand in Triaxial Compression Tests:, Soils and Foundations, December, 12, No. 4, pp. 45-63.

Park, T.K. and Silver, M.L. (1975), "Dynamic Triaxial and Simple Shear Behavior of Sand", JGED, ASCE, 101, No. GT6, pp. 513-530.

Peacock, W.H. and Seed, H.B. (1968), "Sand Liquefaction Under Cyclic Loading Simple Shear Conditions", JSMFD, ASCE, 94, No. SM3, pp. 689-707.

Poulos, H.G. and Davis, E.H. (1974), Elastic Solutions for Soil and Rock Mechanics, John Wiley & Sons, Inc., New York.

Pyke, R.M., Chan, C.K., and Seed, H.B. (1974), Settlement and Liquefaction of Sands Under Multi-Directional Shaking, Report No. EERC-74-2, University of California, Berkeley.

Schofield, A.N. (1981), "Dynamic and Earthquake Geotechnical Centrifuge Modelling", Proc. Int. Conf. on Recent Advances in Geotechnical Earthquake Engineering and Soil Dynamics, Vol. 3, pp. 1-17.

Seed, H.B. (1979), "Soil Liquefaction and Cyclic Mobility Evaluation for Level Ground during Earthquakes", JGED, ASCE, Vol. 105, No. GT2, pp. 201-255.

Seed, H.B., Arango,J. and Chan, C.K. (1975), "Evaluation of Soil Liquefaction Potential During Earthquakes", Report No. EERC 75-28, University of California, Berkeley, October.

Seed, H.B. and Idriss, I.M. (1967), "Analysis of Soil Liquefaction, Niigata Earthquake", JSMFD, ASCE, 93, SM3.

Seed, H.B. and Idriss, I.M. (1971), "Simplified Procedure for Evaluating Soil Liquefaction Potential", JSMFD, ASCE, 97, No. SM9, pp. 1249-1273.

Seed, H.B. and Lee, K.L. (1966), "Liquefaction of Saturated Sands During Cyclic Loading", JSMFD, ASCE, 92, No. SM6, pp. 105-134.

Seed, H.B., Lee, K.L., Idriss, I.M. and Makdisi, F.I. (1973), "Analysis of the Slides in the San Fernando Dams During the Earthquake of 9 February 1971", Report No. EERC 73-2, University of California, Berkeley.

Seed, H.B., Martin, P.P. and Lysmer, J. (1975), "The Generation and Dissipation of Pore Water Pressures During Soil Liquefaction", Report No. EERC 75-26.

Seed, H.B., Martin, P.P. and Lysmer, J. (1976), "Pore-Water Pressure Changes During Soil Liquefaction", JGED, ASCE, 102, GT4, pp. 323-346.

Seed, H.B. and Peacock, W.H. (1970), "Applicability of Laboratory Test Procedures for Measuring Soil Liquefaction Characteristics under Cyclic Loading", Report No. EERC 70-8, University of California, Berkeley, November.

Seed, H.B. and Peacock, W.H. (1971), "Test Procedures for Measuring Soil Liquefaction Characteristics", JSMFD, ASCE, 97, No. SM8, pp. 1099-1119.

Seed, H.B. and Silver, M.L. (1972), "Settlemnt of Dry Sands During Earthquakes", JSMFD, ASCE, 98, No. SM4, Proc. Paper 8844, pp. 381-397.

Selig, E.T., and Chang, C.S. (1981), "Soil Failure Modes in Undrained Cyclic Loading", JGED, ASCE, Vol. 107, No. GT5, pp. 539-551.

Sherif, M.A., Ishibashi, I., and Tsuchiya, C. (1977), "Saturation Effects on Initial Soil Liquefaction", JGED, ASCE, Vol. 103, No. GT8, pp. 914-917.

Silver, M.L., Chan, C.K., Ladd, R.S., Lee, K., Mulilis, J., Tiedemann, D., Townsend, F.C., Valera, J. and Wilson, J. (1976), "Cyclic Triaxial Strength of Standard Test Sand", JGED, ASCE, 102, GT5, pp. 511-523.

Silver, M.L., and Park, T.K. (1975), "Testing Procedure Effects on Dynamic Soil Behavior", JGED, ASCE, Vol. 101, No. GT10, pp. 1061-1083.

Silver, M.L. and Seed, H.B. (1971), "Volume Changes in Sands During Cyclic Loading", JSMFD, ASCE, 97, No. SM9, Proc. Paper 8354, pp. 1171-1182.

Tanimoto, K. (1967), "Liquefaction of Sand Layer Subjected to Shock and Vibratory Loads", Proc. Third Asian Regional Conference, S.M.F.E., Bangkok, Thailand.

Taverna, L.M., The Initial Development of a Radiograph Facility for Geotechnical Engineering Research, S.M. Thesis, M.I.T. Department of Civil Engineering.

Whitman, R.V. (1970), "Evaluation of Soil Properties for Site Evaluation and Dynamic Analysis of Nuclear Plants", Seismic Design for Nuclear Power Plants, R.J. Hansen, ed., The MIT Press, Cambridge, MA, pp. 250-305.

Wood, D.M. (1980), Laboratory Investigations of the Behaviour of Soils Under Cyclic Loading: A Review, Cambridge, University Report CUED/D - Soils/TR 84.

Woods, R.D. (1978), "Measurement of Dynamic Soil Properties", Proc., ASCE Specialty Conf., Earthquake Engineering and Soil Dynamics, Pasadena, Vol. 1, pp. 91-178.

Yoshimi, Y. (1967), "An Experimental Study of Liquefaction of Saturated Sands", Soils and Foundations, 7, No. 2, pp. 20-32.

Yoshimi, Y. and Oh-Oka, H. (1970), "Liquefaction of Saturated Sand During Vibration Under Quasi-Plane-Strain Conditions", Proc. 3rd Japan Earthquake Engineering Symposium, Tokyo.

Yoshimi, Y. and Oh-Oka, H. (1973), "A Ring Torsion Apparatus for Simple Shear Tests", Proc. 8th ISCMFE, Vol. 1.2, Moscow.

Youd, T.L. (1972), "Compaction of Sands by Repeated Shear Straining", JSMFD, ASCE, 98, N. SM7, Proc. Paper 9063, pp. 709-725.

APPENDIX A1

DRAINED CYCLIC TRIAXIAL TEST RESULTS

This appendix presents the results of seven drained cyclic tests on Leighton-Buzzard 120/200 Sand referred to in Chapter Four. Tests DC6 though test DC9, and DC12 were performed on samples prepared by the wet rodding method of sample formation, and Tests DC10 and DC11 were performed on samples prepared by the moist tamped method (with undercompaction).

All values of γ_{pp}, as determined for use in Chapter IV, were corrected for system compressibility. An experimentally-determined curve of vertical strain versus vertical stress for the testing apparatus itself is used to compute the component of vertical strain due to system compressibility, $(\varepsilon_{vpp})s$, for each test (Figure A1-1). This component of strain is subtracted from the measured value of

γ_{pp} as follows:

$$\gamma_{pp} = (\gamma_{pp})\text{measured} - 3/2(\varepsilon_{vpp})s$$

Figures A1-2 through A1-22 give results for the drained tests performed in this investigation. Given for each test is the effective stress path; the stress versus strain plots for various cycles; and the effective stresses ($\bar{p}_o$, q), vertical strain (ε_v), and volumetric strain (ε_{vol}) versus cycle number, N.

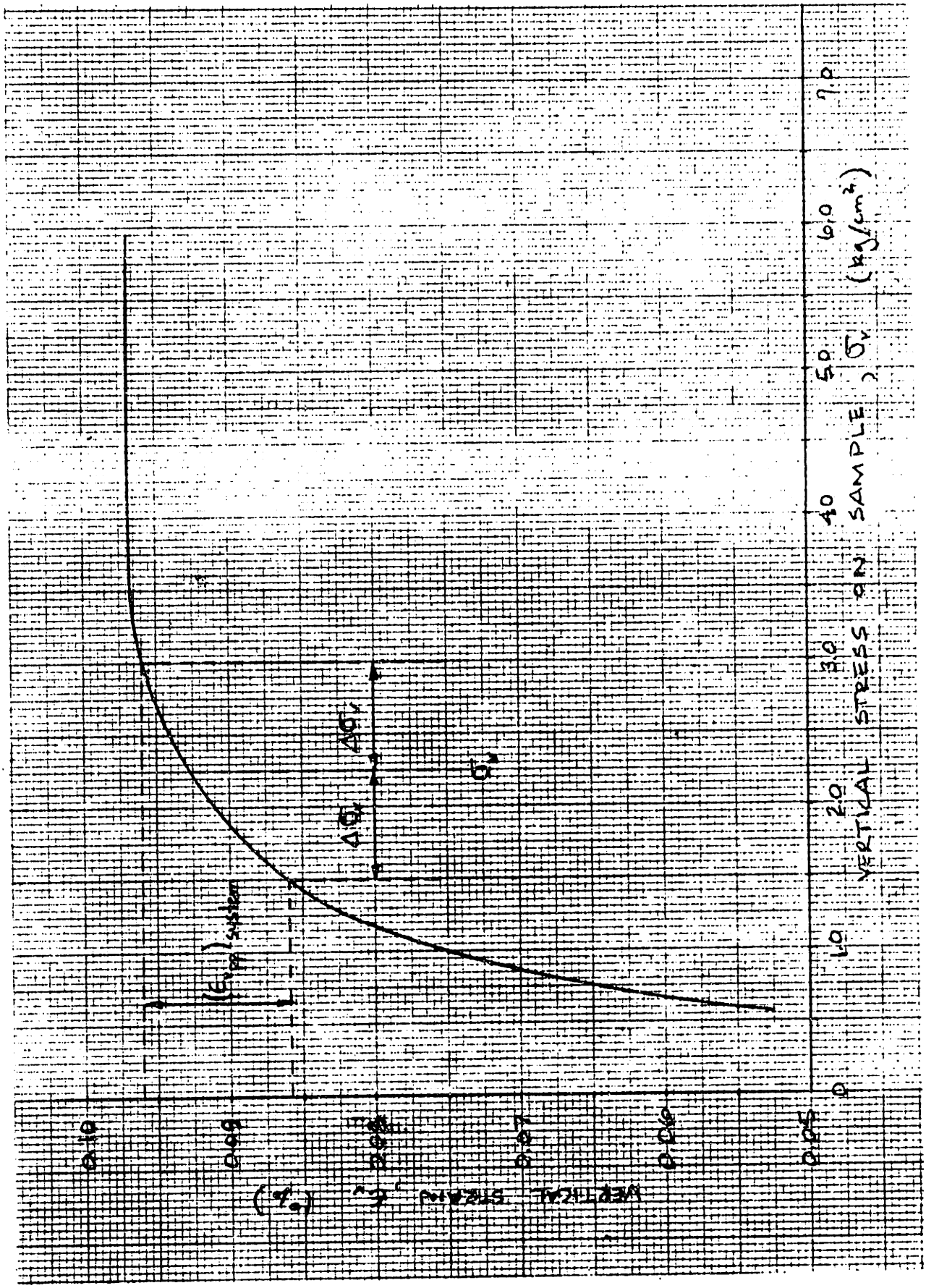

System Compressibility Curve

FIGURE A1-1

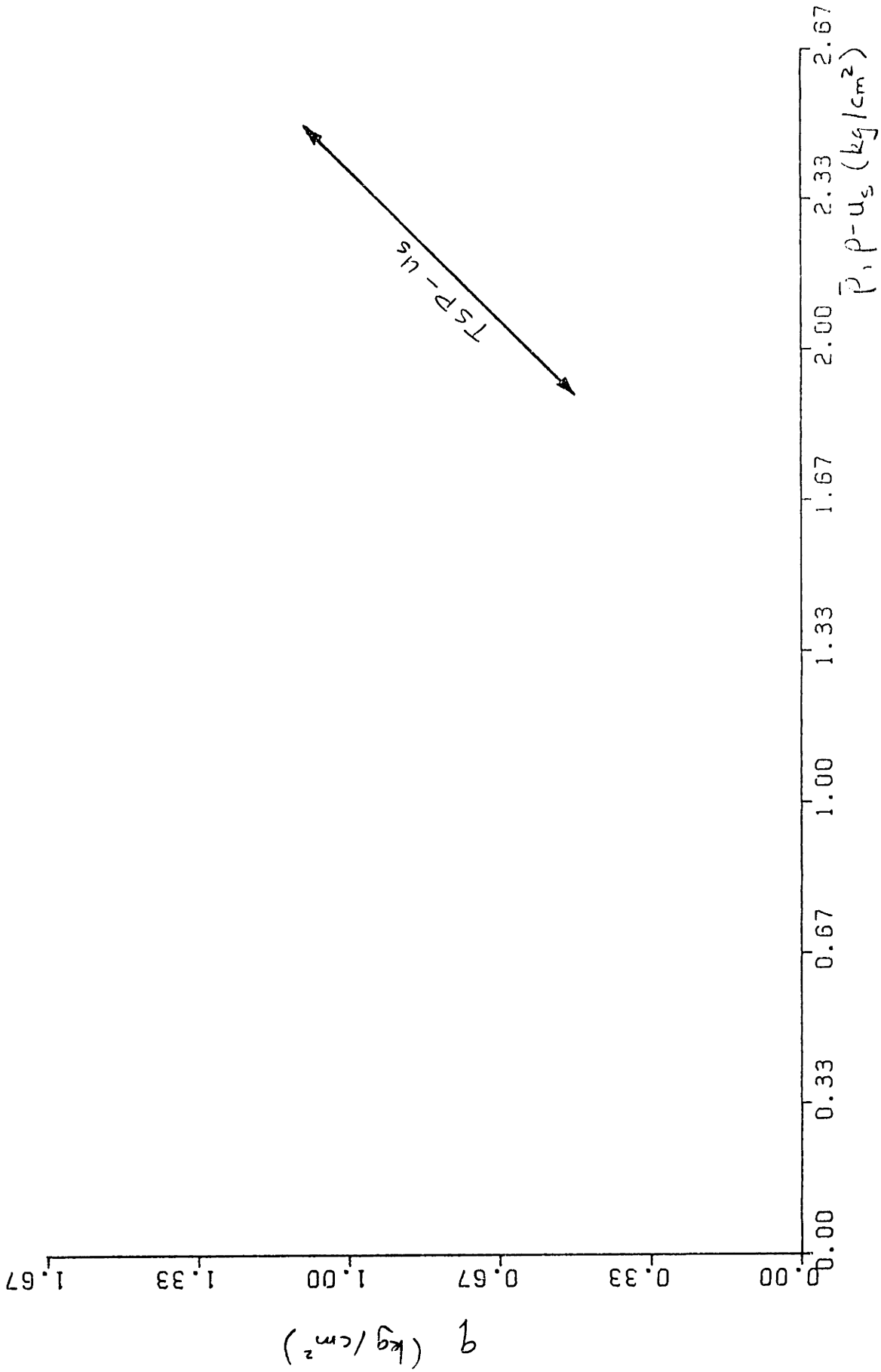

Effective Stress Path - Test DC6

FIGURE A1-2

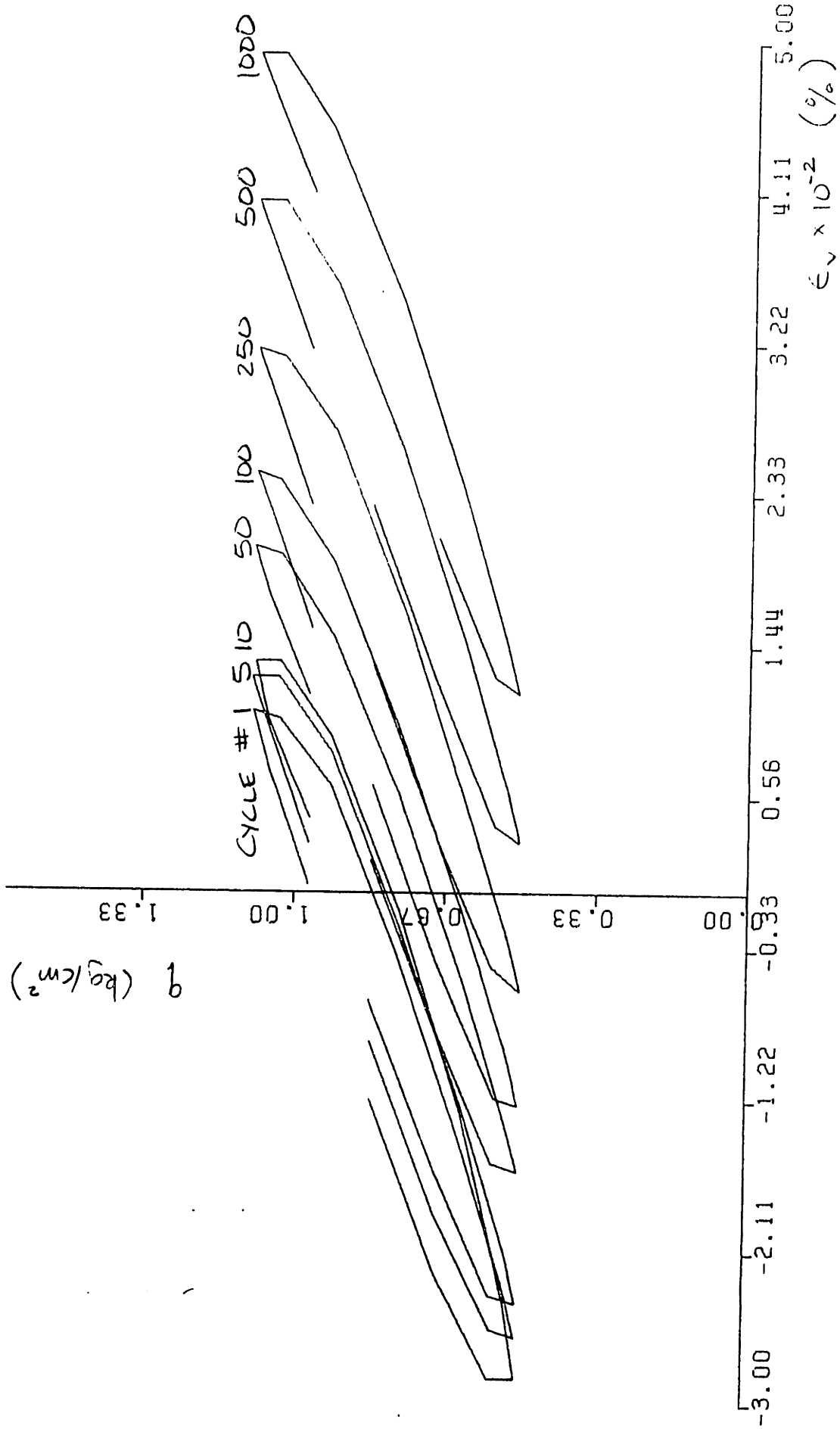

Stress vs. Strain - Test DC6

FIGURE A1-3

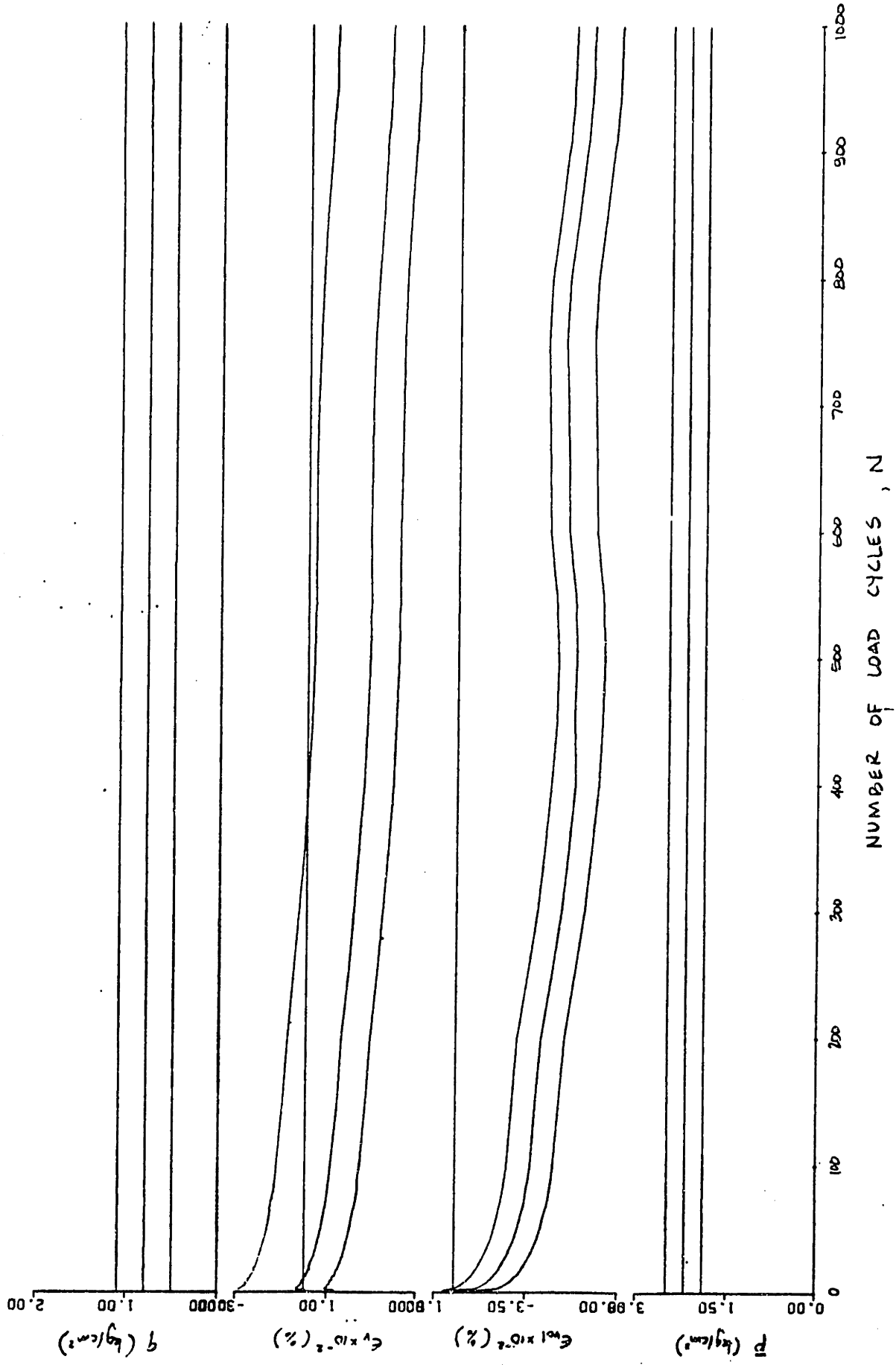

Summary of Stress and Strain Development - Test DC6

FIGURE A1-4

TEST DC7

Plots Not Available

TEST DC8

See Plots Chapter 4

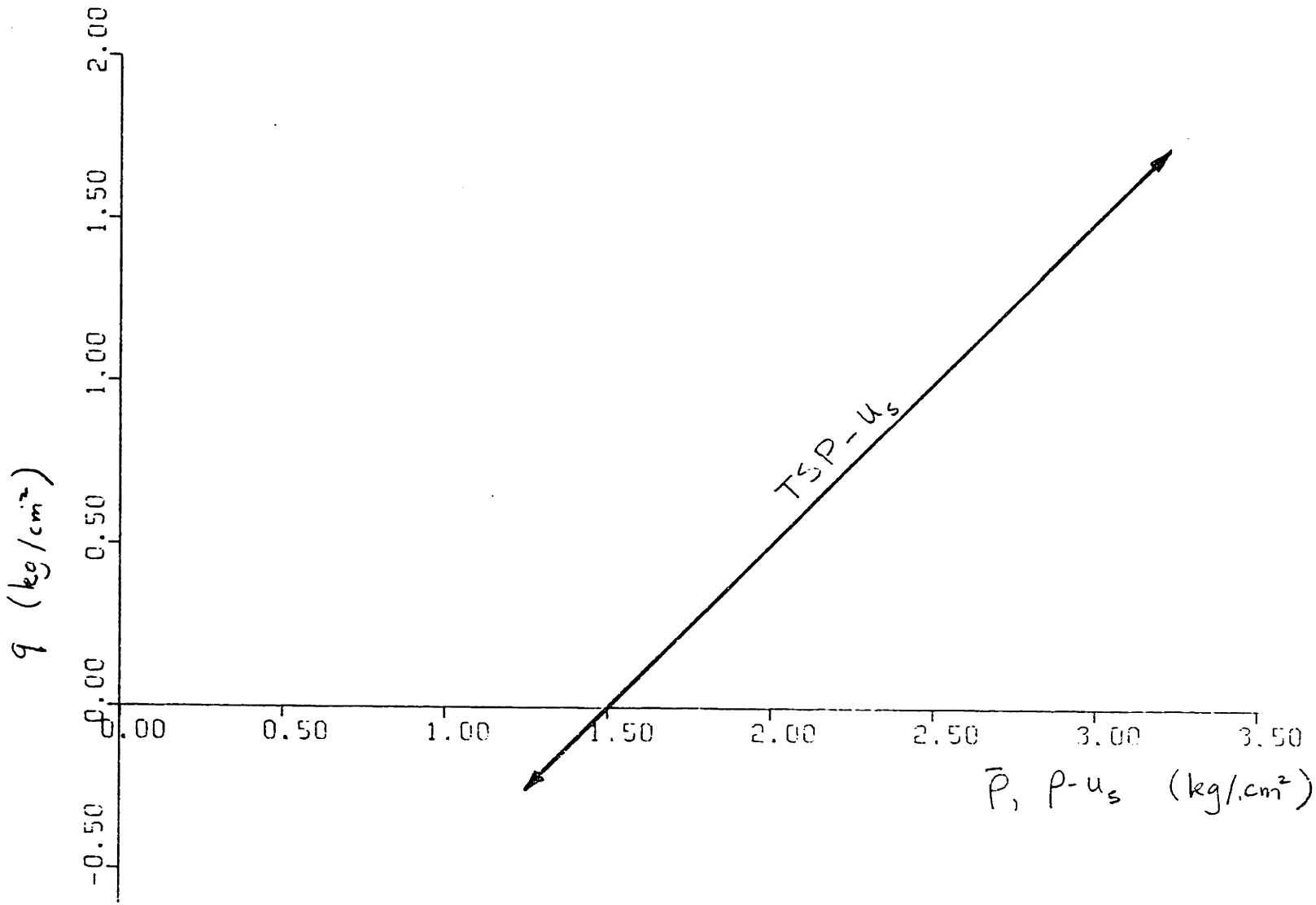

Effective Stress Path - Test DC9

FIGURE A1-5

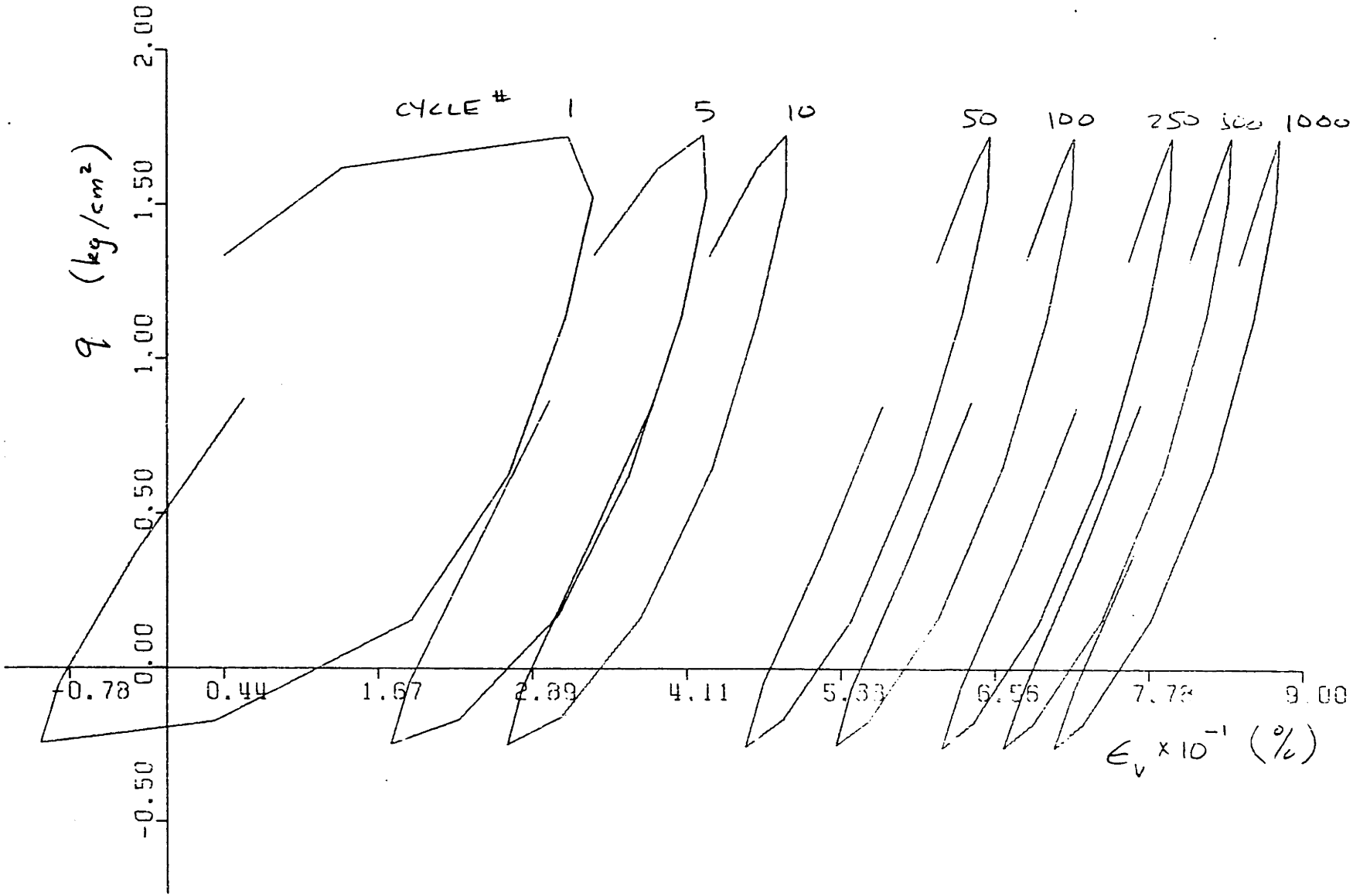

Stress vs. Strain - Test DC9

FIGURE A1-6

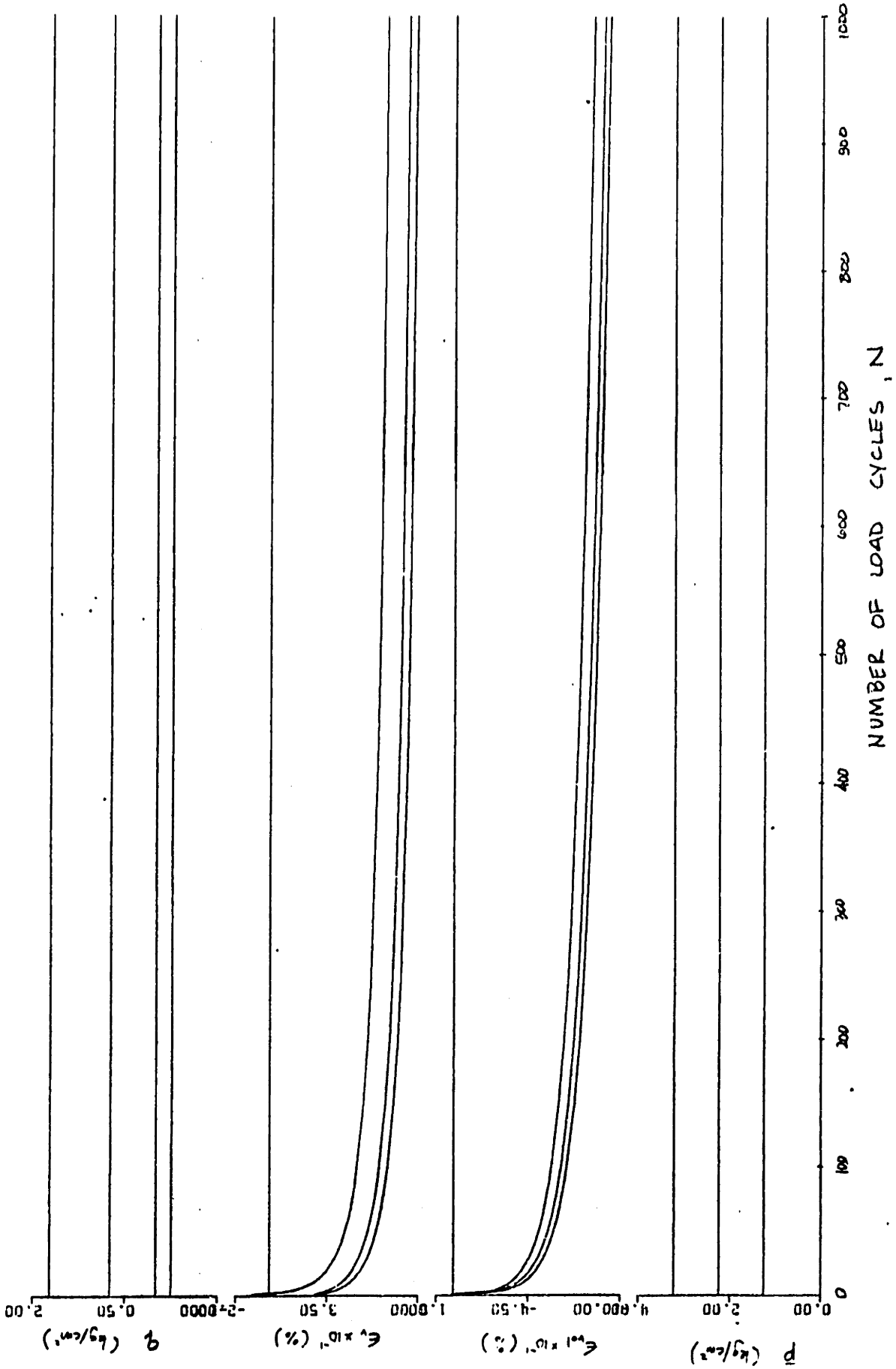

Summary of Stress and Strain Development - Test DC9

FIGURE A1-7

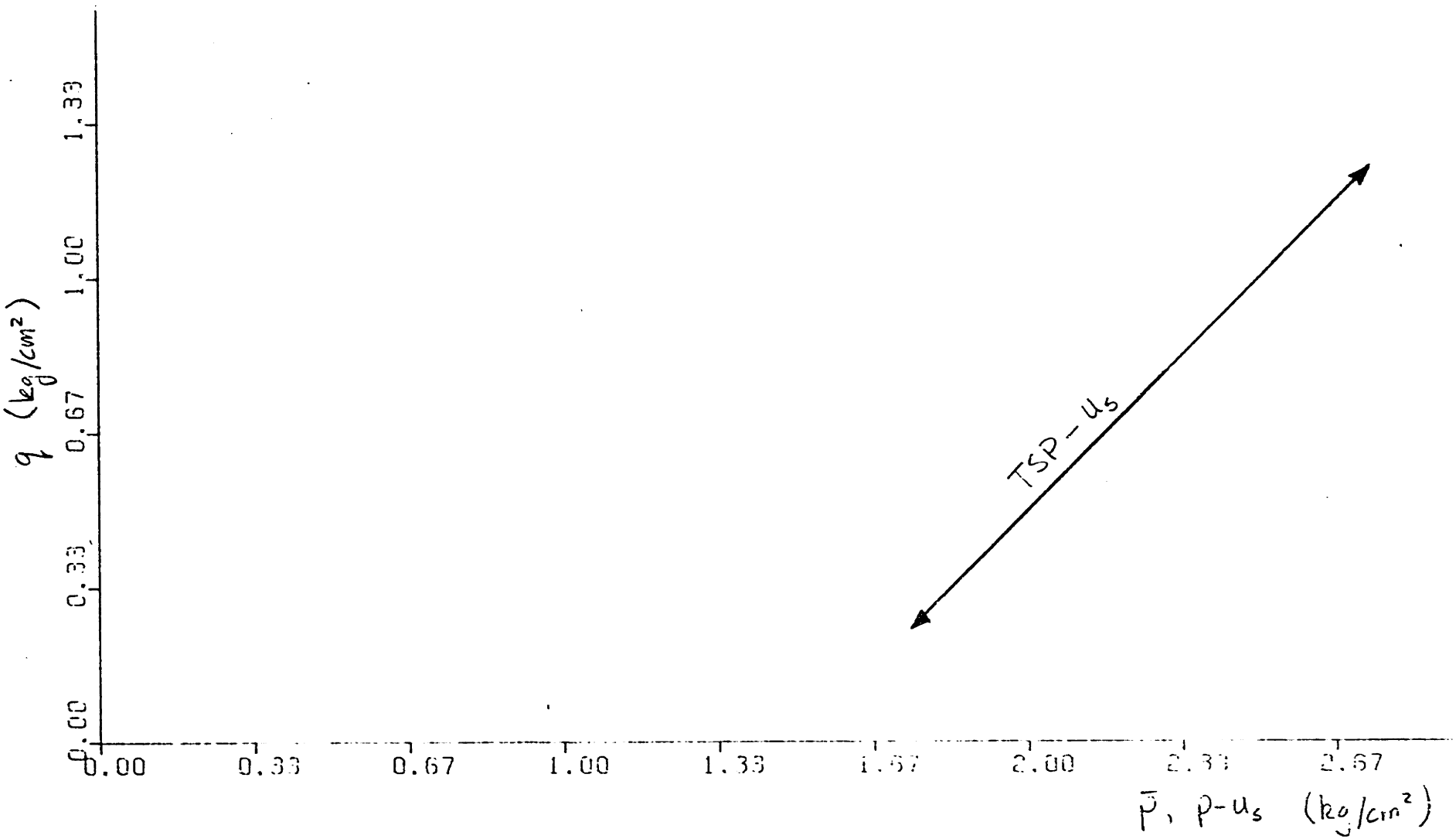

Effective Stress Path - Test DC10

FIGURE A1-8

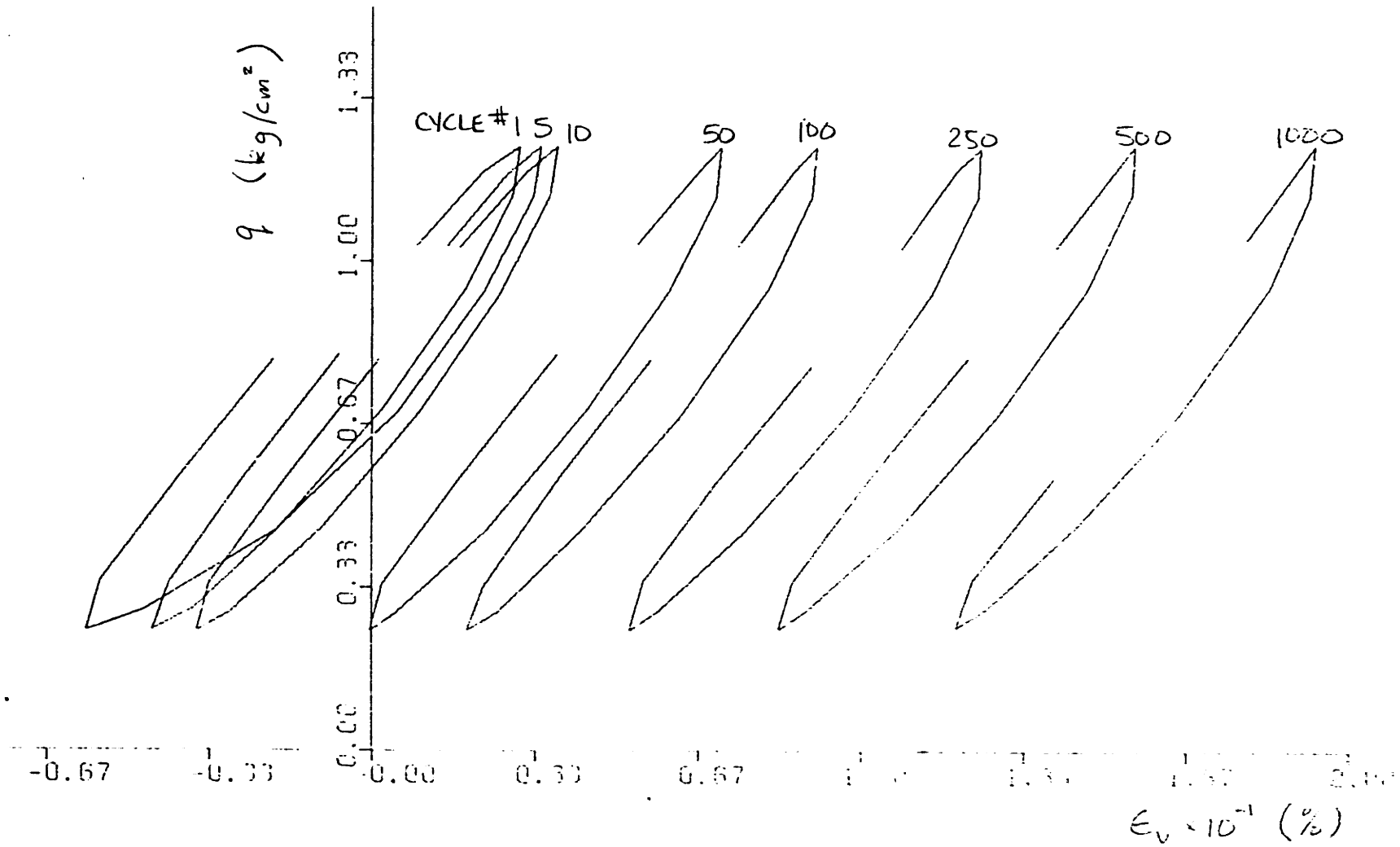

Stress vs. Strain - Test DC10

FIGURE A1-9

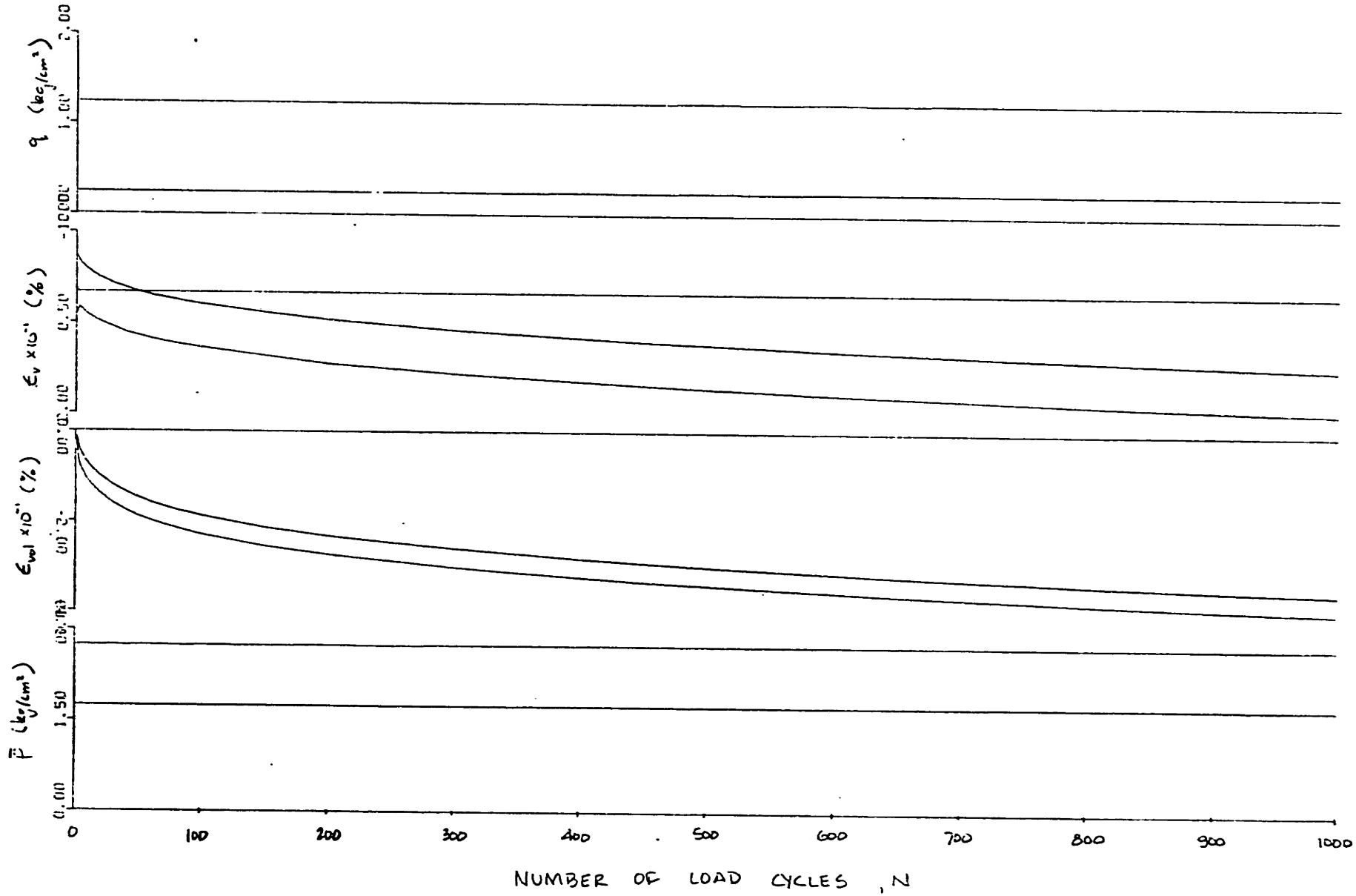

Summary of Stress and Strain Development - Test DC10

FIGURE A1-10

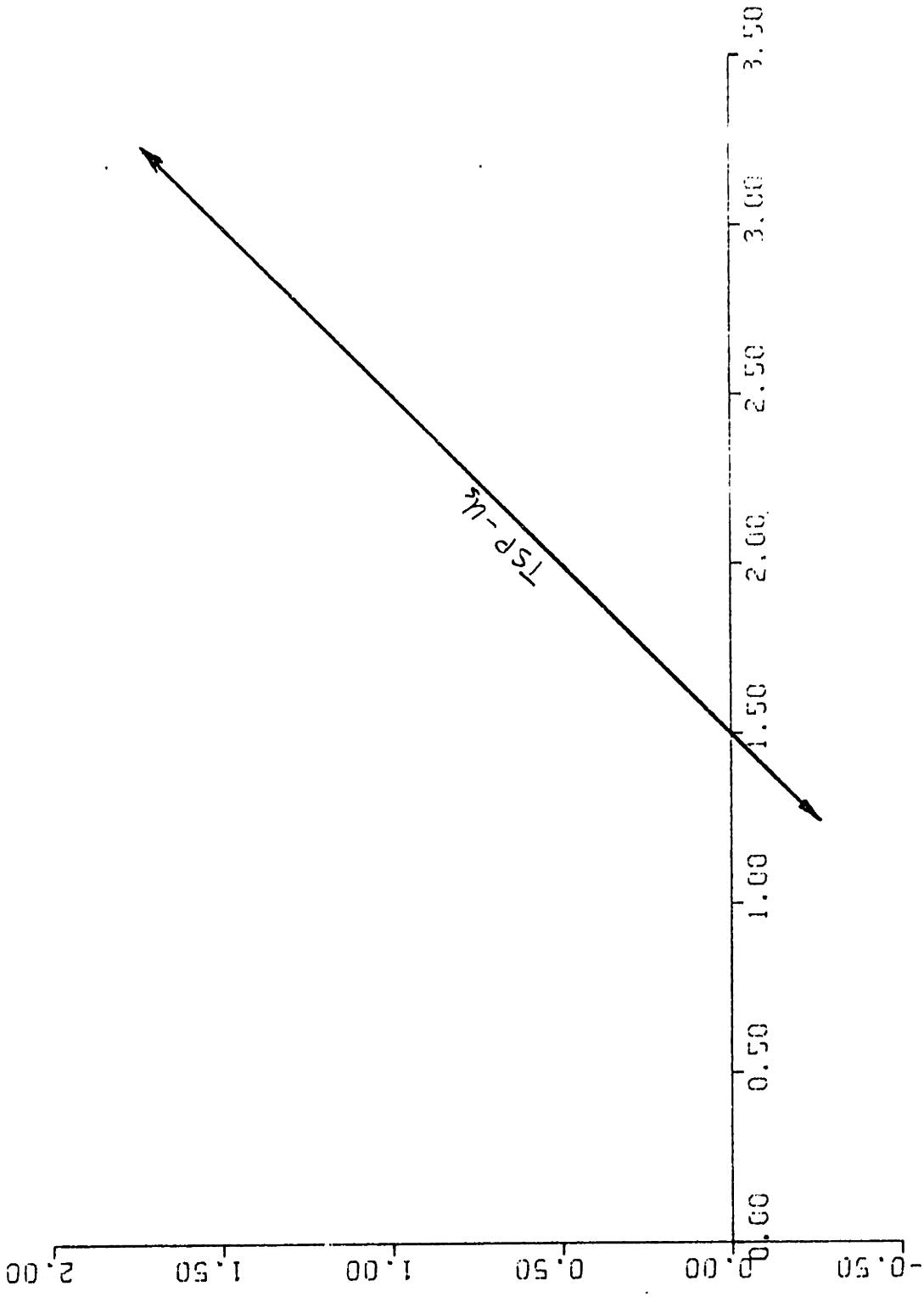

Effective Stress Path - Test DC11

FIGURE A1-11

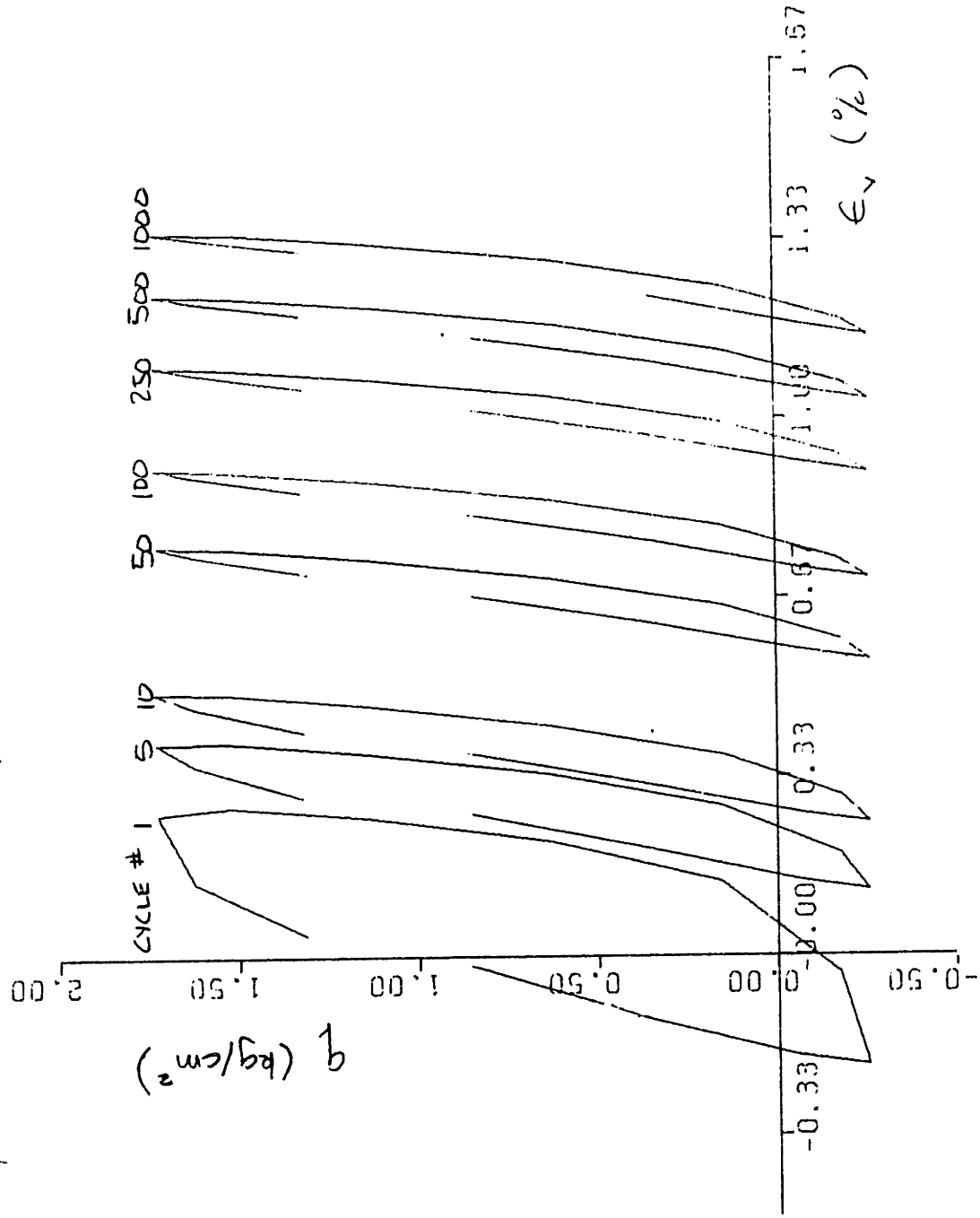

Stress vs. Strain - Test DC11

FIGURE A1-12

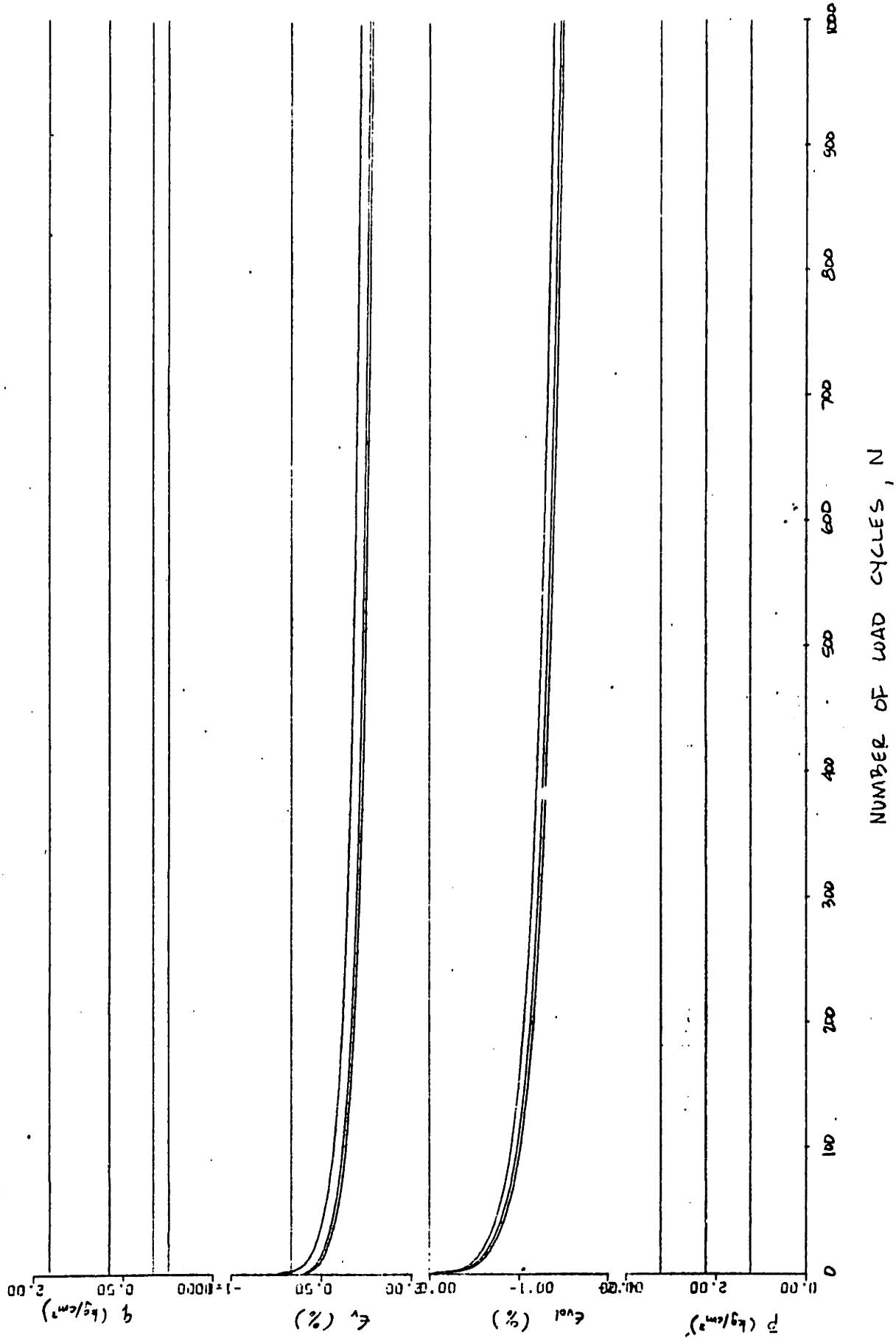

Summary of Stress and Strain Development - Test DC11

FIGURE A1-13

TEST DC12

Plots Not Available

APPENDIX A2

UNDRAINED CYCLIC TRIAXIAL TEST RESULTS

This appendix presents the results of eight undrained cyclic tests on Leighton-Buzzard 120/200 Sand referred to in Chapter Five. Given are the effective stress paths for various cycles; the stress versus strain plots for various cycles; and the effective stresses ($\bar{p}_o$, q), vertical strain (ε_v), and the change in pore pressure (Δu) plotted versus cycle number, N, for each test (excluding Test DC3, which was terminated after 900 cycles).

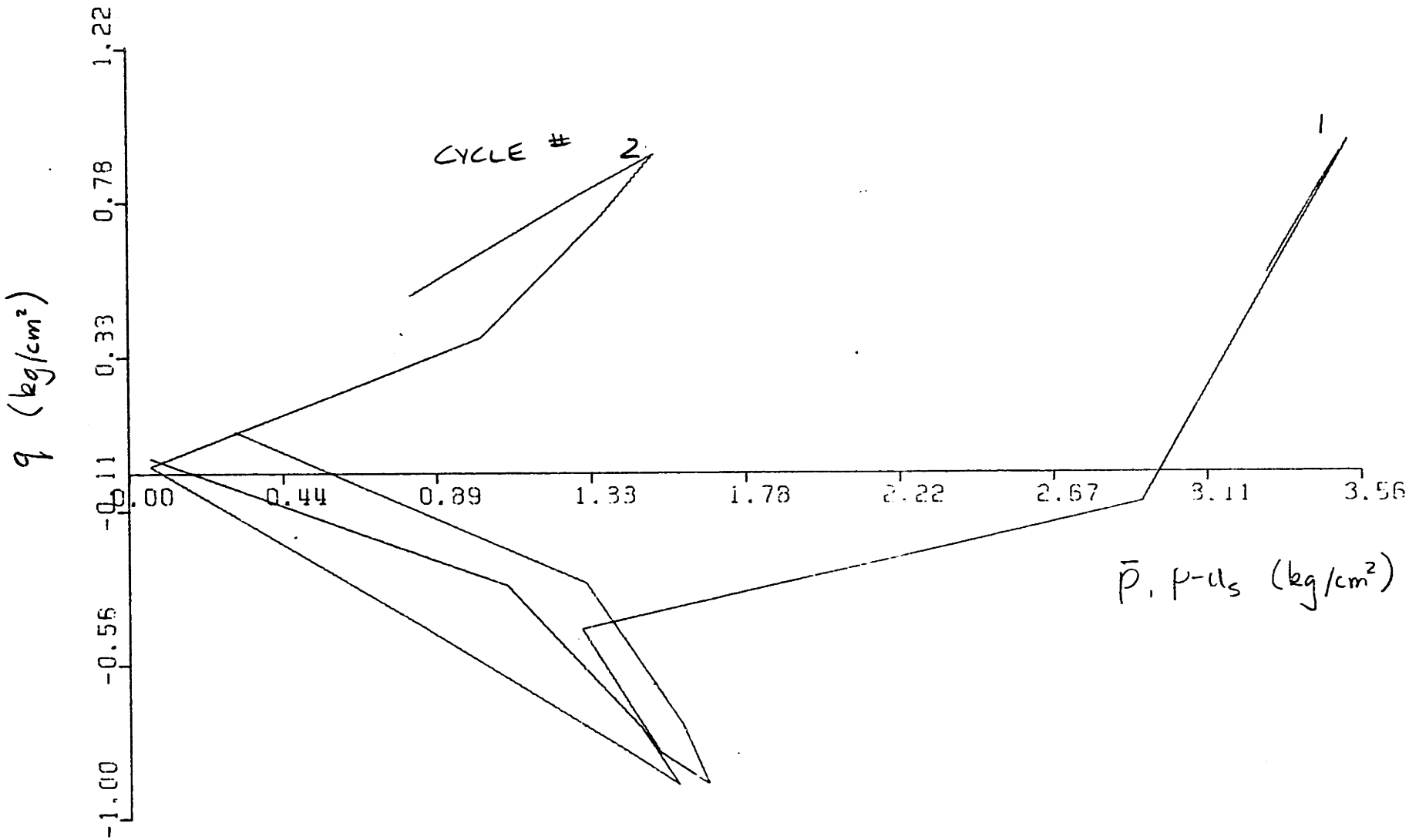

Effective Stress Path - Test UC1

FIGURE A2-1

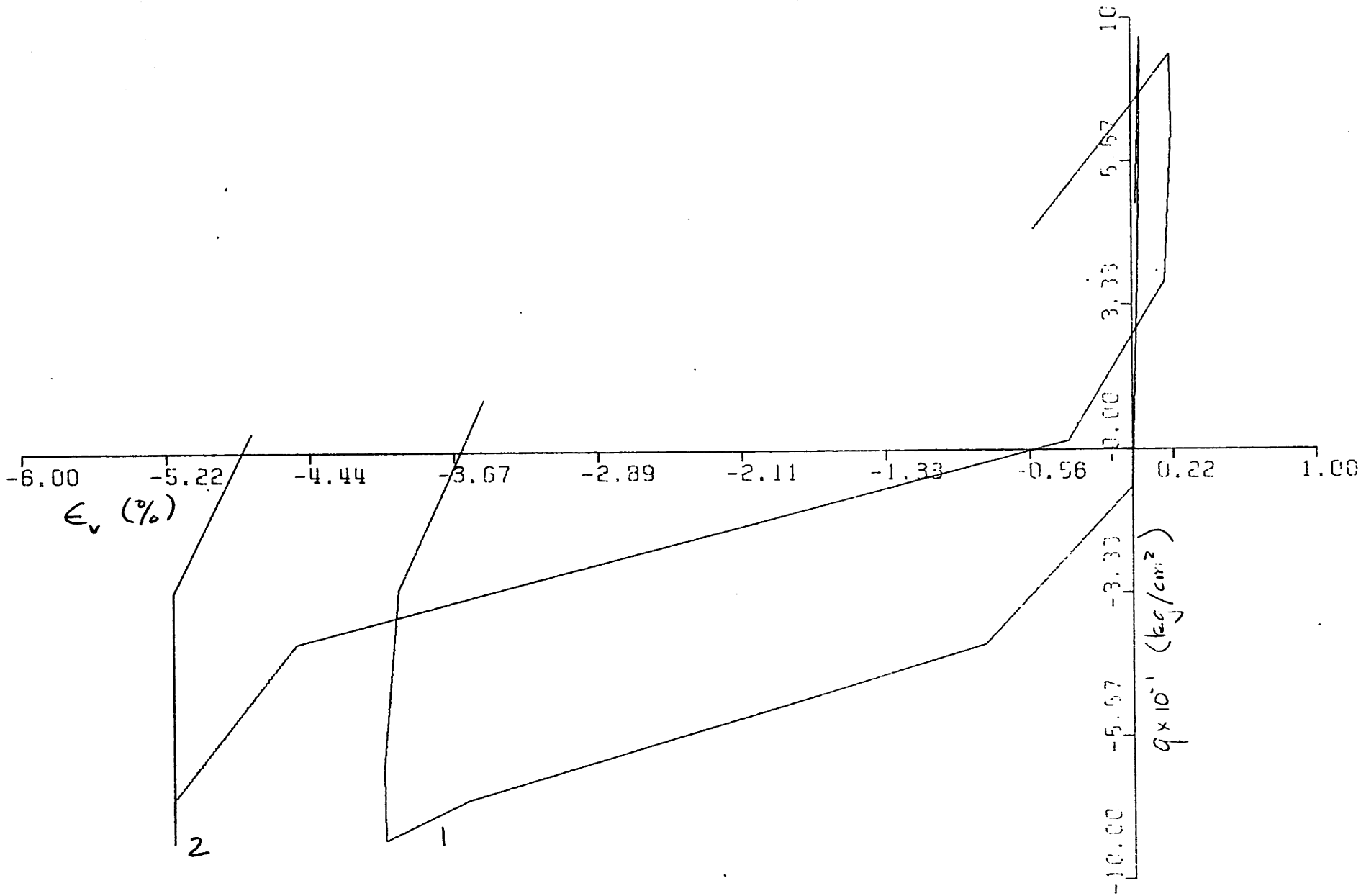

Stress vs. Strain - UC1

FIGURE A2-2

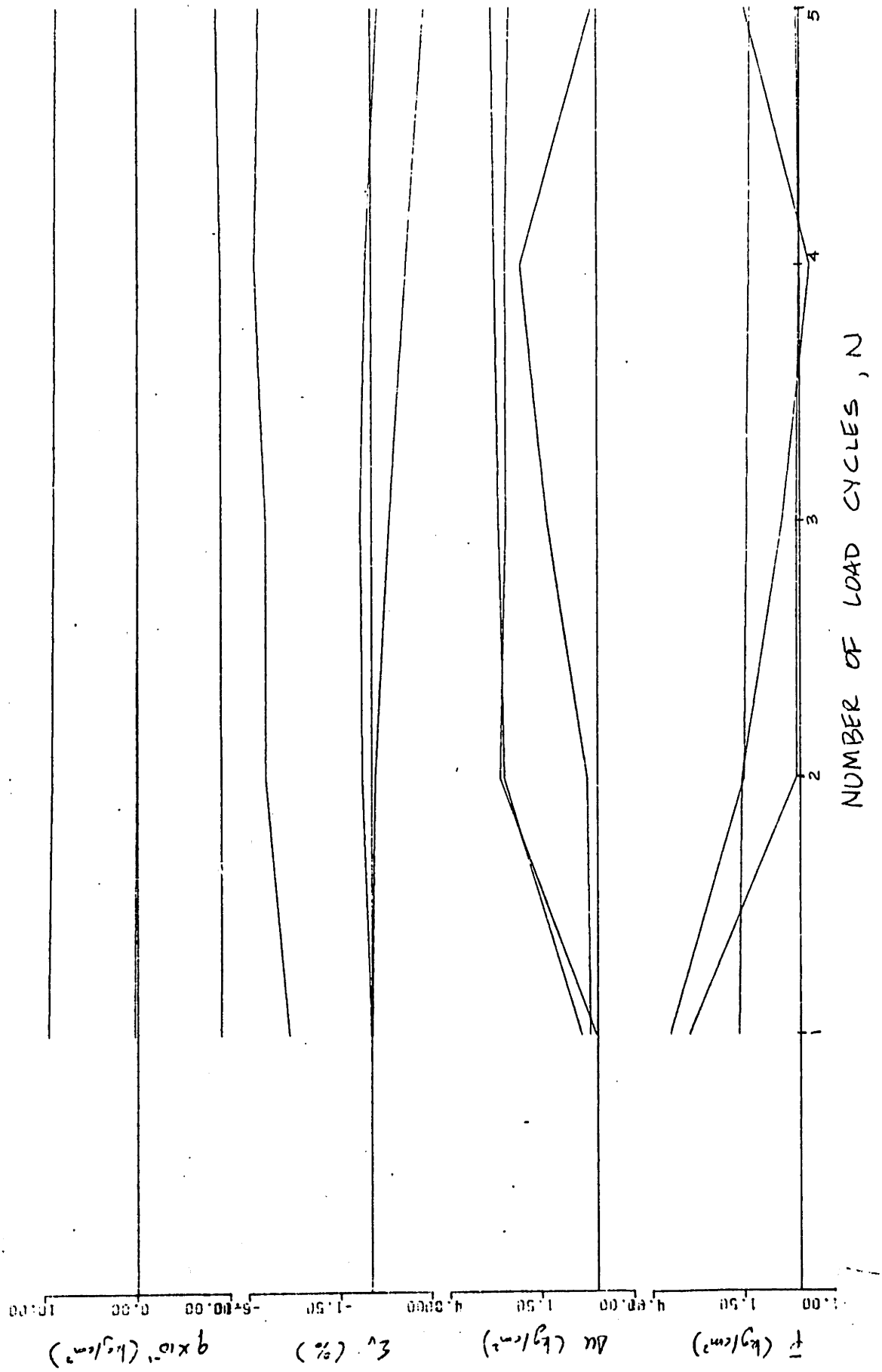

Summary of Stress Strain, and Pore Pressure Development - Test UC1

FIGURE A2-3

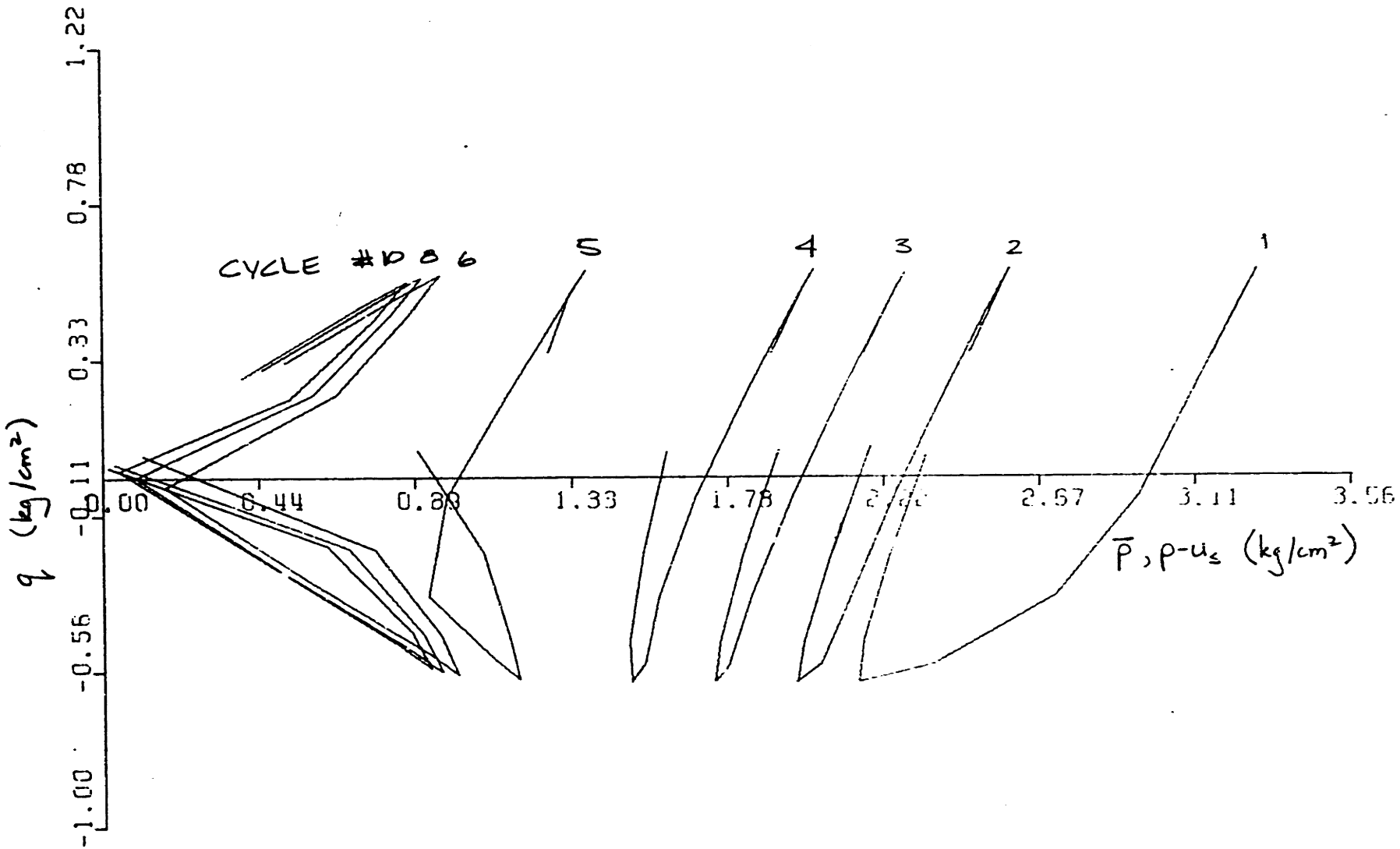

Effective Stress Path - Test UC2

FIGURE A2-4

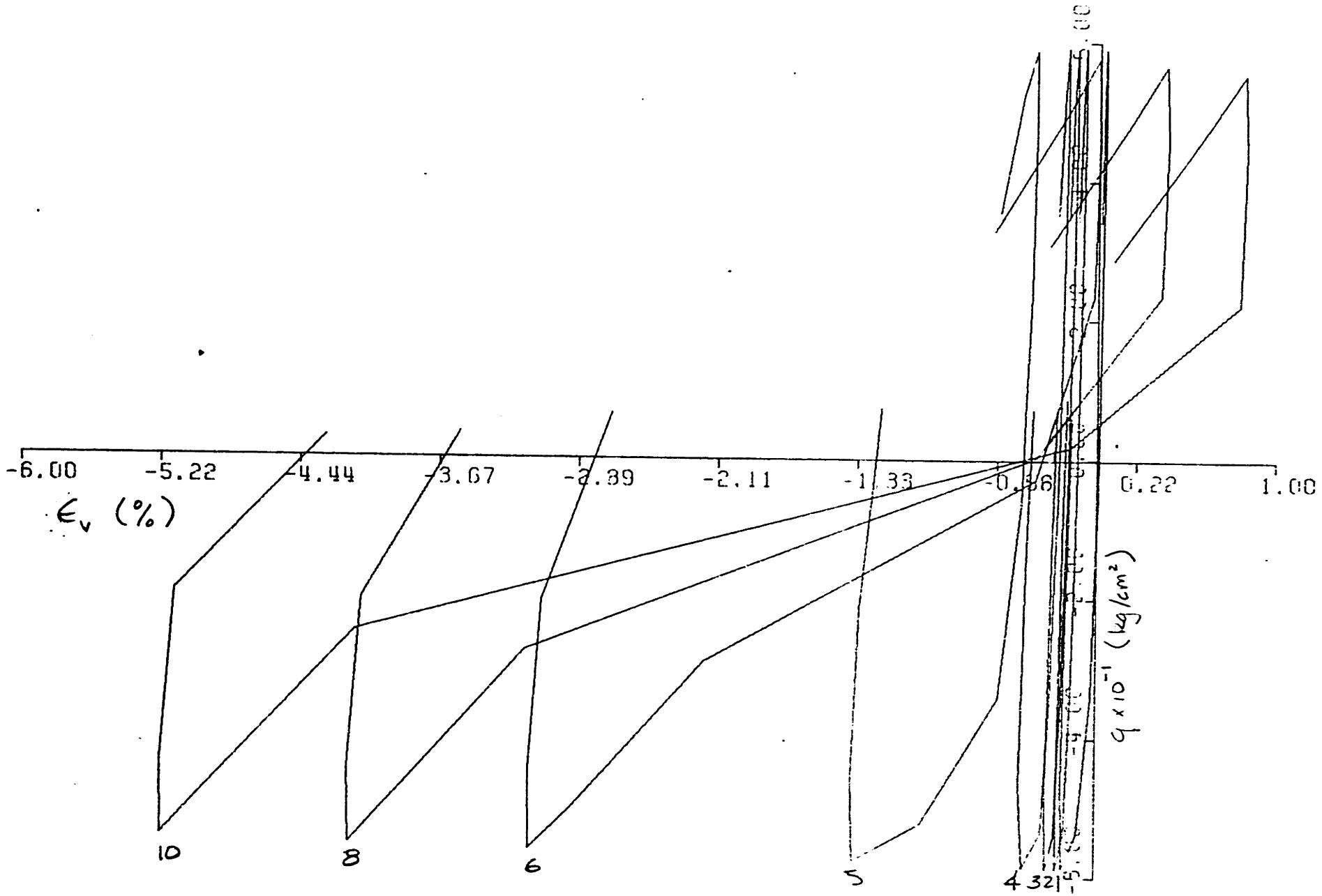

Stress vs. Strain - UC2

FIGURE A2-5

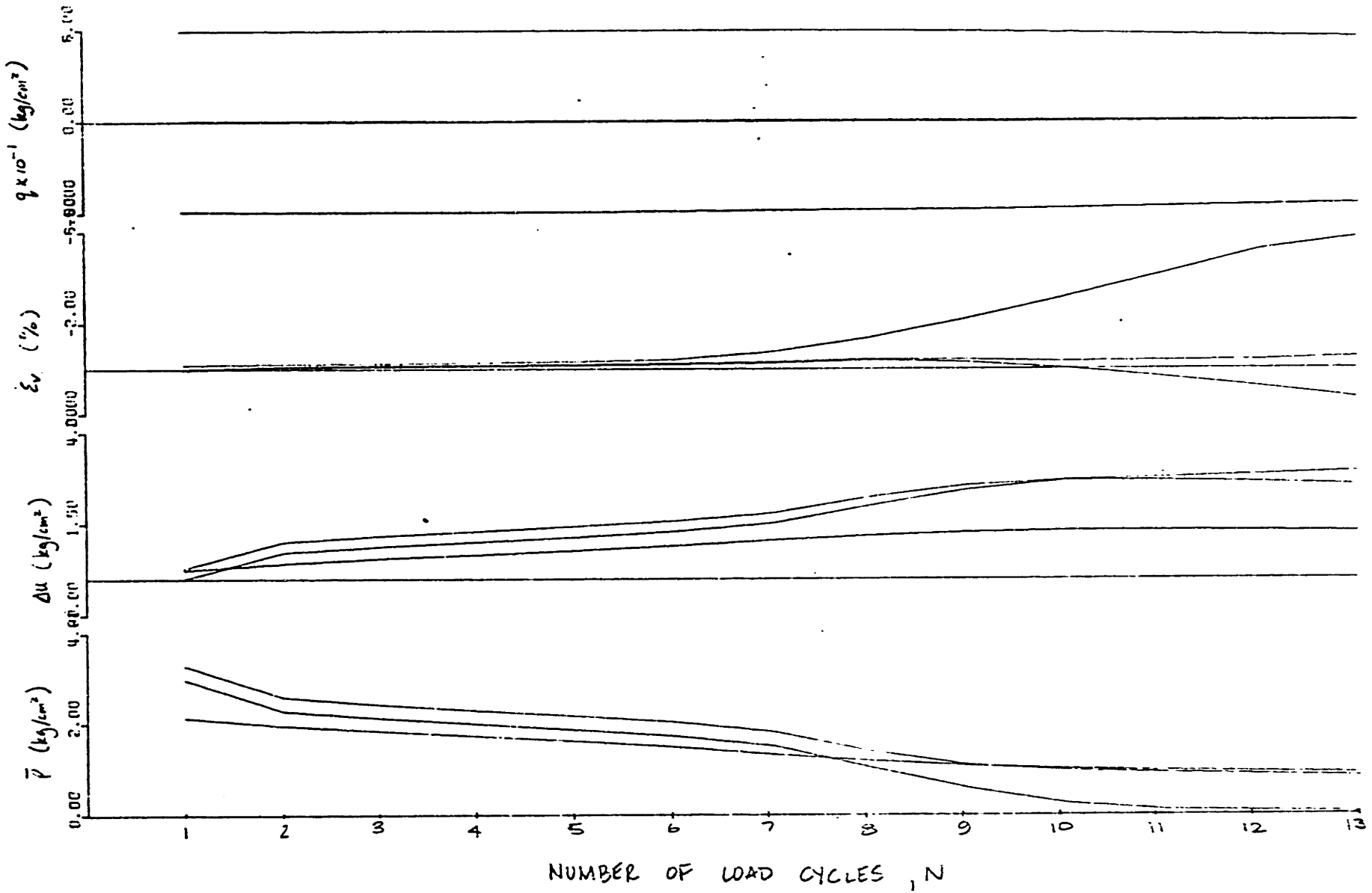

Summary of Stress Strain, and Pore Pressure Development - Test UC2

FIGURE A2-6

TEST UC3

Plots Not Available

TEST UC4

See Plots Chapter 5

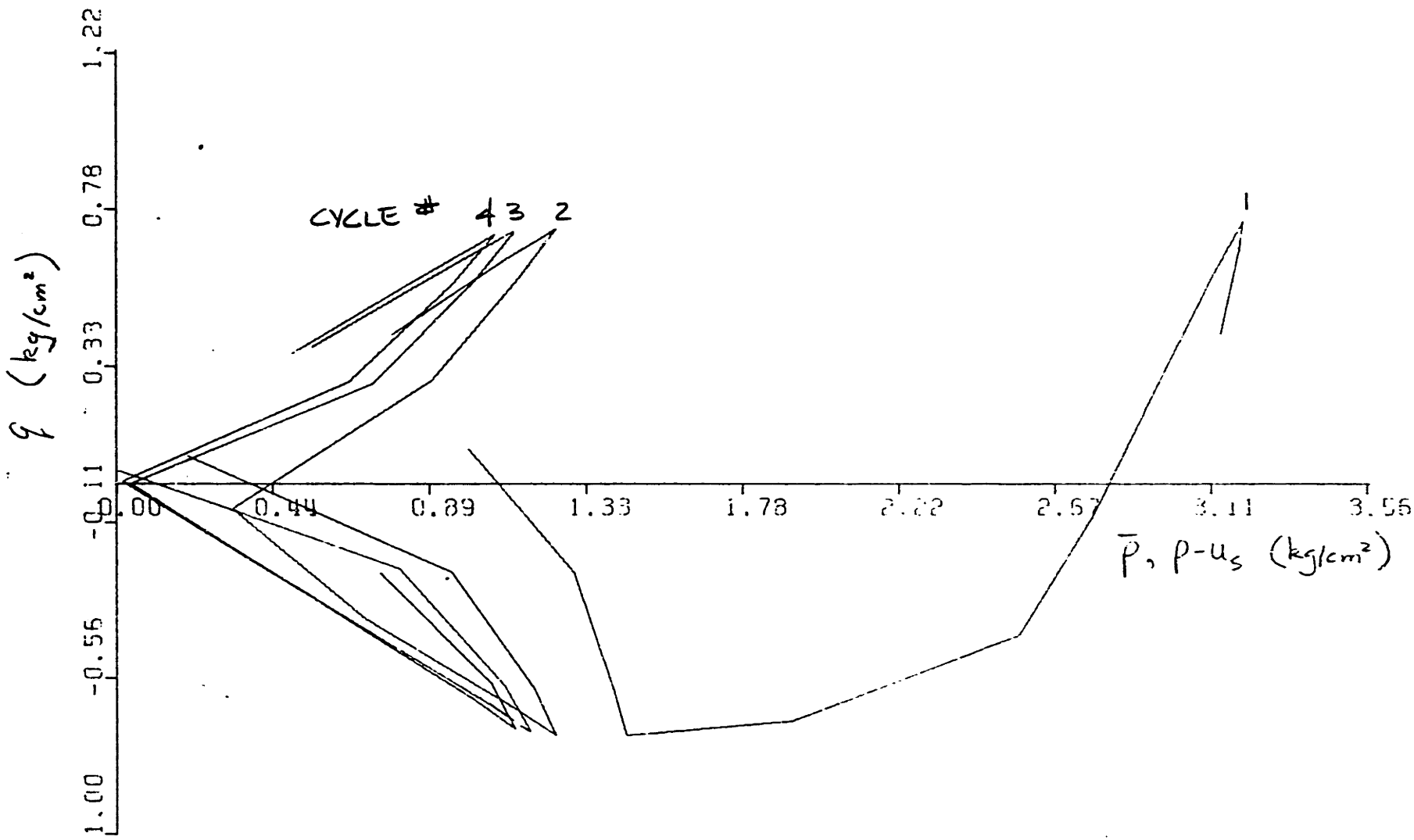

Effective Stress Path - Test UC5

FIGURE A2-7

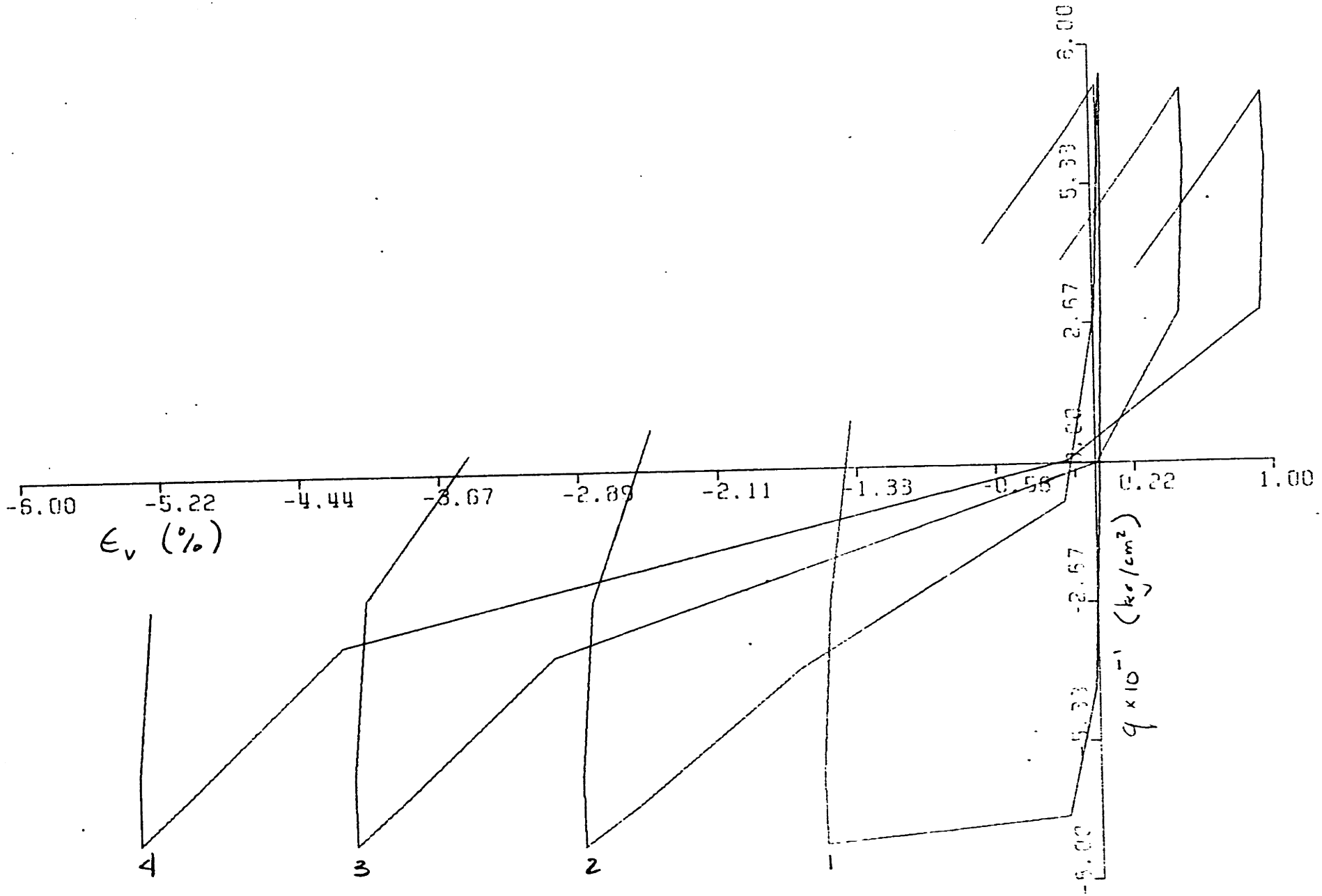

Stress vs. Strain - UC5

FIGURE A2-8

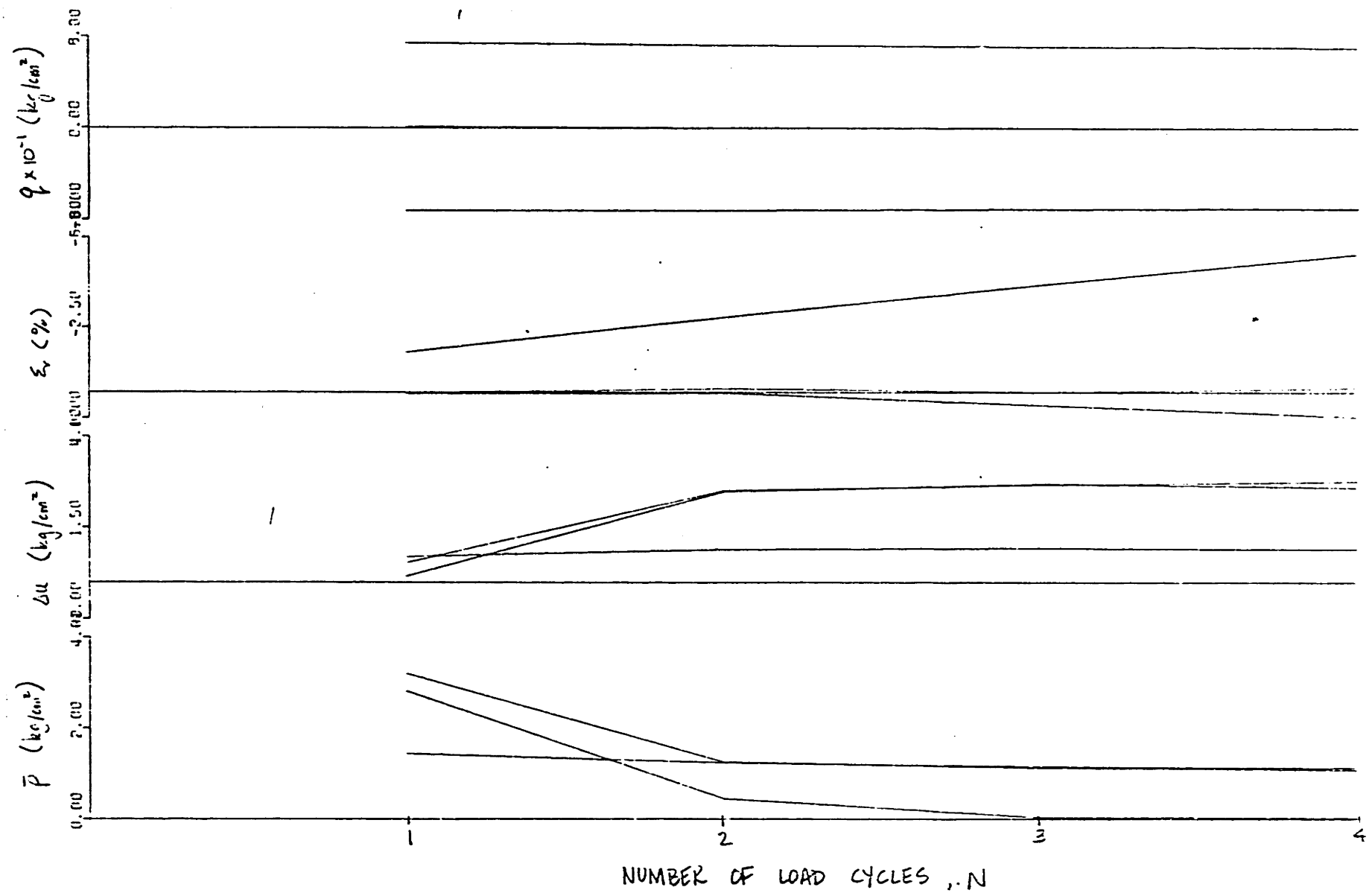

Summary of Stress Strain, and Pore Pressure Development - Test UC5

FIGURE A2-9

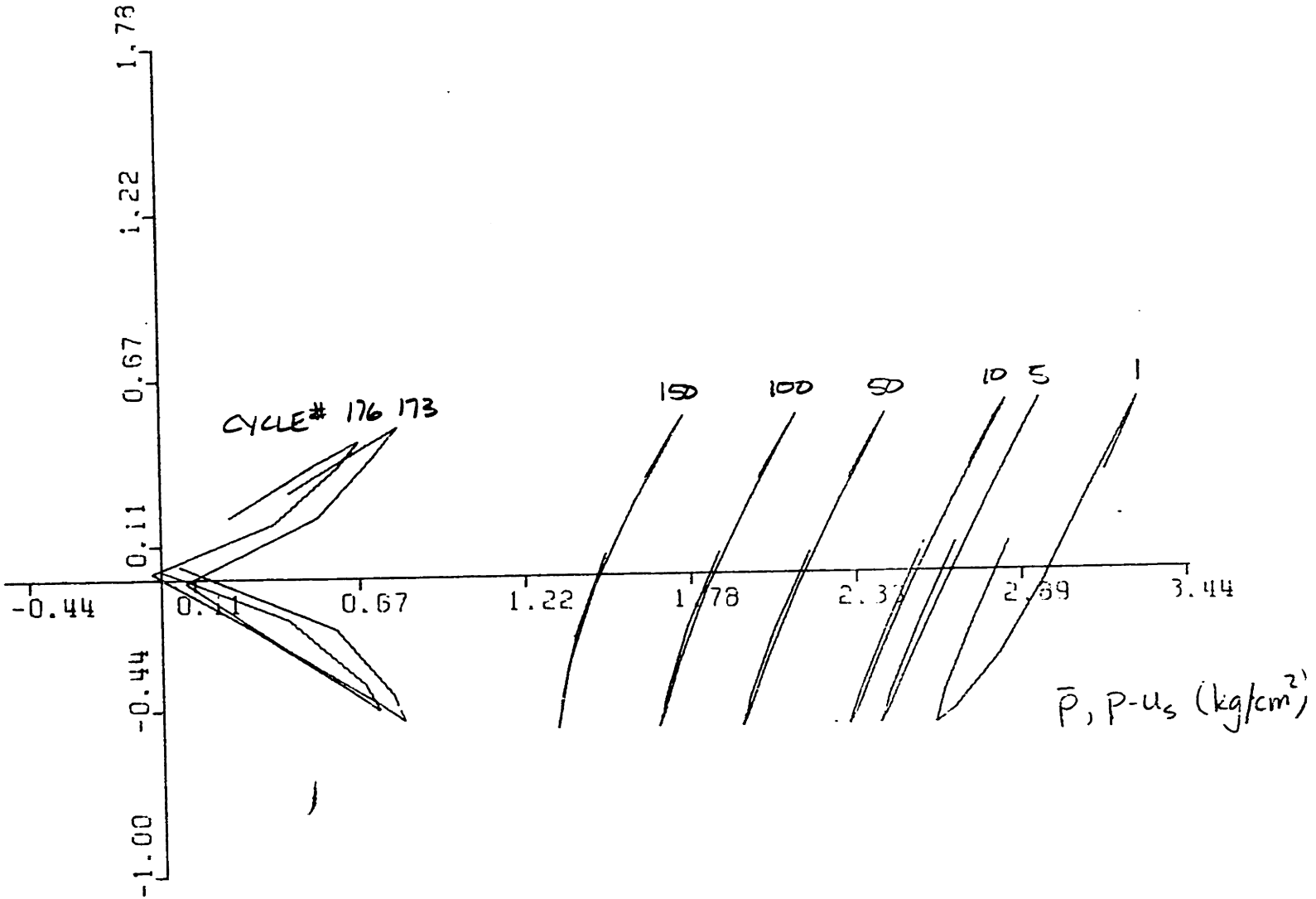

Effective Stress Path - Test UC6

FIGURE A2-10

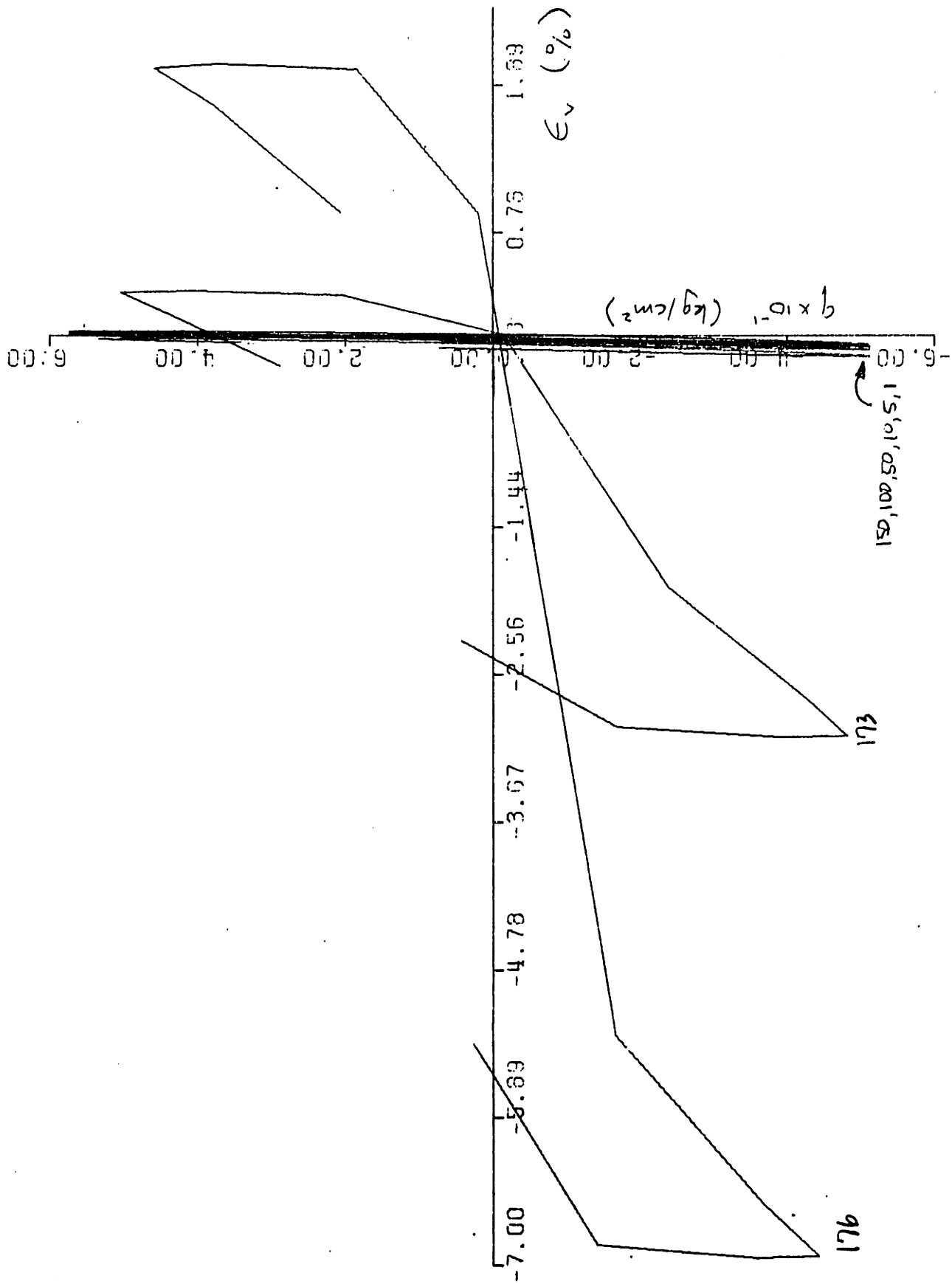

Stress vs. Strain - UC6

FIGURE A2-11

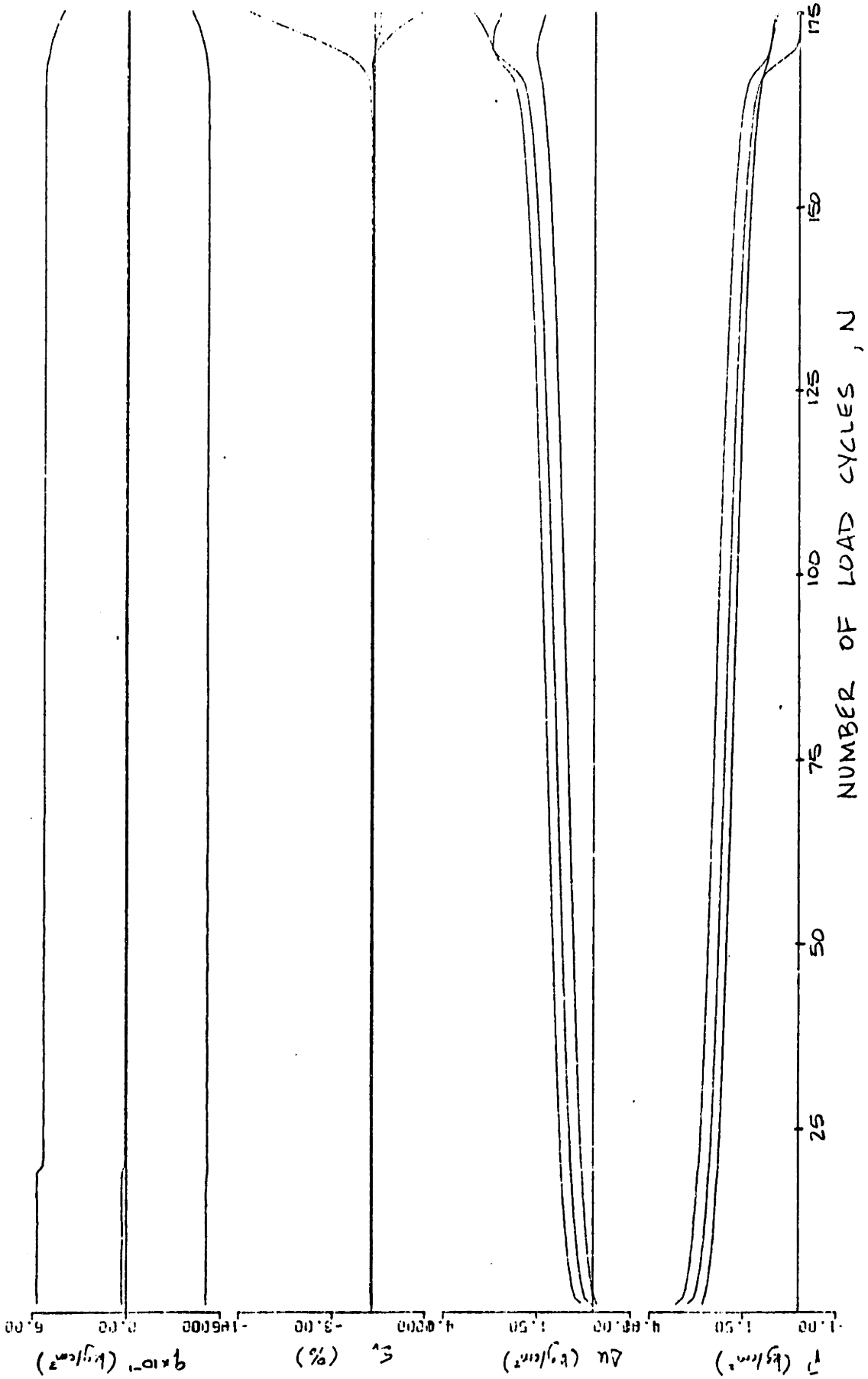

Summary of Stress Strain, and Pore Pressure Development - Test UC6

FIGURE A2-12

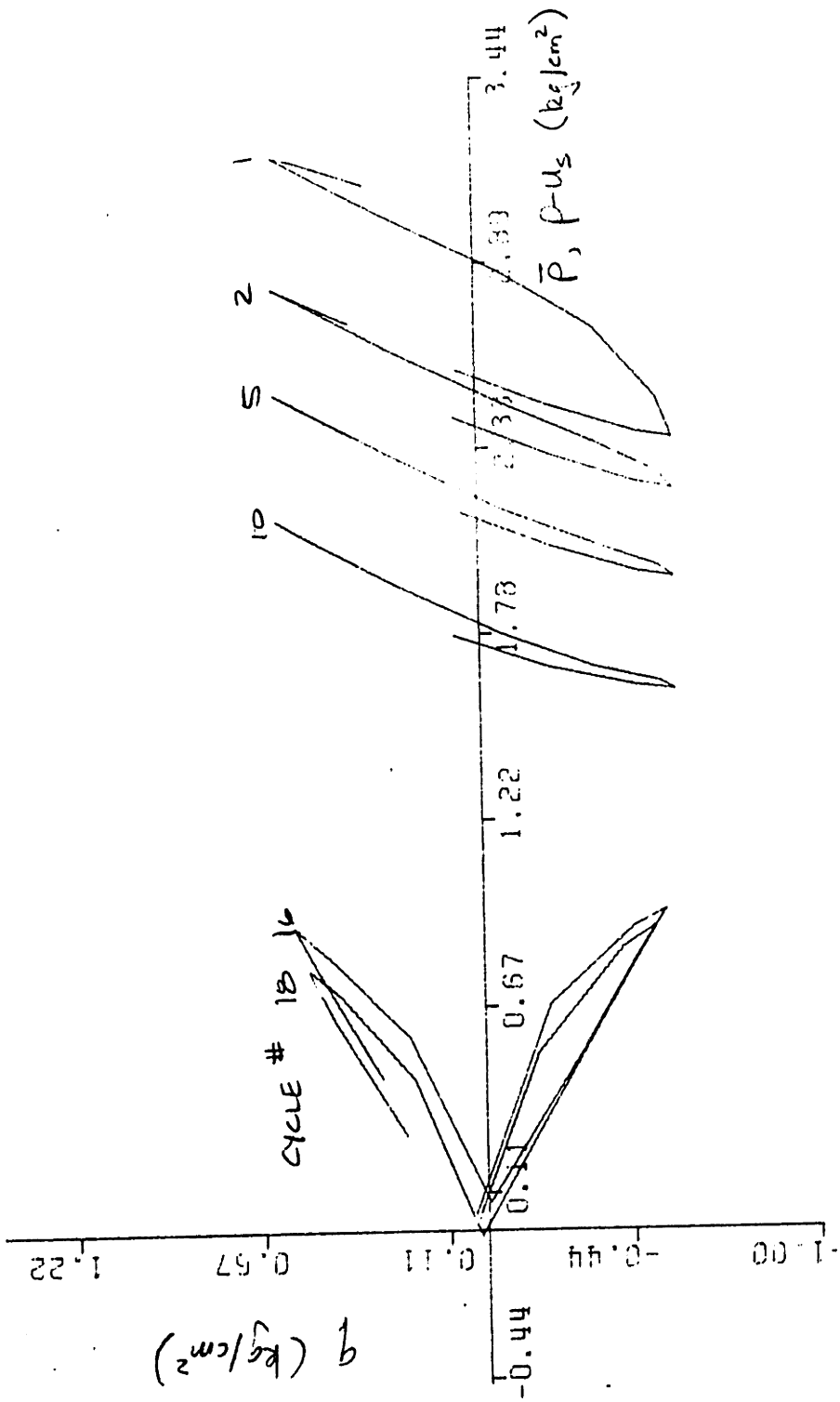

Effective Stress Path - Test UC7

FIGURE A2-13

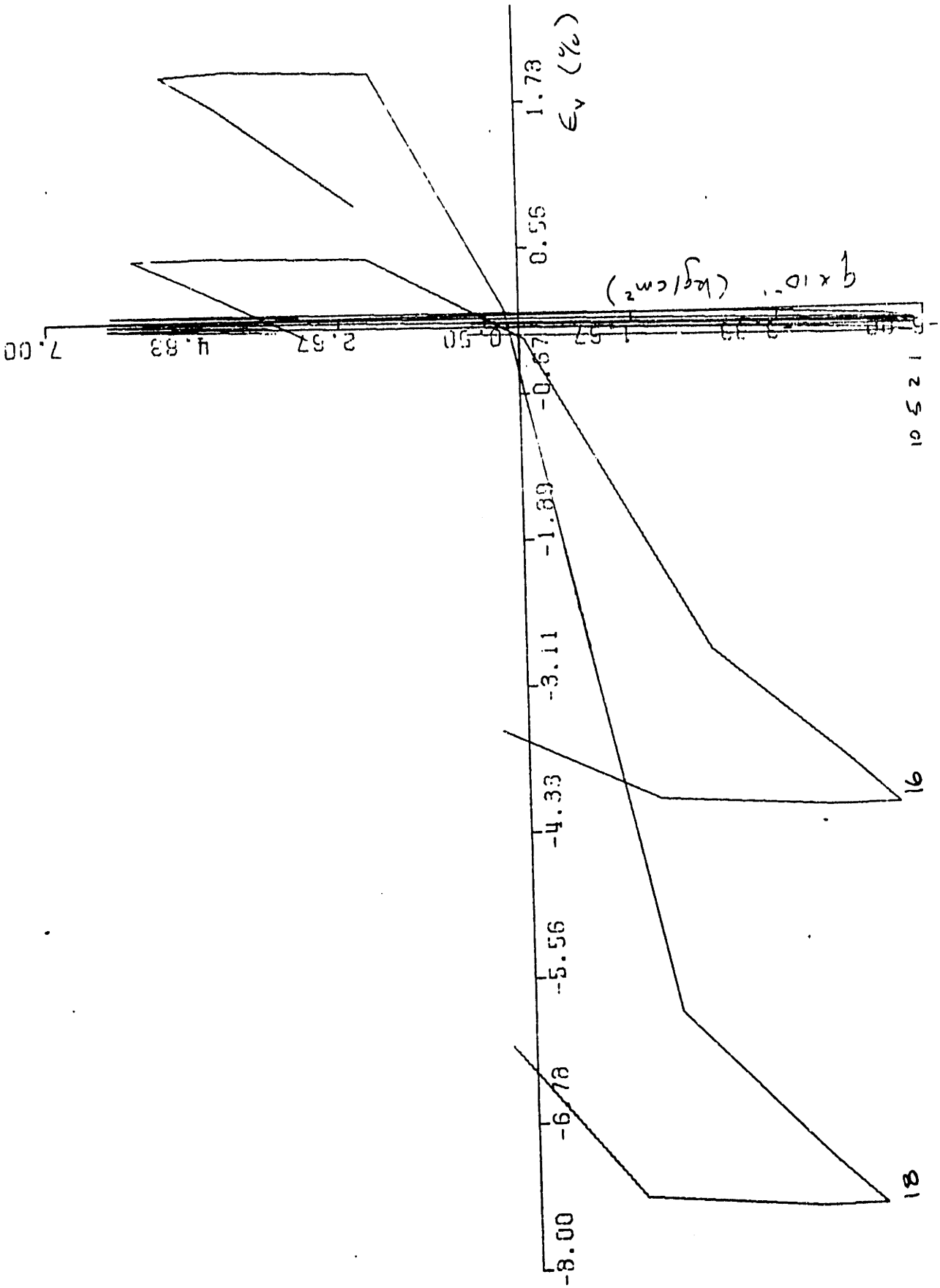

Stress vs. Strain - UC7

FIGURE A2-14

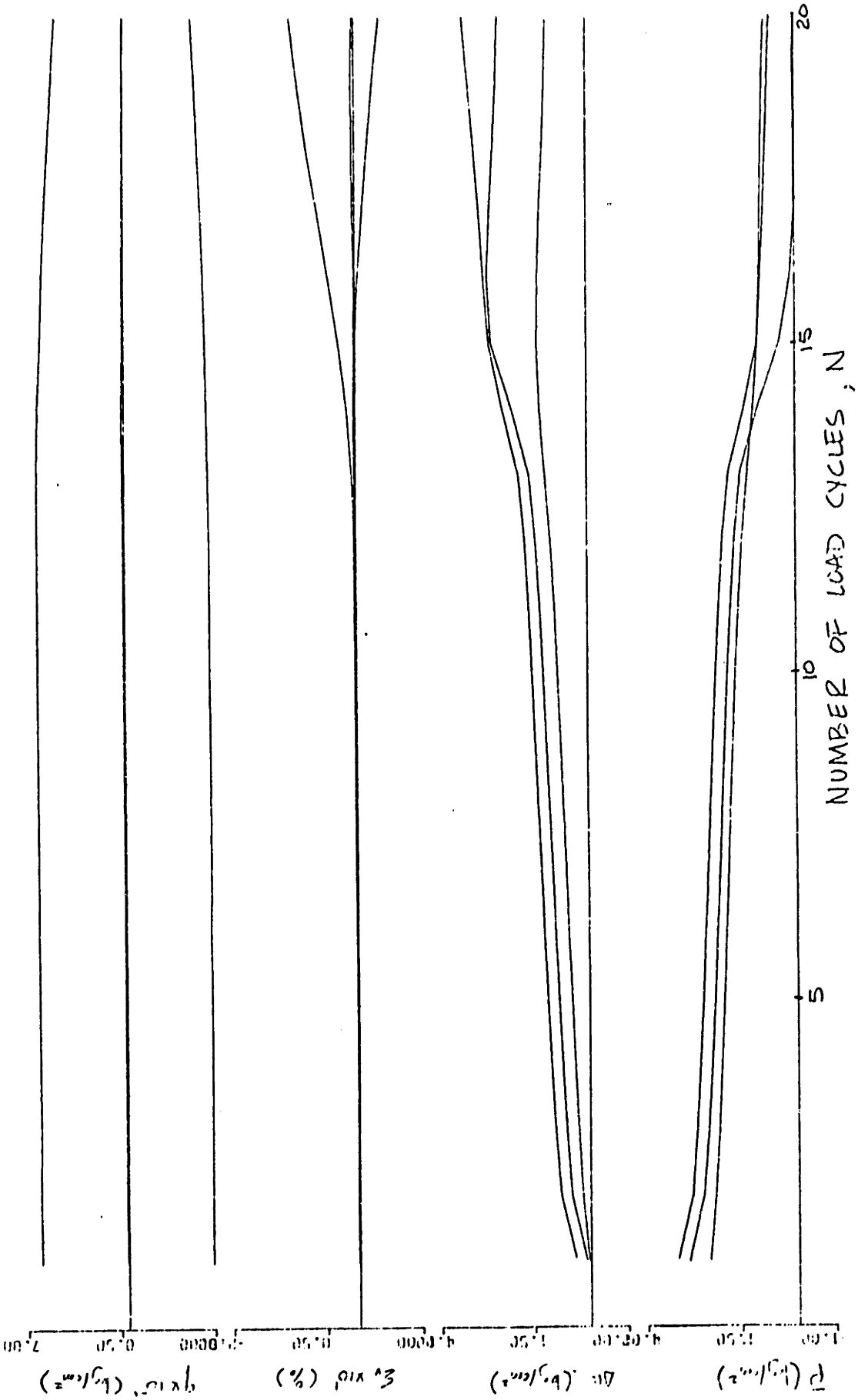

Summary of Stress Strain, and Pore Pressure Development - Test UC7

FIGURE A2-15

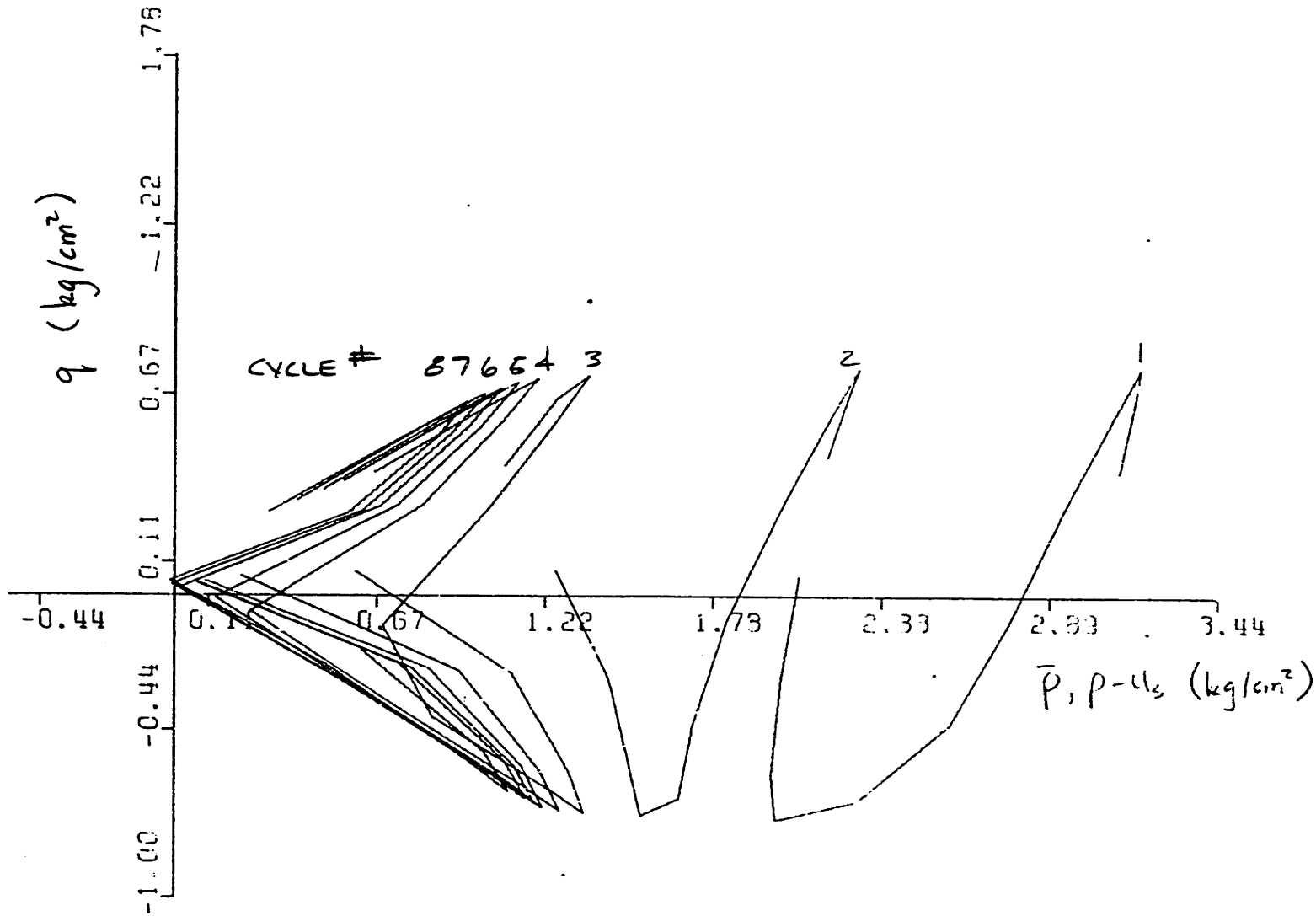

Effective Stress Path - Test UC8

FIGURE A2-16

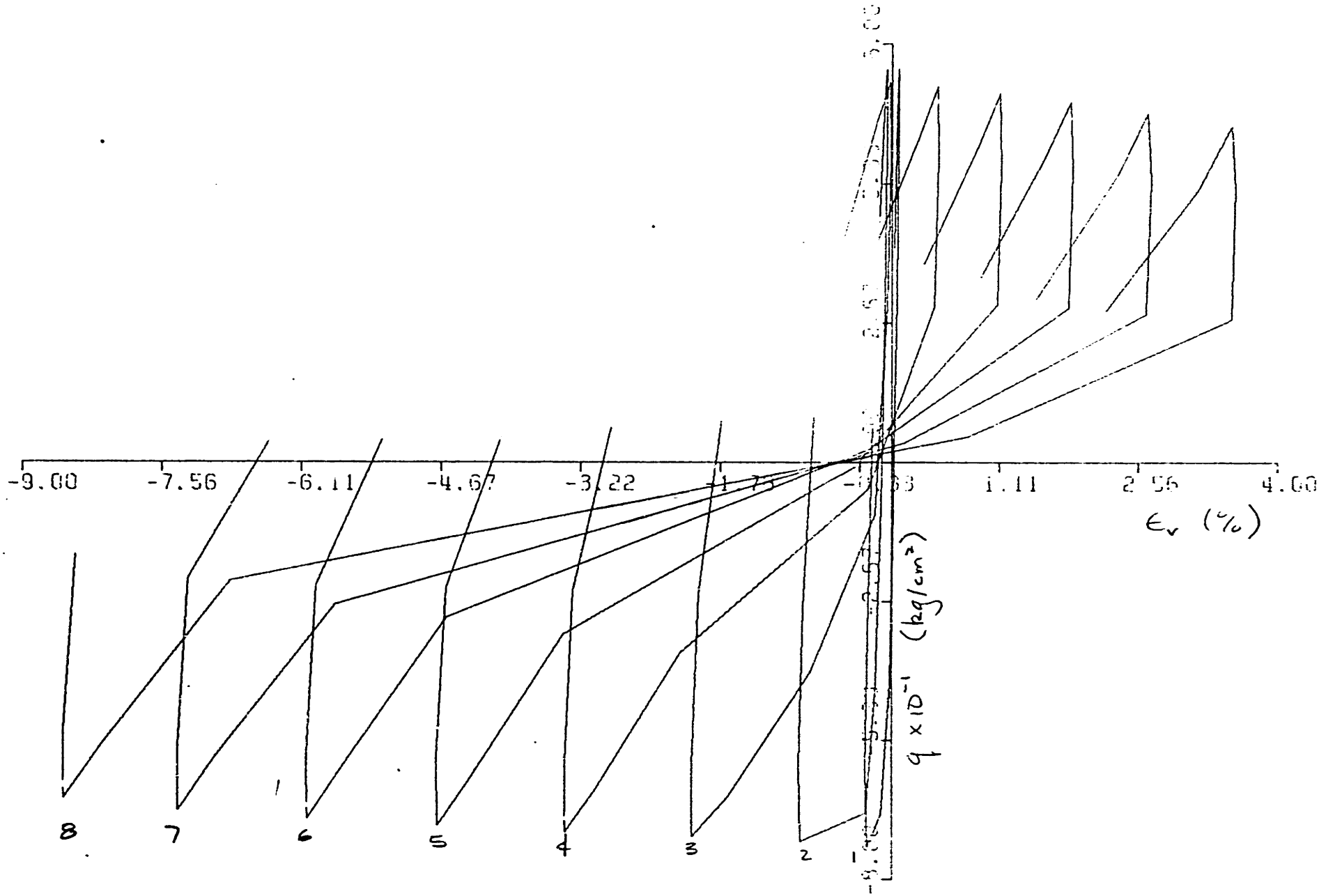

Stress vs. Strain - UC8

FIGURE A2-17

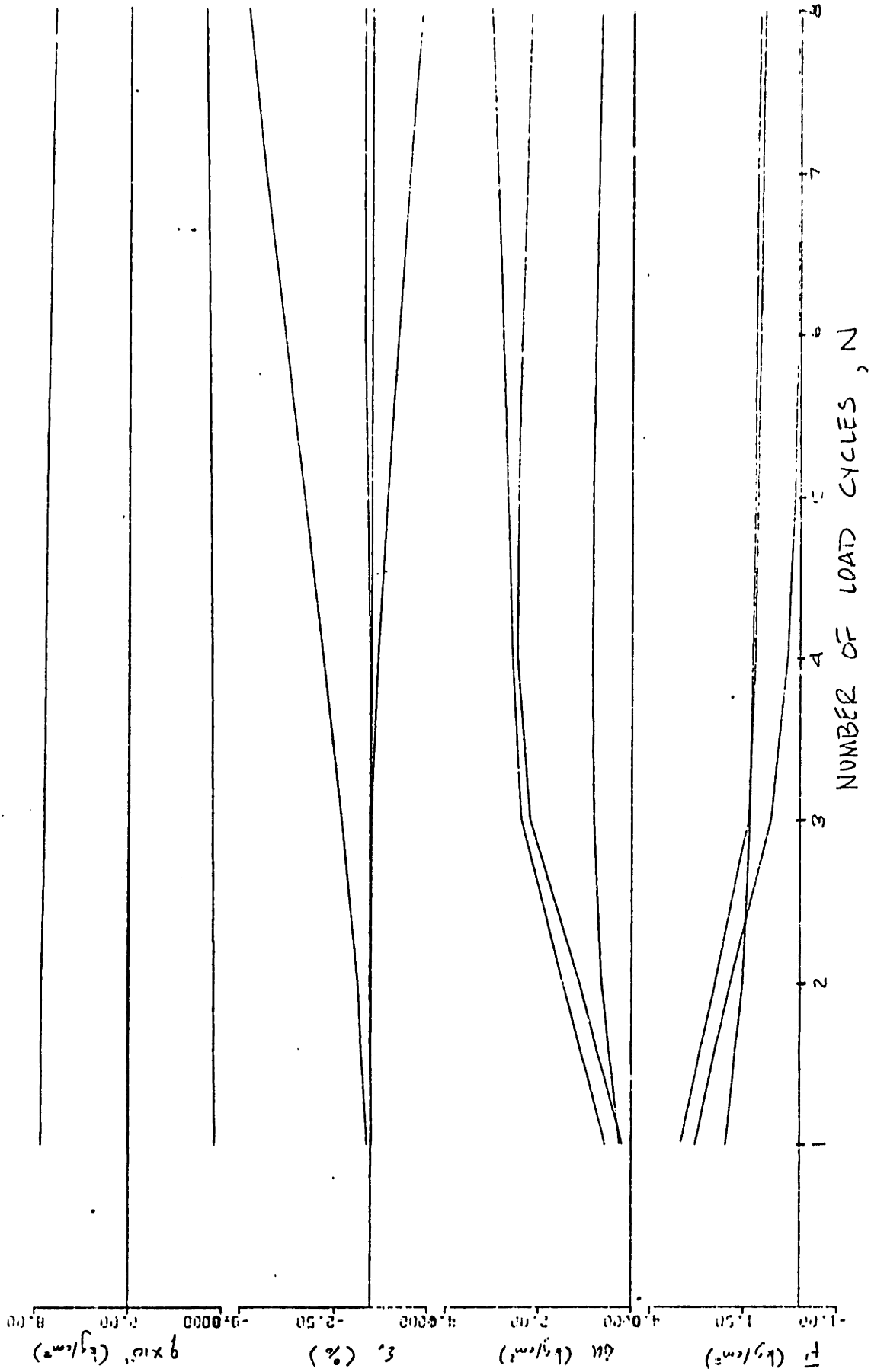

Summary of Stress Strain, and Pore Pressure Development - Test UC8

FIGURE A2-18

APPENDIX B - LABORATORY TESTING PROCEDURE

The triaxial tests were performed on cylindrical soil samples inside a pressure chamber (cell). The sample is oriented with a vertical axis. The horizontal load is controlled by the cell pressure, and the vertical load is applied by a vertical loading piston. The cell pressure and the vertical load can be controlled independently, thus allowing loading under a variety of stress paths.

This appendix describes the equipment used in the testing program. The first section describes the triaxial cell. The second section outlines the two methods of sample preparation used in the program, including saturation and consolidation of the sample. The third describes the cyclic testing apparatus, and procedure the data acquisition system, and the instrumentation used in the test. The final section describes the procedure used in the static triaxial tests.

Triaxial Cell

Triaxial cells, model WF10200 from Wykeham Farrance Eng., Ltd., Weston Road, Trading Estate, Slough, SL14HW, England, were previously modified to perform cyclic tests. The modifications were made to reduce piston friction and to allow better construction of samples to known dimensions. The cells will accept samples with a diameter of 3.5 cm and a height of 7.5 cm, i.e., a H/D ratio of 2.1/1.

Figure B-1 illustrates the modified cell. Friction is reduced by placing linear ball bearings around the piston. A frictionless, rolling diaphram provides an impermeable seal between the piston and the chamber, eliminating the need for sealing oil in the cell. Maximum measured piston friction is less than 100 grams under normal operating conditions.

An alignment frame for the top cap/piston assembly inside the plexiglass cylinder allows connection of the piston and top cap to the sample and membrane while the sample is still in the mold Good seating between the top cap and sample is achieved by pushing the top cap and piston assembly onto the top of the sample and clamping the piston into position with a piston clamping system.

Porous sintered bronze disks are used at the top and bottom of the sample to assist water flow. A top drainage line allows carbon dioxide (CO_2) and deaired water to permeate through the sample in order to displace entrapped air.

Sample Preparation, Saturation and Consolidation

Two methods of sample preparation were used in this investigation: wet rodding, and undercompaction. The following describes the exact technique used to prepare samples in this investigation by each of the two methods. More general procedures for using the undercompaction method is described by Ladd (1978). Wet rodding is more generally described in Chapter II.

Undercompaction:

1. The amount of air-dried sand to be used is calculated using the desired ratio and the volume of the split mold, and weighed.
2. Distilled water is added to the sand until a water content of 10% is achieved.
3. The sand is tamped, in five layers of equal weight, into the compaction mold using the undercompaction method recommended by Silver, et al (1976). The degree of undercompaction used in this investigation was 5%. Hedberg (1977) suggests a degree of undercompaction of 5% for tests with porosities between 41.0 and 43.6%. The primary rubber membrane (Wykeham Farrance cat. no. WF10490, thickness = 0.010 to 0.015 inches) is held to the inside of the mold by a vacuum.
4. The housing containing the top cap/piston assembly is fastened to the triaxial base and the final .6mm of compaction is done with the piston.
5. The vacuum is released and the primary membrane is stretched over the top cap and sealed with O-rings.
6. A slight vacuum of 0.2-0.4 kg/cm^2 is applied to the sample with a screw pump connected to the bottom drainage line, and the split mold is removed.
7. The sample diameter is measured at five (5) locations with a Pi-tape.

8. The secondary membrane (Trojan Latex Condom No. 70, Young's Drug Products, Corp., Piscataway, New Jersey 08854, thickness = 0.003 inches) is pulled up over the sample and sealed with O-rings to the top cap for additional protection against membrane leakage.
9. The cell is assembled and filled with deaired-distilled water.
10. The cell is placed in the consolidation frame and a cell pressure of 0.2 kg/cm^2 is applied using a mercury pot pressure system.
11. The sample height is determined by measuring the piston stickup with a depth micrometer.

Wet Rodding:

1. The amount of air-dried sand to be used is calculated using the desired void ratio and the volume of the split mold. This sand of sand is divided equally into two parts (for a two-layer sample). The sand is weighed and kept in separate containers.
2. The primary and secondary rubber membranes (previously described) are affixed to the bottom pedestal of the triaxial cell base and sealed with O-rings. A bronze disk is set inside the pedestal, and the split mold is set in place. The primary membrane is stretched upward through the mold and pulled over the sides at the top. The secondary membrane remains rolled up at the base, in a void space between the bottom of the mold and the pedestal. A vacuum

is applied to the mold to hold the primary membrane tight against the inside of the mold. An extension collar is secured to the top of the mold by means of a large rubber band which is fastened to the base. The collar is watertight so to allow water to rise above the top of the mold when the sand is rained into the mold.

3. By means of a screw pump connected to the bottom drainage line, the mold is completely filled with deaired-distilled water.

4. The first portion of sand is rained gently into the water-filled mold to form the first layer. The sand settles uniformly at the bottom of the mold at near maximum void ratio. The water which is displaced rises within the extension collar.

5. Rodding is performed with a steel wire rod approximately 0.042 inches in diameter, and sufficiently long enough to extend well above the extension collar. The first layer is densified by pushing the rod to the bottom of the mold a total of 50 times in a random fashion, being sure to cover the whole cross-sectional area. The downstroke of the rod should be brisk. However, because of friction between the rod and the particles within the sample, the upstroke should be gentle. This prevents soil grains from being pulled should be gentle. This prevents soil grains from being pulled upward and

out of the layer. Rodding should be done in sets of five or ten pushes, with a 30 to 60 second pause to allow for some settling action to occur. This enhances the repeatability of the technique.

6. The amount of sand necessary to form the second layer is rained into the mold in a similar fashion. Again, 50 pushes of the rod are used to densify this upper layer. The downstroke, however, is extended 1/16 to 1/8 of an inch into the top of the lower (first) layer in order to densify a thin loose zone which is believed to exist there (see Chapter Two).

7. Upon completion of the densification of the sand within the mold, the water inside the extension collar, (above the sample) is carefully removed. This is done by siphoning the water out of the collar with a small diameter tube (or with a pipette) until the water level is only about 1/4 inch above the top of the sand sample. The remainder of this water is removed and the sample is drained by very slowly backscrewing the screw pump until an airbubble is seen in the hose connecting the screw pump to the triaxial base.

8. The extension collar is removed from the top of the mold. The sand level is generally slightly above the top of the mold at this point. The top bronze disk is placed on the sample and pushed downward (and slightly rotated) in order to level the sample

and provide good seating between the sand and the top cap.

9. The housing containing the top cap/piston is fastened to the base. The top cap/piston is lowered onto the sample and the bronze disk, and held firmly in position while the piston is clamped.

10. The vacuum is released and the primary membrane is stretched over the top cap and sealed with O-rings.

11. A slight vacuum of 0.2 to 0.4 kg/cm^2 is applied to the sample with the screw pump. The split mold is removed.

12. The sample diameter is measured at five (5) locations with a Pi-tape.

13. The secondary membrane is rolled up, over the sample and sealed with O-rings to the top cap.

14. The cell is assembled and filled with deaired-distilled water.

15. The cell is placed in the consolidation frame and a cell pressure of 0.2 kg/cm^2 is applied using the mercury pot system.

16. The sample height is determined by measuring the piston stick-up with a depth micrometer.

Saturation and Backpressuring:

1. Carbon dioxide is flushed through the sample at 5-10 cm^3/minute for 30-60 minutes to displace air in the void spaces. Because CO_2 is heavier than air, and is more soluble in water than air, this procedure enhances saturation.

2. Approximately 200 ml (about 3.5 void volumes) of deaired-distilled water is flushed through the sample, transducer block, and drainage lines under a total head of about 2.5 feet of water.
3. Cell pressure and back pressure (applied by a mercury pot pressure system) are raised incrementally to 4.2 and 4.0 kg/cm^2, respectively, for drained tests; and 5.2 and 5.0 kg/cm^2, respectively, for undrained tests. An axial load is applied in order to maintain an isotropic state of stress during pressurization.
4. The sample sits under backpressure overnight.
5. Pore pressure response is determined by measuring the B-parameter = $\Delta u / \Delta\sigma_c$. The cell pressure is raised by some arbitrary increment, $\Delta\sigma_c$, with the drainage lines to the sample closed. The increase in pore pressure, Δu, corresponding to this increase in confining pressure is measured. B values of 0.98 - 1.00 are desireable and can generally be obtained with little difficulty.

Consolidation:

1. The vertical and horizontal stresses on the sample are increased in increments of $\Delta\sigma_{vc}$ = 05 kg/cm^2 and $\Delta\sigma_{hc} = K_c \, \Delta\sigma_{vc}$. The vertical load is controlled by a proving ring, and the horizontal stress is controlled by the confining pressure within a burette sensitive to ± 0.01 cm^3.

3. In static tests, the stresses are increased until the final consolidation stresses are reached.
4. In cyclic tests, the final increment of consolidation is performed in the cyclic apparatus.

Cyclic Triaxial Testing

Cyclic triaxial tests performed for this investigation were done in a cyclic loading frame built at M.I.T. Following consolidation in the static consolidation frame, the triaxial cell containing the sand sample is moved to the cyclic machine and mounted on the loading frame. The final stage of consolidation is completed in the cyclic machine.

The following description of the cyclic machine is partly taken from the description by Hadge (1979).

Cyclic Load Frame:

Figure B-2 presents a schematic of the M.I.T. - built cyclic load frame. The static weights apply a constant vertical load to the sample. The cyclic component of vertical load is created by the movement of the cyclic weights along a lever arm. A motor-driven wheel moves the weights back and forth along the lever arm, creating a nearly sinusoidal loading pattern. This loading pattern is also shown in Figure B-2, where it is compared to a true sinusoidal pattern. The vertical load on the piston at any one time is given by:

$$W_{total} = W_H + W_s + W_c \cdot 1/8(24 \pm 4 \cos \alpha^* - 400-16\sin^2 \alpha^*)^7$$

where

W_H = static hanger weight in kg

W_s = deadload on static hanger in kg

W_c = total cyclic hanger weight in kg

α^* = angle of rotation on the flywheel measured from maximum load position (see Figure B-2)

$\pm$ = + for $0° < \alpha^* < 90°$ and $270° < \alpha^* < 360°$
- for $90° < \alpha^* < 270°$

It is necessary for the counterweights to balance the cyclic weights in the minimum load position.

A cyclic period of 11 to 12 seconds was used in the testing program. Twelve data readings were made within each cycle. The data acquisition system is unable to record this much information when cycles of less than 10 seconds are used. The minimum period that the cyclic machine can achieve is 2 seconds. Faster periods cause the cyclic weights to swing.

Final consolidation in the cyclic load frame:

1. After consolidation in the static frame is completed, the values at the base of the triaxial cell are closed, the piston clamped to prevent movement, and the cell is carefully transported to the cyclic apparatus.
2. In the cyclic load frame, the final increment of consolidation is applied by increasing the vertical stress on the sample by 0.5 kg/cm^2, increasing the horizontal stresses by $K_c(0.5)$ kg/cm^2 with the cell pressure mercury pot, and opening the backpressure to the electronic volume change device which controls

the backpressure by pressurized air and measures volume change. The position of the hanger during this final consolidation step corresponds to the mean shear stress level, about which the load will be cycled. The loads on the cyclic and counter-weight hangers correspond to the chosen cyclic shear stress, Δq. The load on the static hanger, when combined with the varying load on the cyclic hanger, will produce the total cyclic load on the sample.

Cyclic loading:

All tests are started at mean shear stress, i.e., the cyclic hanger is in mean position on the lever arm. The cyclic period, as mentioned earlier, is 12 seconds, but can be varied at any time within the test. The load, upon beginning cycling, will increase from the mean value to the maximum load position, and then will decrease, and cycle as such.

Transducers:

Four transducers are monitored during the triaxial tests. Pore pressure is monitored at the base of the sample with a Tyco Model AB pressure transducer, manufactured by Tyco Instrument Division, 4 Hartwell Place, Lexington, Massachusetts 02173. The transducer has a linear range from 0 to 14 kg/cm^2 with a given nonlinearity of 0.1% of full scale. Cell pressure is monitored with the same type of transducer. These pressure transducers read pressure to within $\pm$ 0.002 kg/cm^2.

The vertical load on the piston is recorded by a Tyco model FP load cell, with a capacity of $\pm$ 450 kg and a

nonlinearity less than ± 0.1% of full range. The sensitivity of the load cell is ± 0.013 kg.

Vertical displacement of the loading piston is measured with a DCDT (Direct Current Linear Variable Displacement Transformer), manufactured by Hewlett Packard, Medical Electronics Division, 175 Wyman Street, Waltham, Massachusetts 02154. The type used to measure displacement for these tests is 7DCDT-500, with a specified nonlinearity less than ± 0.05 percent with ± 12.5 mm travel, i.e., an accuracy better than ± 0.05 percent strain at 10% vertical strain. The sensitivity of strain measurements is ± 0.003% strain, for the given instrument and size of sample.

During drained tests an electrical volume change device is used to monitor volume changes. This device replaces the cell pressure as the fourth quantity measured. The device has a total range of 160 cm^3 and a sensitivity of 0.002 cm^3 over a range of ± 6 cm^3. It was designed at M.I.T. by Dr. R.T. Martin. A schematic of the device is shown in Figure A-3.

- Data acquisition:

During cycling an electrical scanning system allows the output voltage of the four transducers (vertical displacement, load, pore pressure and cell pressure or volume change) to be read and stored on magnetic tape. The scanning is performed by a Fluke Model 2240A Data Logger, manufactured by John Fluke Mfg. Co., P.O. Box 43210, Mountlake Terrace, Washington 98043. Digital readings of date, time and transducers from the logger are then transferred to a Kennedy Model 1600

Incremental Magnetic Tape Recorder, manufactured by Kennedy Co., 540 West Woodbury Road, Altadena, California.

The number of load cycles is counted by a mechanical counter and an electronic counting system which consists of a reading control box and a photo-electric switch. The switch signals the start of each new cycle. This signal is transmitted to the reading control box which counts the cycles and closes a reading circuit each time a preset number of cycles is reached. Whenthe reading command circuit is activated, another photo-electric switch transmits scanning comman pulses to the Fluke data logger.

Following the completion of the test, the magnetic tape is brought to M.I.T.'s Information Processing Center where it is used as input data for a computer program which reduces the data. The program calculates the stresses and strains for the recorded cycles. The results are tabulated and plotted. Vertical stress on the sample is corrected for membrane stiffness and changes in cross-sectional area of the sample during straining (see Hedberg 1977).

Data reduction computer program:

The data reduction program includes several plotting routines to display test results. The following plots are produced:

1. vertical strain, ε_v; effective stress, $\bar{p}$; shear stress, q; and volumetric strain, ε_{vol}; or pore pressure, Δu versus time for each logged cycle,

2. a summary plot showing ε_v, $\bar{p}$, q, and ε_{vol} or Δu at maximum, mean, and minimum shear stress versus cycle number,
3. the effective stress path for selected cycle numbers,
4. shear stress versus vertical strain for selected cycle numbers.

MEASUREMENT DEVICE	QUANTITY MEASURED	RANGE	ACCURACY & SENSITIVITY
DCDT (Hewlett-Packard)	vertical strain	± 12.5mm	measures to within ± .003% vertical strain specified nonlinearity: less than ± .5% within full range measured accuracy: ± .017% strain at 1% vertical strain ± .019% strain at 10% vertical strain
pressure transducer (Tyco)	pore/cell pressure	0 to 14 kg/cm^2	reads to within ± .002 kg/cm^2 specified nonlinearity: .1% of full range measured accuracy: ± .024 kg/cm^2 at 5.5 kg/cm^2 ± .007 kg/cm^2 at 1.5 kg/cm^2
load cell (Tyco)	vertical load	0 to 450 kg	reads to within ± .013 kg specified nonlinearity: less than ± .1% of full range measured accuracy: ± .06 kg at 50 kg
electrical volume change device (MIT)	volume change	± 6 cm^3	reads to within ± .002 cm^3

DESCRIPTION OF MEASUREMENT DEVICES (from Hedberg, 1977)

TABLE B-1

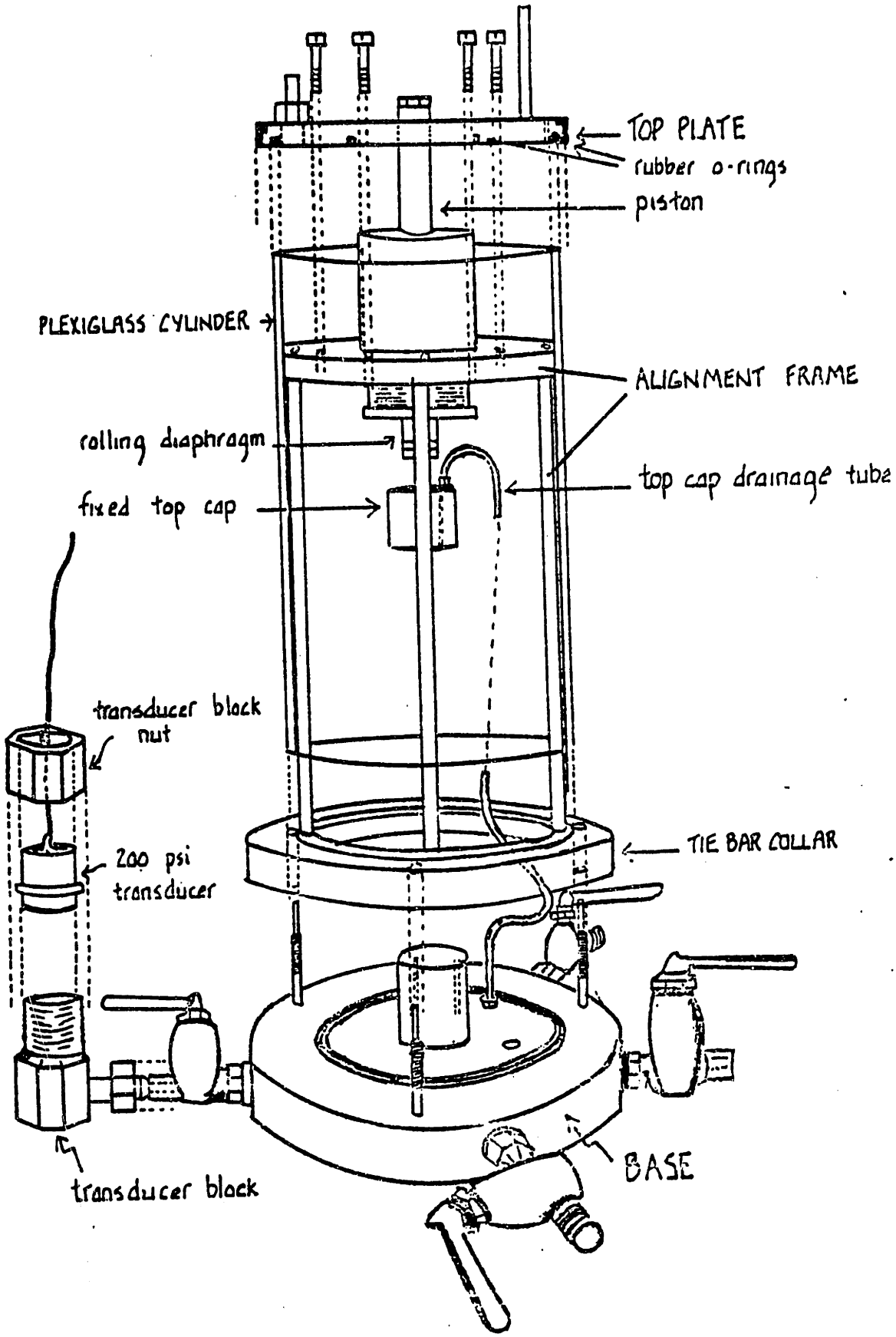

Modified Triaxial Cell
(From Hadge, 1979)

FIGURE B-1

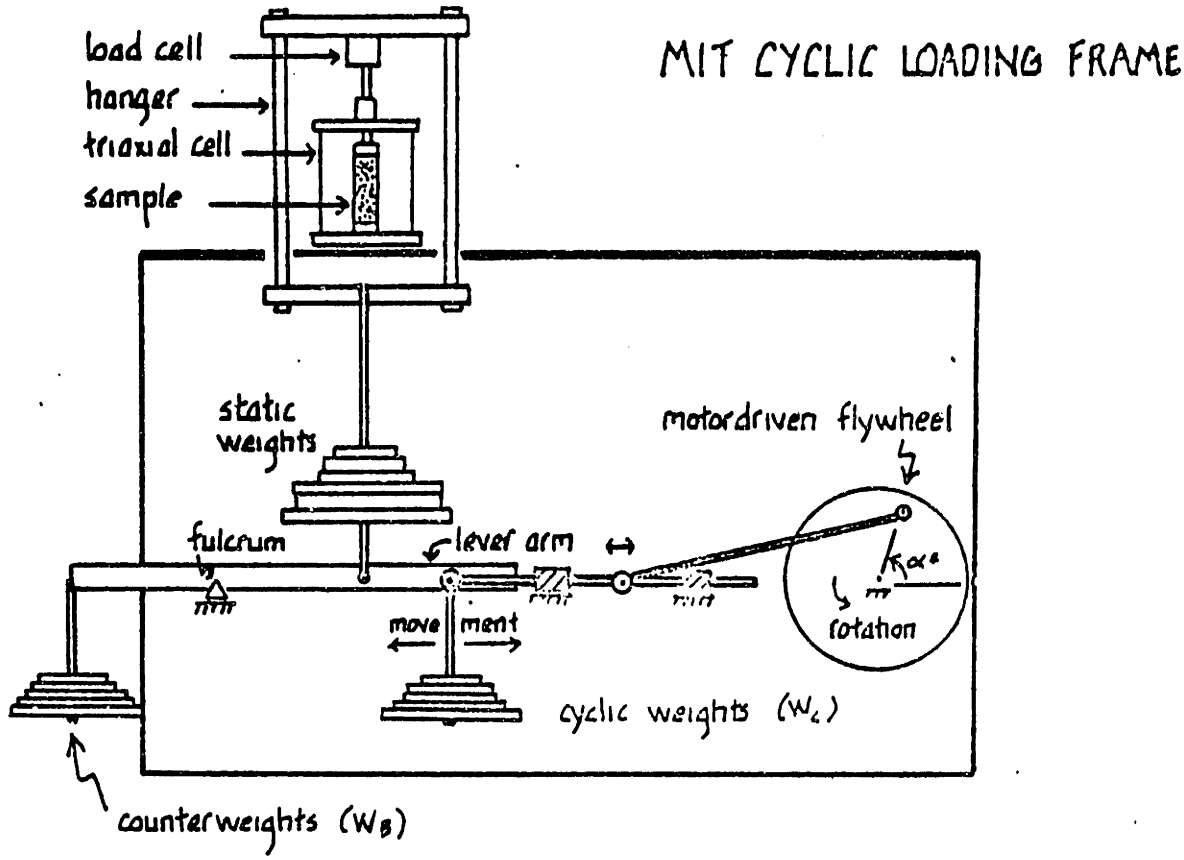

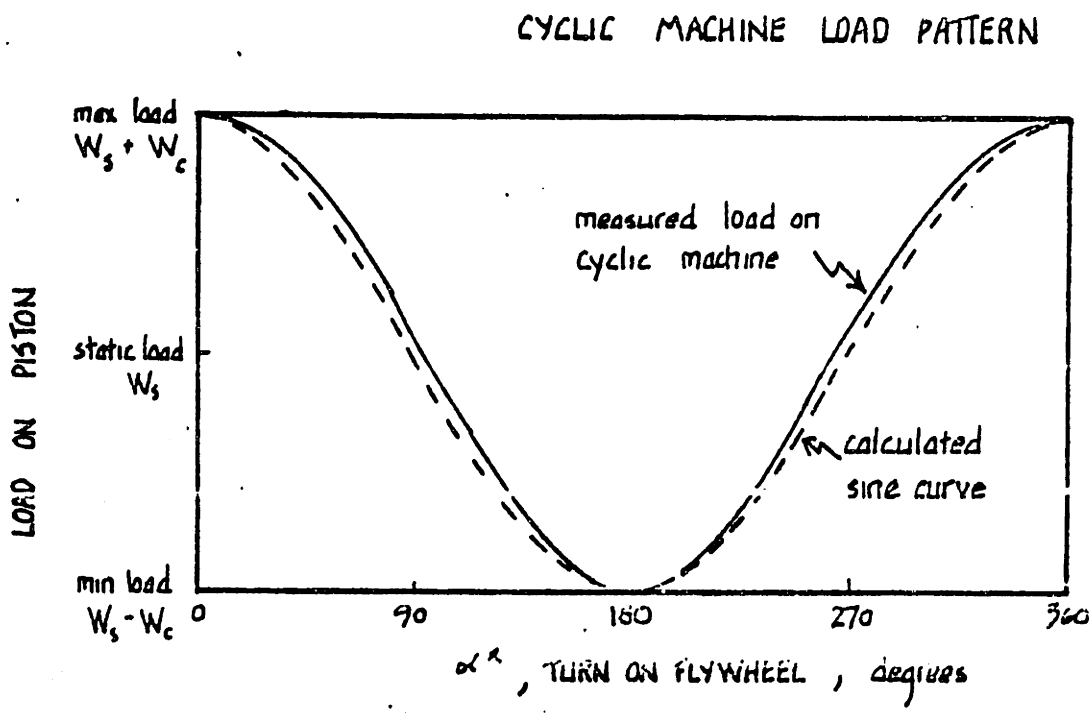

MIT Cyclic Machine
(From Hadge, 1979)

FIGURE B-2

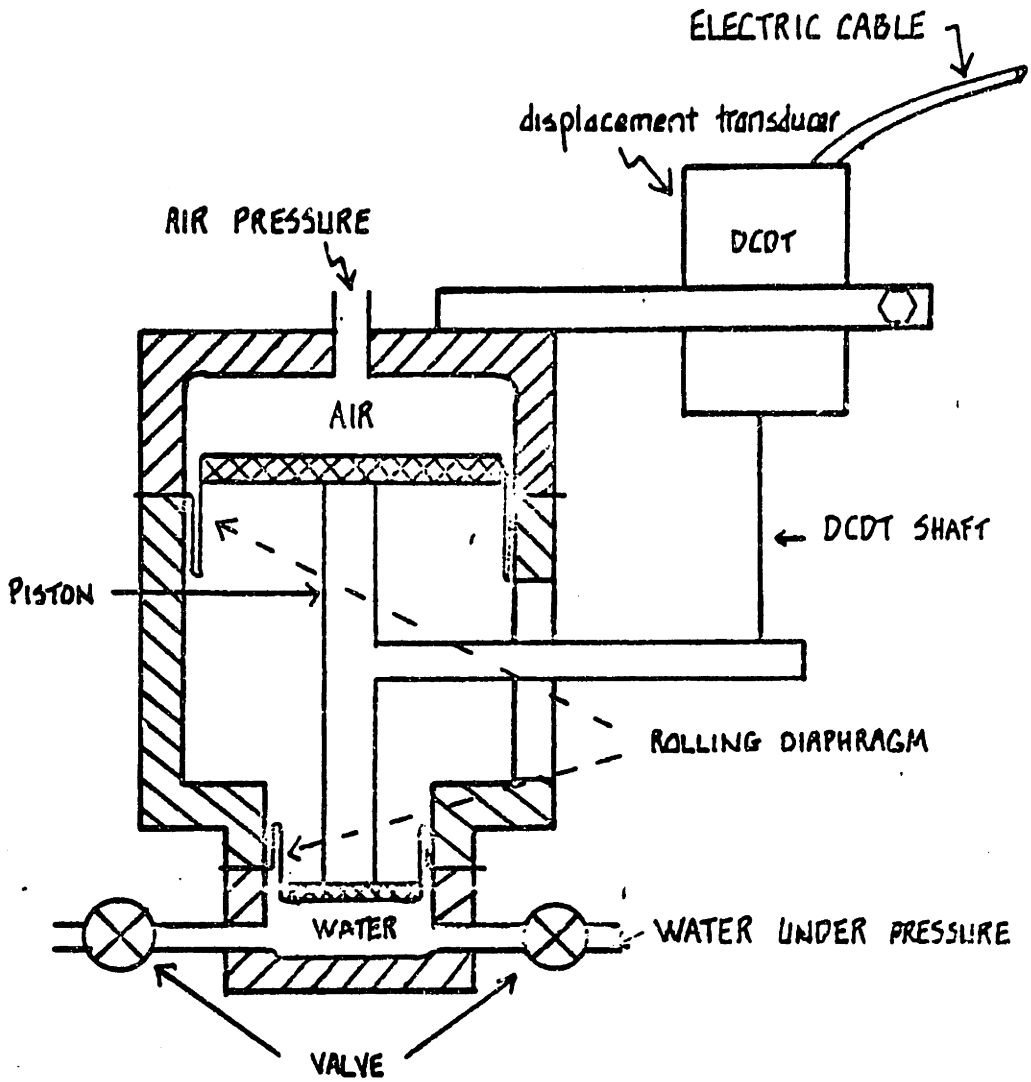

Electrical Volume Change Device
(From Hadge, 1979)

FIGURE B-3

APPENDIX C - STATIC TEST RESULTS

One static triaxial test was performed on a wet rodded sample to determine the friction angle, $\bar{\phi}$. The test was isotropically consolidiated to 1.0 kg/cm^2 and sheared undrained to an axial strain of about 5 percent. Figure C-1 shows the stress paths for this test. The effective stress path indicates an initially contractive behavior in which small positive pore pressures are measured, followed by dilation, in which negative pore pressures are generated and the effective stress path tends to follow the k_f-line. The inclination of the k_f-line, $\bar{\alpha}$, is about 28.5° ($\bar{\phi}$=34°). Figure C-2 shows the stress versus strain curves for this test.

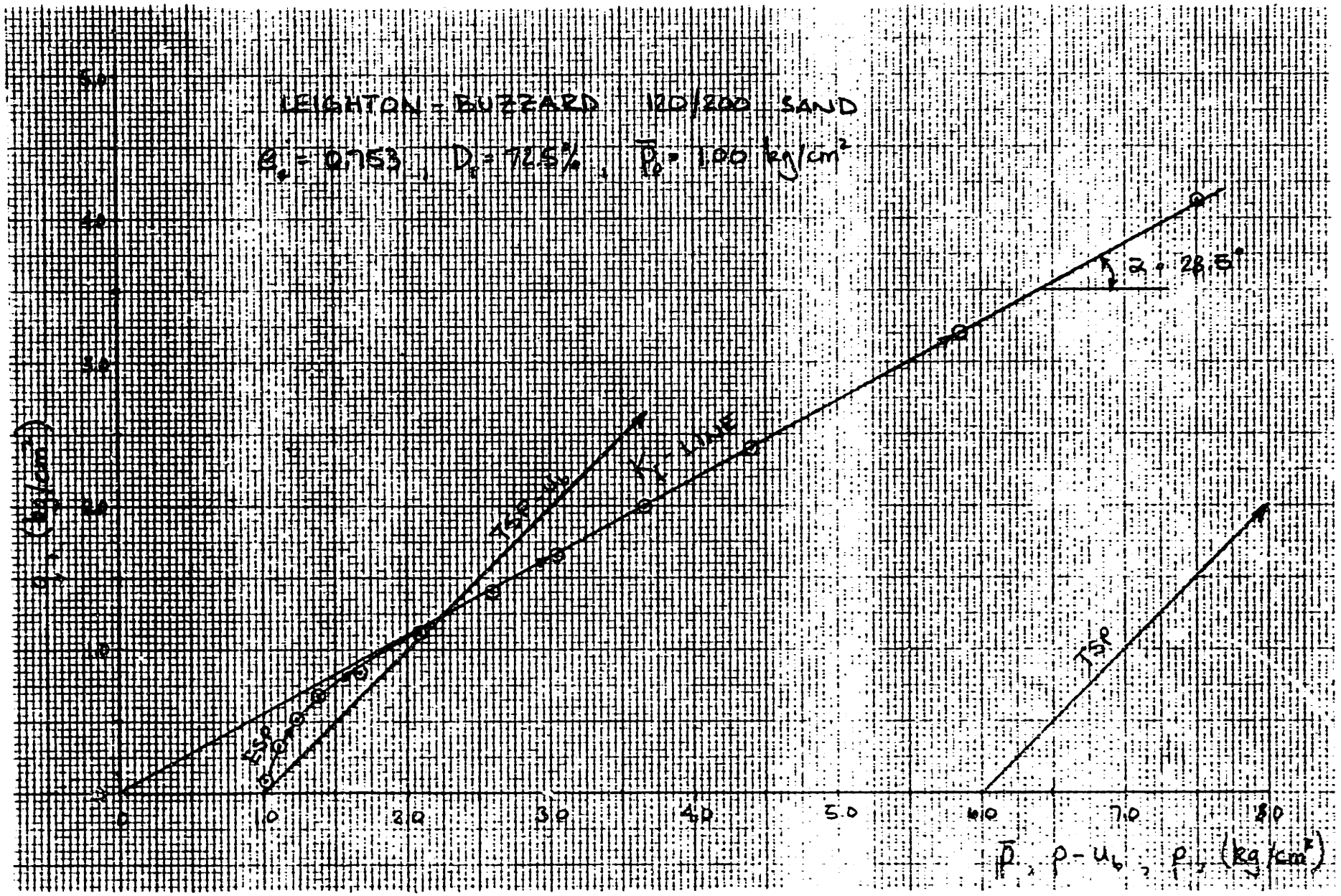

Effective Stress Path - Test US1

FIGURE C-1

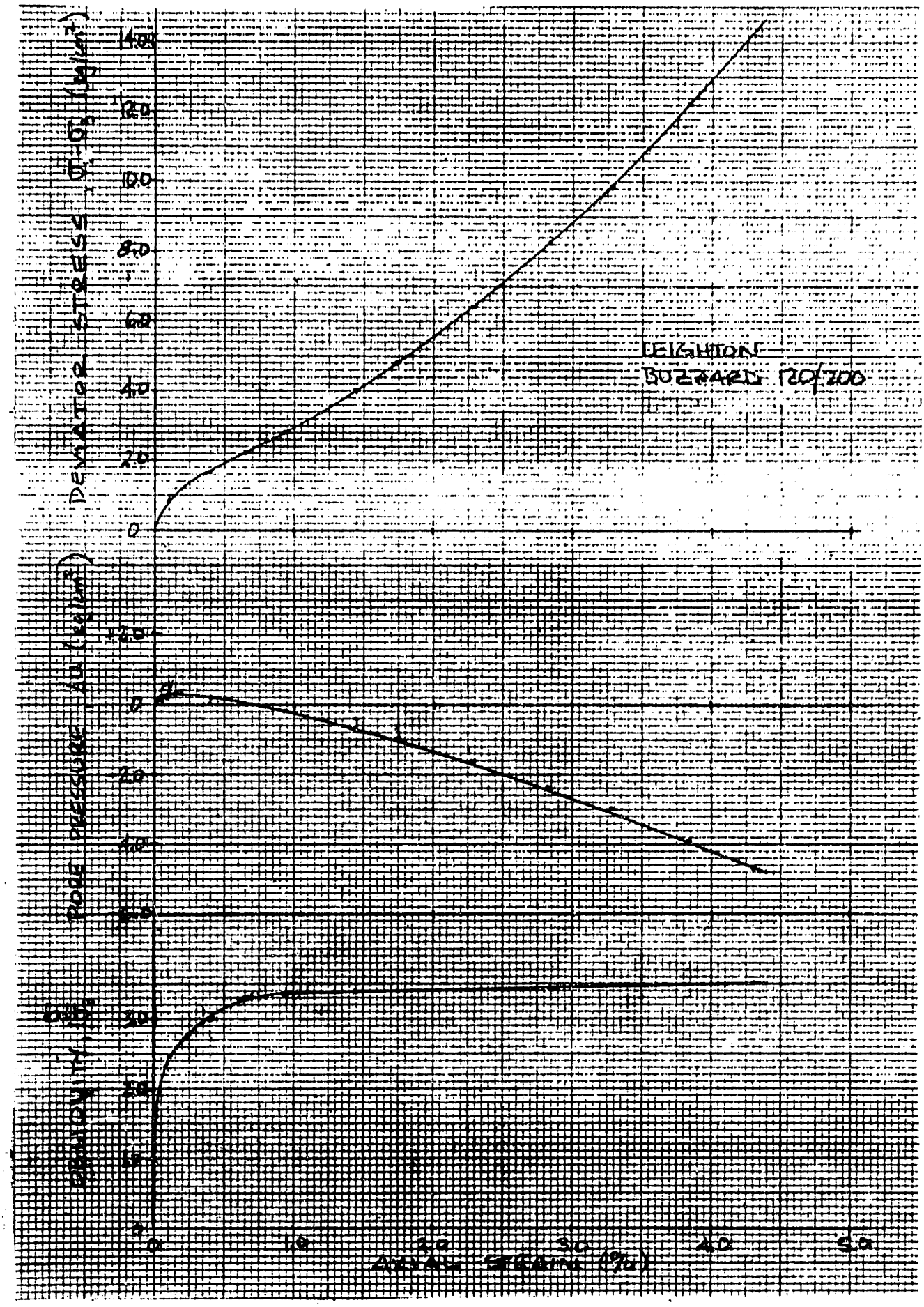

Stress vs. Strain - Test US1

FIGURE C-2